WADING THROUGH THE SPECTRUM OF WETNESS: TAILORED SOLVATION OF

WEAKLY HYDRATED POCKETS

AN ABSTRACT

SUBMITTED ON THE 20TH OF APRIL 2022

TO THE DEPARTMENT OF CHEMISTRY

IN PARTIAL FULFILMENT OF THE REQUIREMENTS

OF THE SCHOOL OF SCIENCE AND ENGINEERING
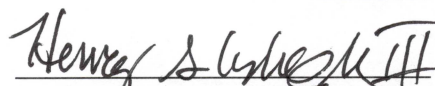
OF TULANE UNIVERSITY
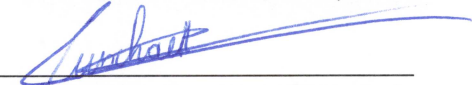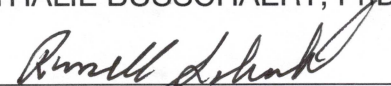
FOR THE DEGREE

OF

DOCTOR OF PHILOSOPHY

BY

_____

PAOLO SUATING

APPROVED: _____
BRUCE C. GIBB, PhD
Director

_____
HENRY S. ASHBAUGH III, PhD

_____
NATHALIE BUSSCHAERT, PhD

_____
RUSSELL H. SCHMEHL, PhD

Abstract

The importance of the influence of the shape of concavities and the nature of those concavities to its solvation in water is oft neglected. The hydration of nanoscopic concavities can be influenced by the addition of functionality to the portal of such concavities. In this dissertation the formation of stable water clusters and stable, vacuous spaces within deep-cavity cavitands is described. Stable water clusters can be formed by the addition of negative charges to the portal of the cavity (as in *exo*-octa-acid), reinforcing the hydrogen bonding network of the bound water molecules. This makes water a better guest for the pocket of the deep-cavity cavitand, inhibiting the binding of guests by making the water cluster more energetically unfavourable to displace. On the hand, the addition of alkyl groups pointing inwards towards the portal (as in tetra-*endo*-ethyl octa-acid) induces a drying transition in the pocket, desolvating the pocket in solution. Alkyl groups are thus functionalities themselves, and not just backbones for functionality. The synthesis and properties of hosts that occupy the two extremes of hydration are herein described

The binding of alkanes to a predominantly vacuous host is also demonstrated. In addition, the synthesis, and preliminary studies of the properties of positively charged analogues of predominantly dry hosts are also described.

WADING THROUGH THE SPECTRUM OF WETNESS: TAILORED SOLVATION OF

WEAKLY HYDRATED POCKETS

A DISSERTATION

SUBMITTED ON THE 20TH OF APRIL 2022

TO THE DEPARTMENT OF CHEMISTRY

IN PARTIAL FULFILMENT OF THE REQUIREMENTS

OF THE SCHOOL OF SCIENCE AND ENGINEERING

OF TULANE UNIVERSITY

FOR THE DEGREE

OF

DOCTOR OF PHILOSOPHY

BY

_____

PAOLO SUATING

APPROVED: _____
BRUCE C. GIBB, PhD
Director

_____
HENRY S. ASHBAUGH III, PhD

_____
NATHALIE BUSSCHAERT, PhD

_____
RUSSELL H. SCHMEHL, PhD

Acknowledgements

Many have come and gone and have made an impact on this work; they may be too numerous to be listed here, but a small number deserve to be especially mentioned.

My supervisor and research director Dr Bruce Gibb once told me in the early days to "…put [my] big boy pants on and figure it out" and that I "think too much and must find a balance between thinking and doing". He and I also spoke in great length about academic politics, scientific quandaries and conundrums, and random the little musings in our heads. Bruce, thanks for the talks, the encouragement, the inspiration, and sometimes the frustrations. Guess what: I've put on my big boy pants (and some), but I still think too much; it's a tough bloody habit to break, you know.

I would be remiss if I didn't mention my dissertation committee. Dr Russell "Russ" Schmehl showed me during his brief stint as department chair the importance of steadfastness and professionalism; Dr Nathalie Busschaert showed me that one can do big and beautiful things even early on in one's career; Dr Henry "Hank" Ashbaugh implicitly and subtly showed me that one can have serious fun whilst doing serious work. To the three of you: thank you. And thanks for taking time out of your busy lives to read through my musings and ramblings.

Life in the University means learning to work with and alongside others. Corinne Gibb, lab manager and lab mother, was both experimental rudder and compass. Without her guidance, this work may have fallen flat on its face. My

of the oft misquoted adage "the blood of the covenant is thicker than the waters of the womb". Without all of them I would be nothing.

Those not listed will forgive me for not having mentioned them. They know who they are, and I am still grateful.

Table of Contents

Part I: Introduction

"Mr Lavoisier and others of the French School have most ingeniously endeavoured to shew that water consists of pure air, called by them oxygene, and of inflammable air, called hydrogene." (Erasmus Darwin, *The botanic garden: a poem in two parts.,*1790)[8]

A brief history of the understanding of water: from the Ancients to the Middle Ages

The importance of water has long been pondered, even by the ancient thinkers (Fig. 1) Archelaus of Athens (fl. 5th century BCE) and Thales of Miletus (625–545 BCE) advocated the thought that matter exists as a continuum of water content, that earth and air are the leavings of water being evapoaretd. In fact, they believed that water was the primal element of the Universe because it was the only substance known to them that can congeal to a solid and disperse as a gas. Indeed, Thales believed that due to its fluid nature, water was the causal agent of all motion and change.[9] Anaximander of Miletus (610–540 BCE) believed that the
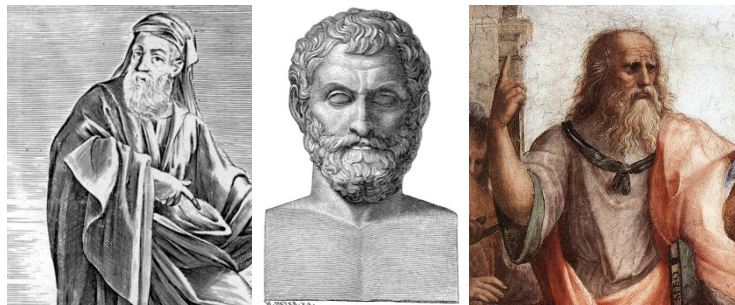
Fig. 1: The Greek thinkers (l-r): Empedocles; Thales of Miletus; and Plato. Images are in the public domain.

action of the sun on water produces life. Empedocles (495–435 BCE) and Aristotle (384–322 BCE) regarded water as one of the four "roots" (ῥιζώματα, rhizōmata) of the Universe alongside fire, air, and earth. These four roots had their own characteristics: water was cold and wet; earth was cold and dry; air was hot and wet; and fire was hot and dry. Differing proportions of these elements gave rise to the characteristics of different objects and materials. The atomist thinkers, which included Stoic and Epicurean philosophers such as Leucippus (fl. 5th century BCE), Democritus (460–370 BCE), Epicurus (341–271 BCE), Zeno of Citium (334–262 BCE), and Plato (427–347) went one step further and consider these four elements (στοιχεῖον, stoicheîon) the indivisible (ἄτομον, atomon) building blocks with which all things are built.[9, 10]

The Daoists in the East wrote about the physical and chemical properties of water, and its importance to Life itself in the *Huainanzi*[11]:

> *When it ascends into the heavens, it becomes the rain and dew.*
>
> *When it descends to the earth, it becomes moisture and dampness.*
>
> *If the myriad things do not gain it, they will not be born.*
>
> *⋮*
>
> *Chop it, and it is not cut apart.*
>
> *Try to set it alight, it will not burn.*
>
> *Seeping, draining, flowing, disappearing,*
>
> *Mixing and blending, intertwining with [things], it cannot be differentiated.*

It is so sharp it can pierce a hole in metal or in stone.

It is so strong it can give sustenance to the entire world.

⋮

Light can be seen but cannot be held,

Water can be held but cannot be destroyed.

Science in the medieval ages was heavily influenced by the ancient Greek philosophers via trade with the Islamic world.[12] The works of the likes of Jābir ibn Ḥayyān (d. 806–816 CE),[13] Abū Bakr al-Rāzī (864–ca. 92 CE),[14, 15] Muḥammad ibn Umayl (ca. 900–ca. 960(?) CE),[16] and Khālid ibn Yazīd (668–704(?) CE),[17] *inter alia*, shaped natural philosophy of the time. Their writings trickled down and transformed into Western alchemy and Hermeticism via the works and translations of those such as Morienus (fl. 700 CE),[17] Thomas Aquinas (1225–1274),[18] Rogerus Baconus (c. 1219/1220 – c. 1290),[19] and Theophrastus von Hohenheim (c. 1493 – 1541).[20] Thus, the belief that water is an indivisible, indestructible, transmuting element persisted well into the 16th century.

Is water indivisible? Discoveries of the Chemical Revolution

The thinkers in the Age of Enlightenment of the 17th and 18th centuries brought about not only political revolutions, but also scientific ones. (Fig. 2). The French chemist Antoine-Laurent de Lavoisier (1743–1794) sought to unravel the mystery of water's composition.[21] Hearing of Henry Cavendish's (1731–1810)

unpublished experiment of the combustion of a mixture of "dephlogisticated[*] air[†]" and "inflammable air" producing visible condensation,[22, 23] de Lavoisier was eager to repeat the experiment to try to reinterpret Cavendish's results. He first extracted "the purest component of air" or dephlogisticated air, using Joseph Priestley's method of heating red mercury calx (cinnabar or mercuric oxide).[24] In a side-experiment he passed a stream of dephlogisticated air through a heated metal pipe and observed the formation of an oxide layer. Then, he collected "inflammable air"— the gas formed by the action of strong mineral acids with metals. In June 1783, he repeated Cavendish's then unpublished experiments with the help of mathematical physicist Pierre-Simon de Laplace, by igniting jets

Fig. 2: The Chemical Revolution and the Age of Enlightenment (*top, l-r*) – de Lavoisier, Cavendish, Priestley, Laplace. (*bottom, l-r*) Dalton, Avogadro, Ampère, Davy. Images are in the public domain.

---

[*] Phlogiston (Greek φλόξ, phlox, flame) was a pseudo-element with fire-like properties which natural philosophers believed imbued substances with the capacity to burn.
[†] "Air" was the term used for any gas, either in a mixture or in the pure state.

of both airs in a mercury-sealed glass container.[25] The combustion generated a condensation in the apparatus; water was formed. This milestone in the history of the sciences proved five things: 1) phlogiston did not exist; 2) dephlogisticated air caused combustion and the formation of oxides in metals and so was renamed *oxygen*; 3) inflammable air was a pure substance – renamed hydrogen – that generated water when combusted with oxygen; water was not simply being condensed from the air by the act of combustion; 4) water was not an element, but rather a combination of both oxygen and hydrogen. Further advances on this and other chemistry fronts by de Lavoisier was cut short on 8 May 1794; at the age of 50 de Lavoisier was convicted and guillotined by the French Revolutionaries on the false accusation of defrauding the State, of which he would be posthumously exonerated.[21]

In 1808 English chemist John Dalton (1766–1844) published an extensive discussion on his atomic-molecular theory, a set of rules which to this day is taught to students of science the world over. His "rule of greatest simplicity" stated that if the atoms of two different elements were known to make one and only one substance, it was assumed that only one atom of each would make up that substance. Thus, with this rule Dalton declared that the composition of ammonia is NH, and that of water is OH.[26]

In 1811 Italian physicist Lorenzo Romano Amedeo Carlo Avogadro (1776–1856) published an essay entitled « *Essai d'une manière de déterminer les masses relatives des molecules élémentaires des corps, et les proportions selon lesquelles elles entrent dans ces combinaisons* » (Essay on a manner of determining the

relative masses of the elementary molecules of bodies and the proportions by which they enter these combinations).[27] In this work he hypothesised that equal amounts of different gasses at the same temperature and pressure have the same volume regardless of the identity of the gas.[28] This hypothesis was independently formulated, tested, and described[29] by French physicist André-Marie Ampère (1175–1836) in 1814, and this principle is now known as Avogadro's law, or the Ampère-Avogadro principle. Indeed, when an electric current is passed through water, the volume of hydrogen generated at the cathode is twice the volume of the oxygen generated at the anode, an experiment first performed by English chemist Humphry Davy (1778–1829), and published in 1806.[30] This experiment, combined with de Lavoisier–de Laplace experiment, provides the solid foundation for water as we know it today: H_2O.

Armed with this knowledge, one is now properly equipped to traverse the modern understanding (and misunderstanding) of water in all its glory.

The modern view: water's micro- and macroscopic properties

Water is the first, and thus smallest of the dihydrogen chalcogenides. A cursory inspection of thermodynamic properties of these molecules (Table 1) very clearly shows that water is an outlier.

	H_2O	H_2S	H_2Se	H_2Te	H_2Po
melting point[31] (K)	273.15	187.55	207.45	222.15	237.85
boiling point[31] (K)	373.15	213.15	231.85	269.15	309.25
formation free energy,[31] $\Delta_f G^\ominus$ (kJ mol^{-1})	−285.9	−21	73.0	99.6	no data
molar heat capacity, $C_{p,m}$ (J mol^{-1} K^{-1}), 298 K	75.4[31]	34.2[32]	34.75[32]	35.56[32]	no data
Acid dissociation constant (0.1 M), pK_a	14	7.0	3.89	2.6	no data
heavy atom electronegativity,[33] χ	3.78	3.44	3.37	3.14	2.85

Table 1: Thermodynamic data for dihydrogen chalcogenides.

At 273.16 K and 611.657 Pa[34] water exists in an equilibrium of three distinct phases: solid, liquid, and vapour.[35, 36] The density gradient of liquid water as a function of temperature is anomalous in comparison to other substances in the fact that it is non-monotonic. In most substances, density and temperature are inversely proportional; the density of water, however, increases from 999.8495 kg m^{-3} at 0.1 °C to the maximum of 999.9749 kg m^{-3} at 3.9 °C. The density then parabolically drops as a function of temperature, where at 25 °C it is 997.6582 kg m^{-3} (Fig. 3). Thus, at ambient pressure any solid water in equilibrium with the liquid will float at the surface of the liquid. This behaviour is important for

life on Earth: during the winter seasons when water freezes any ice that forms floats to the top and any living creatures below the surface will survive in the remaining liquid water.
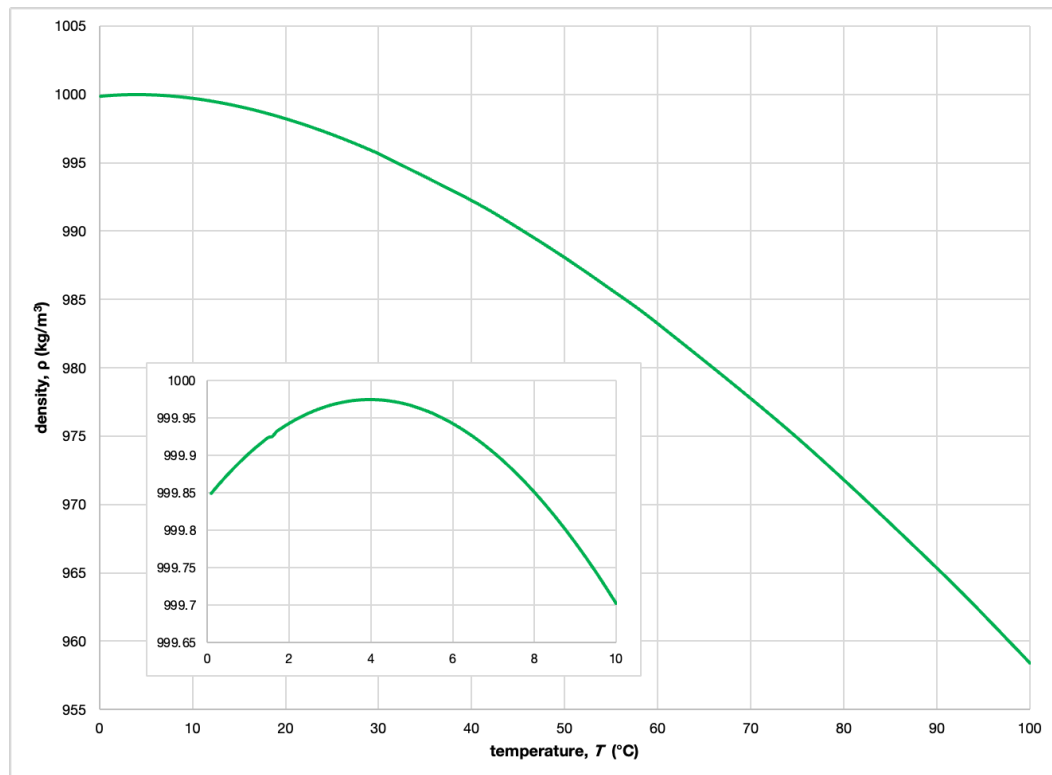
Fig. 3: Plot of the density of liquid water as a function of temperature (0.1–100 °C). Inset is a zoomed-in view of the 0.1–10 °C range showing the maximum density of 999.9749 kg m^{-3} at 3.9 °C. Data were collected from Standard Mean Ocean Water (SMOW) at 101.325 kPa, with known isotopic composition and devoid of all solutes.[37]

The solid form of water at Standard Temperature and Pressure (STP; $T = 273.15$ K, $p^{\ominus} = 100$ kPa)[38-40], known as ice I$_h$ or hexagonal ice, is one of 19 distinct forms.[41] Although Niels Bjerrum deduced the molecular geometry of water using the electrostatic model in 1952,[42] it is ice I$_h$ that definitively gave the correct bond lengths, angles, and intermolecular distances that are used in solid water models. The crystal structure of the I$_h$ form of ice shows a tetrahedral arrangement

of the oxygen atoms in the crystalline domains (Fig. 4).[43] Though crystallographically frustrated in the sense that the oxygen atoms occupy full unit crystallographic sites, and the hydrogen atoms are disordered, ice I_h follows an important Bernal–Fowler rule:[44] there is always a single hydrogen atom between any two oxygen atoms such that a space-filling hydrogen-bonding network is formed (*vide infra*). Thus, a direct measurement of bond angles and lengths can be made. Water is roughly electronically tetrahedral, however, the $\angle HOH$ is less than the ideal i.e., $\cos^{-1}\left(-\frac{1}{3}\right) \approx 109.47°$, due to the strain brought about by lone-pair–lone-pair repulsion. The crystal structure of ice I_h also gives insight into the anomalous behaviour of water's density as a function of temperature (*vide supra*). There exist large voids in the structure which decrease its overall density.
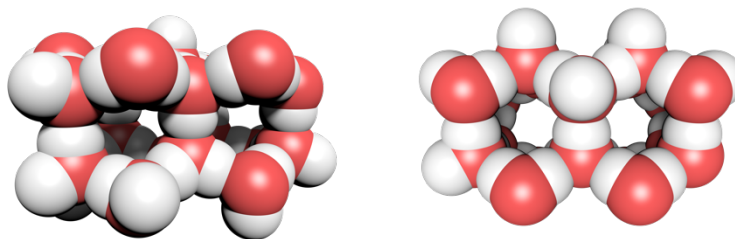
Fig. 4: Space-filling structures of the crystal lattice of ice I_h (CSD-ICSD64772).[43, 45] (l) perspective view; (r) view along the crystallographic *c* axis emphasising hexagonal symmetry. Structures are rendered using ePMV for Cinema 4D.[4]

Liquid water has an unusually high melting and boiling point relative to the other dihydrogen chalcogenides (Table 1). This high cohesivity of water is attributed to the strong hydrogen bonding network that water can form. Liquid

water can form an average of 3.4 hydrogen bonds per molecule, though the bond forming and breaking process can happen at the femtosecond timescale. Using different spectroscopic techniques such as two-dimensional infra-red spectroscopy (2D-IR), Raman spectroscopy, and Raman multivariate-curve resolution (Raman-MCR) spectroscopy the fleeting hydrogen bonding can be observed and counted.[46] Indeed, though the intuitive maximum number of hydrogen bonds that a single water molecule can have is four (two donor sites and two acceptor sites forming a coordination number of 4) in the bulk, there is evidence for the formation of a degree of crowded hydrogen bonding in which a water will have a coordination number of 5.[47] There is mounting evidence that hydrogen bonding in water is purely electrostatic:[48] the oxygen atom, with its partial negative charge, attracts the partially positively-charged hydrogen atom in another molecule.
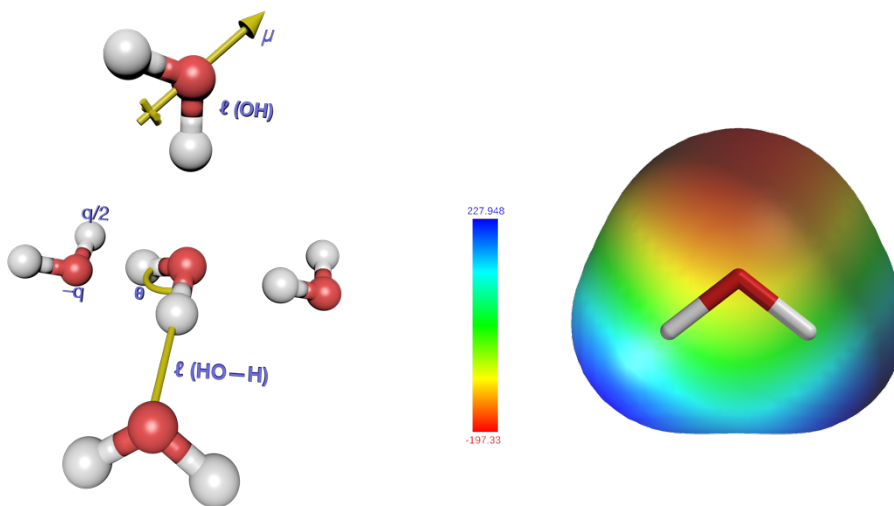
Fig. 5: *left:* A water pentamer. μ: molecular dipole; q: fraction of elementary charge; θ: bond angle; ℓ: bond length. See Table 2 for the values of each. *right*: Electrostatic potential map of an isolated water molecule at an isovalue of 0.002 e au^{-3} (electrons per cubic Bohr) using ωB97X-D correlation with a 6-311+G** basis set. The scale bar represents the electrostatic potential in kJ encountered by a positive point charge on the surface of the molecule.

	Substance		
Parameter	H$_2$O (liquid)	H$_2$O (ice I$_h$)	TIP4P-Ew[¶][49, 50]
ℓ(OH), Å	0.975(1)[51]	0.957(1)[43]	0.9572
ℓ(HO–H), Å	1.78(1)[51]	1.88(1)[43]	1.82
μ, D	2.08(2)[†52], 1.855(1)[‡52, 53]	3.21(9)[†54], 1.855(1)[‡52, 53]	2.321
θ ⊀HOH, °	106.06[51]	109.5[43]	104.52
q, e$^-$	—	—	1.04844

Table 2: Comparisons of different geometric parameters in liquid water, ice I$_h$, and the TIP4P-Ew model. Numbers in parentheses represent the error in the final digit. [†]Dipole moment for the bulk material; [‡]Dipole moment for the isolated molecule. [¶]Values obtained from both parametrisation and calculation at 298 K and 1 bar.

The models for the liquid state of water vary; however, the most accurate and computationally inexpensive model as of this writing is the four-site transferable intermolecular potential with Ewald summation, or TIP4P-Ew. This model closely recreates both the dipole and relative permittivity of water by optimising the geometry and charge distribution, and thus the inter- and intramolecular forces in liquid water.[49, 50] Throughout this dissertation all molecular mechanics simulations involving explicit water will use the TIP4P-Ew model.

The supramolecular chemistry of water
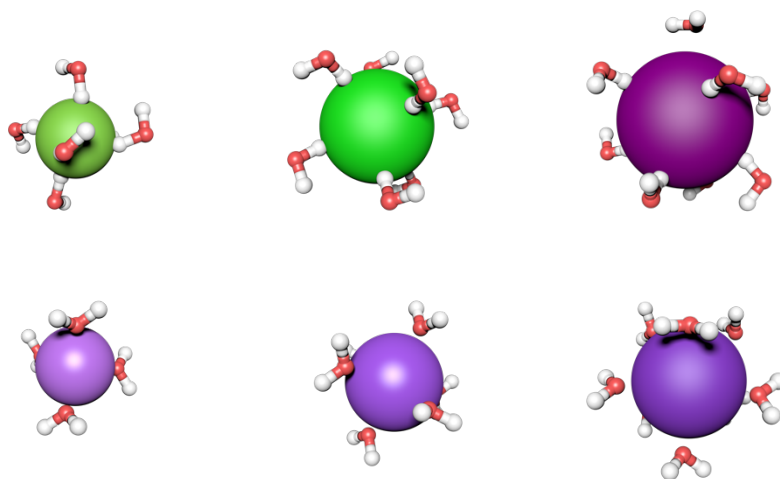
Fig. 6: Various ions with their first solvation shell. Ions are space-filling and are to-scale relative to one another; water molecules are ball-and-stick models with to-scale internuclear distances. *Top, l-r*: F⁻, Cl⁻, I⁻. *bottom, l-r*: Li⁺, Na⁺, K⁺. Geometries were taken from the referenced literature in Table 3 and rendered using ePMV for Cinema 4D.[4]

The high dipole moment of water (1.855 D,[53] see Table 2) presupposes that it is capable of solvating highly charged species via purely electrostatic interactions: the oxygen atom coordinates to the cation, whilst the hydrogen atom coordinates to anions (Fig. 6). The number of individual water molecules that surround each ion depends on the concentration of the individual ions, their sizes, polarizabilities, and excess charge. As the concentration of the salt increases, the number of water molecules in the solvation shell of the individual ions decreases due to the stronger electrostatic attraction between the cation and the anion (ion pairing).[55, 56] The first-shell hydration number, ionic radii, and electronic polarizabilities of a small sampling of important inorganic ions are given in Table 3. The solvation of any solute in a solvent that hydrogen bonds with copies of

Ion	Ionic radius, r_i (Å)[57]	Electronic polarizability α (Å^3)[58]	First hydration number N_1	Hydration free energy, $-\Delta_{hyd}G^\infty$ (kJ mol^{-1}) [59]
Li$^+$	0.74	0.03	4[60, 61]	489
Na$^+$	1.02	0.18	5–6[62, 63]	383
K$^+$	1.38	0.81	8[62]	312
NH$_4^+$	1.49	2.0[64]	5–6[65]	301
Mg^{2+}	0.72	0.075	5–6[66]	1837
Ca^{2+}	1.00	0.49	8–10[67, 68]	1527
F$^-$	1.33	1.3	6[56]	469
Cl$^-$	1.81	3.5	7[56]	344
Br$^-$	1.96	4.6	7[56]	318
I$^-$	2.20	7.5	8[56]	280
PF$_6^-$	2.45	—	4–5[69]	
ClO$_4^-$	2.40	—	12[70]	229
SO$_4^{2-}$	2.30	3.0–5.3[64]	12[71]	975
PO$_4^{3-}$	2.38	—	13[72]	2753

Table 3: Radii, polarizabilities, hydration numbers, and hydration free energies in aqueous solution for certain inorganic ions.

itself, i.e., water, involves the formation of a suitably sized cavity in the bulk solvent. This cavitation may or may not be disruptive to the hydrogen-bonding network of bulk water. Thus, in highly charged species such as smaller inorganic anions, the number of dangling hydrogen bonds (*vide supra*) can be minimised by the electrostatic attraction between the solute and the dipole of water.
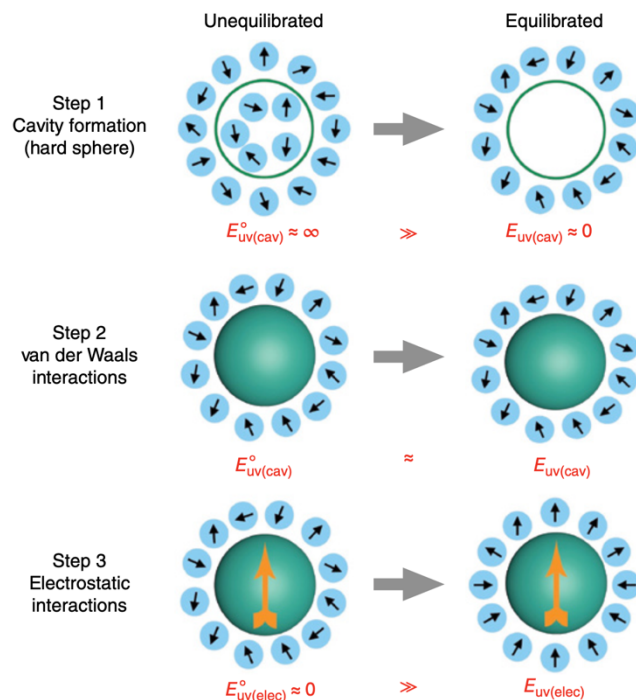
Fig. 7: Introduction of a hard-sphere solute into water. Each step involves a pre- and post-equilibration step where the former is the effect to the solute upon dissolution and the latter is the response of the solvent. Image reprinted with permission from Ref. 43.

The introduction of an ideal hard-sphere solute into water (Fig. 7) initially disrupts the energetics of the system such that there is an instantaneous increase in solvent-solute free energy ($E^0_{uv(\text{cav})} = \infty$) due to the decrease in total entropy ($T\Delta S_{\text{cav}} > 0$). Equilibration of the system brings the free energy of cavitation back to initial state ($E_{uv(\text{cav})} = 0$) since the enthalpy of cavitation (ΔH_{cav}) fully compensates for the loss in entropy. In a purely dispersive system, i.e., solute whose interaction with the solvent is dominated purely by van der Waals forces, the free energy is completely insensitive to the orientations of the individual solvent molecules, and thus the cavitation energy before and after equilibration

remain the same $E^0_{uv(cav)} = E_{uv(cav)}$. In a system where electrostatics dominates, like that of highly polarized, polarisable, or charged solutes, the favourable alignment of the individual dipoles of the solvent molecules makes the solute–solvent interactions distinctly negative even though there is a much larger loss in entropy brought about by the strong solvent dipole reorientation induced by the introduction of a charge or a strong dipole. Thus, in the introduction of large, rigid, cavity- containing molecule (a "host"), and a suitably sized molecule or ion that fills the cavity ("guest"), the interactions between water and the extraneous molecules may ultimately drive the host–guest interaction in water (*vide infra*). Indeed, the amount of work (Table 4) required to create a cavity in water as compared to a liquid alkane is much larger due to its small size (more water molecules need to move out of the way) and strong hydrogen bonding capability.[73]

Solute	ΔG_{cav}	ΔH_{cav}	$-T\Delta S_{cav}$	E_a
Water				
propane	35.8	6.6	29.2	–27.6
isobutane	42.4	10.8	31.6	–32.7
neopentane	46.5	13.2	33.3	–36.0
Liquid alkane				
propane	23.7	40.1	–16.4	–26.7
isobutane	24.4	49.8	–25.4	–35.1
neopentane	27.6	12.4	–15.2	–39.0

Table 4: Energetics at 25 °C of making a cavity in water compared to liquid alkane. ΔG_{cav}, ΔH_{cav}, and ΔS_{cav} are the free energy parameters to make an appropriately sized cavity for the named solutes in either water or liquid alkane; E_a is the van der Waals interaction energy between the solute and solvent. Table was reproduced with permission from Ref. 70.

As mentioned, the introduction of a purely dispersive solute into water disrupts the hydrogen-bonding network of the solvent. This disruption reduces the number of available donors and acceptors for hydrogen bonding and induces the so-called "dangling" hydrogen bond. These dangling bonds do not participate in the hydrogen-bonding network of the bulk and thus do not contribute to the average 3.4 hydrogen bonds[48, 74] (*vide supra*) that each molecule can have. They are enthalpically weaker than inter-water hydrogen bonding, but less entropically penalizing. The number and directionality of these bonds depend heavily on the size and the Euler curvature of the surface (Fig. 8).[75, 76] Starting from one extreme case where a solute is spherical and whose diameter λ is smaller than an individual water molecule (0 Å $< \lambda <$ 2.75 Å, Fig. 8a), each solvating water can have its full complement of hydrogen bonds to other waters: the solute may slip
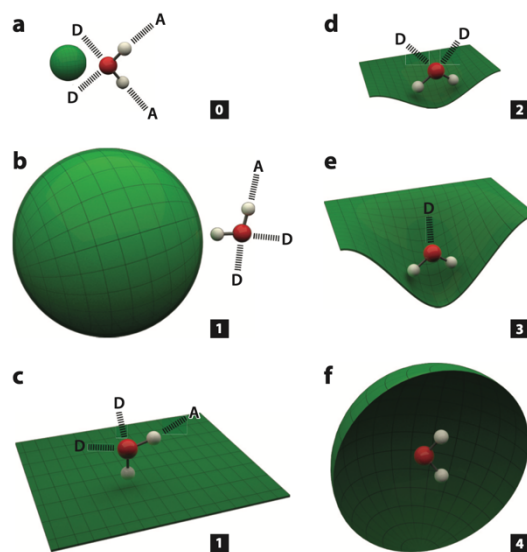
Fig. 8: Number of dangling hydrogen binds as a function of surface type. Numbers indicate the number of dangling bonds. "A": H-bond acceptor. "D": H-bond donor. *a.* Small spherical surface. *b.* Large spherical surface. *c.* Flat plane. *d.*, *e.* Progressively deeper depressions in a flat surface. *f.* Enclosing surface. Image reprinted with permission from Ref. 72.

through the hydrogen bonding network without affecting it. Increasing the size of the solute such that its diameter is much bigger than that of a water molecule (2.5 Å < λ ≪ ∞, Fig. 8b) forces the interaction of water with the surface of the solute, giving rise to a dangling bond. The same can also be said when the size of the solute is infinite and can be approximated as a planar (Euclidean) surface (λ ≃ ∞, Fig. 8c). Introduction of a depression or concavity into the surface will produce an increasing number of dangling bonds as a function of depth. As the water molecule resides deeper in the concavity the hydrogen-bonding capability of the water molecule becomes unidirectional towards the portal of the depression (Fig 8d and 8e) to maximise interactions with the bulk. Eventually the concavity becomes so large that it can be approximated as being the interior of a sphere. This, obviously, is the extreme case where a water molecule is isolated from the bulk and can no longer form any hydrogen bonds (Fig. 8f), effectively a theoretical gas-phase construct.

Ion-ion interactions are governed by the Coulomb force, $\mathbf{F_{12}}$, which describes the attraction or repulsion of ions in solution by way of its sign: attraction, by convention, is negative and repulsion is positive (Eq. 1).[77]

$$\mathbf{F_{12}} = \frac{n_1 n_2 e^2}{4\pi\varepsilon_0} \frac{\hat{\boldsymbol{\lambda}}_{12}}{|\boldsymbol{\lambda}_{12}|^2}$$
<div align="right">Eqn. 1</div>

where:

n_1 and n_2 are the non-zero integer multiples of charge of ions 1 and 2;

e is the fundamental charge (1.6022×10^{-19} C);

ε_0 is the vacuum permittivity (8.854×10^{-12} C^2 J^{-1} m^{-1}); and

$\boldsymbol{\lambda}_{12}$ is the vector between ions 1 and 2.

Integration of Eq. 1 with respect to the unit vector $\hat{\boldsymbol{\lambda}}_{12}$ gives the potential energy $\mathbf{U_{12}}$ of ion 2 held at a distance λ from ion 1 (Eq. 2). Again, the sign of the potential energy indicates favourability: negative potential energies are favourable, attractive interactions, whilst positive potential energies are unfavourable, repulsive interactions.

$$\mathbf{U_{12}} = \int_0^{\lambda_{12}} \mathbf{F}_{12} = -\frac{n_1 n_2 e^2}{4\pi\varepsilon_0} \frac{\hat{\boldsymbol{\lambda}}_{12}}{|\boldsymbol{\lambda}_{12}|} \qquad \text{Eq. 2}$$

It is apparent that the Coulomb force and potential as written in Eqs. 1 and 2 are valid only in vacuum; however, it is also clear that the forces exerted on ions 1 and 2 are attenuated as a function of the square of the distance between them. Thus, for two negative charges the repulsive force is reduced by a factor of one-fourth as the distance between them is doubled.[77]

The equation for the Coulomb force can be modified for charges embedded in a dielectric material, i.e., ions in solution. An extra factor ε_r is inserted into the denominator and is defined as the relative permittivity of the material within which the charges are embedded (Eq. 3). The potential energy is similarly attenuated by a factor of ε_r. Values of ε_r at 298 K for common solvents are given in Table 5.

$$\lambda_B = \frac{n_1 n_2 e^2}{4\pi\varepsilon_0\varepsilon_r k_B T}$$

<div align="right">Eq. 3</div>

Material	relative permittivity, ε_r, at 298 K[78]	Bjerrum length, λ_B, in Å
vacuum	1*	560.2
hexane	1.88	298.2
benzene	2.27	247.0
diethylamine	3.78	148.3
methoxybenzene	4.33	129.5
oxolane	7.88	71.15
pyridine	12.91	43.43
propanone	20.56	27.27
N,N-dimethylformamide	36.71	15.27
water	78.36	7.155

Table 5: Relative permittivities, ε_r, of different materials at 298 K with Bjerrum lengths at $k_B T$. *The relative permittivity of vacuum is, by definition, unity.

Because molecular motion is governed by thermal vibrations, it is worth investigating the effect of the relative permittivity of the solvent on the effective distance between two ions of like charge as a function of thermal energy. If a benchmark potential is set to be $k_B T$ (or ~2.50 kJ mol^{-1} at 298 K) the interaction energy between the two charged particles is comparable in magnitude to the thermal energy scale. The distance between the two charged species is the Bjerrum length λ_B (Eq. 3), which in vacuum is ca. 561 Å, whilst in water is 7.15 Å—a reduction by a factor equal to the relative permittivity of the solvent. Thus, it would take 1$k_B T$ worth of energy to hold two like charges 7.15 Å apart in water at

298 K, whilst it would take $78.36 k_B T$ (ca. 194 kJ mol⁻¹), *cæteris paribus*, in vacuum. Or, in another sense, the distance between two like-charged particles in vacuum with an interaction energy of $1 k_B T$ is ca. 561 Å. Fig. 9 shows a plot of Bjerrum length λ_B as a function of multiples of $k_B T$ for different solvents, and a plot of Bjerrum length as a function of relative permittivity at $1 k_B T$.
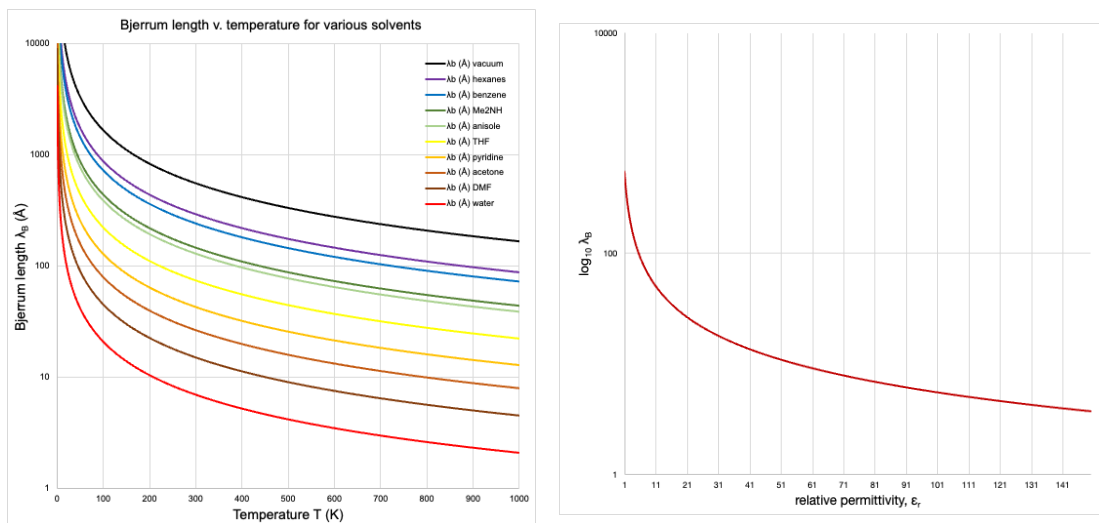
Fig. 9: *left*: Plot of Bjerrum length as a function of multiples of $k_B T$ for various solvents at 298 K. *right*: Plot of Bjerrum length at 298 K and 1 $k_B T$ as a function of relative permittivity ε_r.

The hydrophobic effect: bound water, hydrophobic collapse, and water wires

The hydrophobic effect is one that is unique to water; each requires the other to exist. If water cannot fully interact with a solute in a meaningful way, i.e., in hydrogen bonding, ion–dipole, or dipole–dipole interactions, water will aggregate and will preferentially interact with copies of itself in bulk solution.[74] As

a consequence, apolar solutes will then tend towards interacting with copies of itself. Thus, the hydrophobic effect is a self-sorting phenomenon.[79]

The hydrophobic effect can be driven by entropy ($\Delta S > 0$), enthalpy ($\Delta H \ll 0$), or both. The former case is called the classical hydrophobic effect: when two apolar molecules are dissolved in water a hydrophobic collapse occurs where the solutes associate to one another because of the energetic penalty of creating two smaller cavities in the bulk solute compared to one larger cavity. In a 2004 report by Choudhury and Pettitt,[80] it was observed computationally that when two parallel, nanometre-sized, non-polar plates were brought together in water, the intervening water molecules would rush out from between the plates to re-join the bulk when the plates were within a certain distance from one another.

In cases where solutes are concave and water can be "trapped" within the concavity, the non-classical hydrophobic effect dominates where $\Delta H \ll 0$. The concavity reduces the number of ideal hydrogen bonds in the bound water (*vide supra*), and thus, when water is released from the concavity the formation of hydrogen bonds to the bulk there is a net release of heat from the system.[81-84]
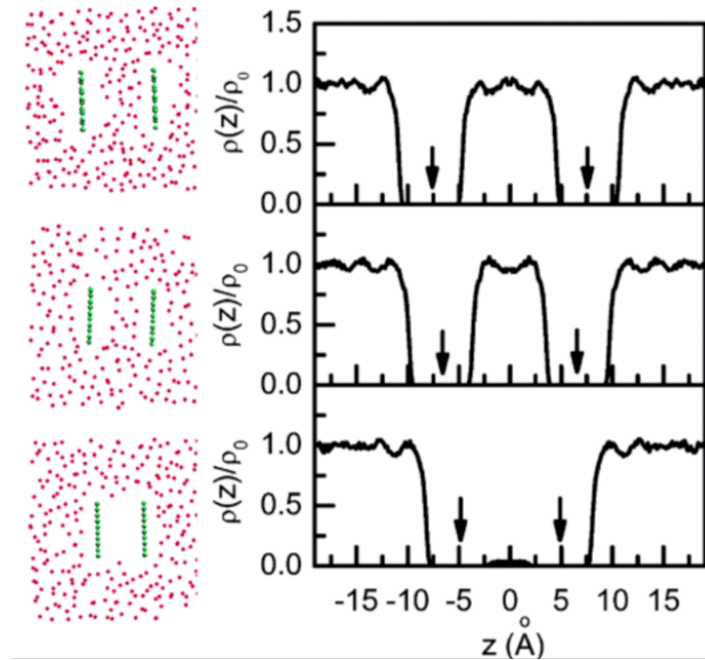
Fig. 10: Illustration of the drying transition between two apolar plates composed of carbon atoms in water. (*left*) Plot of a configuration for the system with interpolate separations (*top*) $r_0 = 15.4$ Å, (*middle*) $r_0 = 13.4$ Å, (*bottom*) $r_0 = 10$ Å. Red circles are the positions of the water oxygens atoms, and blue circles are the carbon atoms on the solute plates for a slab through the sample. (*right*) Plots of the normalised single particle density $\rho(z)/\rho_0$ vs z corresponding to the systems on the left. Arrows indicate the positions of the plates along the z-axis. Image reproduced with permission from Ref. 77.

It is a well-known phenomenon in the physical community that apolar concavities in water possess drying transitions, i.e., a fluctuation between being wet and de-wetted. An alternative explanation for the driving force behind the non-classical hydrophobic effect has been put forth by Nau and co-workers[85-90] stating that the bound water molecules/clusters within apolar concavities in water are "high energy" despite the fact that the chemical potentials (μ_i) of bound water and bulk water are exactly the same in a equilibrated system. For water-soluble hosts with apolar concavities the binding event is almost always driven by the hydrophobic effect, and in water, these pockets are almost always weakly hydrated unless there exists groups at the portal of the pocket that spontaneously induce a drying

transition,[84] or have blocking groups that compete with water and have stronger binding than water (*vide infra*), or are small enough that the entropic gain of filling a small void would not compensate for the enthalpic penalty of breaking hydrogen bonds in the bulk (Fig. 11).[91, 92]
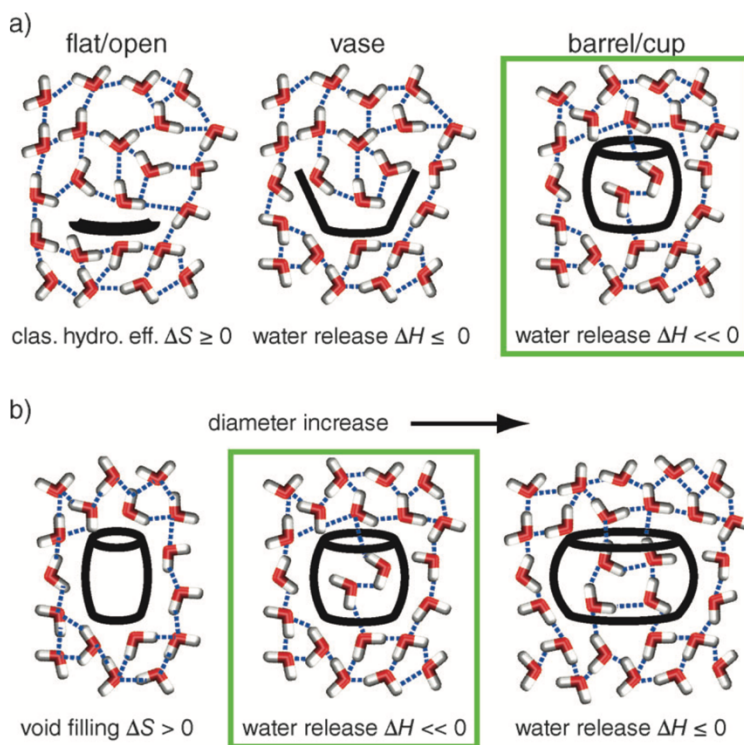
Fig. 11: Different host geometries and associated effects on the dehydration thermodynamics accompanying host–guest binding as interpreted in terms of the 'classical' ($\Delta S > 0$) or 'nonclassical' ($\Delta H < 0$) hydrophobic effect. a) Concave hosts shield water molecules better from hydrogen bonding with bulk solvent than open/flat structures. b) An optimal cavity diameter exists for which the host cavity is not empty but contains an intermediary number of water molecules that do not have the full complement of hydrogen bonds. Hydrogen bonds of water molecules near/ inside the host are indicated by dashed lines. Image and caption reproduced from Ref. 85 with permission from John Wiley & Sons.

In cases where the cavity is of sufficient length and just wide enough to hold one water molecule, water wires may occur. Indeed, in the MD simulation of a single-walled, uncapped (6,6)-carbon nanotube 13.4 Å long and 8.1 Å wide, a spontaneous and continuous filling of the carbon nanotube pore occurs which

forms wires (one-dimensional order) of hydrogen-bonded water molecules within the tube when immersed in a bath of water (Fig. 12). The number of water molecules within the tube fluctuate between 2 and 7; if the attraction between the water molecules and the nanotube walls is reduced by lowering the Lennard-Jones ε parameter[‡], the tube is predominantly dry, which leads to a two-state transitions between the filled and empty states.[91]
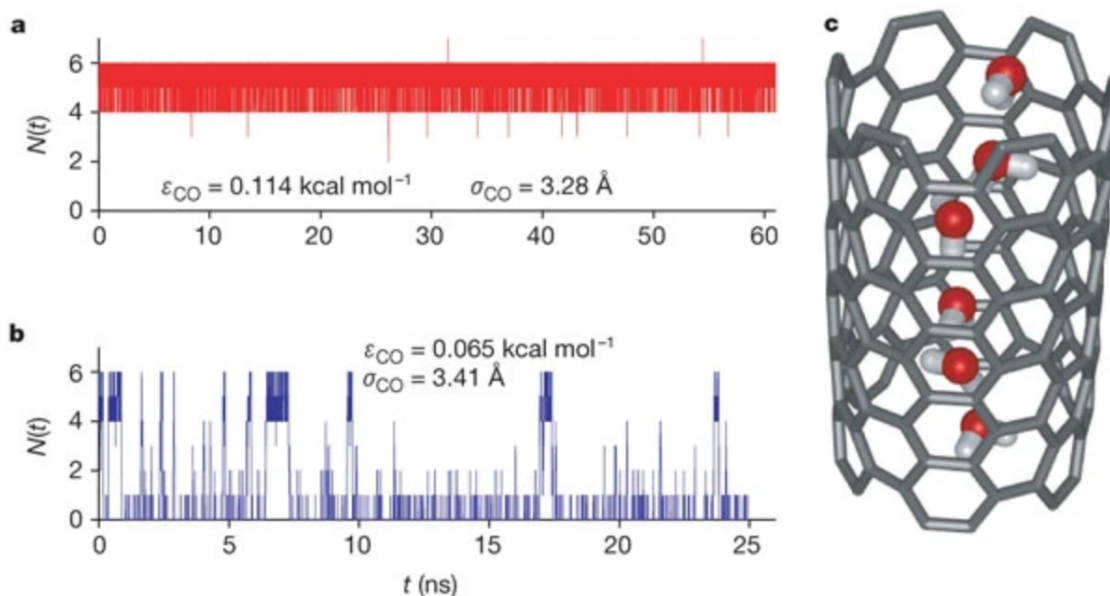
Fig. 12: a) Number N of water molecules inside the nanotube as a function of time for sp² carbon parameters and for b) reduced carbon–water attractions. c) Structure of the hydrogen-bonded water chain inside the nanotube. Image and caption reproduced from Ref. 91 with permission from SpringerNature.

[‡] The Lennard-Jones potential $V_{LJ}(r) = 4\varepsilon\left[\left(\frac{\sigma}{r}\right)^{12} - \left(\frac{\sigma}{r}\right)^{6}\right]$ is a computationally inexpensive intermolecular potential between two neutral particles which takes into consideration the depth of the potential well (i.e., dispersion) between the two particles (ε) as a function of distance (σ) between the two, as described by using an attractive (n^6) term and a repulsive (n^{12}) term.

The Hofmeister effect

It has been well-established since 1888[93] that salts have a profound effect on the aqueous solubility of proteins and other molecules. Indeed, the purification and or/fractional precipitation ("salting-out") of certain proteins from solution involves the addition of salts such as ammonium sulfate $((NH_4)_2SO_4)$.[94] In some cases, the protein becomes more soluble in water ("salting-in") in the presence of salts such as sodium thiocyanate (NaSCN) and sodium perchlorate (NaClO$_4$) at pH levels at or below the isoelectric point (pI)[§] of the protein. These examples represent the two extremes of the gradation of salts according to their ability to "salt-in" or "salt-out" proteins; this gradation is called the Hofmeister series (Fig. 13) in honour of Franz Hofmeister who discovered the effect of salts on aqueous solutions of chicken albumin. There exists a Hofmeister series for anions, and for cations. However, in general, the Hofmeister series for anions is more well-studied than that for cations because of the larger effects that the anions have on solvation.

Salting-out   Salting-in

$$F^- \sim SO_4^{2-} > HPO_4^{2-} > MeCO_2^- > Cl^- > NO_3^- > Br^- > ClO_3^- > I^- > ClO_4^- > SCN... \quad BF_4^- > IO_4^- > ReO_4^- > PF_6^-$$

Traditional Hofmeister anions

Expanded Hofmeister series
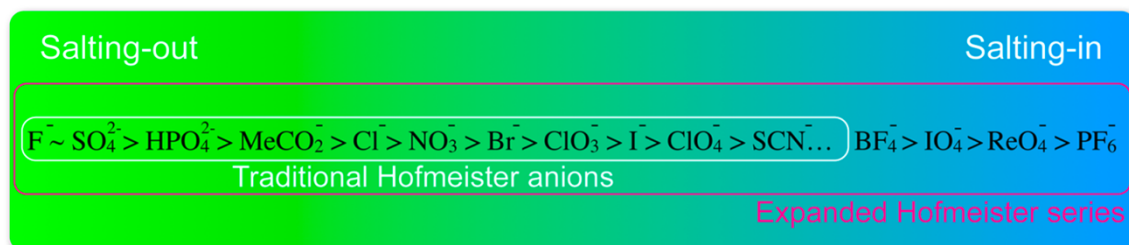
Fig. 13: The Hofmeister series for illustrating the "salting-in" and "salting-out" extremes, and the expansion of the series beyond the traditional anions. Image courtesy of BCG.

[§] The isoelectric point (pI) of a protein is defined as the pH of a protein-containing solution where the sum of all charges on the protein is 0.

At first glance the anions that salt out seem to be charge dense and hard, while those that salt in are charge diffuse and polarisable. However, there is no universal rule that determines the ordering of anions in the series. Most computational models that attempt to explain the Hofmeister effect point to the effect of the ion on its first hydration shell. Indeed, an inspection of the structural entropy of the ion in water (ΔS_{struct}) shows that salting-out anions tend to have a negative structural entropy and a net increase in the number of hydrogen bonds in the first solvation shell; the contrapositive also holds true (Table 6).[95]

Anion	radius, r (Å) [96]	ΔS_{struct} (J K^{-1} mol^{-1}) [97]	ΔG_{HB} [97]
SO_4^{2-}	2.30	−94 [98]	0.78 [98]
HPO_4^{2-}	2.00	−57	0.41
F^-	1.33	−27	0.10
Cl^-	1.81	58	−0.76
Br^-	1.96	81	−1.00
I^-	2.20	117	−1.36
NO_3^-	1.79	66	−0.85
ClO_4^-	2.40	107	−1.26

Table 6: Water structural entropy ΔS_{struct} and net effects on hydrogen bonds in surrounding water molecules (ΔG_{HB}) for a selection of anions differing in their ionic radii r.

Evidence has been presented that correlates electrostatic interactions and the Hofmeister effect based on radial charge densities in the anions.[99] This model attempts to explain ion effects such as hydration enthalpies, diffusivity, or the free energy of transfer from MeOH to water. However, these arguments presuppose that the only effects that anions have are only on water and completely ignores solutes such as synthetic macrocycles (*vide infra*) and

biomacromolecules. Indeed, as will be discussed in **§H** of this chapter, salts, and indeed the buffers that control the pH of the solution, have profound effects on macromolecules, their binding affinities, and their aggregation states. Briefly, salting-in ions interact with protein surfaces to improve their solubility, while salting-out salts exclude (or draw out) water from the surface of the protein which effectively desolvates it and reduces its solubility.[100-104]

The Hofmeister effect has practical utility to the organic chemist in so much as certain reaction workups that involve a water/organic partitioning will almost always involve a final wash with an aqueous salt solution to either remove bulk water from the organic phase, or to force the migration of the intended organic product from the aqueous phase to the organic (or *vice versa*). This choice of salt can be guided by the Hofmeister series. In a report by Hyde *et al*. it was noted that the extraction of a water-soluble nucleoside was improved by the addition of Na_2SO_4.[105]

Measuring the strength of host-guest complexes

The strength of host–guest complexes are measured using association constants K_a. Interactions between host (H) and guest (G) to form the complex (HG) are equilibrium phenomena of the form

$$H \quad + \quad G \quad \rightleftharpoons \quad HG \qquad\qquad \text{Eqn. 4}$$

where the association constant K_a is defined as

$$K_a = \frac{[HG]}{[H][G]}$$ Eqn. 5

and where [X] is the molar concentration of the relevant species at equilibrium, with mass balance equations

$$H_t = [H] + [HG]$$ Eqn. 6

$$G_t = [G] + [HG]$$ Eqn. 7

where X_t is the total amount of that species in solution at any given moment.

The energetics of the association can be quantified using the equation that relates free energy (ΔG) to the equilibrium constant, and thus to the enthalpy (ΔH) and entropy (ΔS) of complexation:

$$\Delta G = -RT \ln K_a = \Delta H - T\Delta S$$ Eqn. 8

There are myriad methods of measuring binding affinities; in this dissertation two methods shall be highlighted: nuclear magnetic resonance (NMR) spectroscopy and isothermal titration calorimetry (ITC), both of 1:1 host/guest complexes in water.

1. **Affinity determination by nuclear magnetic resonance (NMR) spectroscopy**

The determination of association constants by NMR involves the observation of the change in chemical shift of a reporter atom (or set of reporter atoms) in the host as a function of increasing guest concentration. For practical purposes ^{1}H NMR spectroscopy is commonly employed because of the ubiquity of protons in organic molecules, the wide dispersity of signals, *inter alia*.[106, 107] Depending on the specific system being observed, the reported signal can either be shielded or de-shielded, i.e., the change in the isotropic shielding $\Delta\sigma_{iso}$ is more positive or more negative, respectively. This translates to a change in chemical shift $\Delta\delta$ that is more negative in the former case, and more positive in the latter.[108]** Indeed, when a guest which has a distinct NMR signal is bound inside a host composed of aromatic rings (*vide infra*) the guest becomes physically shielded from the external magnetic field inside the NMR instrument and thus its signals appear shielded during the binding event.

In an ideal world where all binding events are perfect, an NMR spectral signal for the free state will be well resolved and a separate signal can be obtained for the bound state. Recall, however, that binding events are equilibrium processes, and because of the kinetics of exchange between the free and bound states there will occasionally be instances where signal broadening occurs. Reducing the temperature of the sample can slow down the kinetics of exchange and can resolve a broad, coalesced signal into two separate resonances. Increasing the temperature increases the kinetics beyond the ability of the

---

** Isotropic chemical shifts are defined in such a way that their direction is in the opposite sense as that of shielding: $\Delta\delta \equiv -\Delta\sigma$.

spectrometer to distinguish between the energy difference of the two states and thus one time-averaged resonance frequency will be observed. The common cause of these effects is the very small energy difference that exists between the magnetic states of different Larmor frequency.[tt] In order to observe and fully resolve these differences the residence lifetime, τ, of the nucleus at each state must be sufficiently large. Indeed, the lower limit for τ is given by the Heisenberg relation

$$\tau(\Delta v) \approx \frac{1}{2\pi}$$

<div align="right">Eqn. 9</div>

where:

τ is the residence lifetime of the exchange process

and $\Delta v = \frac{\Delta E}{h}$ is the frequency difference $v_A - v_B$ involved.

For large τ values separate signals v_A and v_B are observed. This is the regime of *slow exchange*. At the *coalescence point* the two signals come together and form a broad signal, and in the *fast exchange* regime, the spectrum becomes a single, time-averaged signal that is recorded at the frequency $\frac{v_A+v_B}{2}$.[107] Since reaction and binding kinetics are affected by temperature, titrations need to be performed isothermally. Thus, to ensure the accurate observation of states with τ close to the time scale of the NMR experiment,[109] higher external magnetic fields

---

[tt] The Larmor frequency ω is the angular frequency at which a charged particle (in the case of NMR, a nucleus) precesses about the externally applied magnetic field $\vec{B}_0$ at a rate proportional to the particle's gyromagnetic ratio γ ($\omega = -\gamma\vec{B}_0$).

can be employed to force the separation of two distinct energy states and effect the resolution of the exchanging resonances without adjusting the temperature of the sample.

In the regime where the binding event is slow on the NMR time scale, the relative integrations of the signals that correspond to free host, free guest, and complex can be used in Eq. 5 to give the binding affinity K_a for systems that have an affinity between 10–10^4 M^{-1}. In fast-exchanging systems, the change in chemical shift of some reporter nucleus can be recorded as a function of the molar concentration of the total guest added (Fig 14c). For a 1:1 host/guest binding system, the NMR binding isotherm can be expressed as
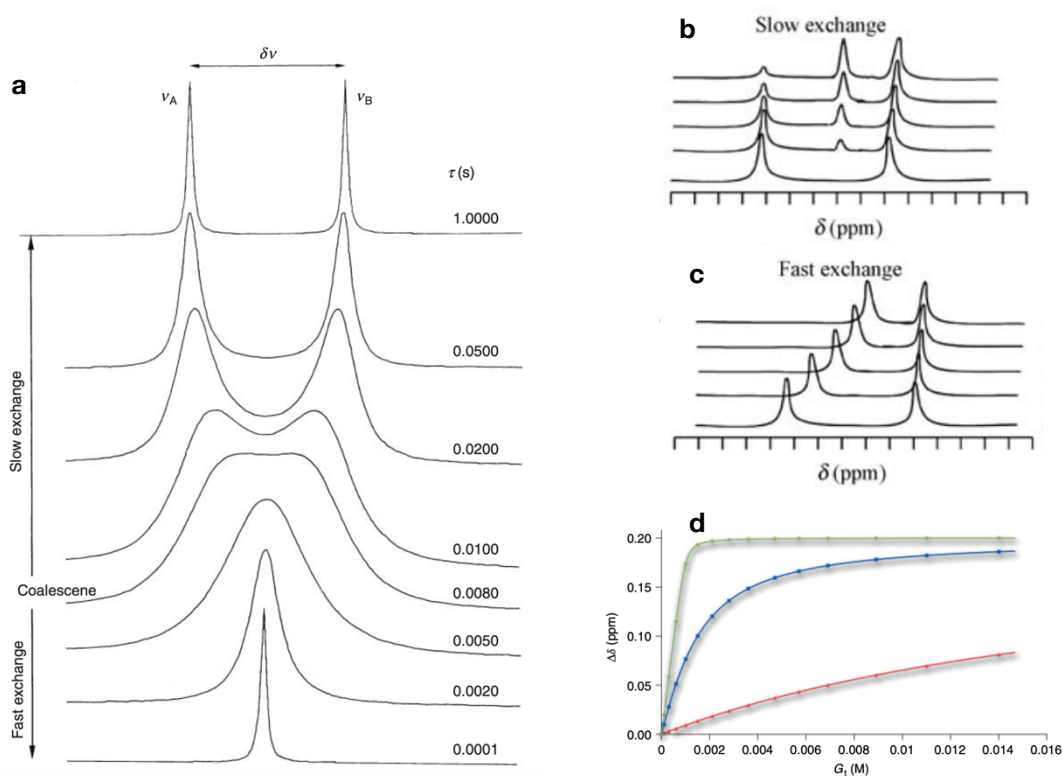
Fig. 14: **a**. Theoretical NMR spectra for an exchange process A⇌B as a function of τ;Δν = 30 Hz, with populations $p_A = p_B = 0.5$; line width without exchange broadening is 1.0 Hz. Image reproduced from Ref. 107 with permission from Wiley-VCH **b**, **c**. Schematics of spectra of fast and slow equilibration of a mixture of free host, guest, and complex. Images reproduced from Ref. 77 with permission from Wiley. **d**. Three theoretical binding isotherms for 1 mM host titrated with guests of association constants $K_a = 50$ (red), 10^3 (blue), and 10^4 (green). Image courtesy of BCG.

$$\Delta\delta_{obs}= \frac{\Delta\delta_{max}}{\dfrac{1}{K_a[G]}+1}$$

<div align="right">Eqn. 10</div>

where $\Delta\delta_{obs}$ and $\Delta\delta_{max}$ are the observed ppm shift of the signal as a function of added guest and the maximum shift at the end of the titration, respectively. A quadratic can be obtained in the combination of Eqns. 5, 6, and 7, to which Eqn. 10 can be substituted to obtain the fitting equation relating G_t and $\Delta\delta_{obs}$:

$$\Delta\delta_{obs}= \frac{\Delta\delta_{max}}{\dfrac{2}{K_aG_t-K_aH_t-1+\sqrt{(1-K_aG_t+K_aH_t)^2+4K_aG_t}}+1}$$

<div align="right">Eqn. 11</div>

A theoretical binding isotherm is given in Fig. 14d for a 1 mM solution of host with guests of three different affinities.[110]

2. Thermodynamics of complexation by isothermal calorimetry

Isothermal titration calorimetry (ITC) involves the measurement of the heat released or absorbed during the complexation event. In a typical ITC experiment, a well-insulated guest solution is titrated into a well-insulated host solution in aliquots, during which time the heat released is measured and plotted against the mole fraction of guest to host. In a typical thermogram the differential power applied to the sample to keep it in thermal stasis as a function of time per injection is plotted (Fig 15), and the area under the peaks are integrated to give the amount of heat released or absorbed as a function of guest molar ratio. The titration points are then plotted to a 1:1, 1:2, or 2:1 binding curve, and the fit reveals the

thermodynamics of binding. The slope of the resulting sigmoidal curve determines the association constant K_a, the furthest point from the baseline determines $\Delta H_{complex}$, and the inflection point of the curve gives the binding stoichiometry.

The ITC experiment gives both K_a and $\Delta H_{complex}$, which can be substituted into Eqn 8 to give ΔG and $-T\Delta S_{complex}$. The quality of the data depends on the Wiseman c parameter which is defined as

$$c = nK_aH_t$$

Eqn. 12

where n is the binding stoichiometry. Low c values (<5) are less than ideal[111] and certain modifications such as increasing the concentration of both host and guest, or modifying the injection schedule can be performed to improve the overall quality of the data.[112, 113]
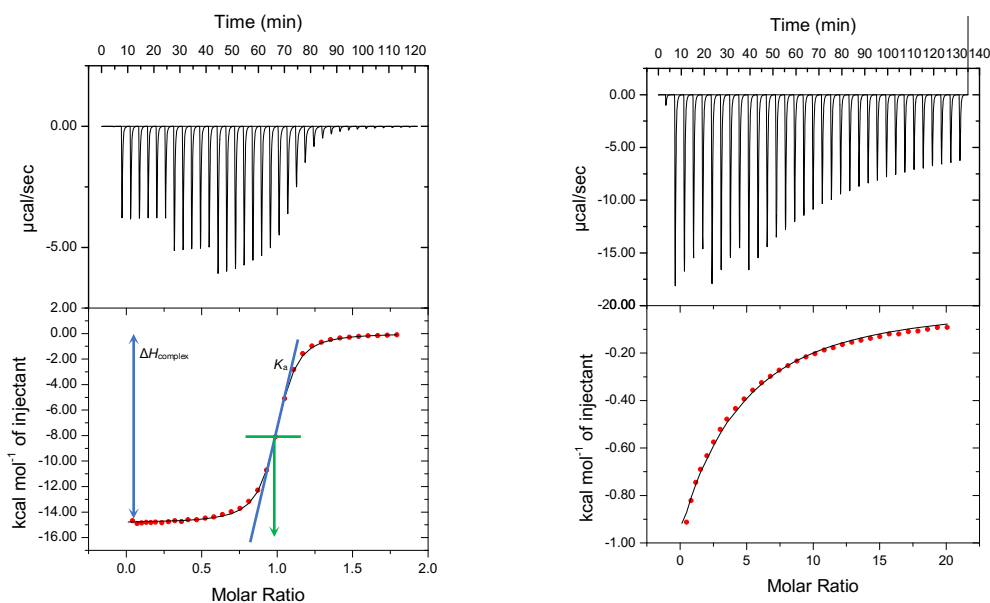
Fig. 15: Examples of ITC thermographs for a strong association with a high Wiseman c parameter (*left*), and a weak association with a low Wiseman c parameter (*right*).

Host–guest chemistry: preorganisation and recognition in macrocyclic hosts

When transferring a solute, whether neutral or ionic from the gas phase into the solution phase a cavity must be formed in the solute whose radius is large enough for the solute to interact with its surroundings. The formation of this cavity is endergonic, i.e., has a positive Gibbs free energy because of the entropic penalty of rearranging water molecules to form such a cavity and because of the amount of energy (in the form of heat) required to break hydrogen bonds and to maintain dangling bond acceptors and donors.[59] In order to circumvent the problem of the entropic cost of cavity formation, the entropy cost can be "pre-paid" by synthesising macromolecular entities that either have an enforced cavity, or can spontaneously form a cavity upon sequestration of the solute. This is more evident in the synthesis of molecules with dipoles that all point in one direction to bind cations in solution. Furthermore, macrocycles have been shown to bind solutes far better than macromolecules that have more degrees of freedom. Indeed, increasing the rigidity of the macromolecule increases the binding affinity of the solute at the cost of the work required to synthesise the macromolecule.

Host–guest chemistry presupposes the existence of two distinct entities: the host and the guest. Host molecules are those that contain specific molecular recognition groups that can bond non-covalently to a particular set of molecular functionalities.[74] These interactions are manifold, but most examples almost

always include hydrogen bonding, π-π interactions, ion-π interactions, and more recently, halogen bonding. These complexations are generally reversible, except for some extreme cases where the binding interactions are so strong that they are generally considered irreversible (cf. streptavidin–biotin complex, $K_a \sim 10^{14}$ M^{-1}). These interactions are almost always driven by the interactions between complementary functionalities between host and guest, including solvophobicity (specifically hydrophobicity in water). The next subsections will highlight both preorganisation and host–guest complementarity during the binding event, including recent advances in host–guest chemistries in water.

1. Crown ethers, podands, and cryptands
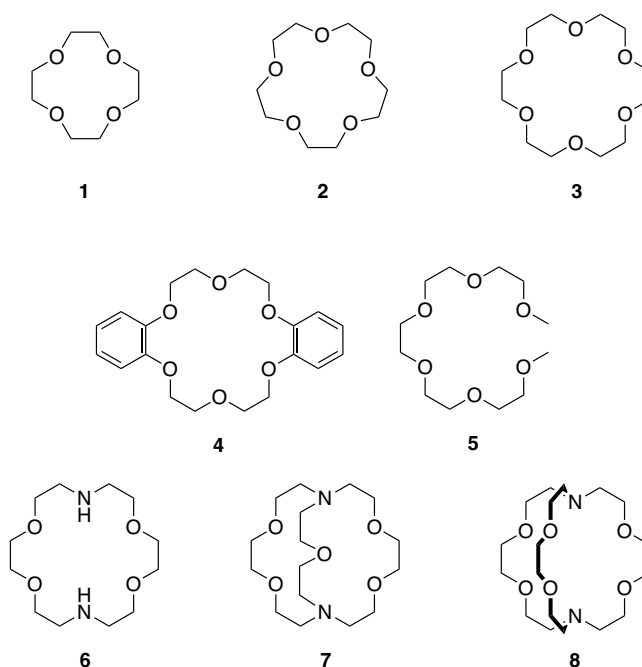
Fig. 16: A small selection of ether-type macrocyclic hosts. **1–4**: crown ethers; **5**: a podand; **6**: an aza-crown ether; **7**, **8**: cryptands.

The first host molecules that were systematically studied were crown ethers—macrocycles composed of poly(ethylene glycol) units whose most common forms number from 4 to 6 units (Fig. 16). The parent compound (**4**), dibenzo-18-crown-6 was discovered by Pedersen in 1961 whilst working on the reactivity of phenolic compounds on vanadium ions.[114] The compound was not soluble in methanol, but was solubilised by the addition of sodium salts. Analysis suggested that the solubility change was brought about by the complexation of a sodium ion within the polyether core, where the cation is chelated by the strong dipole moment of the ethereal oxygens. Indeed, its co-solubility with certain salts in methanol increases by orders of magnitude in the presence of dibenzo-18-crown-6.[115] These compounds (**1**–**4**) have different cavity sizes and thus have different size complementarities for various alkali metal cations and can improve the solubility of the metal salts in organic media, i.e., they can act as phase-transfer catalysts. In general, it is observed that 12-crown-4 (**1**) selectively binds Li^+; 15-crown-5 (**2**) binds Na^+; 18-crown-6 (**3**) binds K^+ and NH_4^+. This selectivity comes about purely from the size complementarity of the cavity of the macrocycle to the cation; a comparison of cavity sizes and cation diameters are given in Table 7. A cursory inspection of the electrostatic potential surface of 18-crown-6 reveals a strongly negative potential brought about by the strong dipole of the ethereal oxygens (Fig. 17).

Cation	Diameter (Å)[57]		Host	Cavity size (Å)[74, 116]
Li$^+$	1.48		12-crown-4 (**1**)	1.20–1.50
Na$^+$	2.04		15-crown-5 (**2**)	1.70–2.20
K$^+$	2.76		18-crown-6 (**3**)	2.60–3.20
NH$_4$$^+$	2.98			

Table 7: Comparison of cation diameters to host cavity sizes.
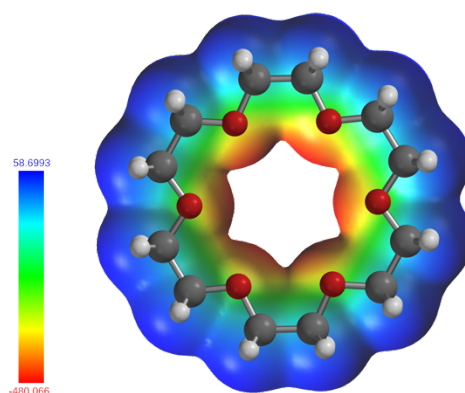
Fig. 17: Electrostatic potential surface of **3**. The colours on the scale bar represents the amount of electric potential exerted on a positive point charge at a particular point on the surface.

Podands, from the Greek for "leg" (πούς, pous), are a class of polyether hosts that are the acyclic analogues of the crown ethers. They may be terminated at the ends by any group, however, the most common are those terminated by methyl units (e.g., Fig 16 compound **5**). Their binding patterns mimic those of the cyclic polyethers, however, the binding strength of analogous podands to alkali metal cations are much weaker due to the flexible nature of the host and their intrinsic lack of pre-organisation. For example (Table 8), the binding constant of K$^+$ in methanol drops by four orders of magnitude going from host **3** to host **5** due to the entropic cost of having **5** wrap around K$^+$ during the 1:1 binding event.[117]

The replacement of two oxygen atoms with nitrogen atoms in a crown ether gives rise to aza-crown ethers (**6**). This insertion of a trivalent atom into the macrocycle opens the door to the synthesis of bicyclic hosts known as cryptands (**7**, **8**). In comparison, aza-crowns of the same size as their fully oxygenated analogues fare no better than the analogous podands. The cryptands, on the other hand have a large enhancement of binding affinity, in part because of the macrobicyclic rigidity (Fig. 18), but also because of the increase in number of Lewis donor groups.

Host	$K^+ \subset$ host			
	K_a (M^{-1})	ΔG (kJ mol^{-1})	ΔH (kJ mol^{-1})	$-T\Delta S$ (kJ mol^{-1})
5	100.0	−11.37	−36.40	25.04
3	1.260×10^6	−34.82	−56.00	21.17
6	63.10	−10.27		
7	1.0×10^7	−39.96		
8	1.0×10^{10}	−57.08		

Table 8: Thermodynamic parameters for the binding of K$^+$ (as the picrate salt) to various polyether hosts in MeOH at 25 °C.[74]
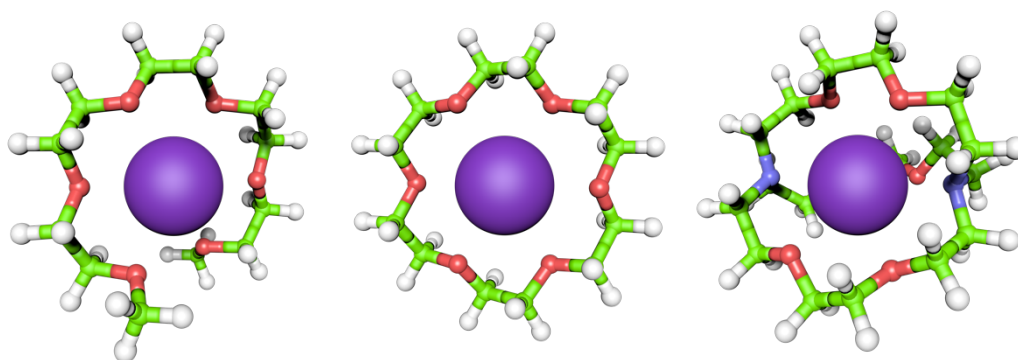
Fig. 18: *l–r* Binding pose of K$^+$ into **5**, **3**, and **8**. Violet: potassium; green: carbon; white: hydrogen; blue: nitrogen. Structures were generated by semi-empirical PM6 calculations by Spartan '14[1] and rendered using ePMV for Cinema4D.[4]

Recent reports by the Kamigata and Shimizu groups shows that the substitution of the oxygen atoms in crown ethers for softer Lewis bases such as sulfur atoms can bias crown ether complexations towards softer Lewis acids such as Hg^{2+}, Cd^{2+}, and Ag^+ in acetone.[118, 119] In addition, the introduction of further preorganisation in the form of *Z*- carbon-carbon unsaturation which forces the sulfur lone pairs inwards creates a complementary pocket for such cations. In a follow-up report by the Gagliardi and Despotopulos groups it was shown that dilute HCl or HNO_3 increases the extraction kinetics from the aqueous phase to CCl_4–solution of the unsaturated thiacrown ether.[120] They further demonstrate, albeit computationally, that there may be some potential for the unsaturated thiacrown to extract Cn^{2+} even though it has noble-gas-like behaviour as predicted by Pitzer in 1975[121] and confirmed by Schwerdtfeger in 2019.[122]

2. Cyclodextrins

Fig. 19: Bond-line structures of α-cyclodextrin (**9**), β-cyclodextrin (**10**), γ-cyclodextrin (**11**), sugammadex (**12**), vecuronium bromide (**13**), and rocuronium bromide (**14**). Bolded bonds on the host represent the secondary, or larger, portal of the host which is closer to the viewer.

Cavitands, as defined by Cram in 1983,[123] are synthetic organic compounds that have enforced cavities of dimensions at least equal to smaller ions such as Li^+, and whose cavities persist even in the absence of a guest molecule. Thus, polyether type host molecules such as crown ethers and cryptands that collapse in the absence of an organising guest are not part of this class of host molecule.

One of the most studied cavitands are cyclodextrins—macrocyclic molecules composed of α-D-glucopyranoside units connected via α-1,4 glycosidic bonds. Three major cyclodextrins (abbreviated as CD) are studied and are most commonly available: α, β, and γ-cyclodextrin, composed of 6, 7, and 8, glucose units each, respectively (Fig. 19, compounds **9**, **10**, and **11**). They are of the form of hollow, truncated right cones, i.e., containing two portals–the primary and secondary, where the former portal is smaller than the latter. Cyclodextrins are economical to synthesise in that they are a by-product of industrial enzymatic cleavage of starch by amylases and glucosyltranferases, and are obtained as a
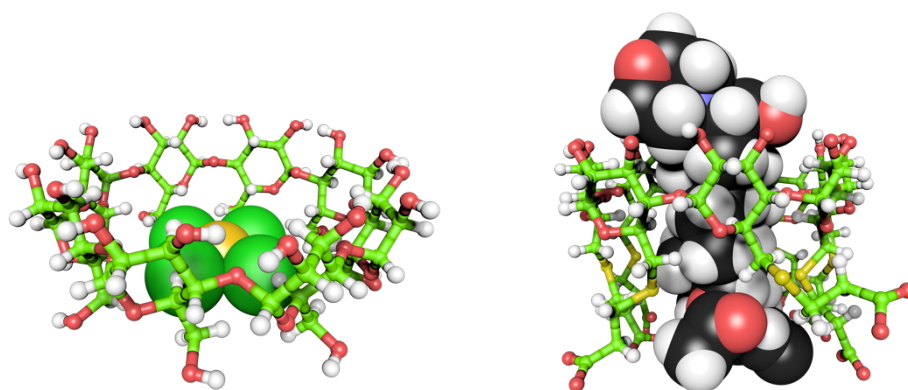
Fig. 20: (*l*) $AuCl_4^-$ in γ-cyclodextrin (**11**) (CCDC OWIPOB). (*r*) rocuronium (**14**) in sugammadex (**16**) (CCDC IDIVOG). Counterions and solvent removed for clarity. Structures were generated using crystal structures from their respective CCDC identifiers, and rendered using ePMV for Cinema 4D. Light green: host carbon; red: oxygen; white: hydrogen; light yellow: gold; dark green: chlorine; black: guest carbon; blue: nitrogen; dark yellow: sulfur.

mixture of the three major forms. They are then separated by portal size via the inclusion of a non-polar guest to selectively precipitate one form over the others.[124] The solubility of cyclodextrins in water are anomalous in so much as the even-numbered oligomer macrocycles are more soluble than the odd. This, presumably, is because of the symmetry of the molecule: the six-fold and eight-fold symmetry of **9** and **11**, respectively, are more compatible with the solvent cage of water than the seven-fold symmetry of **10**. This is the reverse of the pattern found in cucurbit[n]urils (*vide infra*, Table 9).

Cyclodextrins are arguably the most commercially important host molecules. Their ease of synthesis and isolation, and their non-toxicity lend them myriad uses.[124] One oft-cited commercial, household use of cyclodextrins is in water-soluble air fresheners: as aqueous solutions of cyclodextrin are aerosolized, the weakly hydrated pocket binds malodorous molecules suspended in the air.[125] Cyclodextrins have also been used as excipients in drugs as vehicles for drug delivery;[126] indeed, derivatised versions of **11** where the primary portal has been functionalised with pendent thiopropanoate moieties has been commercialised with the generic name sugammadex (**12**) and sold under the brand Bridion™. Sugammadex is the first agent which selectively binds neuromuscular binding agents vecuronium (**13**) and rocuronium bromide (**14**).[127] The quaternary ammonium groups on the guest molecules coordinate selectively to the pendent carboxylates which increases the binding affinity of the non-polar surface of the drug to the weakly hydrated pocket of sugammadex, as evinced by the crystal structure of the complex (Fig 20).[128] Cyclodextrins have also been

investigated for use in heavy metal recovery and recycling. γ-Cyclodextrin has been shown to selectively solubilise and stabilise Au(III) complexes in the form of $NaAuCl_4$ and $NaAuBr_4$, and has been tested on site in a gold mine.[129] Heavier alkali metal salts of AuX_4^- complexed in cyclodextrins have been shown to precipitate and form higher order structures such as nanowires, 2D metal–organic networks, and 3D scaffolds where the AuX_4^- binds to the narrower primary portal of the host (Fig 20).[130, 131]

3. Cucurbit[n]urils
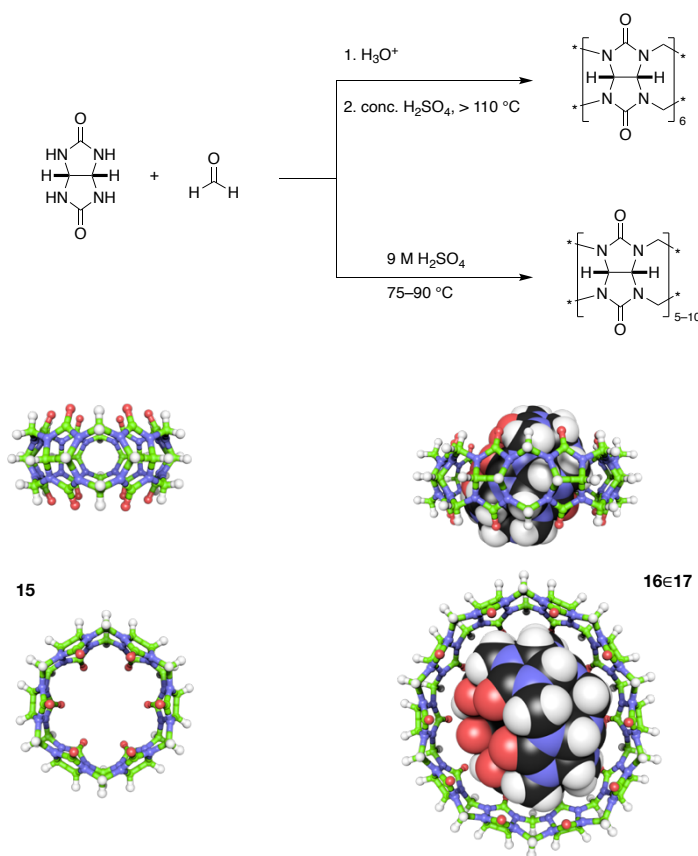
Fig. 21: *top* – Synthesis of CBs. *bottom* – Crystal structures of CB[6] (**15**) (CCDC BEBDOB) and CB[5]∈ CB[10] (**16∈17**) (CCDC HUMXAR). Structures are to scale and are rendered using ePMV for Cinema 4D. *green*: host carbon; *black*: guest carbon; *white*: hydrogen; *blue*: nitrogen; *red*: oxygen.

Cucurbit[n]urils (Latin: *cucurbita*, gourd), abbreviated CB[n], are toroidal macrocycles composed of *n*-glycoluril units condensed with formaldehyde. Five different sizes are most studied: CB[5], CB[6], CB[7], CB[8], and CB[10]. Forcing conditions will bias the formation of the cyclic hexamer, whilst careful control of heat and amount of acid will give a range of cyclic oligomers ranging from the pentamer to the decamer.[132] The X-ray structures of CB[6], and CB[5]∈CB[10] are shown in Fig. 21 (**15**, **16**, **17**, respectively). Unsurprisingly, because of the large cavity of **17** it is rarely isolated on its own; it crystallises with **16** as a guest and can only be purified by displacing **16** via competition with a stronger binding melamine guest.

The presence of the urea carbonyls at the portals of CBs makes the portal markedly polar and thus will attract and bind positively charged groups and ions, whilst the interior is apolar and weakly hydrated and will thus bind similarly apolar moieties. A view of the electrostatic potential surface of **15** is shown in Fig. 22, the general binding pose of positively-charged bolaform amphiphiles is shown in
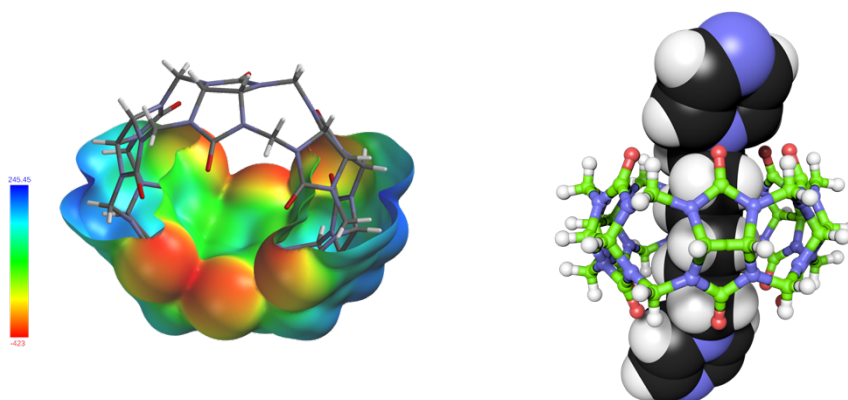
Fig. 22: *left*– Electrostatic potential surface of CB[6] (**15**) calculated using the semi-empirical PM6 method from crystal geometry (CCDC BEBDOB). The colours, and thus the scale bar, represent the force in kJ applied on a positive point charge at the surface of the molecule. *right*– crystal structure (CCDC BIKXUQ) of the pseudorotaxane formed between **15** and α,ω-bis(pyrazinium)hexane; counterions and solvent removed for clarity.

Fig. 22, and the binding constants of different group 1 and 2 cations to **15** in comparison to 18-crown-6 (**3**) is given in Table 10.[133] A higher affinity for cations can be observed with **15** for a variety of monovalent and divalent cations in acidic water (Table 10). One can surmise that this is due to the permanent dipole engendered by the unidirectionality of the carbonyls in **15** (along with its rigidity) , whilst the permanent dipole does not exist in **3** due to its flexibility (the crown ether is pre-organised to a lesser degree than CB[6]).[133]

Host	$\mathcal{M}$ (g mol^{-1})	V (Å^3)	s_w (mM)
α-CD	972.85	174	149
β-CD	1134.99	262	16.3
γ-CD	1297.13	427	179
CB[5]	830.70	82	20–30
CB[6]	996.84	164	0.018
CB[7]	1162.98	279	20–30
CB[8]	1329.12	479	<0.01
CB[10]	1661.40	—	—

Table 9: Comparison of CDs and CB[n]— $\mathcal{M}$: molar mass; V: cavity volume; s_w: molar solubility in water.[133]

	Li$^+$	Na$^+$	K$^+$	Rb$^+$	NH$_4^+$	Ca^{2+}	Sr^{2+}	Ba^{2+}
CB[6]	2.38	3.23	2.79	2.68	1.92	2.80	3.18	2.83
18-crown-6	—	0.80	2.03	1.56	1.10	<0.5	2.72	3.87

Table 10: Calorimetrically determined $\log_{10} K_a$ values for the complexation of monovalent and divalent cations with CB[6] in HCOOH/H$_2$O (1:1) at 25 °C, and with 18-crown-6 in water. Table reproduced from Ref. 131 with permission from Wiley.

CBs have also been used to explore the cavitation mechanism for the dissolution of noble gasses in water. A report by Nau *et al*. shows that the collapse of the cavity formed in water by the dissolution of polarisable noble gasses such as Kr and Rn drives the binding of the gasses to **16**. They show that the cavitation

energies dominate the binding processes over the electronic dispersion effects of polarizability.[86]

4. Resorcin[n]arenes and velcrands

Resorcin[n]arenes are a class of cavitands formed via the equilibrium condensation of resorcinol with an aldehyde to form cyclic oligomers, of which the cyclic tetramer is preferentially formed. Resorcinarenes have a saucer-shaped cavity rimmed with phenolic hydroxyls, and bridging carbon atoms upon which pendent functionalities are attached (Fig. 23).
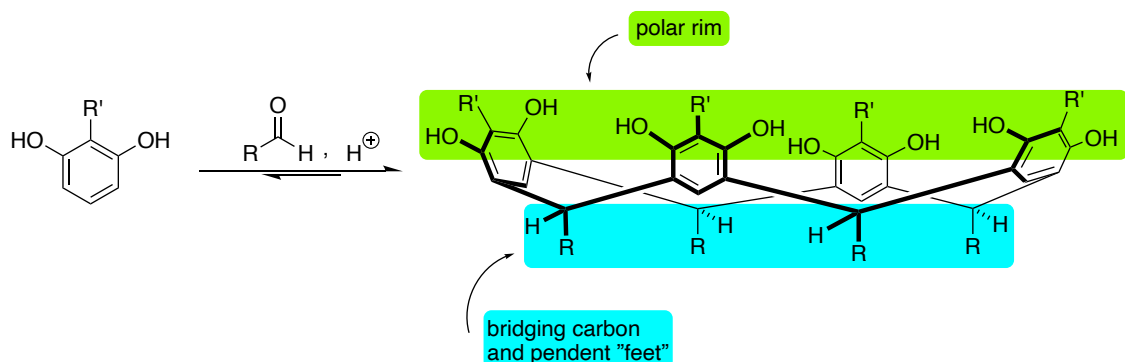
Fig. 23: Synthesis and general form of a resorcin[4]arene highlighting the polar, functionalisable rim in green, and the bridging methines and pendent moieties in blue.

In resorcin[4]arenes where the bridging carbon atoms derived from the aldehyde are the same in all four sites, four achiral diastereomeric forms are possible: *r*ccc, *r*cct, *r*ctt, and *r*tct, where the descriptors *r*, c, and t specify *relative* configuration, *cis*, and *trans*, respectively (Fig. 24).[134] In a study by Högberg in

1980,[135] it was found that the formation of the resorcin[4]arene is not a concerted tetramerization, but rather a stepwise process which goes through the acyclic tetramer and finally into the product. Product analysis as a function for time for the resorcinol–benzaldehyde system in HCl/EtOH shows that the kinetic product is the *r*cct diastereomer (Fig. 25a, Fig. 25b). Further analysis showed that higher acyclic, oligomeric homologs are also formed, however the reverse reaction to re-form the acyclic tetramer has a higher rate constant, and that the formation of the *r*ccc cyclic tetramer is the thermodynamic sink of the complex equilibria, in part because of the extensive hydrogen bonding of the phenolic hydroxyls at the rim which hold the conformation in its C_{4v} form. In almost all cases, the solvent
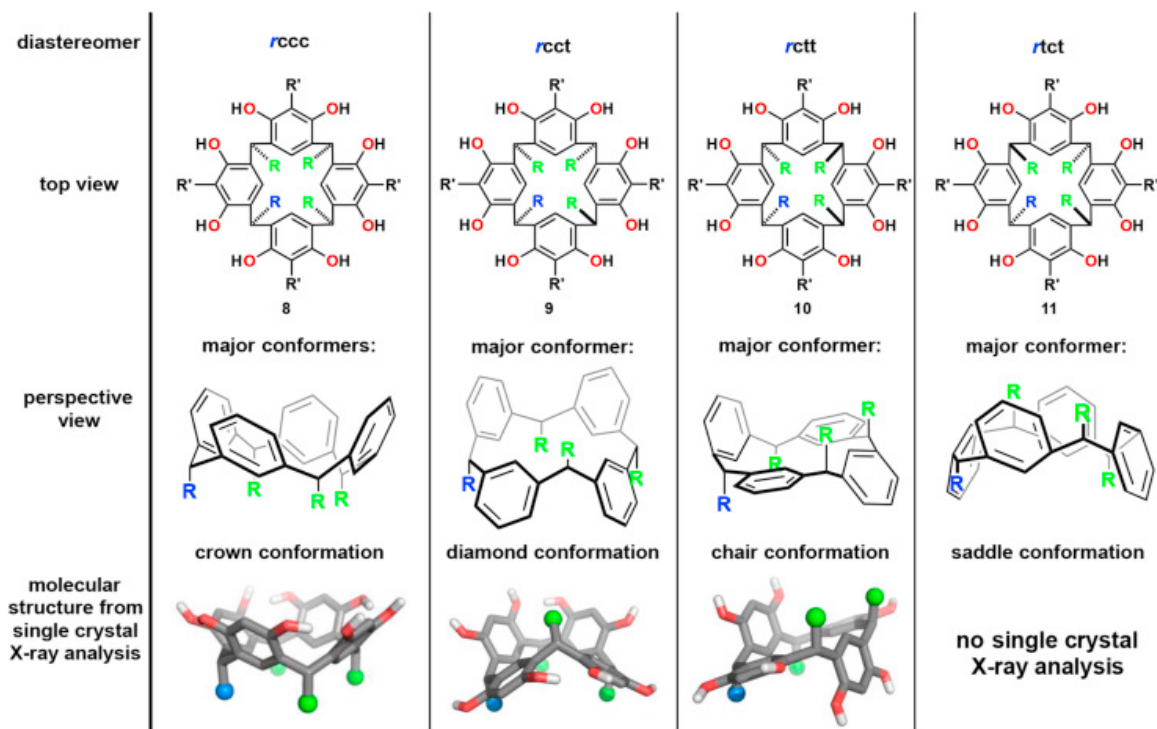
Fig. 24: Different views of the four possible diastereomers of "feet"-substituted resorcin[4]arenes and the four most important conformations of these structures, with representative molecular structures from single crystal X-ray analyses. OH groups are omitted for clarity. Image and caption reprinted from Ref. 131 with permission from Elsevier.

conditions for the reaction are such that the *rccc* form preferentially precipitates

out of solution
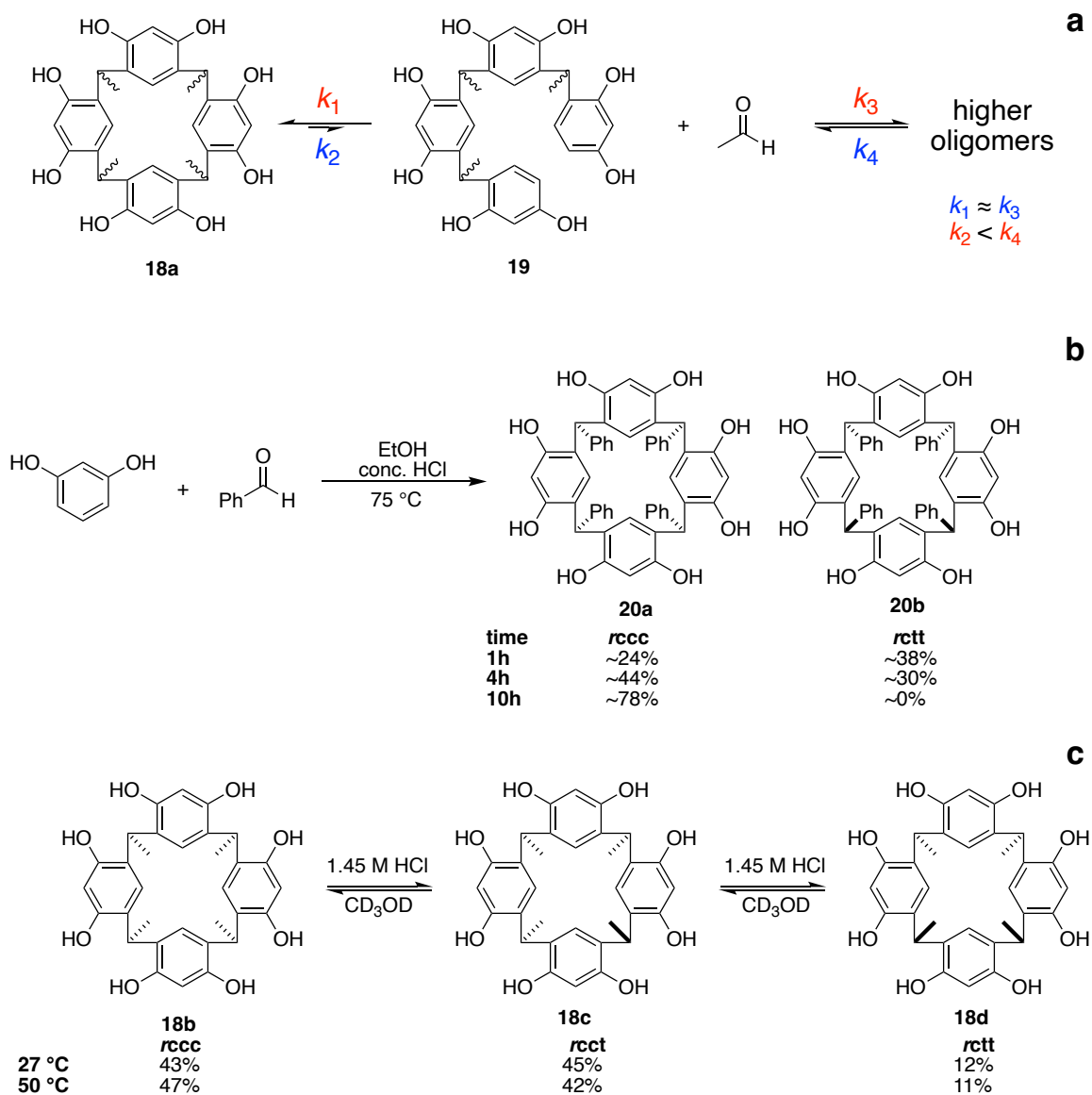
Fig. 25: **a.** Scheme of the formation and fast degradation of higher acyclic oligomers of the resorcinol/aldehyde condensation. **b.** Results of a kinetic study showing the thermodynamic preference for the *rccc* diastereomer over the kinetic *rctt* diastereomer. **c.** Distribution of stereoisomers in the equilibrium epimerisation reaction of methyl-footed resorcin[4]arene from its *rccc* form to its *rcct* and *rctt* forms. Image adapted from Ref. 131.

In a related study by Weinelt and Schneider (Fig 25c)[136] pure *r*ccc methyl-footed resorcinarene was shown to isomerize into the *r*cct and *r*ctt diastereomers when dissolved in acidic methanol at elevated temperatures, with a distribution favouring a 45:45:10 ratio of *r*ccc/*r*cct/*r*ctt. This shows the ease in which the cyclic tetramer can form, break, and re-form in homogeneous acidic solution.

Due to the extensive hydrogen-bonding capabilities of the polar rim of resorcin[4]arenes, they can form well-behaved, quantifiable aggregates such as dimers and hexamers. These aggregates can be held together non-covalently by bridging water molecules[137-144] or via metal ions,[145-147] or covalently to form encapsulating host molecules.[148-153] The covalent dimers, called carcerands (Latin: *carcer*, prison), can protect even the most reactive of molecules via a constrictive binding mechanism whereby the guest is fully enclosed in the cavity of the dimer, the most famous example of which is butadiene (Fig 26b, **19**).[148, 150, 152-156] The
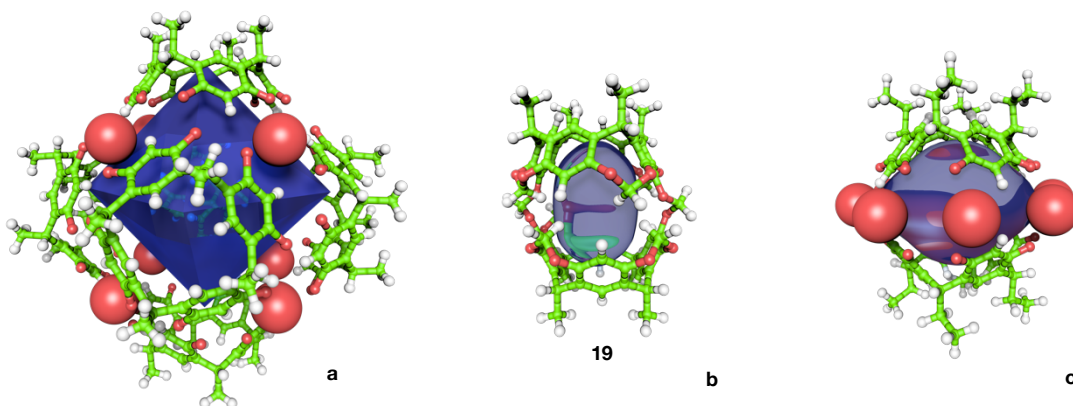
Fig. 26: *l-r* a) Non-covalent resorcinarene hexamer (CCDC LIWQIR); b) dimeric carcerand—– feet have been truncated to methyl groups for clarity; c) non-covalent resorcinarene dimer (CCDC PUJQOA). All figures are to scale relative to one another. Blue objects within each assembly represents the general shape of the void space within the assembly, and large red spheres represent bridging water molecules whose hydrogen atoms are absent in the crystal structure. Disordered solvent and guest molecules have been omitted for clarity. Green: carbon; red: oxygen; white: hydrogen. Structures were generated from their respective crystal structures and rendered using ePMV for Cinema 4D.

hexamers (Fig. 26a), on the other hand, are only formed in the presence of water in apolar solvents such as in CHCl$_3$, where 60 hydrogen bonds hold the hexamer together, with the void space of 1375 Å^3 filled with disordered nitrobenzene molecules. A similar motif is found in an analogous non-covalent dimer held together by the complexation of a tetraethylammonium cation which fills the void, and is bridged at the rim by 8 water molecules (Fig 26c).
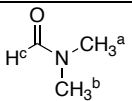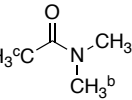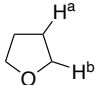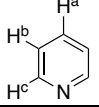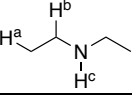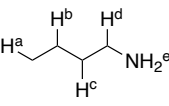
Guest structure	proton	δ^{free} (ppm)	δ^{bound} (ppm)	Δδ = δ^{free} − δ^{bound}
H^c–C(=O)–N(CH$_3$^{a})(CH$_3$^{b})	^{a}H	2.86	−0.43	3.99
	^{b}H	2.94	0.22	2.73
	^{c}H	7.99	4.04	3.95
H$_3$C–C(=O)–N(CH$_3$^{a})(CH$_3$^{b})	^{a}H	2.94	−1.43	4.37
	^{b}H	3.02	0.97	2.05
	^{c}H	2.09	−2.24	4.33
(CH$_3$)$_2$SO		2.61	−1.20	3.81
H$_2$O		1.55	−1.87	3.42
H$_3$CCN		2.00	−2.42	4.42
2 H$_3$CCN		2.00	−2.15	4.15
CH$_2$Cl$_2$		5.30	2.64	2.66
CH$_2$Br$_2$		4.95	2.50	2.50
tetrahydrofuran (H^a, H^b)	^{a}H	1.85	−2.20	3.07
	^{b}H	3.75	−0.23	3.98
pyridine (H^a, H^b, H^c)	^{a}H	7.68	6.24	1.44
	^{b}H	7.30	2.84	4.46
	^{c}H	8.62	4.08	4.54
C$_6$H$_6$		7.36	3.87	3.49
H^a, H^b, H^c amine	^{a}H	1.08	−2.94	4.02
	^{b}H	2.65	−0.48	3.13
	^{c}H	—	−1.48	—
H^a, H^b, H^c, H^d, NH$_2$^{e}	^{a}H	0.90	−3.39	4.29
	^{b}H	1.33	−1.24	2.57
	^{c}H	1.41	−0.94	2.35
	^{d}H	2.27	−1.13	3.80
	^{e}H	—	−3.18	—

Table 11: Chemical shifts (δ) in ppm of guest signals in the bound state within **19** as G∈**19** in comparison to the free state, and the change in chemical shift Δδ. Signals were extracted from ^{1}H NMR spectra taken in CDCl$_3$ in a 500 MHz instrument at 22 °C. Table reprinted from Ref. 152 with permission from the Royal Society of Chemistry.

Evidence for the binding of guests into the void space of the carcerand (Fig. 26b) is via ^{1}H NMR spectroscopy. Any bound guest will be physically shielded from the external magnetic field of the NMR instrument by the magnetic anisotropy of the walls of the resorcinarene and will thus have a more negative chemical shift relative to the free state. Table 11 shows the chemical shifts of various guest signals within a carcerand in CDCl$_3$.

The depth of the monomeric cavitand may be increased by bridging the phenolic sites. The simplest bridging is by using a dihalomethane or dihalomethane surrogate such as bromochloromethane or dichlorodimethylsilane to form bridged resorcinarenes (Fig. 27). Gibb, Chapman, and Sherman in 1995,[157] and Jordan, *et al*. in 2021[158] demonstrated that the proximal phenols at the rim of propanol-footed resorcin[4]arene (**19**) can be bridged by methylene units by reaction with either bromochloromethane (BCM, CH$_2$BrCl), diiodomethane (DIM, CH$_2$I$_2$), or methylene ditosylate (MDT, CH$_2$(OTs)$_2$) in the presence of a non-nucleophilic base such as potassium carbonate (K$_2$CO$_3$), or 1,8-diazabicyclo[5.4.0]undec-7-ene (DBU) to form compound **21**. The bridging reaction is stereoselective: one hydrogen atom is pointing inwards towards the C_4 axis of the resorcinarene, while the other is parallel to it. Indeed, ^{1}H NMR spectroscopy of the bridged resorcinarenes show two doublets, one for each diastereotopic proton, which points to the magnetic dissimilarity between the two atoms: the inwards-pointing proton is shielded from external magnetic fields by the resorcinarene cavity, while its partner is not.
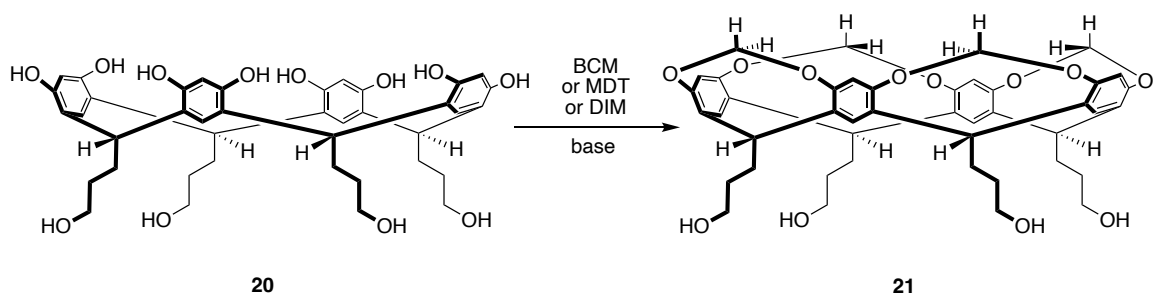
Fig. 27: Conversion of propanol-footed resorcinarene **20** to methylene-bridged resorcinarene **21**. BCM: bromochloromethane; MDT: methylene ditosylate; DIM: diiodomethane.

Resorcinarenes can also be bridged in such a way that the cavity is deepened. In 1991, Moran *et al.* demonstrated that resorcinarenes may be deepened to have vertical walls.[159] An eight-fold nucleophilic aromatic substitution (S_NAr) was performed on 2,3-dichloroquinoxaline using the phenolic oxygens on the resorcinarene in the presence of caesium carbonate and [2.2]paracyclophane as a template in dimethyl sulfoxide to yield cavitand **22** (Fig. 28).
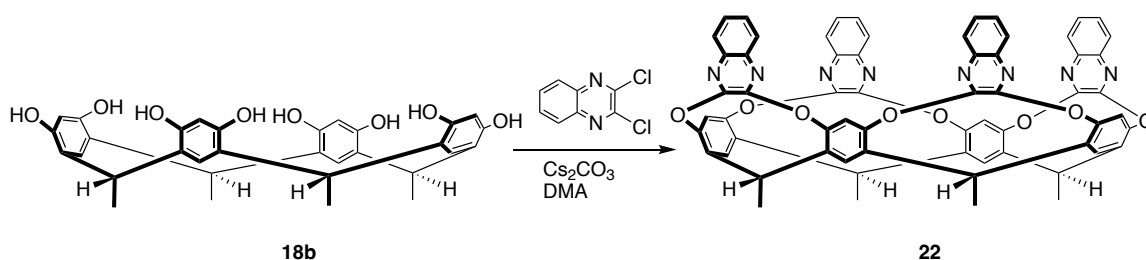
Fig. 28: Synthesis of velcrand **22** from resorcinarene **18b**.

Dalcanale and coworkers observed that in **22** (Fig 29) the presence of a templating guest would make the quinoxaline walls stand parallel to the C_4 axis of the host. This conformation resembles a tall cylindrical vessel and was thus called the "vase". A structural modification by Knobler *et al*., such that the starting

resorcinarene was tetramethylated at the resorcinol 2-position prior to reaction with 2,3-dichloroquinoxaline, showed that the resulting cavitand dimerised in both the solid state and in solution. All four walls were splayed outward, and the resulting increase in exposed surface induced face-to-face dimerization. This conformation was thus called the "kite". This proclivity for the kite conformers to dimerise in both solution and the solid state led to this class of molecules to be called velcrands, in reference to the propensity of hook-and-loop fasteners to stick to one another, cf. Velcro®.
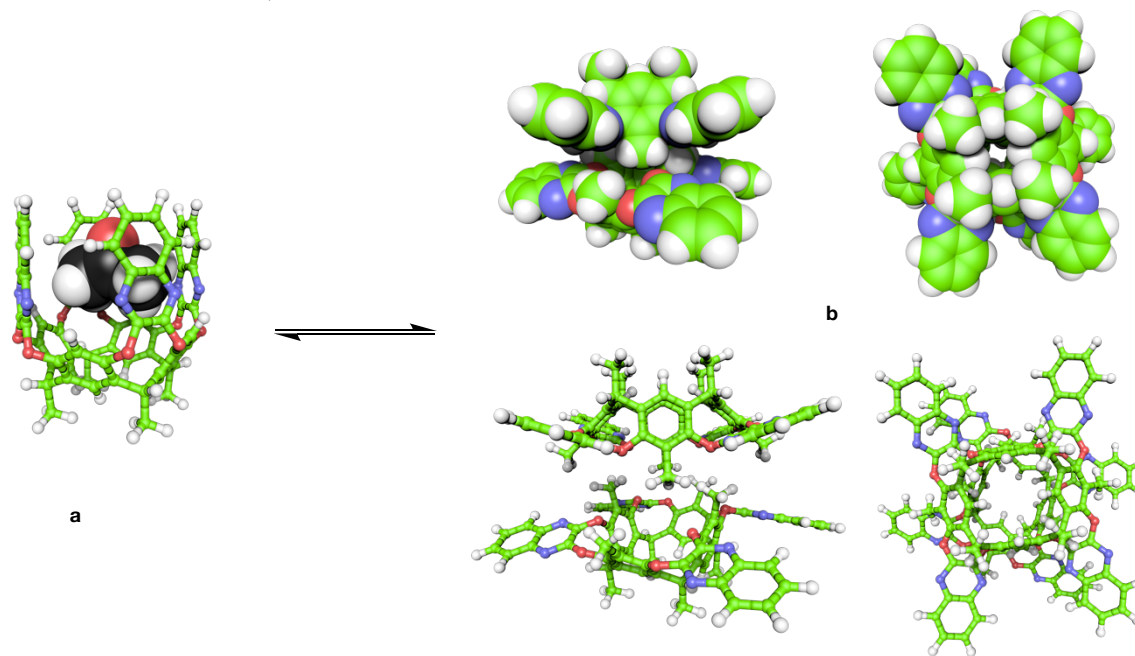
Fig. 29: Conformations of velcrand **22**. a) vase conformation with a bound acetone molecule (CCDC KAJFAC01). b) side (*left*) and top (*right*) views of the kite dimer in CPK (*top*) and ball-and-stick (*bottom*) forms. Green: host carbon; white: hydrogen; red: oxygen; blue: nitrogen; black: guest carbon. Images were rendered using ePMV for Cinema 4D.

In a 1998 communication,[160] Rebek and co-workers described the synthesis of an imide-rimmed velcrand **23** (Fig. 30). This host molecule dimerises into a capsule in apolar solvents such as $CDCl_3$, C_6D_6, and toluene-d_8. The ^{1}H NMR signals of the imide protons are sharp, characteristic of high (C_{4v}) symmetry
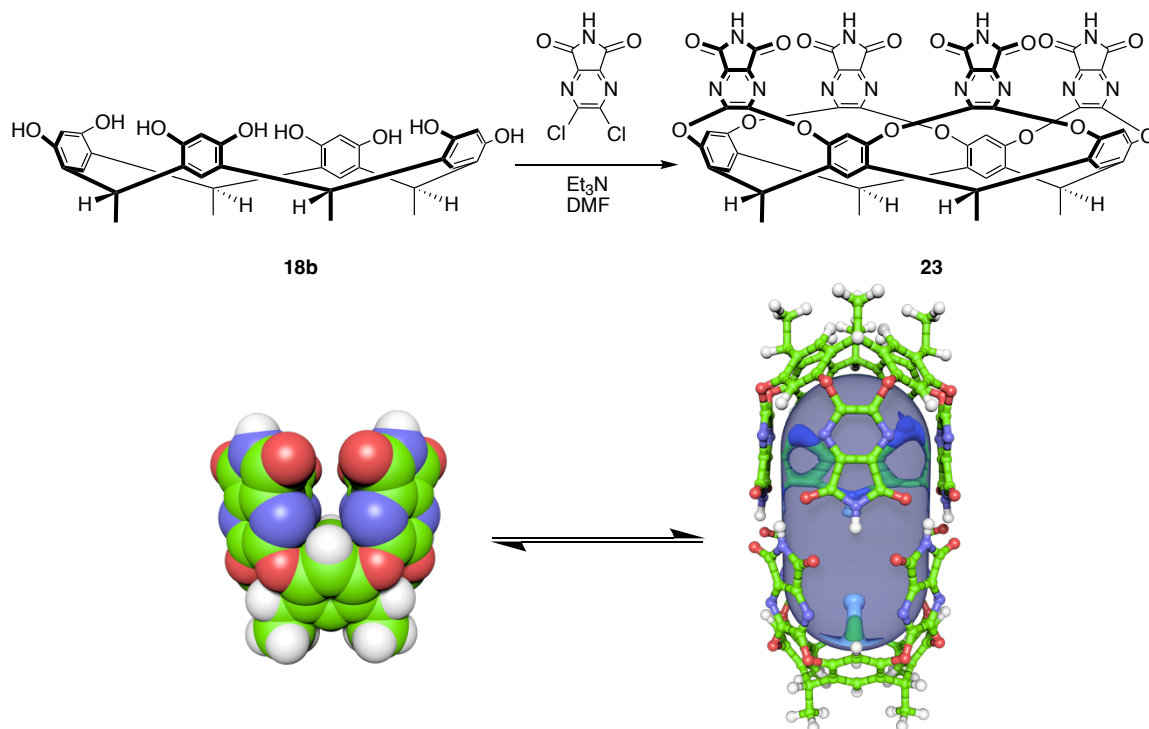
Fig. 30: (*top*) Synthesis of velcrand **23** and (*bottom*) its dimerization equilibrium. Green: carbon; white: hydrogen; red: oxygen; blue: nitrogen. Blue object within the dimer capsule represents the approximate size and shape of the cavity. Images were rendered using ePMV for Cinema 4D.

and lack of exchange. An NH vibrational band at 3332 cm^{-1} was also observed in the solution-state FTIR spectrum of the host indicative of strong hydrogen bonding. In guests that are sufficiently sized, a 2:1 host/guest pair can be observed using ^{1}H NMR spectroscopy, and small guests induce a 2:2 motif. In follow-up reports,[161, 162] they observed that *n*-alkanes can adopt motifs that are not found in the solid state or in solution. These helical geometries (where the methylene units of the sufficiently-sized *n*-alkanes adopt *gauche* conformations[163, 164]) are enforced due to the confinement of the guests within the cylindrical void of the capsule. Because of the shape of the cavity and the rigid walls composed of aromatic rings, the magnetic shielding anisotropy is intensified. In fact, the further away from the hydrogen-bonded seams the guest is located, the more

shielded it becomes, and the Δδ shift of the signals of the guest become increasingly negative.

In a more recent communication by Wu and Rebek,[165] it was demonstrated that a non-dimerising per-*N*-methylated imide-rimmed velcrand can act as a chaperone for a macrocyclization in water. As an α,ω-diisocyanoalkane is complexed in the cavitand a 'yo-yo' motion can be observed by ^{1}H NMR spectroscopy. In some cases the motion is on the time scale of the NMR experiment which broadens and obliterates guest signals. It is clear that because of the hydrophobicity of both the interior of the host and the guest, the alkane region of the guest is preferentially bound inside the host, and any polar moieties will stick out and into the bulk water. In analogous guests where one functional group can directly interact with water (10-isocyano-1-decanamine) the motion is slowed in such a manner that the depth of the guest can be ascertained. The host then acts as an external template that brings the two ends of the guest molecule together to facilitate the reaction. The product of the macrocyclization, *N,N'*-decen-1,10-diylurea, is now less hydrophobic, and is thus bound less deeply into the cavitand as evinced by the less negative Δδ shifts of the guest signals.
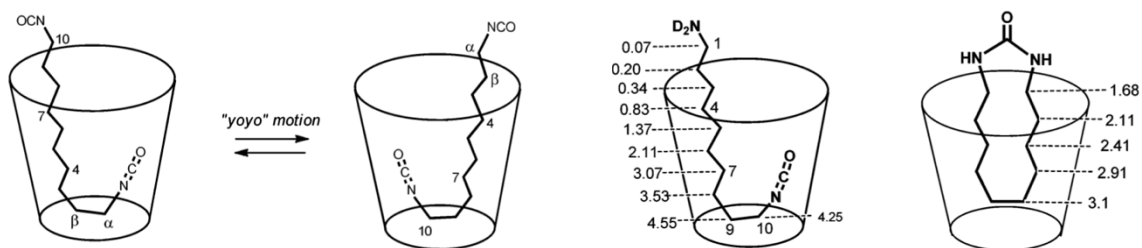
Fig. 31: (*left*) Cartoon of the 'yo-yo' motion of 1,10-diisocyanodecane. (*right*) Cartoon of the binding modes of the starting isocyanate and the cyclised urea, with their corresponding –Δδ shifts within the host. Image reproduced from Ref. 162 with permission from the American Chemical Society.

5. Rigid, deep-cavity cavitands

A natural extension to the deepening of resorcin[4]arenes is the rigidification of the cavity and the freezing of the conformational mobility of the cavitand. Two strategies may be employed to freeze the conformational mobility of the cavitand: non-covalent and covalent.
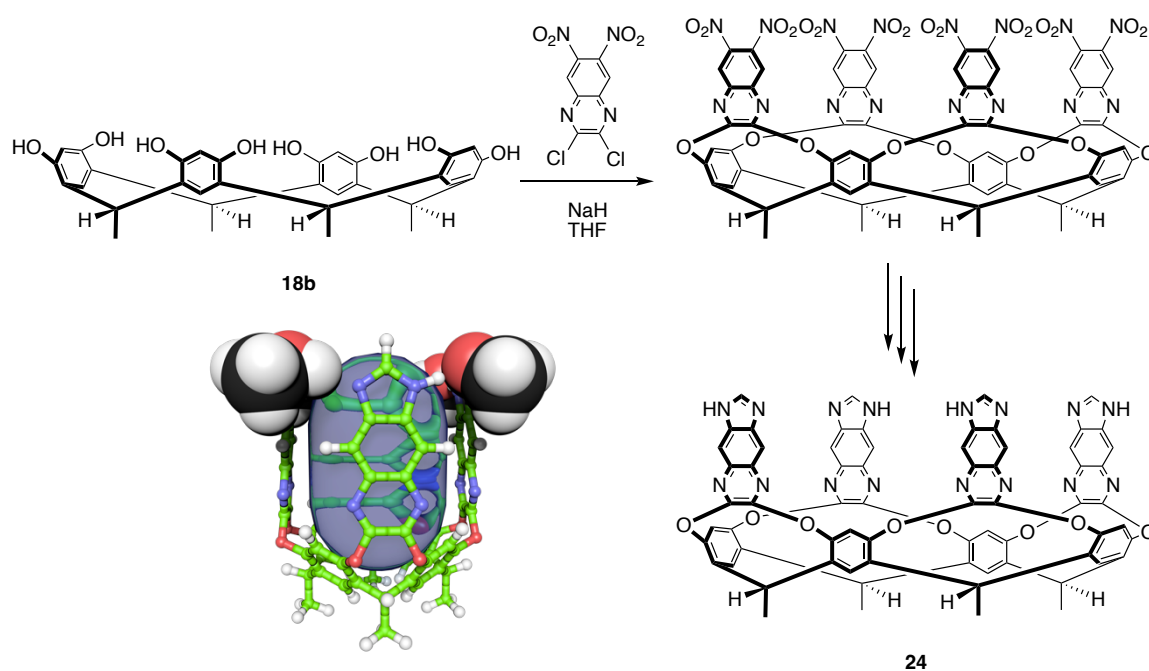
Fig. 32: Synthesis of imidoquinoxaline velcrand **24** and its 3D structure. Green: host carbon; white: hydrogen; red: oxygen; blue: nitrogen; black: bridging methanol carbon. Blue object within cavitand represents the approximate size and shape pf the cavity. Image rendered using ePMV for Cinema 4D.

In 2009[166] Choi and co-workers reported on the synthesis and binding properties of an imidazoquinoxaline velcrand **24** (Fig. 32). Due to its hydrogen bonding geometry this cavitand does not dimerise in the way that **23** does; rather, its shape is enforced by intramolecular hydrogen bonds between the imidazole moieties at the rim that are bridged by methanol molecules. The binding

properties of the host is what one would expect for velcrand-type hosts: the magnetic anisotropy spread out guest signals, with large $-\Delta\delta$ values indicative of guest depth within the cavitand.

In 1999 Xi, Gibb, and Gibb[167] reported the synthesis of benzal-bridged resorcinarenes functionalised at the rim with aryl groups. Functionality ranged from σ-donors such as H and Me, to σ-acceptors/π-donors such as halogens, to strong π acceptors such as esters, acids, and nitriles (Fig 33).[168] The synthesis involves the eight-fold stereoselective substitution at the benzal position by the proximal phenolic oxygen atoms of resorcinarene **25** in the presence of a non-nucleophilic base in a polar aprotic solvent to yield deepened cavitand **26**.
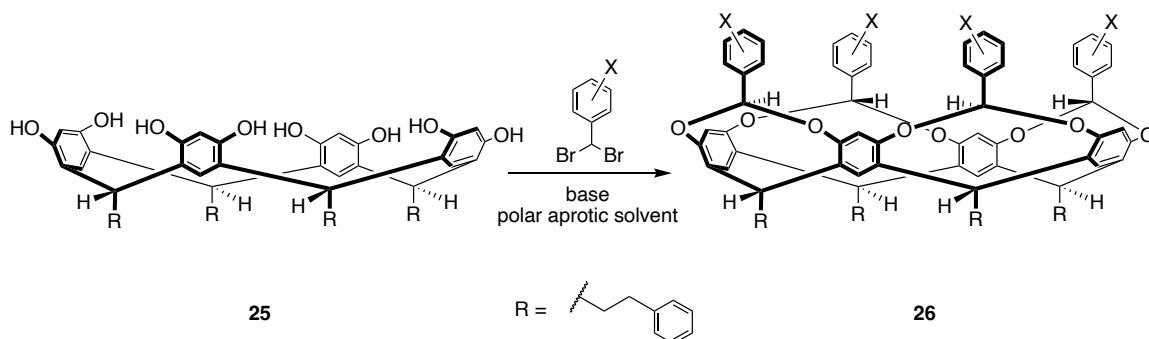
Fig. 33: Synthesis of benzal-bridged resorcinarenes. Successful (yield ≥25%) functionalities: X= H, 2-Br, 3-Br, 3-Me, 3-OMEM, 4-Br, 4-I, 4-Me, 4-Ph, 4-COOEt, 3,5-Br$_2$.

The attachment of the benzal bridge was found to be highly diastereoselective, and that even though some intractable polymer occurs as a side product, the isolated product is always the C_4-symmetric cavitand, with a bond efficiency of ca. 86% for the first benzal bridge attached.[169] The correct addition of the first benzal bridge templates the addition of the other three (**28**, Fig. 34). If one benzal bridge attaches incorrectly, i.e., with the proton 'up' instead

of 'in' (**27**, Fig. 34), the addition of the next benzal bridges fails, presumably because of the steric interference brought about by the aryl rings partially covering the opening of the resorcinarene, especially in the case of the 3,5-dibromobenzal-bridged resorcinarene.
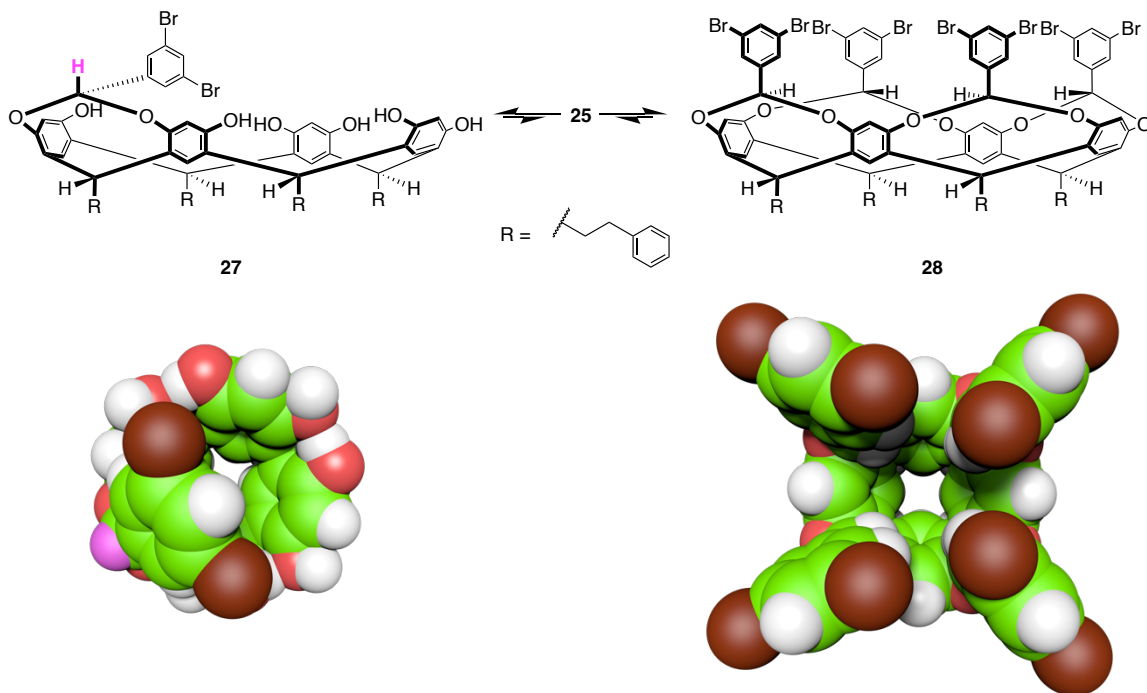
Fig. 34: Bridging of resorcinarene **25** to form successfully bridged octabromide **28** and mis-bridged dibromide **27**. Space-filling models are directly below each structure, with a view down the C_4 axis of the resorcinarene. Benzal proton from the mis-bridged reaction is highlighted in pink. Images were generated using ePMV for Cinema 4D.

The addition of functionality to the resorcinarene opens the door to more chemistries performed on the host molecules. Specifically, the addition of halogens to the aromatic rim of the host enables transition-metal catalysed reactions such as Ullman-type, Heck, Negishi, Sonogashira, and Suzuki reactions. In 2001[170] Gibb, Stevens, and Gibb reported on the eight-fold Ullman biaryl-ether condensation reaction[171] between octabromide **28** and resorcinol in the presence of CuO in pyridine to form deep-cavity cavitand **29** (Fig. 35). Compound **29** has a truncated right circular[‡‡] cone-shaped cavity— the bowl-shaped molecule is ~8 Å wide as measured between diametrically opposite inward-pointing (*endo*) hydrogen atoms at the rim, and ~8 Å deep from the ethereal oxygens at the rim to the base hydrogen atoms at the resorcinarene core
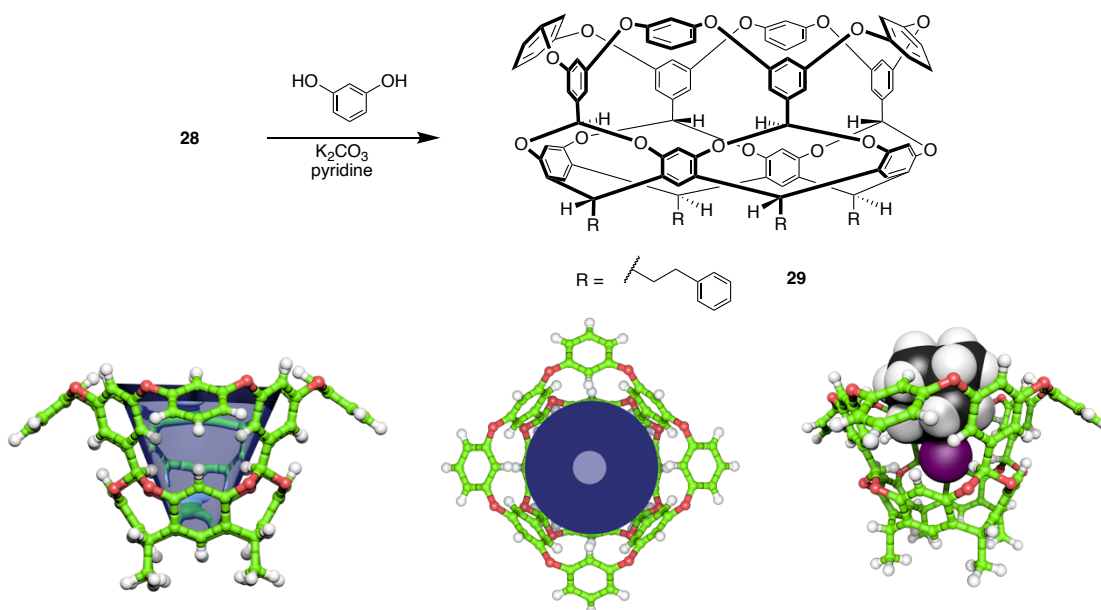
Fig. 35: *top*: Synthesis of deep-cavity cavitand **29** from octabromide **28**. *bottom*: 3D models of **29**– *left*: side view; *middle*: view from the top along the C_4 axis; *right*: binding mode of 1-iodoadamantane to **29**. Green: host carbon; white: hydrogen; red: oxygen; black: guest carbon; purple: iodine. Blue object represents approximate size and shape of cavity. Structures generated from x-ray data (CCDC RAKHIU) and rendered using ePMV for Cinema 4D.

[‡‡] A right circular cone is one whose base is a circle and whose axis passes through the centre of the circle normal to its plane.

(Fig 35). The inward pointing benzal protons participate in C-H···X hydrogen bonding with halogenated guest molecules, as evinced by the deshielding of the ^{1}H NMR signal of the benzal protons during the binding event, and the packing motif of the guest in the solid state (CCDC RAKHIU).

In a follow-up communication, Gibb and Gibb described the synthesis (Fig. 36)[172, 173] of octa-acid **30** and the binding of a hydrophobic guest in water. Host **30** shares the same bowl-shaped cavity as **29**, however, **30** is coated with eight carboxylic acid groups which engender water-solubility where at high pH values the host is at the very least hexa-anionic[174] and nominally octa-anionic.[172] The synthesis of **30** begins with the bridging of propanol-footed resorcinarene **31** to form octabromide **32**, which was subjected to an eightfold Ullmann biaryl ether condensation with 3,5-dihydroxybenzyl alcohol to form octol **33**. The poorly
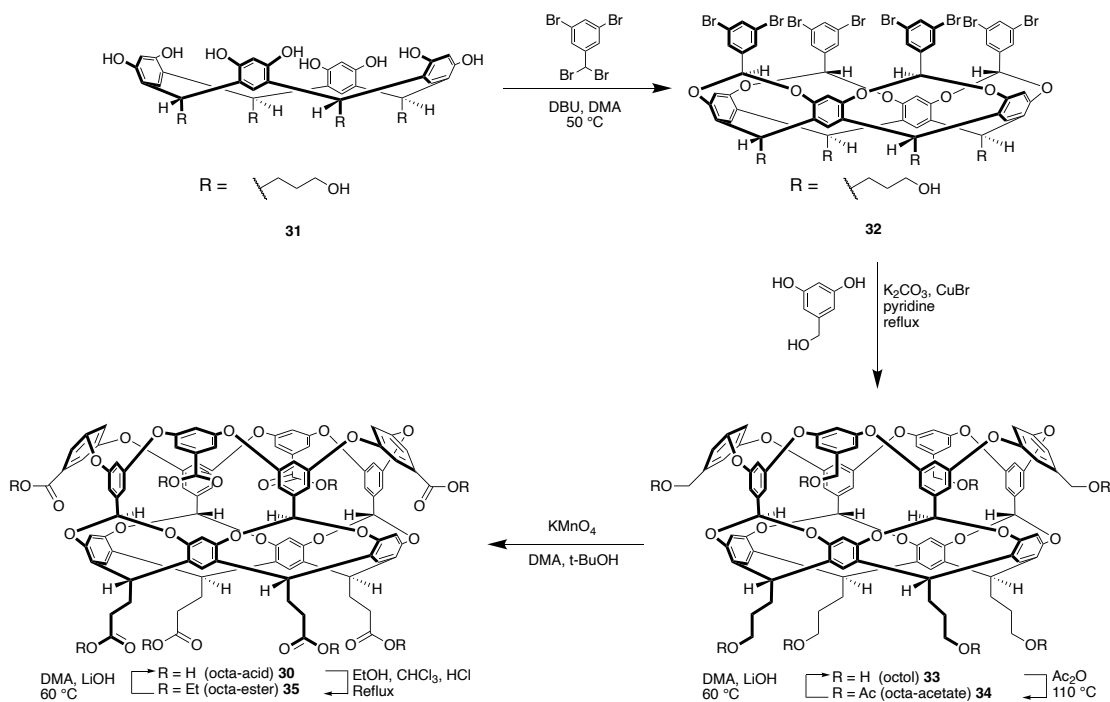
Fig. 36: Synthesis of deep-cavity cavitand **30**.

soluble **33** can be purified using chromatography via its octa-acetate ester **34**, however operationally, the oxidation to form crude **30** may be performed using KMnO$_4$ in the crude state. Crude **30** is purified using chromatography via its octa-ethyl ester **35**, and then hydrolysed to give pure **30**.

Octa-acid **30** has been studied in organic photochemistry,[175-183] in the investigation of the Hofmeister effect,[184-189] in the heterophasic sequestration of hydrocarbons,[190-196] and in the kinetic resolution of isomers and selective isomer protection.[190, 197-201] In recent years, **30** has been studied and used as a benchmark molecule for a set of computational challeges called the Statistical Analysis of the Modeling of Proteins and Ligands (SAMPL), details of which will be discussed in the next chapter.

A cursory inspection of the interior of **30** reveals a completely apolar interior engendered by the aromatic walls which compose the cavitand. In aqueous solution, compound **30** is weakly hydrated. Its volume can comfortably hold up to 7 water molecules; however, in equilibrium, there is only an average of 4 water molecules in a hydrogen bonding network within its pocket.[174] Much like **23** and **24**, **30** can also self-assemble in the presence of non-polar guests whose length exceed that of the depth of the cavitand (Fig 37). Indeed, spectroscopic evidence has been provided for the templation of a supramolecular capsule in water by the presence of *n*-alkanes as determined by Diffusion-Ordered NMR Spectroscopy (DOSY-NMR).[191] For *n*-alkanes C$_4$–C$_7$, the host is dimeric and in a quaternary complex, i.e. in a 2:2 host/guest complex. A switching point occurs in C$_8$, where

the diffusion constant hovers between that of a dimer and that of a monomer indicating that there is an exchange between the two states at the NMR time scale.[109] Increasing the length of the guest to C_9 induces another switch: the formation of the 2:1 host/guest complex where this binding stoichiometry persists until C_{17} (Fig. 37a). Again, analogous to the velcrands, the increasingly negative $\Delta\delta$ shifts of the encapsulated guest signals indicate the depth of the guest within the cavitand (away from the hemispheres). Plotting the $-\Delta\delta$ of the terminal methyl groups of the n-alkanes reveals that C_{12} occupies the entire length of the cavitand void space, and that any increase in length forces the guest to contort into geometries that will make the terminal methyls pull away from the depths of the capsule (Fig. 37b). In a follow-up report[194] it was shown that the guest packing motifs of the n-alkanes can range from being fully 'extended' in C_4–C_{11} where the relevant C–C torsions are *trans*; to 'helical' in C_{12}–C_{14} where the torsions are closer to *gauche*, to 'hairpin' in C_{15}–C_{22} where a hairpin turn occurs in the guest, to 'spinning top' where the two ends are deep within the capsule and the rest of the guest does a turn around the equator (Fig. 31c). In some cases, a haemorrhaging of the guest occurs where the capsule is completely full and the only way for the guest to fit is for the two hemispheres of the capsule to come slightly apart and for part of the guest to be exposed to the bulk solvent.[196]
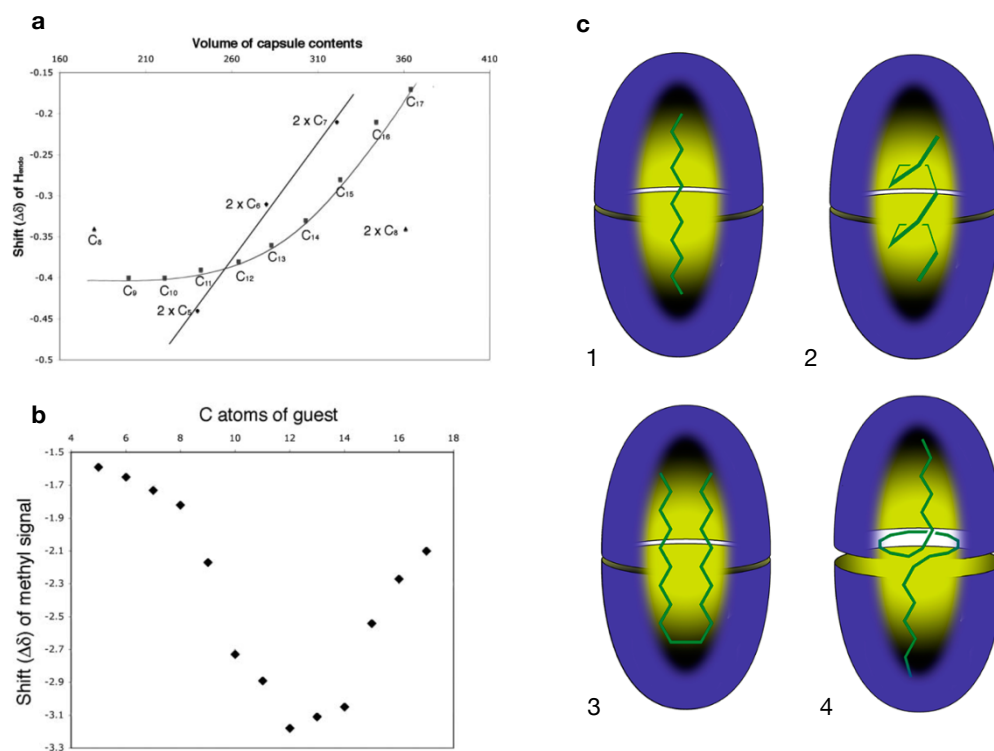
Fig. 37: a) Plot of binding stoichiometry as a function of guest size. b) Plot of terminal methyl $\Delta\delta$ as a function of guest size. c) binding motifs of *n*-alkane guest as a function of size: 1– extended/compressed; 2– helical; 3– hairpin; 4– spinning top. Note the separation of the hemispheres in the spinning top motif and the potential for guest haemorrhage.

Compound **30** has been used to probe the Hofmeister effect on host–guest complexes in water. In a 2011 report[184] it was demonstrated that adamantane-1-carboxylate (AdCOO⁻, $K_a^{30} \sim 3.95 \times 10^6$ M⁻¹) binds more strongly to **30** in the presence of salting-out anions, and much more weakly in the presence of salting-in salts. This is attributed to the fact that salting-out salts dehydrate the pocket of **30** and the surface of AdCOO⁻ and thus enhances the hydrophobic effect which increases the binding affinity. Salting-in salts, on the other hand, compete with AdCOO⁻ for the pocket of **30**, and thus weakens the affinity. In the case of ClO_4^-, although the strength of interaction is four orders of magnitude weaker than that of AdCOO⁻ ($K_a^{30} \sim 100$ M⁻¹), the competition is enough to inhibit

the binding of AdCOO⁻. Using van 't Hoff analysis of the resulting data for the binding of ClO_4^- to **30**, it was determined that the interaction is highly exothermic, with a significant entropic penalty. This, along with previous *in silico* work on the binding of anions to **30**,[174] point to the fact that ClO_4^- binds as an aqua complex in the pocket, with an average of 3.1 water molecules included along with the anion. Indeed, in the ITC analysis of the complexation of AdCOO⁻ and **30** in the absence of salt it was found that the binding event is slightly endothermic with a large gain in entropy.

To probe the effect of host charge on the binding of anions and the Hofmeister effect, positand 1 was synthesised (P1, **36**, Fig. 38).[202] Unlike its parent (**30**) it is soluble in solutions whose pH is well below alkaline. Its synthesis diverges from **30** at **33**, where it is subjected to the Appel reaction which converts the alcohols to halides,[203] and then to a Menshutkin reaction which forms the quaternary ammonium groups.[204] Because of the inherent switch in charge of the host, binding affinities of anions to **36** are much stronger. Still, however, just like in **30**, F⁻ and Cl⁻ do not seem to bind (or bind too weakly) to **36**, presumably because of the high barrier to dehydration of the anions (Table 3)[59, 96] which cannot be overcome by the Coulomb potential of the host–guest pair. Compound **36** is a ditopic host molecule: aside from the obvious binding site at the pocket, it also contains a "crown" of charges at the feet of the cavitand within which anions can bind.
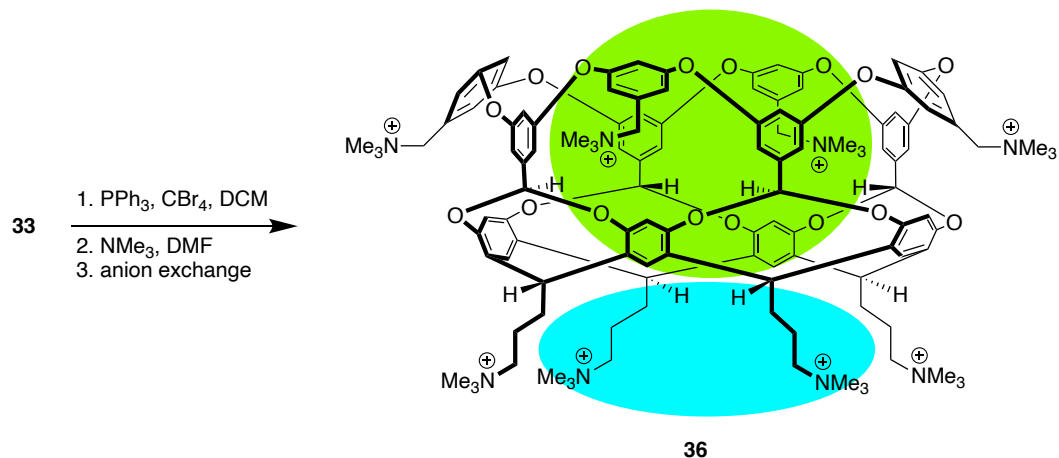
Fig. 38: Conversion of **33** to **36**. Compound **36** exists as a salt whose counteranion is Cl⁻. The green region highlights the pocket binding site, while the blue region describes the crown of ammoniums at the feet.

A range of Hofmeister anions were used to study salt effects on **36**.[187] As expected, salting-out salts induce aggregation and precipitation of **36** by binding to the weakly hydrated pocket of **36**. To probe the affinity for the salts to the crown, the pocket was blocked using AdCOO⁻ ($K_a^{36} = 7.2 \times 10^6$ M⁻¹) to ensure that any salts would preferentially bind to the feet. Indeed, when ClO_4^- is titrated into a solution of **36** in buffered D_2O a binding constant to the feet can be determined (2400 M⁻¹ cf. 4300 M⁻¹ to the pocket; 160 M⁻¹ to **30**). In certain cases, such as that for trichloroacetate (TCA, Cl_3CCOO^-) and dichloroacetate (DCA, Cl_2CHCOO^-) the binding to the pocket is stronger in that they can competitively displace AdCOO⁻. In this set of experiments, it was found that there can be a "role-reversal" for certain salting-in salts where they induce the aggregation and precipitation of **36**. This is called the reversed Hofmeister effect which is attributed to the non-specific binding of an anion to the charge carriers of the host. This non-specific binding screens the charges and effectively neutralises them by forming an ion pair, and

thus weakening solvation by ion–dipole interactions with water and inducing aggregation.

Two analogues of **30** were synthesised such that the Ullman biaryl-ether coupling introduces four methyl groups at the rim: one analogue with methyl groups at the *endo-* position pointing inwards towards the C_4 axis of the cavitand, and another with methyl groups pointing upwards and parallel to the C_4 axis (Fig 39). These compounds were called tetra-*endo*-methyl octa-acid (TEMOA, **37**) and tetra-*exo*-methyl octa-acid (TExMOA, **38**), respectively, and are constitutional isomers of one another. These two cavitands, just like their parent **30**, are soluble in water at pH levels above 8. The hydration properties, however, are different from **30**.[84] Compound **37** can bind amphiphilic guest molecules and anions such as ClO_4^- and PF_6^-. Overall, the free energy of binding of amphiphiles ($CH_3(CH_2)_nCOO^-$, n = 4–8) is stronger in **37** by ~4 kJ mol^{-1}. Densimetry measurements (which give partial molar volume) and MD simulations offer a viable explanation: the placement of methyl groups at the *endo-* position induces a drying transition in the host, and thus **37** is vacuous and devoid of water in its pocket; there is one water molecule in the cavity at equilibrium at ambient pressure. Compound **38**, on the other hand, though slightly deeper, has the same solvation as that of **30**, and thus the binding thermodynamics of amphiphiles is comparable to **30**. Simulations also point to the fact that if the ambient pressure is increased to 2500 bar (2.5×10^5 kPa), the hydration of the pocket of **37** is the same as that of **30**.
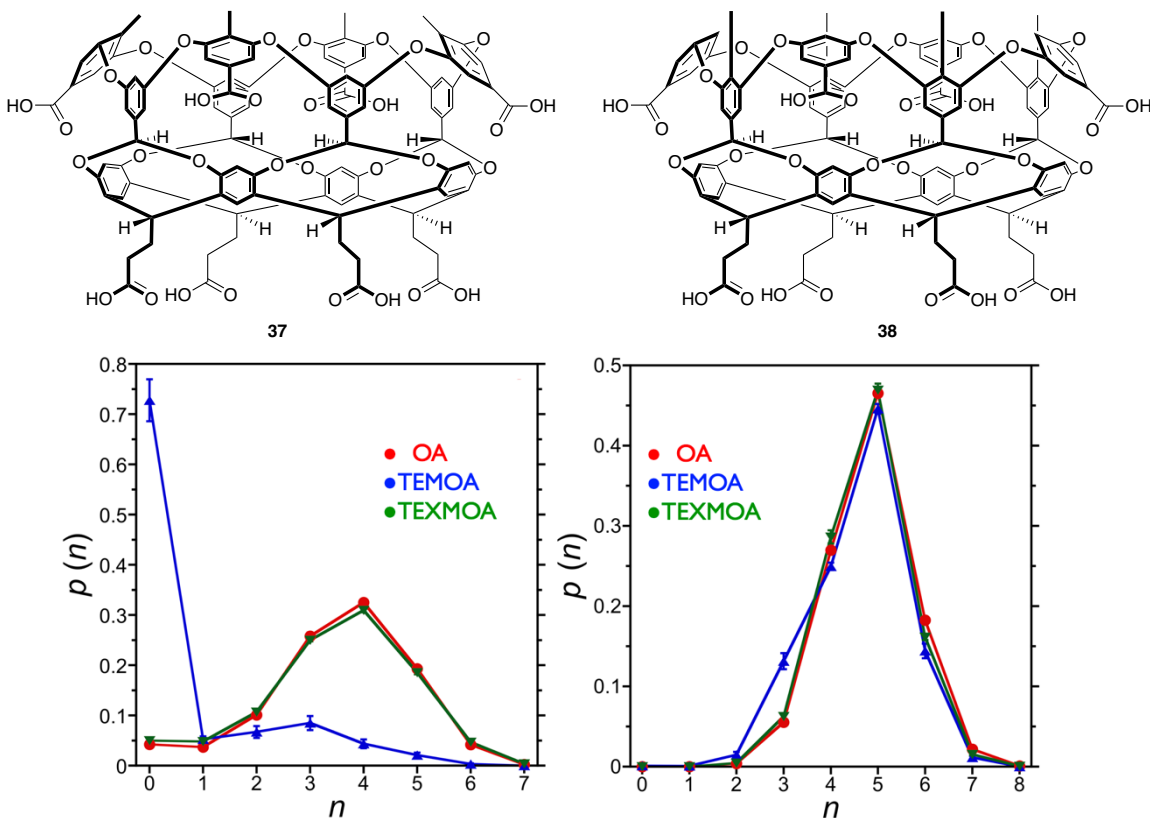
Fig. 39: *top*: Tetra-*endo*-methyl octa-acid **37**, and tetra-*exo*-methyl octa-acid **38**. *bottom*: Pocket hydration probabilities as a function of number of water molecules at 1 bar (*left*) and at 2500 bar (*right*).

Anions also bind to the pocket of **37**: in a 2018 report[188] the anion binding properties of **37** was probed in comparison to **30**. On average, anions such as perrhenate (ReO_4^-), triflate (trifluoromethanesulfonate, $F_3CSO_3^-$), and hexafluorophosphate (PF_6^-) bound much more strongly to **37** compared to **30** by at least one order of magnitude. The answer probably lies in "steric desolvation" of the anions during the binding event: the methyl groups strip sterically encumbers the passage of the anion with its solvation shell into the cavity, and thus the methyl groups physically strip the anion of its bound waters. However, in the case of thiocyanate (SCN^-) and perchlorate (ClO_4^-), the binding is comparable,

if not stronger, to **30** rather than to **37**. Thus, it would seem, then, that the explanation is incomplete.

Part II: Comprehensively Cataloguing Complicated Clammy Chemistry

An overview

Drug discovery relies on the synthesis of tens, if not hundreds, of lead compounds and testing them against substrates identified as underpinning a specific disease or disorder. Ideally, a "hit" or productive compound will be discovered in the assay and will then be further modified to give the best pharmacological results. Indeed, a large part of the cost of drug design and new drugs themselves are in the trial-and-error method of synthesis–assay–modification of lead compounds.[205, 206] Ideally, once the underlying cause of a disease or disorder is discovered and a biomacromolecule target identified and structurally characterised, a computer would be able to predict the design of the drug that would bind into the target and modulate its activity. However, our ability to predict the ideal ligand based in a structurally known binding site is poor.

There are very rudimentary ways via molecular dynamics simulations to predict the affinities of certain drugs and small molecules to the protein. However, current models that these simulations employ do not consider protuberances and concavities, the solvation of the pocket (whether wet or dry, strongly solvated or weakly solvated),[207-212] the polarizability of the solvent, the hardness of the ions

present, hydrogen bond donors and acceptors, charged groups proximal to the binding site, and so on. All these complexities make the accurate prediction of ligand affinities to bind sites difficult and complex.[65, 79, 213-217] To simplify things somewhat, artificial binding sites have also been investigated to probe the different non-covalent interactions involved.[84, 86, 87, 174, 218-221] Towards this, a major component of the Statistical Assessment of the Modeling of Proteins and Ligands (SAMPL) is to analyse the binding affinities and thermodynamics of small molecules to artificial macrocycles. The SAMPL exercise is a series of blind challenges designed to test the limits of state-of-the-art forcefields and develop benchmarks for the quality of the predictions generated by computational predictions.[222] A set of carefully designed hosts and guests are released at the beginning of every cycle, and wet chemists involved with the exercise determine binding affinities using spectroscopic and calorimetric techniques. At the same time, computational chemists attempt to predict the results of the experiments using simulations, and the differences between the results of the wet experiments and the computations are compared and statistically analysed. In the work described in this Dissertation, the syntheses of hosts and thermodynamic results will be presented and discussed for two cycles: SAMPL7 and SAMPL8, where the former deals with wet cavities, and the latter, dry.

Wetter pockets: Synthesis and properties of exo-OA; contributions to SAMPL7

Water, water, every where,
Nor any drop to drink
(Samuel Taylor Coleridge, *Rime of the Ancient Mariner*, 1814)[223]

It has been established that at a certain separation a drying transition will occur between two apolar plates (*vide supra*), and that certain concavities will de-wet if they are smaller than a context-dependent "drying lengthscale".[224-226] The effect of polar groups proximal to a concavity influences the binding of substrates to the concavity due to the dipole–dipole interactions between the cohesive, highly polar, strongly hydrogen bonding water with the polar moieties in the concavity, such as the sidechains in a binding site triad in a protein. This can affect the binding of substrates in so much as water can be harder to displace and can competitively bind to the active site.

To probe this, *exo*-octa-acid (*exo*-OA, **39**, Fig. 40) was synthesised and compared to **30** (Fig 36). *exo*-OA **39** is a constitutional isomer of **30**, in so much as the carboxylates at the outer rim (the *peri*- position) have been moved to the *endo*- position and point "upwards" parallel to the C_4 axis of the host. Correspondingly, compound **39** shares the same apolar concavity with **30**. The synthesis of **39** starts with a common compound to **30**, octa-bromide **32**. A similar Ullman biaryl-ether condensation is performed between **32** and resorcinol using CuBr·SMe₂ complex as a catalyst to form tetrol-footed *meta*-basket **40**. The feet
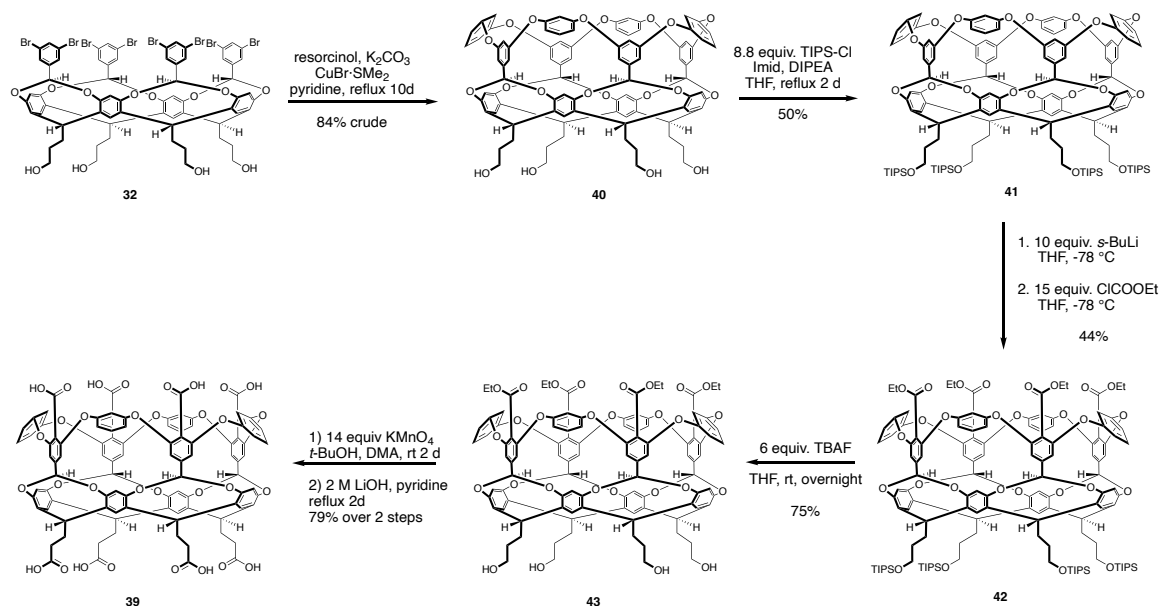
Fig. 40: Synthesis of *exo*-octa-acid **39**.

were then protected using triisopropylsilyl chloride to form the tetrakis-TIPS *meta*-

basket **41**. Directed *ortho*- metallation[227, 228] using *sec*-butyllithium was used to

form the tetra-*exo*-lithiate which was not isolated, but rather was quenched with

ethyl chloroformate to give tetra-*exo*-ester TIPS-*meta*-basket **42**. This compound

was then subjected to fluoride-assisted de-silylation to form cavitand **43**, which

was subjected to oxidation by $KMnO_4$ to convert the alcohols at the feet to

carboxylates, and then a base-promoted de-esterification and re-protonation to

finally give cavitand **39**.

Using both spectroscopic and calorimetric techniques the

thermodynamics of guest binding to *exo*-octa-carboxylate **39** was compared to

30 at pH 11.5 (10 mM phosphate buffer). Eight different guests were used (Fig.

41)— four that are negatively charged carboxylates at the experimental

parameters, and four positively charged trimethylammoniums: *n*-hexanoic acid

(**44**), 4-chlorobenzoic acid (**45**), (*S*)-perillic acid (**46**), (*S*)-citronellic acid (**47**), β-phenylethyl(trimethyl)ammonium (**48**), *n*-hexyl(trimethyl)ammonium (**49**), *trans*-4-methylcyclohexyl(trimethyl)ammonium (**50**), and adamantyl-1-(trimethyl)ammonium (**51**). The thermodynamic data are given in Table 12.
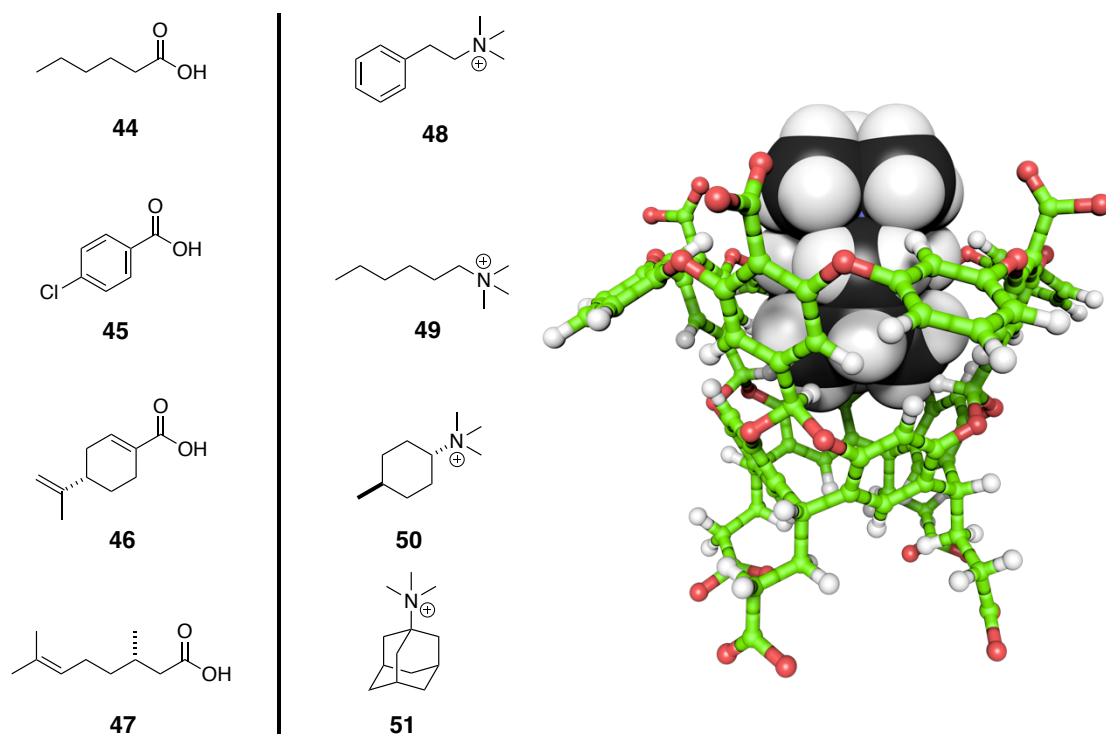
Fig. 41: (*left*) Guests used in the SAMPL7 exercise. *(right)* Model of the binding of guest **51** to *exo*-octa-acid **39**. Green: host carbon; white: hydrogen; red: oxygen; blue: nitrogen; black: guest carbon.

Guest	OA 30				exo-OA 39			
	$\log_{10} K_a$	ΔG (kJ mol^{-1})	ΔH (kJ mol^{-1})	$-T\Delta S$ (kJ mol^{-1})	$\log_{10} K_a$	ΔG (kJ mol^{-1})	ΔH (kJ mol^{-1})	$-T\Delta S$ (kJ mol^{-1})
44	3.6	−20.8 ± 0.1	−23.2 ± 0.1	2.4 ± 0.3	—[b]	—[b]	—[b]	—[b]
45	5.1	−28.9 ± 0.1	−40.2 ± 1.1	11.0 ± 1.0	1.0	−5.5[c]	—	—
46	5.9	−33.9 ± 0.1	−50.2 ± 0.0	16.3 ± 0.1	2.5	−14.1 ± 0.3	−25.2 ± 0.6	11.1 ± 0.3
47	5.0	−28.3 ± 0.2	−28.0 ± 0.7	−0.3 ± 0.5	2.6	−15.1 ± 0.1	−30.5 ± 2.9	15.4 ± 2.8
48	3.5	−19.8 ± 0.0	−31.3 ± 0.2	11.5 ± 0.2	4.1	−23.3 ± 0.1	−25.8 ± 0.0	2.5 ± 0.1
49	3.7	−20.8 ± 0.1	−30.5 ± 1.4	9.6 ± 1.4	4.3	−24.4 ± 0.0	−13.6 ± 0.1	−10.8 ± 0.1
50	4.5	−25.4 ± 0.2	−24.0 ± 0.7	−1.4 ± 0.5	5.1	−29.2 ± 0.4	−20.8 ± 0.3	−8.4 ± 0.2
51	6.0	−34.5 ± 0.1	−32.7 ± 0.8	−1.7 ± 0.6	5.6	−32.1 ± 0.0	−21.1 ± 0.2	−11.0 ± 0.1

Table 12: Thermodynamic data[a] from ITC and/or NMR for the binding of guests **44–51** with hosts **OA 30** and **exo-OA 39**. All titrations were performed in 10 mM phosphate buffer at pH 11.5, and equilibrated at 25 °C. Rows highlighted in pink represent data for negatively-charged guests, and in blue for positively-charged guests.

[a] The ΔH and K_a values were obtained by carrying out at least three separate experiments, averaging each set of data, and calculating the respective standard deviations. ΔG was obtained from K_a via the standard thermodynamic equation. The average ΔH and ΔG values were then used to calculate an average $-T\Delta S$, and the corresponding standard deviations calculated using the standard equation for the propagation of uncertainties for subtraction. The deviations of ΔG were obtained by using the standard equation for the propagation of uncertainties for logarithms. The errors on $\log_{10} K_a$ are smaller than what is significant.
[b] Binding is too weak to be observed by NMR or ITC.
[c] Determined by ^{1}H NMR spectroscopy

As with **30**, the small amphiphilic guests bound to **39** in a 1:1 stoichiometry (DOSY NMR spectroscopy), but unlike **30** where the exchange between the free and bound states is usually slow on the NMR time scale, the exchange in **39** was found to be generally fast or on the time scale of the NMR at 500 MHz. Thus the bound guest signals were broad. Only in the case of **51** with its large, spherical, globular body did sharper signals appear in the NMR spectrum.

In both cases guest **51** was the strongest binder. Aside from the fact that it is one of the most saturated guests, it is compact and pre-organised: there are no available degrees of freedom for it to change its shape upon binding. The strength of binding of **51** came as no surprise, since, short of having a halogen to anchor the guest to the bottom of the host, adamantan-1-yl derivatives almost always bind on the order of 10^6 M^{-1} to **30**. All host–guest pairs gave an appreciably measurable binding affinity, save for **44**∈**39**. Based on the binding of **51** to **39** which was approximately one order of magnitude weaker than that to **30**, we predicted that the other guests would bind weaker to **39** by at least one order of magnitude.

The binding of the anionic guests to **30** is stronger than to **39** ($\langle \Delta G \rangle_{\ominus}^{\mathbf{30}}$ = –28.0 kJ mol^{-1}, $\langle \Delta G \rangle_{\ominus}^{\mathbf{39}}$ = –9.1 kJ mol^{-1}). This follows intuition in the sense that the negative charges on the portal of **39** should weaken binding of carboxylate guests **44**–**47**. However, one might expect that electronic repulsion should turn off binding to **39** completely; this is not the case. Combining the argument of electrostatic repulsion and guest flexibility it is no surprise that **44** is the weakest

binding guest to **39**. Indeed, the binding is either non-existent or so weak that it is below the limit of detection for NMR spectroscopy (≤ 5 M^{-1}).[74, 110] The fact that binding negatively-charged guests to **39** is not switched off points to what could very likely be either a charge attenuation or charge screening effect. It has been well-established that cations such as Na$^+$ and Li$^+$ can condense onto carboxylates.[229-231] This can cause a net charge decrease on the carboxylates, reducing Coulombic screening that attenuates anion binding, and allowing the hydrophobic effect to dominate binding. Regarding the former, the Bjerrum attenuation can be invoked. Carboxylates are highly solvated, with a $\Delta G_{\text{hydr}}^{\text{COO}^-} = -$374 kJ mol^{-1}, and thus, charge–charge interactions between two carboxylates are attenuated in solution. The distance from the C_4 axis of **39** to one of the *exo–*carboxylates is ~6.1 Å, just shy of the Bjerrum length in water (~7.5 Å at 298 K) this effect is more pronounced in the binding of the ammoniums to **39** ($\langle \Delta G \rangle_{\oplus}^{\textbf{30}} = $–25.1 kJ mol^{-1}, $\langle \Delta G \rangle_{\oplus}^{\textbf{39}} = $–27.2 kJ mol^{-1}). Intuitively, because the charged guest headgroup is that much closer to the carboxylates on **39** than to **30**, the expectation would be that the binding would be much stronger than a difference of ~2.1 kJ mol^{-1}. Thus, the effect of moving the carboxylates from the *peri-* to the *exo-* positions only marginally affect the binding of charged guests. This stark asymmetry is more clearly shown in Fig. 42.
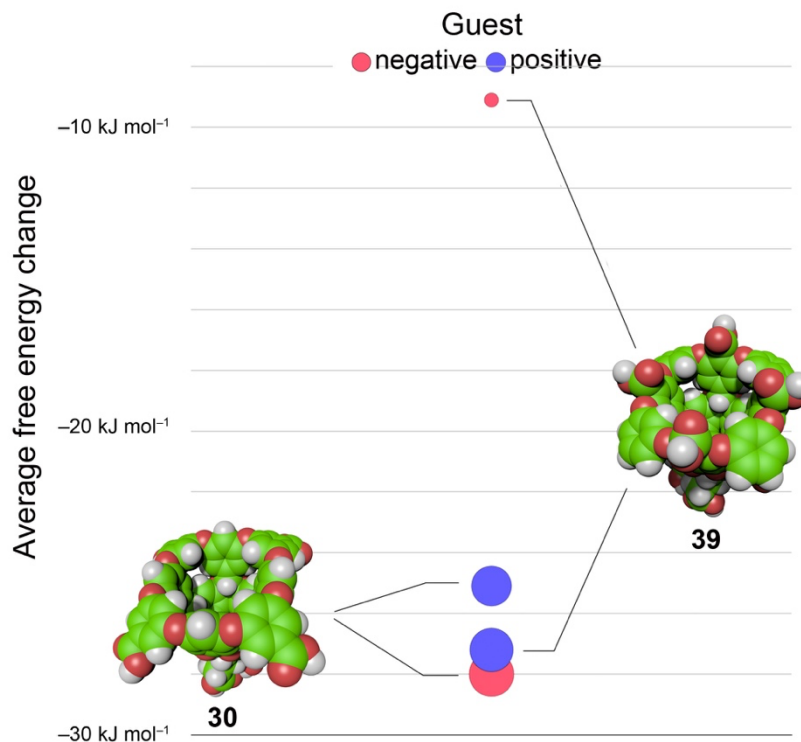
Fig. 42: Differences in the average free energy change ($\langle \Delta G \rangle$) of binding of negative (red circles, **44–47**), and positive (blue circles, **48–51**) guests to **30** and **39**. Both the position on the vertical axis and the circle diameters correspond to the magnitude of the average free energy complexation. Image courtesy of BCG.

To ascertain what other phenomena may be coming into play in the binding of carboxylates to **39**, MD simulations were performed in collaboration with Henry Ashbaugh and Yang Wang (Tulane Department of Chemical and Biomolecular Engineering). This was driven by the hypothesis that because carboxylates are highly solvated, the presence of these groups at the *exo-* position proximal to the portal of the pocket must be increasing the solvation of the cavity of **39** relative to **30**. In addition, a theoretical host tri-*exo*-mono-*endo*-octa-acid **52** was simulated to probe whether increasing the proximity of the charged groups to the concavity would induce better solvation (Fig. 43). Simulations show that in all three hosts, the probability of finding the same number of water molecules within the pocket

is the same, i.e., in equilibrium there are on average four water molecules within the pockets at any one time. Since there is practically no difference in the solvation of the pockets, the next logical step would be to probe the energy required to dehydrate the pockets. The difference in energy required to dry out **39** is not that different to **30** (~1 k_BT, or ca. 2.5 kJ mol^{-1} at 298 K), which means there is a net stabilisation of the water network within **39**. However, because of the inward pointing carboxylate in **52**, the energy difference relative to **30** becomes much greater by ~4 k_BT (~10 kJ mol^{-1} at 298 K).
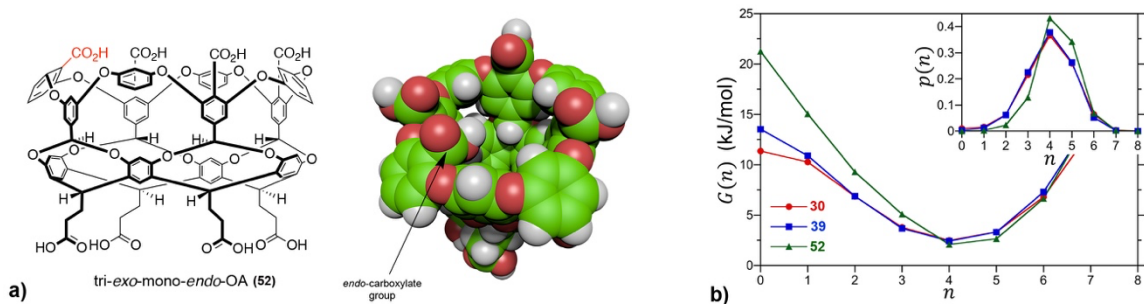
Fig. 43: a) Chemical structure and space-filling model of theoretical host tri-*exo*-mono-*endo*-OA **52**. The unique *endo*-carboxylate in indicated in red in the former and by an arrow in the latter. b) Free energies for observing n waters within the non-polar pockets of **30**, **39** and **52**. The probabilities, $p(n)$, of observing n waters within the pocket are reported in the inset. The free energy is determined from the probability as, $G(n) = -RT \ln p(n)$, which corresponds to the free energy required to constrain the pocket to contain only n waters. In the case of guest binding the empty pocket ($n = 0$) is the most important state to consider. The error bars in the simulation data are comparable to or smaller than the figure symbols. The maximum error estimate across all hosts for the free energy of emptying a cavitand, $G(0)$, is ±0.4 kJ mol^{-1}.

This series of experiments does not give the full picture as to why the affinity of different guests vary but results point to two main facts: 1) the position of the charges influence the strength of binding directly via Coulombic attraction or repulsion and changes in counterion condensation; and 2) charges closer to the portal of a weakly hydrated cavity indirectly affect binding by changing the hydrogen bonding network of waters in the cavity. In other words, only

considering Coulomb's law and host-guest attraction or repulsion does not give a full picture; the binding free energy to **39** is only ca. 70% of what is expected if Coulomb's law dominates. However, there may be myriad other non-covalent interactions behind the binding that may be affecting free energies. Does the effect of the charge go beyond only a few atoms beyond the charge carrier? If it does, then will simulating a more charge-diffuse host, or indeed synthesising a more charge-concentrated host, give more insight to the other interactions taking place? More studies need to be performed, and more hosts need to be synthesised in order to probe such scenarios.

From dry to arid: SAMPL8

Deep calleth on deep, at the noise of your flood-gates. (Ps 41:8, Douay–Rheims Bible, 1609)

The presence of static alkyl groups at the portal of a cavity can induce a drying transition in water. This can be shown using physical experiments such as ITC where the binding of amphiphilic guests to **37** is stronger than in **30**. MD simulations also show that **37** is dry and vacuous contrary to natural intuition about synthetic cavities in solution.[81-84, 188]

To further probe the effect of evacuating and dehydrating pockets, tetra-*endo*-ethyl octa-acid **53** was developed. Much like **37**, the cavitand's portal is lined with alkyl groups, but as the name suggests, with ethyls instead of methyls.

This change induces 1) host flexibility since the ethyl groups can point either into or out of the pocket and can introduce an induced-fit mode of guest binding; and 2) the shape of the pocket is changed because the ethyl groups occupy space within the pocket itself.

The synthesis of **53** begins with chemistries that form the weaving reagent for the Ullmann biaryl-ether condensation (Fig. 44). First, using known chemistries, 3,4,5-trimethoxybenzaldehyde was converted to the dimethyl acetal **54** using trimethyl orthoformate in benzene using *p*-toluenesulfonic acid as a catalyst at quantitative yields.[232, 233] Acetal **54** was then subjected to a reductive metalation using elemental sodium which selectively removes the methoxy group at the 4- position to form a natriated anion. This is a modification of a directed *ortho*- metalation, where the adjacent methoxy groups direct the position of, and chelate, the sodium cation. This deep red-coloured anion was then quenched with ethyl bromide to alkylate the 4- position, and the reaction is quenched with aqueous HCl to remove any unreacted elemental sodium and to regenerate the aldehyde.[234] This reaction gave a 7:3 mixture of the alkylated/protonated products which were chromatographically separated to isolate 4-ethyl-3,5-dimethoxybenzaldehyde **55**. Compound **55** was then subjected to a triphasic Baeyer–Villeger oxidation using Oxone[§§] as the oxidant to form the benzoic acid **56** in high yields. This oxidation selectively oxidised the aldehyde to the acid without affecting the available benzylic position in the way that $KMnO_4$ or MnO_2

[§§] Oxone® is 2:1:1 potassium peroxysulfate ($KOSO_3OH$)/potassium hydrogen sulfate ($KHSO_4$)/potassium sulfate (K_2SO_4).

would. Compound **56** was then subjected to a double de-etherification reaction using BBr$_3$ to free the phenols, and the resulting dihydroxy acid **57** was subjected to a reduction using H$_3$B·SMe$_2$ complex to form the benzyl alcohol **58**.

To form the basket, an Ullmann biaryl-ether coupling was performed between **58** and known octa-bromide **32** in refluxing pyridine in the presence of K$_2$CO$_3$ and CuBr·SMe$_3$ as a catalyst. This reaction afforded crude **59** in moderate yields. Serendipitously, **59** precipitated out of solution during the workup as a high purity micaceous solid. This cavitand could then be further purified using chromatography via its octa-acetate ester **60** and subsequent hydrolysis to pure **59**. However, operationally, crude **59** can be taken to the next step without purification. Octol **59** was then oxidised to crude **53** using KMnO$_4$ at elevated temperatures and was then purified using chromatography via its octa ethyl ester **61**, and subsequent base hydrolysis.
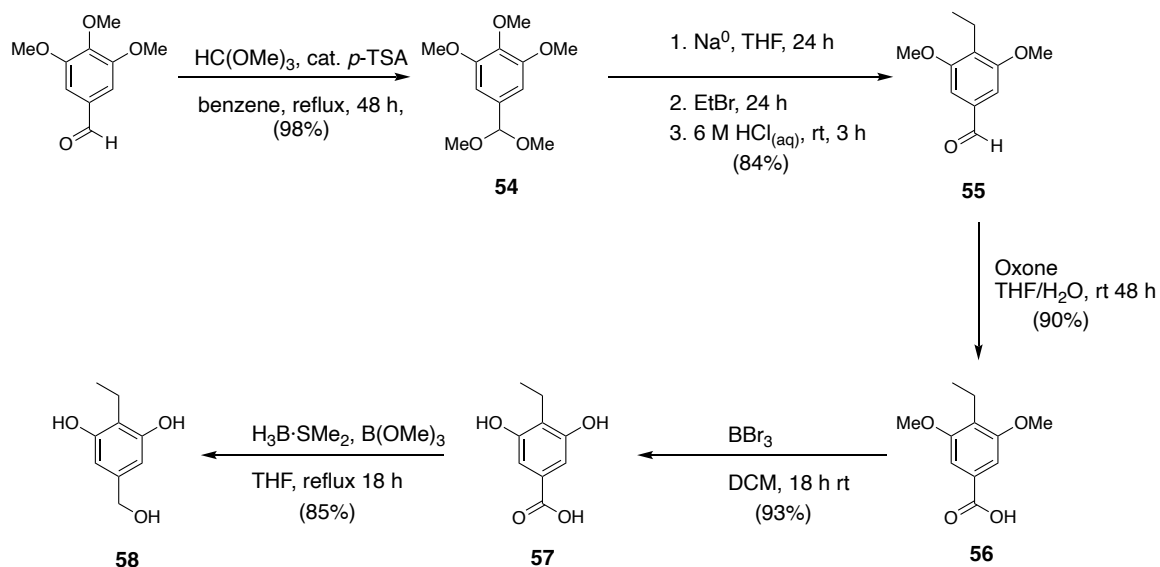
Fig. 44: Synthesis of Ullmann "weaving" compound **58** from 3,4,5-trimethoxybenzaldehyde.
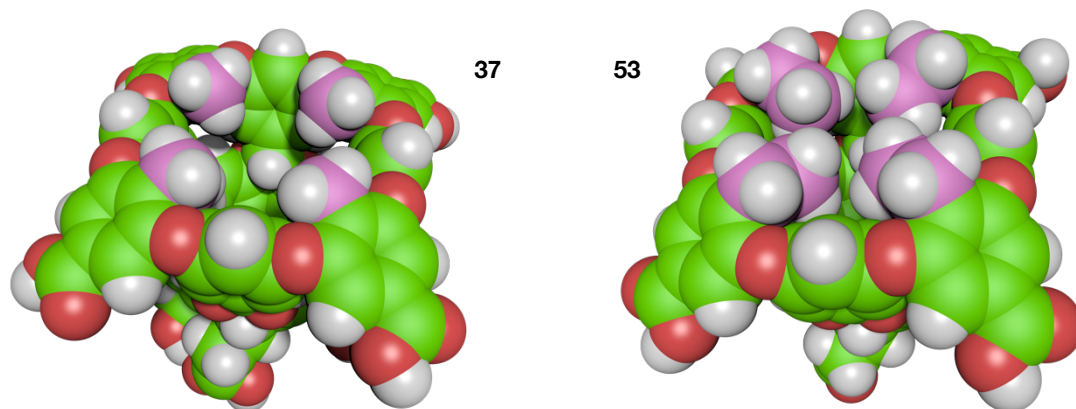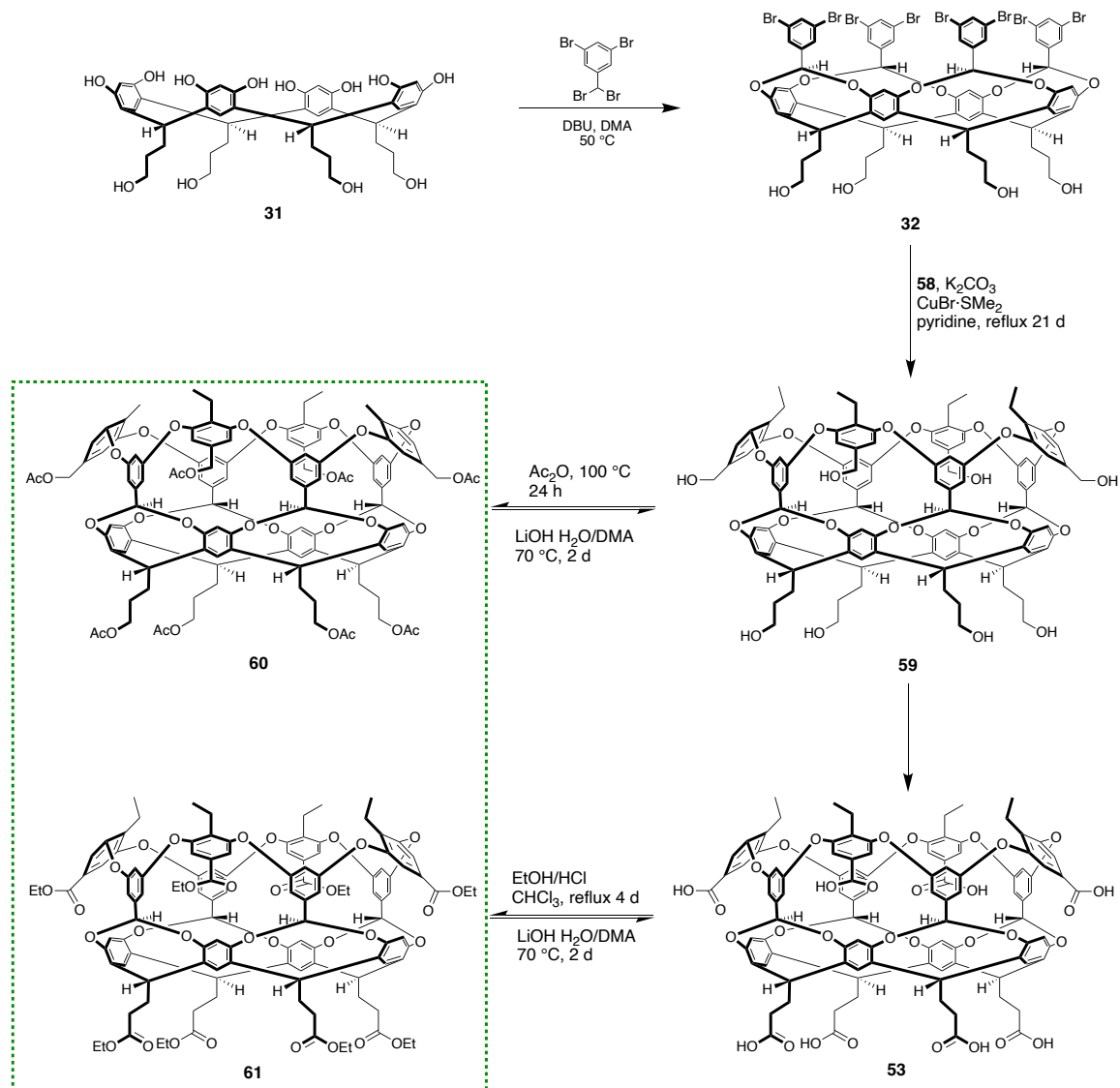
Fig. 45: (*top*) Synthetic path towards tetra-*endo*-ethyl octa-acid **53** starting from resorcinarene **31**. Purification steps are performed on compounds in the green dashed box. (*bottom*) Space filling structures of **37** and **53**, with the alkyl groups at the portal highlighted in pink. Green: carbon; pink: portal alkyl carbons; white: hydrogen; red: oxygen. Images rendered using ePMV for Cinema 4D.

Modelling suggests that the ethyl groups are free to rotate between the 'in' and 'out' positions with a relatively low barrier. To probe this, variable-temperature NMR (VT NMR) spectroscopy was performed on a 1 mM sample of **53** in 10 mM pD 11.5 phosphate-buffered D_2O (Fig. 46). A standard ^1H NMR spectrum was taken as the temperature was increased gradually from 5–60 °C and the peak shifts as a function of temperature observed. The signals corresponding to the pendent inward-pointing ethyl groups, particularly the terminal methyl designated as $H_{c''}$, became progressively more deshielded ($\delta \rightarrow +\infty$), and the attached methylene designated $H_{c'}$, became progressively more shielded ($\delta \rightarrow -\infty$). This points to the ease at which the ethyl groups rotate and exchange between the 'in' and 'out' conformations (the out conformation designated as **53-4o**). The broadness of $H_{c''}$, $H_{c'}$, H_b, and H_d indicate a moderate to fast exchange between the conformers at the time scale of the NMR experiment.[106, 107, 109] At 23 °C H_b and H_d sharpen compared to at 5 °C, but $H_{c''}$, $H_{c'}$ still retain their broad linewidths.*** At 55 °C all peaks not only shift but also resolve to a sharp triplet and a sharp quartet, respectively. It is noteworthy that as the temperature was raised, the $H_{c'}$ and the $H_{c''}$ signals indicated a deshielding of the protons that were distinct from the mean temperature-dependent chemical shift of the protons distal to the $H_{c'}$ and $H_{c''}$. Although the temperature does influence the chemical shift of all host signals, the change in conformational preference of

---

*** The linewidth-at-half-height is defined to be $\Delta_{\frac{1}{2}} = \frac{2}{T_2^*}$ with $T_2^* = \frac{\gamma \Delta B_0}{2} + \frac{1}{T_2}$, where the first term stands for the magnetic field inhomogeneity contribution to the linewidth, and the second term is the true transverse relaxation. The most common T_2 relaxation mechanism is via molecular/group motion: slow movement shortens T_2 relaxation and broadens lines; the contrapositive is true.

the ethyl groups has an additional influence to the shielding. This is consistent with the idea that the frequency difference between the in and out positions is considerable, and that **53-4o** is the higher energy conformer that becomes more prevalent with increasing kinetic energy.
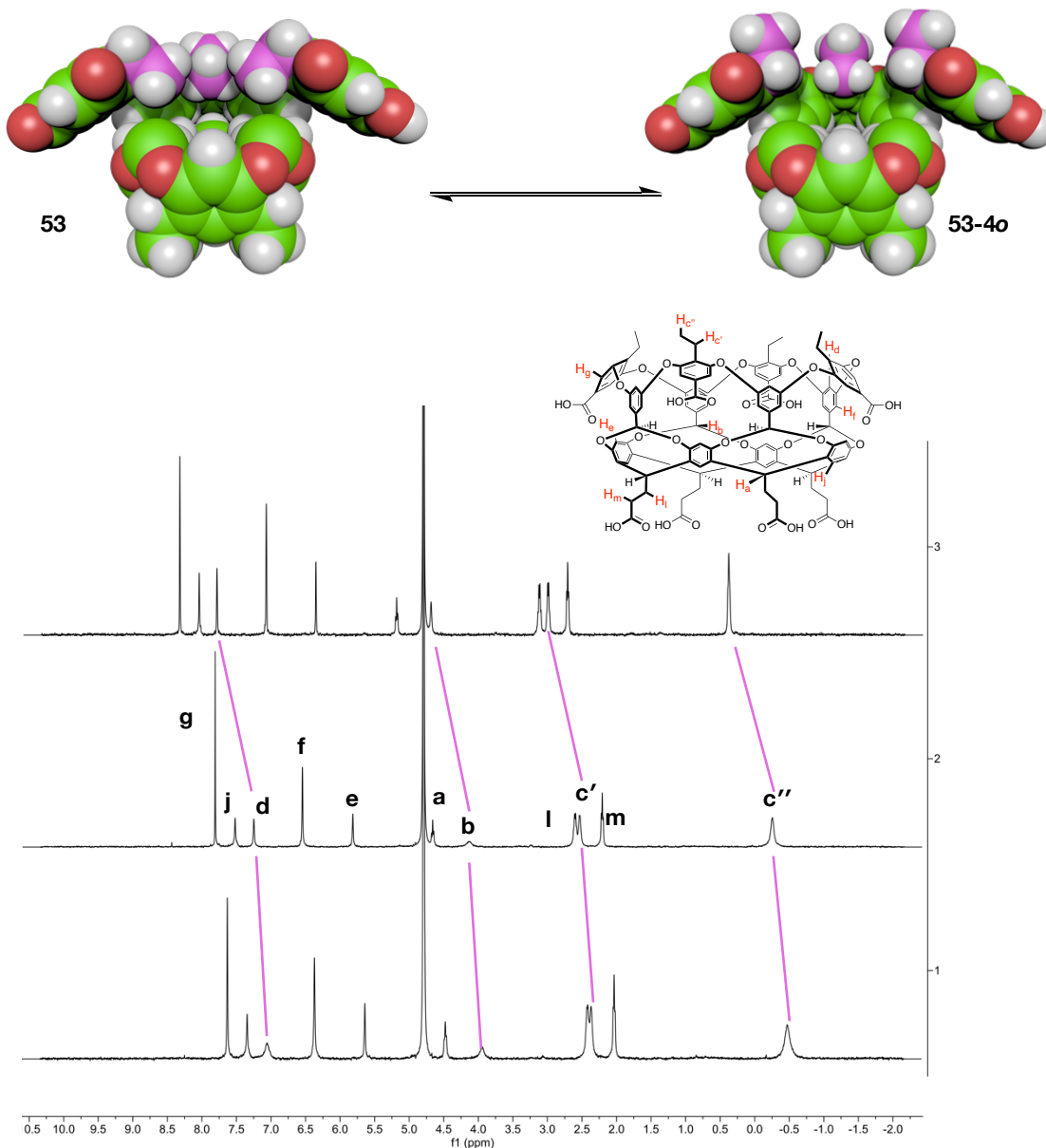
Fig. 46: (*above*) Space-filling models of **53** (with cut-away) showing equilibrium between the 'in' and 'out' conformations of the ethyl rim groups. Pendent propanoate feet have been truncated to methyls for clarity. (*below*) Selected VT ^{1}H NMR spectra of the host in 10 mM pD 11.45 phosphate-buffered D_2O: 5 °C (*bottom*), 23 °C (*mid*), 55 °C (*top*).
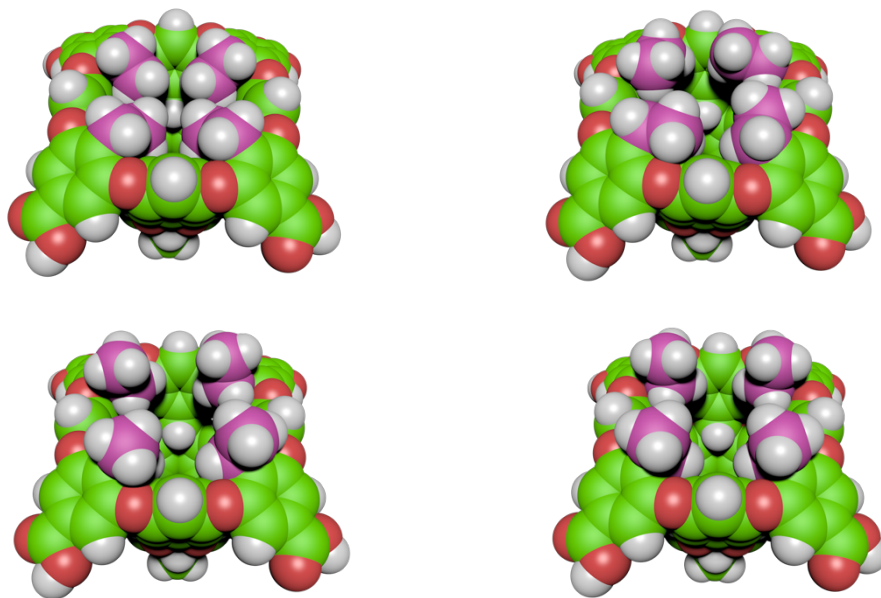
Fig. 47: (*left to right, top to bottom*): Representative van der Waals structures of the theoretical methyl-footed variant of **53** at different critical points in the energy profile as the four ethyl groups are simultaneously rotated out of the pocket: 0°, 80°, 160°, and 180°. The ethyl groups undergoing rotation are highlighted in pink for clarity. van der Waals structures are generated using ePMV for Cinema 4D.

To probe this further, gas-phase studies using the semi-empirical Parametric Method 6 (PM6)[1, 235] were performed on a theoretical variant of **53** (Fig 47) where the pendent propanoate feet were truncated to methyls. The ethyl groups were then rotated unidirectionally, and the free energy of formation was measured every 5° of rotation from the zero point (ethyl in) through to 180° (ethyl out), and back to 360° (Fig. 48). As expected, there is a barrier to rotation of the ethyl groups from in to out that costs $\Delta G^{\ddagger} = 46.5$ kJ mol^{-1} due to the sterics inherent to the position of the ethyl groups. This barrier is the same as the bowl-to-bowl inversion exchange energy in corannulene ($T_{coal} = -67$ °C)[236] and the
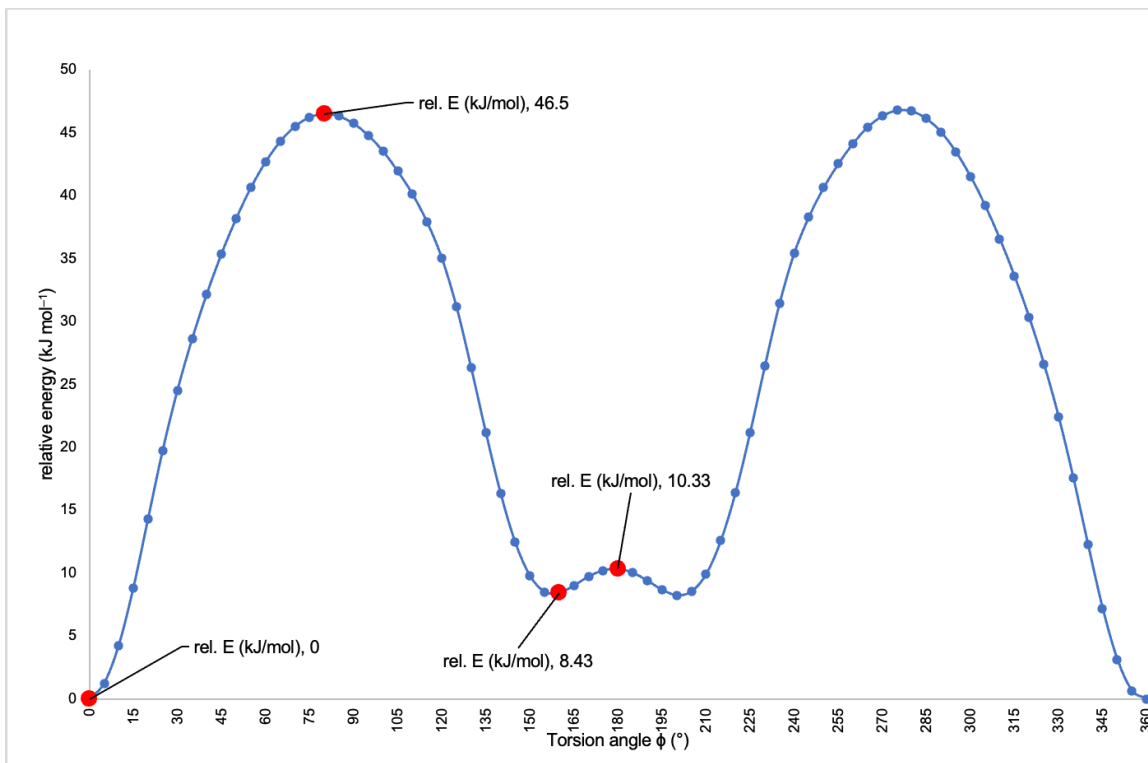
Fig. 48: Plot of relative energies of the theoretical methyl-footed variant of **53** versus torsion angle φ in degrees, with critical points highlighted in red and called out with their individual values.

cyclohexane ring inversion energy in cyclohexane (T_{coal} = –80 °C)[164] as observed by NMR spectroscopy. It is noteworthy that the local minimum of the potential energy profile is not at the point where the ethyl groups are 180° relative to the starting point, but instead it occurs at ca. 160° where the ethyl groups are just resting on the rim of the cavitand. This is presumably a stabilisation brought about by the increase in the intramolecular van der Waals interactions at this point in the energy profile. The free energy difference between all 'in' and all 'out' was calculated to be ΔG = 10.3 kJ mol^{-1}. If only one ethyl is rotated, i.e., **53** → **53-1o**, a free energy difference of ΔG = 2.17 kJ mol^{-1} was found, with a barrier of $\Delta G^{\ddagger}$ = 11.4 kJ mol^{-1}. This barrier is significantly lower than the rotation of the ethyl moiety

in ethylbenzene which was calculated to be 4 kJ mol^{-1}. Nevertheless, this corresponds to a coalescence temperature $T_{coal} < 200$ °C which is well below the freezing point of D_2O (~3 °C). The line broadening of H_b, $H_{c'}$, and $H_{c'}$ suggests that the barrier to rotation of the ethyl groups would be significantly higher in water than it is in vacuum. However, the evidence given by both gas phase analyses and VT NMR spectroscopy point to the fact that the ethyl groups are free to rotate.

62, 3-hydroxy-2-naphthoic acid

63, p-bromophenol

64, cyclopentylacetic acid

65, piperonylic acid

66, p-toluic acid
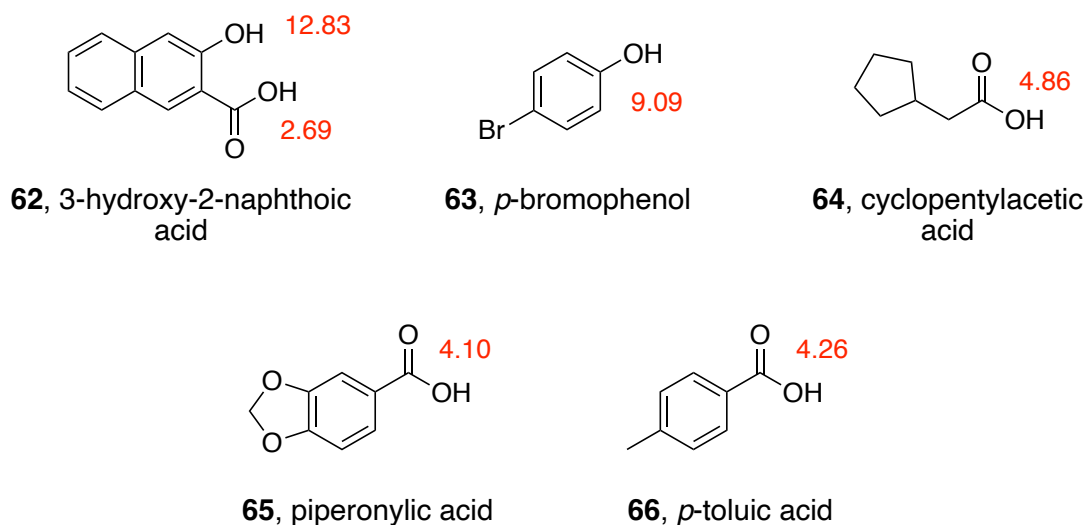
Fig. 49: Guests used in the SAMPL8 exercise. $pK_a^{H_2O}$ values of the ionisable protons are in red text and were calculated using Chemicalize by ChemAxon.

For the 8th Statistical Assessment of the Modeling of Proteins and Ligands (SAMPL8), the thermodynamics of binding of five guests (Fig. 49) to hosts **37** and **53** was probed using ITC (and for very weak binders, NMR spectroscopy). At experimental conditions (~25 °C, 10 mM pH 11.5 phosphate-buffered water) both hosts are soluble just like parent cavitand **30**, and all guests are deprotonated and thus anionic. Guest exchange was found to be fast but bordering on the time

scale of the NMR experiment in a 11.75 T (500 MHz) external magnetic field, as evinced by the broad, ill-defined guest peaks in the NMR spectra, whose shifts were quite large. On the other hand, the shifts of the resonances for $H_{c'}$ and $H_{c''}$ were smaller but still well-resolved. Indeed, at saturation, $H_{c'}$ was shielded, and $H_{c''}$ becomes deshielded ($\Delta\delta$ –0.48 and +0.98, respectively, in the binding event between **63** and **53**). In the resting state of **53** where all the ethyl groups are pointing inwards, the pocket is too small for any of the guests to bind. As such, during the binding event at least one ethyl group must turn outwards for the pocket to accommodate the guest. Thus, the signal shifts of $H_{c'}$ and $H_{c''}$ can be attributed to the conformational change from out to in during the binding events.

As with SAMPL7, ITC was used to obtain the thermodynamic parameters of the binding of guests **62**–**66** to hosts **37** and **53**. The data obtained are summarised in Table 13. In two out of ten triplicated determinations (**64**∈**53** and **66**∈**53**) the binding affinities were too low to be determined by ITC. Thus, titrations tracked via ^{1}H NMR spectroscopy was used as an alternative to ascertain binding strength. Although the attempt was successful in the case of **66**∈**53**, **64**∈**53** was still too weak and could not be determined by either technique.

Guest	TEMOA (37)				TEEtOA (53)			
	$\log_{10} K_a$	ΔG (kJ mol^{-1})	ΔH (kJ mol^{-1})	$-T\Delta S$ (kJ mol^{-1})	$\log_{10} K_a$	ΔG (kJ mol^{-1})	ΔH (kJ mol^{-1})	$-T\Delta S$ (kJ mol^{-1})
62	5.1	−29.1 ± 0.2	−72.1 ± 5.3	42.1 ± 5.1	3.3	−13.8 ± 0.2	−57.1 ± 0.7	38.3 ± 0.6
63	6.2	−35.2 ± 0.1	−65.6 ± 1.0	30.3 ± 1.0	3.8	−21.6 ± 0.1	−48.7 ± 1.2	27.2 ± 1.1
64	4.2	−24.2 ± 0.1	−33.2 ± 1.0	9.0 ± 0.8	—[b]	—[b]	—[b]	—[b]
65	5.7	−32.3 ± 0.1	−74.1 ± 1.4	41.8 ± 1.3	3.3	−18.7 ± 0.2	−54.3 ± 3.6	35.6 ± 3.4
66	4.9	−27.9 ± 0.1	−59.6 ± 3.2	31.7 ± 3.1	2.4	−13.9 ± 0.1[c]	—	—

Table 13: Thermodynamic data[a] from ITC and/or NMR for the binding of guests **62–66** with hosts TEMOA **37** and TEEtOA **53**. All titrations were performed in 10 mM phosphate buffer at pH 11.5., and equilibrated at 25 °C

[a] The ΔH and K_a values were obtained by carrying out at least three separate experiments, averaging each set of data, and calculating the respective standard deviations. ΔG was obtained from K_a via the standard thermodynamic equation. The average ΔH and ΔG values were then used to calculate an average $-T\Delta S$, and the corresponding standard deviations calculated using the standard equation for the propagation of uncertainties for subtraction. The deviations of ΔG were obtained by using the standard equation for the propagation of uncertainties for logarithms. The errors in $\log_{10} K_a$ are smaller than what is significant.
[b] Binding is too weak to be observed by NMR or ITC. Based on the difference in the average free energy of complexation to both hosts ($\langle\Delta\Delta G\rangle$ = 12.9 kJ mol^{-1}) and the value for **64** binding to **37**, an affinity maximum to **64** binding to **53** can be estimated to be approximately −10 kJ mol^{-1} or $K_a \lesssim 60$ M^{-1}.
[c] Determined by ^{1}H NMR spectroscopy

Ranking guests by increasing binding free energy ΔG yields **64** < **66** < **62**, **65** < **63**. All binding events were enthalpically driven, i.e., exothermic with $|\Delta H| > |T\Delta S|$. This signature for the non-classical hydrophobic effect is seen for most binding events that involve an apolar concavity because of the poorly solvated pocket. This in turn translates to a lack of competition of the guest with water for the binding site, and maximises all other non-covalent interactions, such as dipole–dipole, π–π stacking, dispersion forces, and C-H···X hydrogen bonding. Indeed, the strongest binder in the series, **64**, has a pendent bromine atom which has been shown to drive the binding via C-H···X hydrogen bonding to the H_b atoms of the two hosts.[170] This is evinced by the strong enthalpic contribution to the free energy of binding of **64** to both hosts and the significant shift in H_b ($\Delta\delta$ = 0.52 ppm).

The strength of binding of the next strongest guest in the series, **66**, goes against intuition. The presence of the two ethereal oxygens composing the acetal in **66** was expected to increase solubility in water, and thus would engender weak binding. However, the presence of the acetal itself, with its highly electron-deficient methylene, drives its binding to the pockets of both hosts, presumably due to C-H···π interactions between the electron-deficient methylene and the electron-rich aromatic walls of the hosts. It was shown previously that the binding

of methyl esters drives the formation of host–guest complexes due to the same C-H···π interactions that anchor the methyl group to the bottom of the pocket.[197]

Salicyloid guest **62** has the largest non-polar surface area for dewetting during the binding event. This dewetting is evidently more significant than the energetic advantages of the anchoring of the methyl group in **66** to the base of the pocket. In contrast, the smallest, and weakest binder of the series is **64**, which is more water-soluble due to its size and contains no anchoring groups.

A comparison of the $\Delta\Delta G$ values for each guest binding to **37** and **53** shows an average difference of 12.9 ± 1.7 kJ mol^{-1}. This can be attributed to the energy required to flip the ethyl groups from 'out' to 'in' in order to accommodate any incoming guest (calculated to be 10.3 kJ mol^{-1}, *vide supra*). Because ITC and NMR only indirectly point to what is happening in solution, MD simulations were performed in collaboration with Henry Ashbaugh and Busayo Alagbe (Tulane Department of Chemical and Biomolecular Engineering) to visualise any interaction in solution between the host and water, host and guest, and guest and water. Specifically, the hydration state of **37** and **53** were probed, along with the

potential of mean force of the binding of **66∈53**, and the partial molar volume of both hosts.
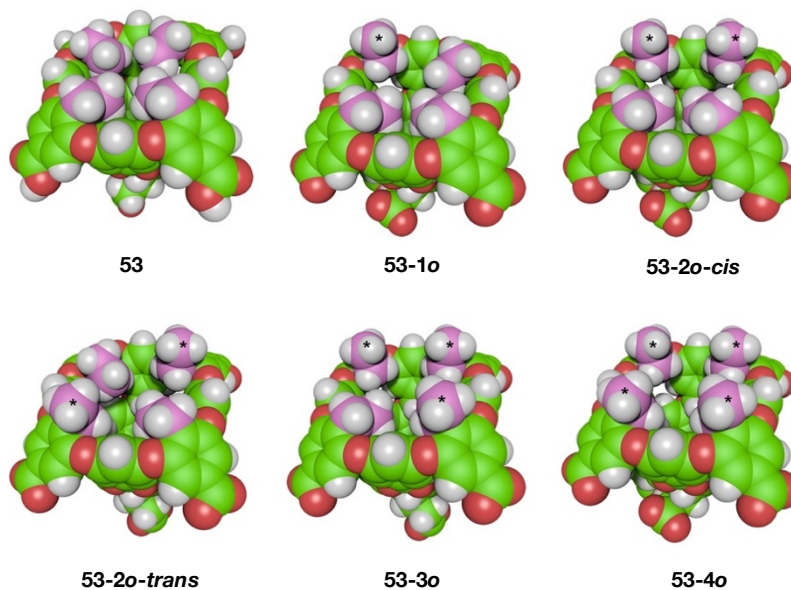
Fig. 50: Conformations of the rim ethyl groups of **53**. For clarity, the ethyl groups are highlighted in pink, with those oriented out of the pocket in each structure marked with *. *Top row*, *l-r*: four ethyls in (**53**), one ethyl out (**53-1o**), two adjacent ethyls out (**53-2o-cis**). *Bottom row*, *l-r*: two opposing ethyls out (**53-2o-trans**), three ethyls out (**53-3o**), and four ethyls out (**53-4o**).

    Host **53** can exist in six different rim conformations (Fig. 50): all ethyls in (**53**, host resting state), one ethyl out (**53-1o**), two adjacent ethyls in (**53-2o-cis**), two opposite ethyls out (**53-2o-trans**), three ethyls out (**53-3o**), and all ethyls out (**53-4o**). Intuition suggests that because the shape of the pocket in **53-4o** is similar

to **37** their hydration states would be similar, and that as ethyl groups were successively turned in, the pocket would be increasingly drier.
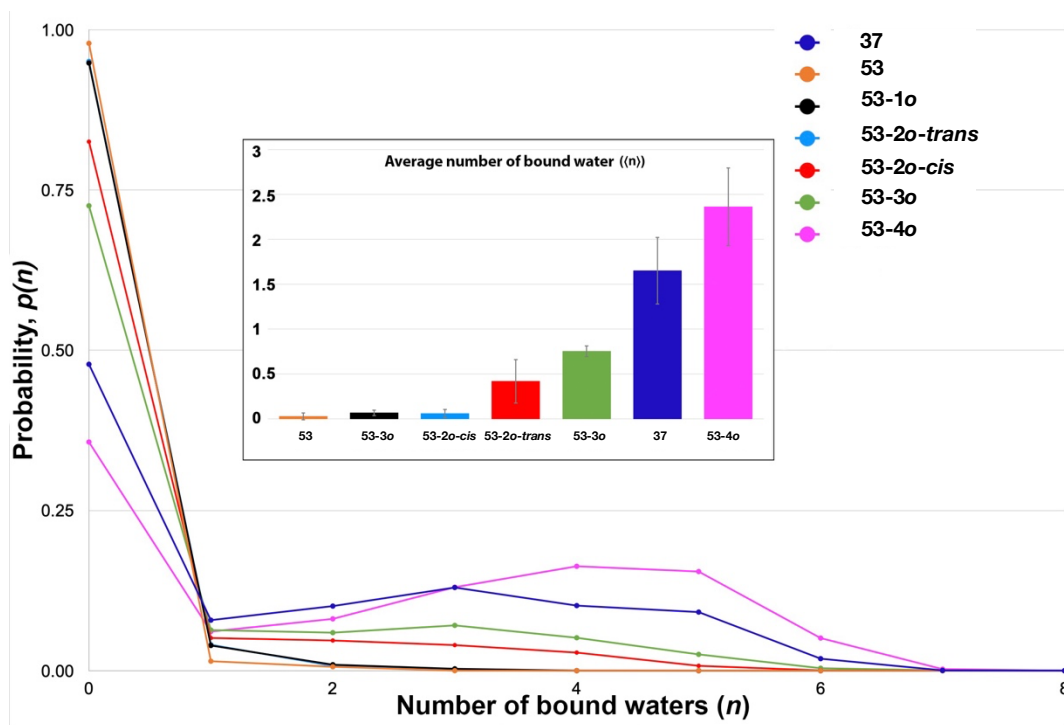
Fig. 51: Probability distribution of the hydration (number of water molecules, *n*) of the pockets of **37**, **53**, **53-1o**, **53-2o-trans**, **53-2o-cis**, **53-3o**, and **53-4o**. Error bars have been omitted for clarity. The probability distribution for **53-1o** and **53-2o-trans** are close enough that they appear overlaid. *Inset:* bar graph of the average hydration number ⟨*n*⟩ of each host.

To probe this, the pocket hydration states of every conformation was evaluated: the probability of finding *n* water molecules in the pocket was found, which was averaged to get the number of bound water molecules in equilibrium. Figure 51 shows a plot of the hydration states of both hosts and every conformer of **53**. Both **37** and **53-4o** show a bimodal distribution: there is a 48% and 36% chance, respectively, to find a vacuous, i.e., empty pocket; there is a 13% and

17% chance of finding three and four water molecules, respectively, to **37** and **53**. As expected, **53** in its resting state shows a unimodal distribution, with a ca. 96% chance of finding no waters in the pocket. There is then a continuum of increasing hydration from **53-1o** to **53-3o**: as each ethyl group adopts an 'out' conformation the probability of finding an evacuated pocket decreases from 96% to 48%, and the probability of the pocket filling with three water molecules increases from 0% to 17%. Models predict that **53-2o-trans** is drier than **53-2o-cis**, presumably because the opposing ethyl groups pointing inwards divide the pocket into two smaller pseudo-pockets, whereas two adjacent ethyls only create one.

Taking the weighed hydration average of each of the probabilities of hydration for each host and conformer gives the host/conformer's degree of hydration (Fig. 51 inset). From wettest to driest, the hosts can be ranked as follows: **53** ~ **53-1o** ~ **53-2o-trans**, **53-2o-cis**, **53-3o**, **37**, **53-4o**. The pockets of **53**, **53-1o**, **53-2o-trans** are, within error, the same hydration as one another; all three are vacuous in solution. Conformer **53-2o-cis** is wetter still than its *trans* counterpart because of reasons previously stated. Indeed, the one order of magnitude difference in hydration can be attributed to the fact that any bound water in **53-2o-cis** can hydrogen bond to one another and to the bulk, while waters in **53-2o-trans** cannot. Thus, water is a better guest for **53-2o-cis** because more than one can bind due to hydrogen bonding stabilisation. Turning one more ethyl group increases the hydration of the pocket, as expected. What is unexpected is the fact that, as a first approximation, **53-4o** is much wetter than

37 even though the shapes and volumes of the pockets are similar (283.1 ± 1.2 versus 280.5 ± 1.4 Å^3 for **53-4o** and **37** respectively). However, the error bars are large and that to see any differences in **53-4o** and **37** would require a much more powerful and a much longer simulation time than what is feasible.
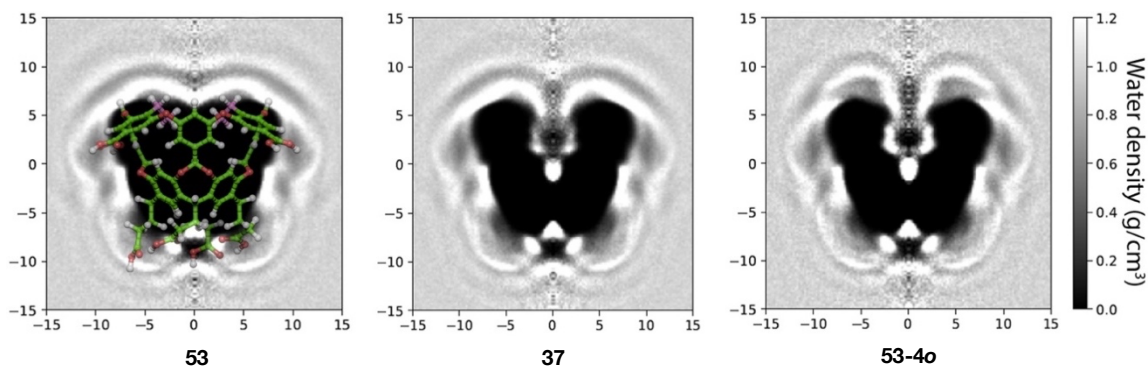
Fig. 52: Water density maps about **53**, **37**, and **53-4o**. The general orientation of the host in the three images is highlighted for host **53**. Each figure representing a cross-section of the cavitand (at 25 °C and 1 bar). The densities are cylindrically averaged around the C_4 axes of each host and are reported in greyscale, with the very high electron density (cross-section) of each host masked out in black. The unsolvated pocket of **53** also appears in black

The degree of hydration of the hosts can be translated into water density maps— images of the average hydration in and around the pocket of the hosts that have been cylindrically averaged about the idealised C_4 axes of the hosts (Fig. 52). The maps were generated for **37**, **53**, and **53-4o**. Each image shows a cross section of the host with the locations of the oxygen atoms of water shown in greyscale. In each image, the high electron density of the cross section of each host is masked out in black. As expected, the interior of **53** is completely dark, i.e., completely devoid of water, while there is some electron density residing within the interior of **37** localised around the ethereal oxygens at the rim and at

the very bottom of the pocket. The same is true about **53-4o**, although the density

of water is slightly higher.
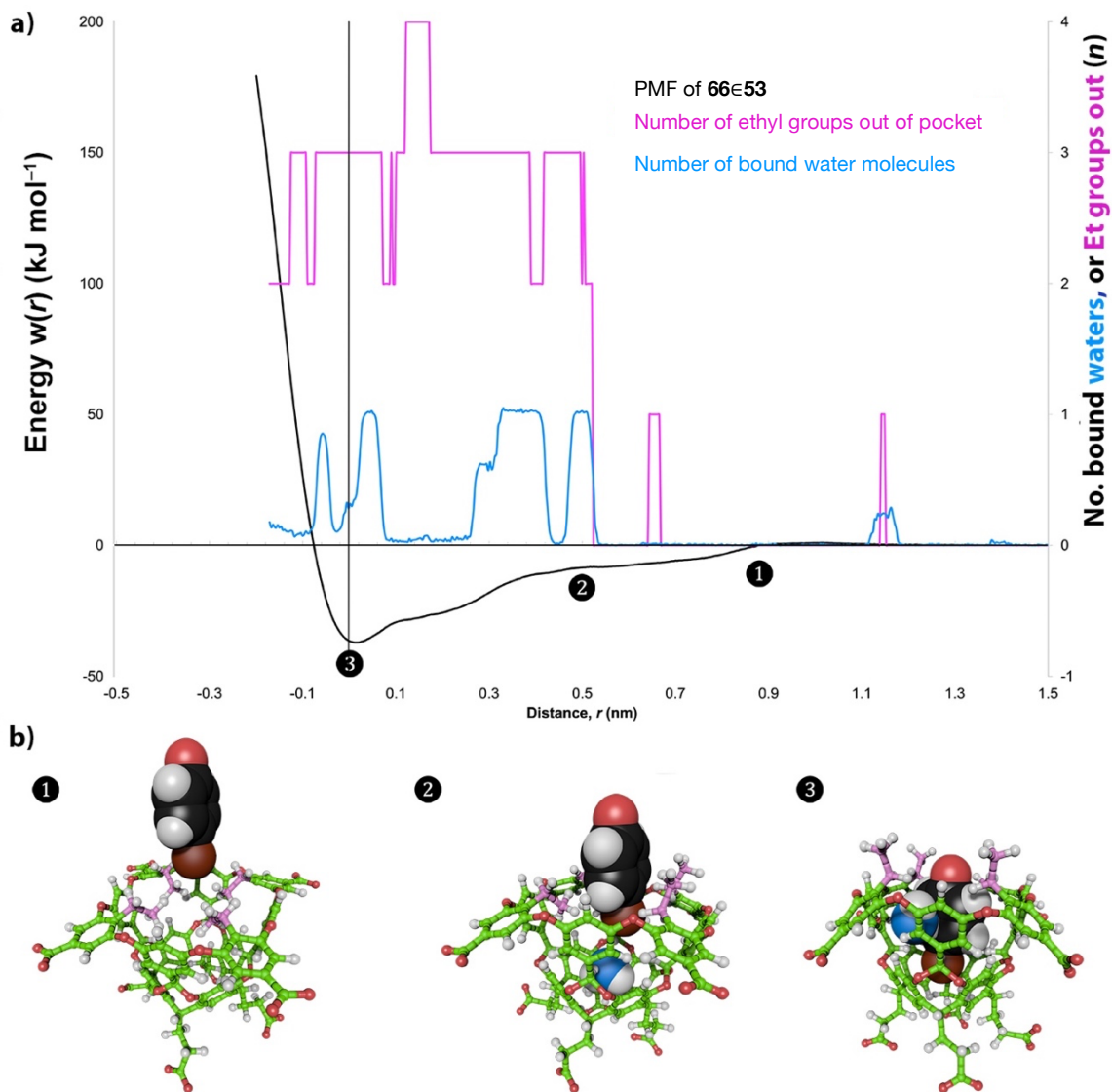
Fig. 53: Detailed mechanism for the formation of the complex between **53** and **66** calculated from simulations of the host, guest, and complex solvated by 2,500 water molecules. a) In this graph the x-axis shows the depth of the guest as it is inserted into the host. The potential of mean force (PMF, left y-axis) is shown as a black curve with a minimum at 0 nm. Superimposed on this plot is the number of ethyl groups in the host pointing out (pink line and right y-axis), along with the average number of bound waters (blue line and right y-axis). The data are taken from 10,000 saved configurations from the simulation. The indicated points on the PMF curve (❶, ❷, and ❸) correspond to the structures shown below in; b) Structures ❶, ❷, and ❸ showing the positions of **66** relative to **53** at the indicated points on the PMF profile. In the three structures, the flexible ethyl groups are highlighted in pink, and any bound water molecules shown in blue

As mentioned, and as intuition would dictate, for a guest to bind to the pocket of **53** the ethyl groups must move out of the way of the guest, swinging outwards to do so. The pocket hydration of **53**, as seen above, is very sensitive to the orientations of the ethyl groups, and thus the relationships between the conformation, pocket hydration, and guest complexation was probed with further MD simulations. The PMF of the **63∈53** complex was obtained, along with the number of water molecules in the pocket and the number of outwards-pointing ethyl groups during the binding event. The PMF (the calculated free energy of complexation) was found to be –30 kJ mol^{-1} (~12 RT)— a number complementary to the experimental value of –21.6 kJ mol^{-1}.

Figure 53 shows the PMF profile for this complexation (black line), with $r = 0$ defined as a dummy atom where the C_4 axis intercepts the plane defined by the centers of the four benzylic carbons to which the H_a protons are attached. In general, the PMF landscape is uneven compared to that of guest binding to a similar host devoid of ethyl groups.[220] As the guest approaches the portal of the pocket ($r \geq 0.9$ nm, ❶) the host is in its resting state with the four ethyl groups oriented into the pocket (pink line in Figure 53a; ethyls highlighted in pink in Figure 53b). During this segment of the simulation, only very occasionally were the ethyl groups observed to flip outward to give the **53-3o** state (Figure 53a). As expected, the pocket is essentially dry (blue line in Figure 53a) in this conformation.

As the guest begins to enter the pocket ($r \approx 0.5$ nm, ❷) three ethyl groups move out of the cavity. There are occasional fluctuations to the **53-2o** and the **53-**

4o states, but to a first approximation the switch from the **53** conformation to the **53-3o** conformation is complete. Presumably, the fourth ethyl group does not have to swing out because of the slim nature of the guest. As the guest is entering the cavity, a water molecule (Figure 53a) slips in to occupy the void at the very base of the pocket (Figure 53b, c.f. water density in Figure 52). The switching from a dry cavity to one with a bound water suggests that wetting represents a thermodynamic minimum, but higher levels of sampling are required to accurately determine this. Regardless, most snapshots have this guest water oriented as shown in Figure 53b, acting as a double hydrogen bond donor to two opposing aromatic rings in the wall of the pocket. Here, the guest water has little option but to only hydrogen bond with the host, at least transiently until the slower binding **66** 'catches up'.

As guest **66** binds completely into the pocket ($r \approx 0$, ❸) the bound water is pushed out of the bottom of the pocket; the hydrogen bonding between it and the host is no thermodynamic match for the formation of four X···H–C hydrogen bonds between **66** and the H_b atoms of the cavitand.[170] However, this guest water does not entirely vacate the pocket. As Figure 53a and 53b shows, frequently one water molecule can be found in the pocket bound with **66**, sandwiched between the aromatic face of the guest and the aromatic wall of the pocket. Labeling the bound water in structure ❷ reveals that ~90% of the time it translocates to the upper section of the pocket as **66** docks. In other words, in most saved configurations the bound water in structure ❷ and ❸ are one and the same. Presumably the

bound water in ❸ is stabilized by both hydrogen bonding to the bulk, and its weaker dangling hydrogen bonding to the wall of the host and the aromatic ring of **66**. However, an estimation of its precise thermodynamic stability would require much longer simulations to obtain accurate exchange kinetics with water in the bulk. What is clear however is that in the case of **66** (and presumably the other aromatic guests), the pocket of the host is wetter when it binds a guest than when it is empty; the bound water is integral to the stability of the host-guest complex. The final stages of **66** binding result in little change in the conformations of the ethyl groups (Figure 53b); barring the occasional flipping of one ethyl group into or out of the pocket, the dominant form is the **53-3o** conformation. Thus, in the bound state the pocket of host **53** is occupied by **66**, a water, and one of its ethyl groups.
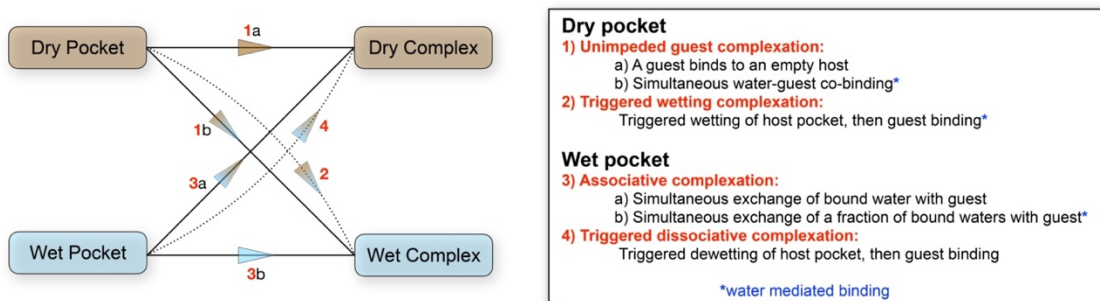
Fig. 54: Mechanisms for host–guest complexation in aqueous solution, treating dry and wet hosts separately for simplicity.

This, naturally, leads to the following question: what are the mechanisms for binding to rigid hosts, and does **53** fall into any of them? One can envision a dichotomy of complexes that involve water, and those that don't.

In a completely dry pocket, a guest can bind without being impeded by competition by water. This is the simplest case, and quite possibly theoretical (Fig. 55-1a). On the other hand, there may also be the case where a fully solvated guest brings in part of its solvation shell into the completely dry host to form a wet complex from a dry host (Fig. 55-1b). A wetting of the complex may also be achieved by a triggered mechanism, where the approach of the guest induces a binding of water in the first step prior to the docking of the guest; the pocket remains wet on the inside along with guest forming a wet complex from a dry host (Fig. 55-2). This is the regime where the triggered wetting of **55** lies.

In a wet pocket, one can envision a pocket that contains some water molecules that are free to equilibrate between being free and bound to the cavity. For certain hosts that are tubular or toroidal, a guest may enter from one portal and push water out the other in an associative way much like an S_N2 process. This is an associative guest binding regime where there is a water–guest exchange (Fig. 55-3a). Note that not all of the water molecules have to displaced; the mechanism holds for situations where only a fraction of water molecules are pushed out of the cavity (Fig. 55-3b).

Finally, the last mechanism considered is a triggered dissociative binding, where the approach of the guest induces a dewetting of the pocket to allow the guest to bind (Fig. 55-4). This happens when the approach of the guest disrupts the hydrogen bonding network of the bound water molecules to the bulk, and thus a dewetting transition takes place. This is famously seen in MD studies of **30** by Rick and coworkers.[174]

These studies with **53** elucidate a new mechanism of host–guest binding, in particular the triggered wetting of a dry host. Along with MD simulations, thermodynamic experiments reveal the ability of finely tuned functionalities at the rim to selectively wet or dewet the pocket

An exploration of the binding of alkanes to a dry host

With the 1:1 binding profile of **53** evaluated, its capsule formation was then probed by exposing free host dissolved in pH 11 phosphate-buffered water to neat hydrocarbons. Just like **30** and **37**, host **53** can also form capsular assemblies in the presence of sufficiently long and apolar guests.

Host **53** was found to form well-defined 2:1 host–guest complexes with C_{11} – C_{14} *n*-alkanes (Fig. 55). Analyses of $\Delta\delta$ shifts of the bound guest peaks show that undecane and dodecane adopt an extended/compressed motif within **53** (Fig 56). Extending the chain length by one carbon shows a slight transition towards the next motif – spinning top – which can be seen fully in tetradecane. This is in comparison to host **30** where the spinning top motif is not observed until hexacosane ($C_{26}H_{54}$). The ordering of motifs of alkanes in **30** (extended → helical → hairpin → spinning top) is not strictly followed in **53**: the ethyl groups engender a constriction of the pocket and a narrowing of the portal, thus inhibiting the formation of the helical and the hairpin motifs.[189] The ethyl groups also act as pseudo-guests in so much as they add bulk to the interior. Thus, in an empty host

dimer there already exists 16 carbon atoms that can occupy space in the capsule; the addition of 14 carbon atoms from the alkane guest brings the total number to 30, the largest number of carbon atoms ever to be encapsulated in a dimer capsule of a deep-cavity cavitand. The aggregation state has been confirmed using DOSY NMR spectroscopy: in all five cases the diffusion constant of the complex ($D = 1.33 \times 10^{-6}$ cm^2 s^{-1}) points to a dimeric species (cf. **30** monomer: $D = 1.81 \times 10^{-6}$ cm^{2}s^{-1}).
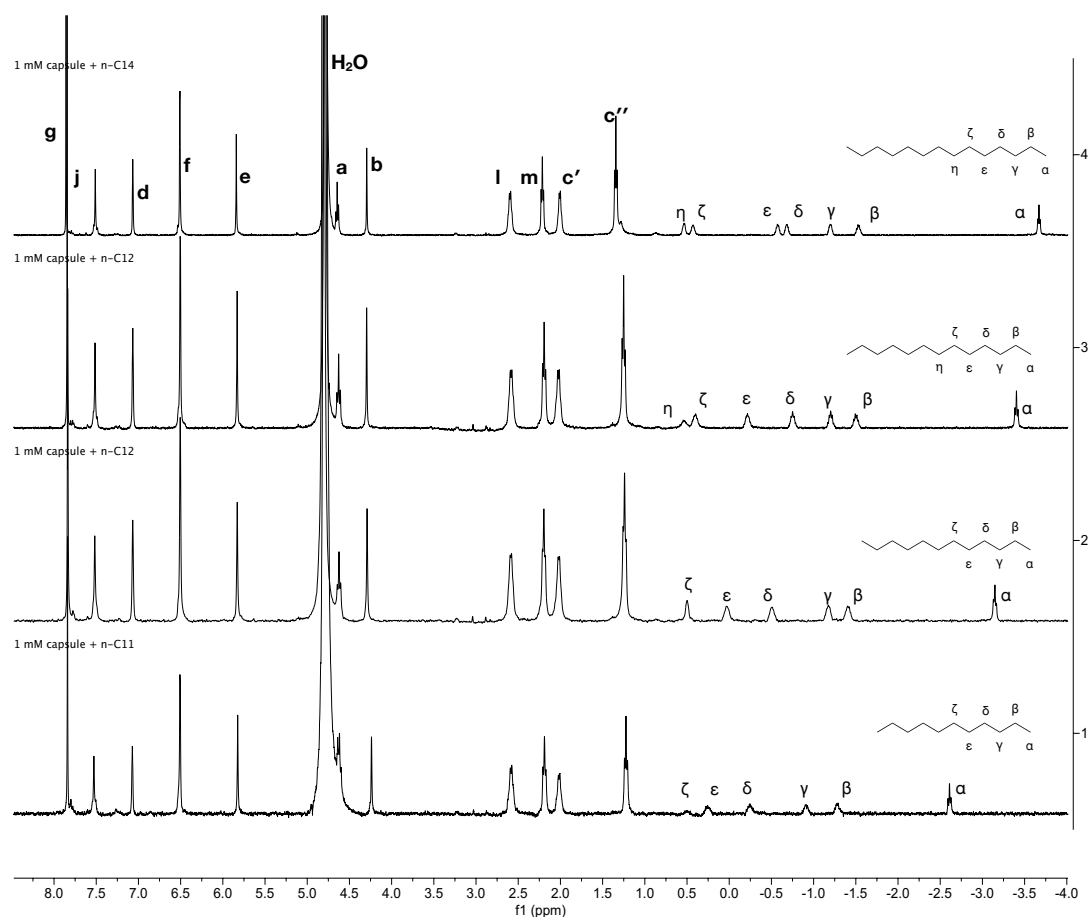
Fig. 55: Stack of 1H NMR spectra of **53** with alkanes (bottom to top) undecane, dodecane, tridecane, and tetradecane. Host signals are labelled in Latin letters, while guest signals are in Greek. The guest binding region for alkanes is below 1.0 ppm

The complexes of **53** with lower alkanes are less well-defined. Although sharpening of host peaks occurs, particularly in H_d, H_b, $H_{c'}$, and $H_{c''}$, guest peaks remain broad due to the presumably weak binding of the guests that undergo fast exchange close to the NMR time scale. In some instances, the $H_{c''}$ resonances
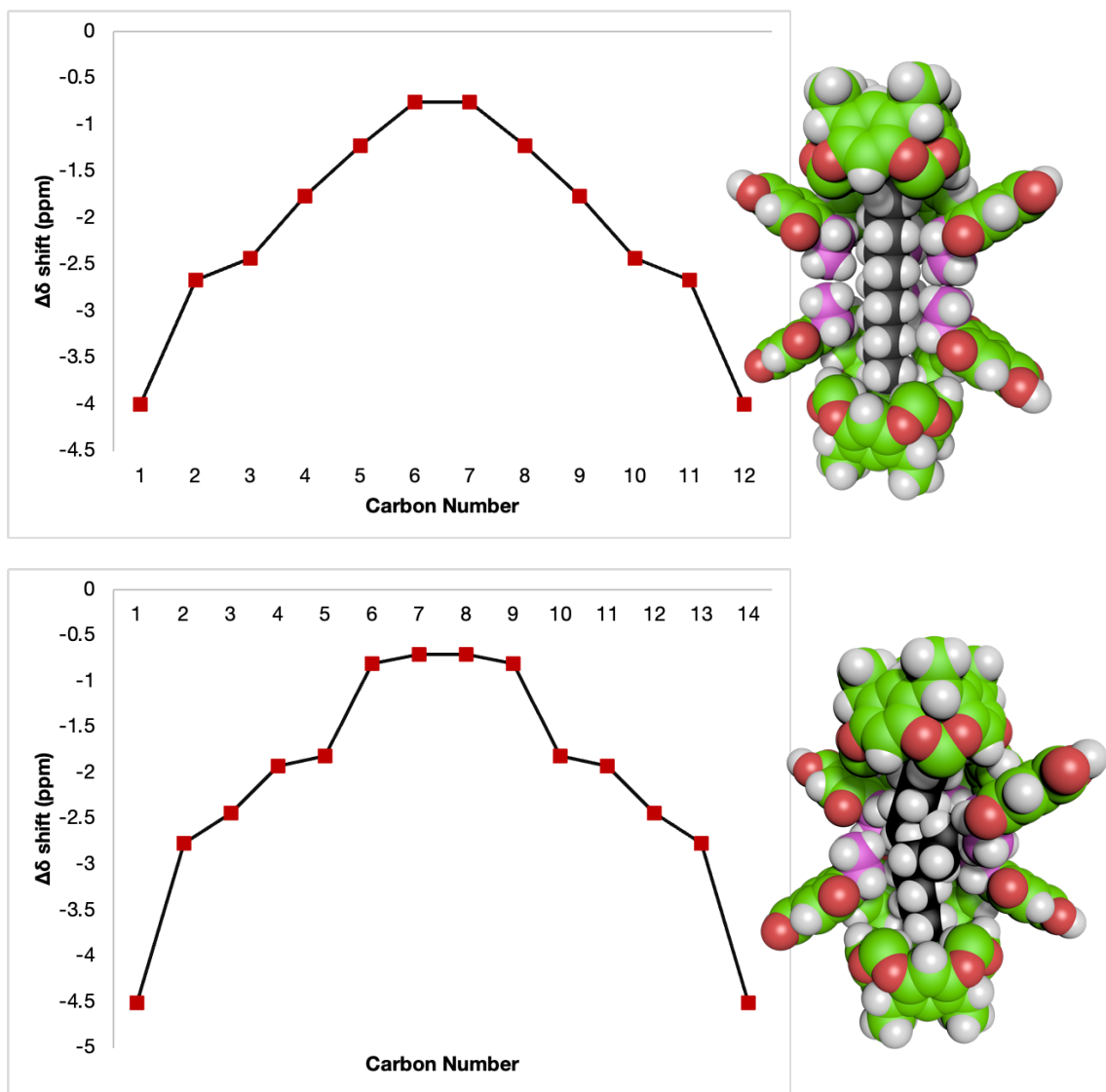
Fig. 56: Plots of Δδ shifts of the ^{1}H resonances of dodecane (*top*) and tetradecane (*bottom*) which points to the binding motif within **53** as depicted in the corresponding idealised CPK renderings. Green: host carbon; pink: host ethyl carbons; white: hydrogen; red: oxygen; black: guest carbon.
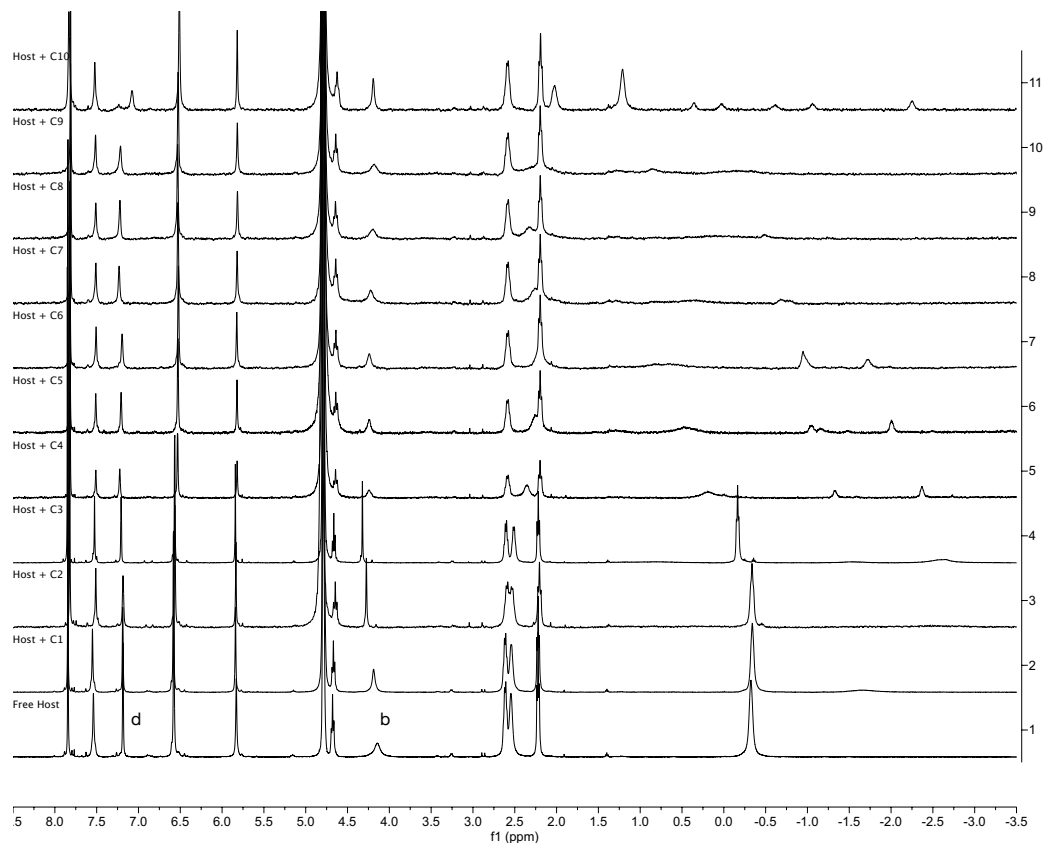
Fig. 57: (*top*) Stack of ^{1}H NMR spectra of **53** with alkanes methane to decane; reference spectrum of the free host is at the bottom of the stack.

almost completely disappear into the baseline; this is almost always accompanied by a concomitant broadening of H_b (Fig. 57). Going from C_1 to C_3 there is deshielding of $H_{c''}$ and H_b, and a shielding of $H_{c'}$ indicative of a binding event and of the ethyls slowly turning away from the pocket; there are no visibly sharp guest resonances in the spectrum, although increasing the intensity of the spectrum reveals very broad guest signals in the bound guest region. A switch occurs in the case of C_4, C_5, and C_6: guest resonances are visible above the baseline, albeit broad and ill-behaved, and $H_{c''}$ disappears/broadens. The binding of C_7, C_8, and C_9 are even less well-behaved. Guest and $H_{c''}$ resonances progressively become broader; only in the case of decane does the situation improve. Guest resonances

are more well-defined and integrable, and every host resonance is above the baseline. The H_d resonance is generally used as an indicator of capsule formation
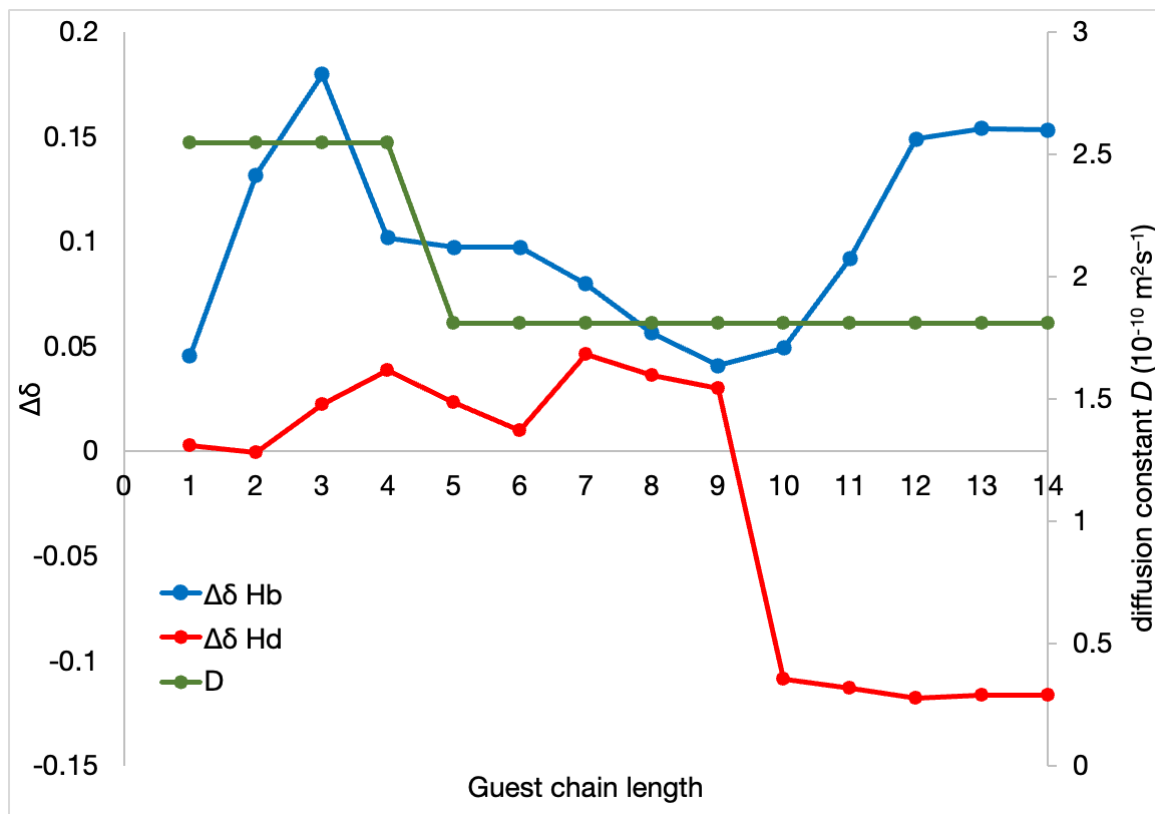
Fig. 58: Plot of Δδ shifts for H_d and H_b, and diffusion constant D as a function of guest chain length.

when $\Delta\delta \rightarrow -\infty$. Both H_b and H_d show a non-monotonic behaviour in $\Delta\delta$ as a function of increasing guest carbon chain length (Fig. 58).

The case of methane is complex. Methane's small size (d_k = 3.8 Å)[35†††] means that it can slip in and out of the host molecule. However moderate solubility in water ($[CH_4]_{satd}^{H_2O}$ = 1.415 mM)[37] means that it can bind to a deep-cavity cavitand via the hydrophobic effect. Indeed, NMR experiments (Fig 59) conducted on $CH_4 \in$ **53** reveal that binding involves fast exchange close to the time scale of the NMR experiment at 11.75 T (500.13 MHz). A characteristic negative $\Delta\delta$ shift of the methane peak can be observed, going from 0.17 ppm with a line width $\Delta_{\frac{1}{2}}$ of
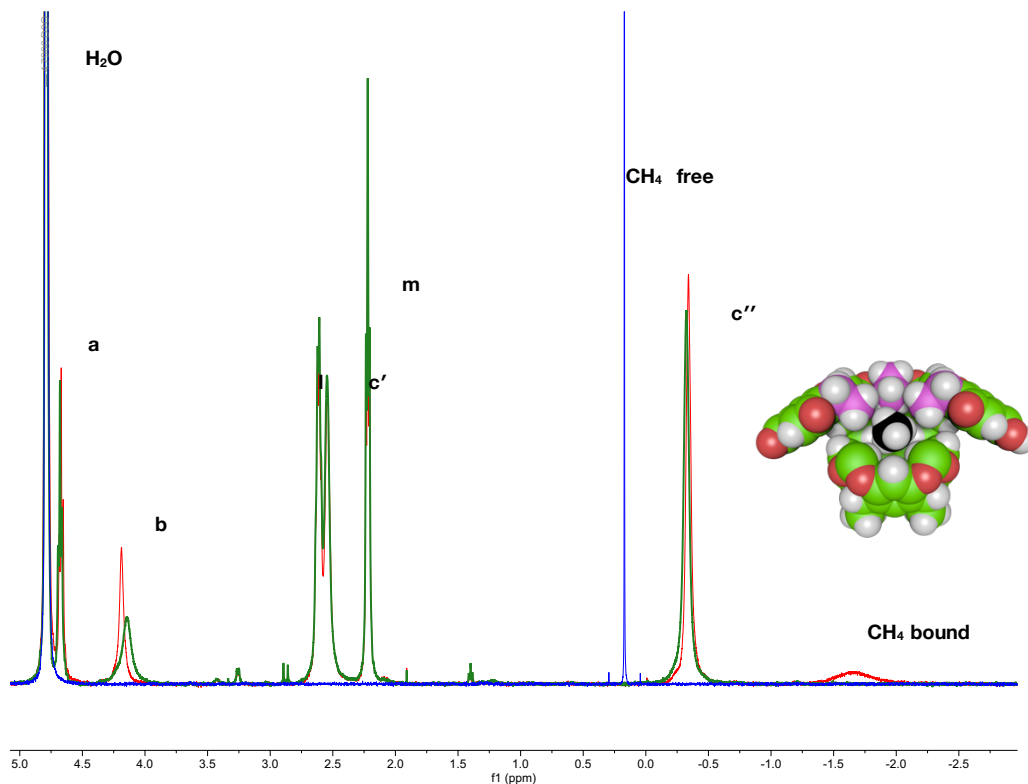
Fig. 59: Superimposed ^{1}H NMR spectra in the –3-5 ppm region of (*blue*) free CH_4, (*green*) free **53**, and (*red*) $CH_4 \in$ **53**. A cutaway CPK of the idealised structure of $CH_4 \in$ **53** is provided.

———————————

††† The kinetic diameter of a gas d_k is defined as $d_k^2 = \frac{1}{\sqrt{2}\pi l n}$ where l is the mean free path of the gas molecule and n is the number density of the particles.

0.97 Hz in the free state in 10 mM pD 11.5 phosphate-buffered D_2O, to −1.67 ppm

with a line width of ca. 171 Hz in the bound state within **53**. The resonances for

$H_{c'}$ and $H_{c''}$ do not show any movement from those of the resting state of **53**

indicating that although there is a bound methane molecule within the host, its

size is not nearly enough to induce a switch to the ethyls pointing out. Leaving the

solution open to air does not cause CH_4 to desorb from the host; only when the

solution is sparged with N_2 or subjected to freeze–pump–thaw cycles is CH_4

released.

DOSY NMR spectroscopy at low fields does not prove to be useful in the

case of $CH_4 \in$ **53** because of the larger-than-normal linewidths brought about by
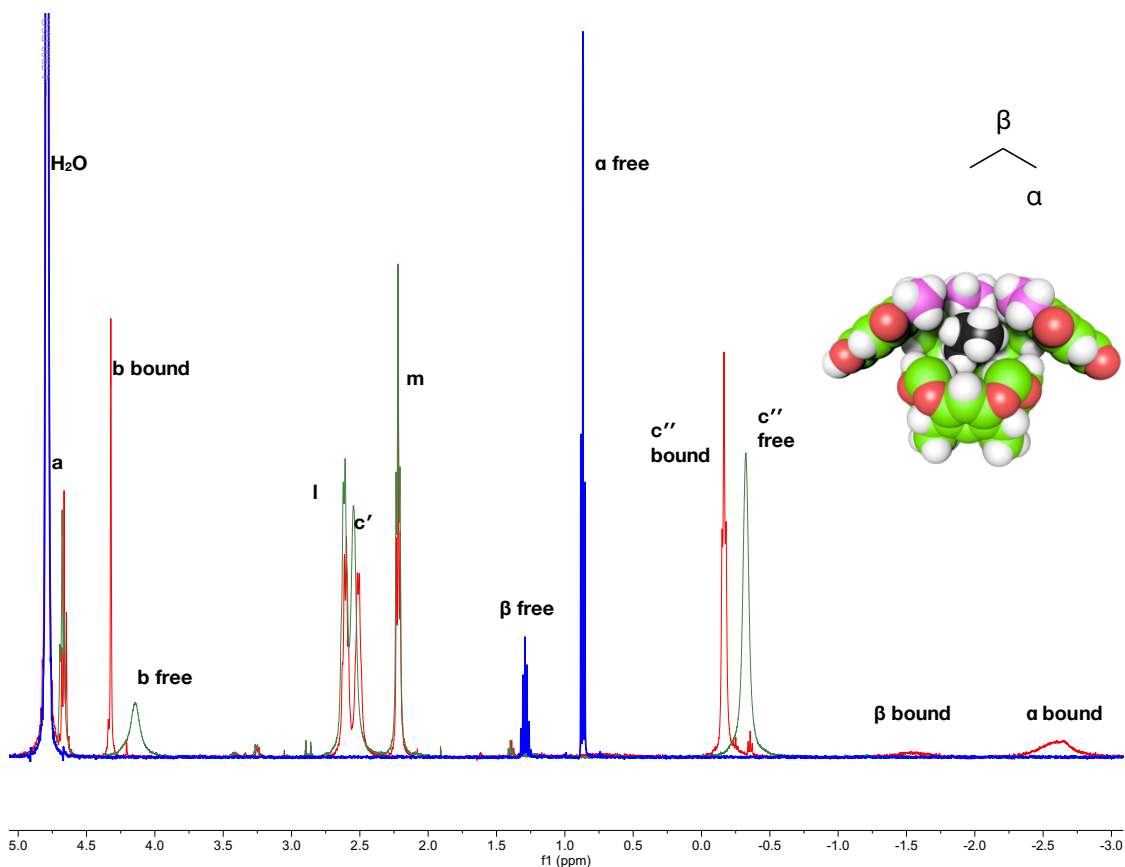
Fig. 60: Superimposed ^1H NMR spectra in the −3-5 ppm region of (blue) free C_3H_8, (green) free **53**, and (red) $C_3H_8 \in$ **53**. A cutaway CPK of the idealised structure of $C_3H_8 \in$ **53** is provided.

exchange. However, the Δδ shifts of H_d in $CH_4 \in$ **53** (Fig. 57) are completely different from the Δδ shifts of H_d in $C_{14}H_{30} \in$ **53$_2$** which indicates that $CH_4 \in$ **53** may be monomeric in nature.

The case for propane (d_k = 4.30 Å, $[C_3H_8]_{satd}^{H_2O}$ = 1.53 mM)[35, 237] is similar to that of $CH_4 \in$ **53** in so much as the guest resonances are broad and that the exchange is fast and close to the time scale of the NMR experiment (Fig. 60). However, the host resonances are sharp and well-defined. The resonances for $H_{c'}$ and $H_{c''}$ point to a regime where the ethyl groups begin to point outwards. In this instance, DOSY NMR spectroscopy points to a monomeric complex (D = 2.55 × 10^{-6} cm^2 s^{-1}), but the H_d Δδ value suggests otherwise. This is indicative of fast exchange close to the timescale of the NMR experiment between the free, monomeric state, and the bound, possibly aggregated state. Again, just with CH_4, the propane does not spontaneously desorb from the host, and additional work such as an N_2 sparge or freeze–pump–thaw cycles is required to decomplex propane from **53**.

DOSY NMR experiments in higher fields, i.e. 700 MHz (16.45 T) narrows exchange linewidths sufficiently to glean a relative diffusion constant. All complexes with alkanes from CH_4 to C_4H_{10} seem to be monomeric (D = 2.55 × 10^{-10} m^2 s^{-1}) relative to the known dimeric species with $C_{14}H_{30}$ (D = 1.81 × 10^{-10} m^2 s^{-1}); complexes with C_5H_{12} to $C_{13}H_{28}$ share the same diffusion constant with dimer. This is a stark shift from the non-monotonic behaviour of **37**.[192, 238, 239] One possible explanation could be that as the guest becomes larger, the pendent ethyl groups

at the rim of **53** turn outwards to a larger degree, increasing the apolar solvated surface area. In turn, to stabilise itself, the hosts aggregate in a portal-to-portal manner to reduce the area of the apolar surfaces exposed to the bulk solvent.

Conclusions

The introduction of functionality to the portal of a water soluble deep-cavity cavitand can change the binding properties of the cavitand by the inclusion of water molecules into (or exclusion from) the pocket.

In the case of *exo*-octa acid (**39**) the added functionalities are carboxylates. These functional groups are known to be well-solvated in water due to its relatively small size and high charge-to-volume density. The placement of these carboxylates stabilises the cluster of four water molecules in the pocket of the host via charged hydrogen bonds; the stability was calculated to be ~1 $k_B T$ (~2.5 kJ mol^{-1} at 298 K). This points to the fact that the carboxylates make the water clusters a better guest to **39** than to parent compound octa acid (**30**), and thus a better competitor for binding to the pocket compared to 'unstabilized' water clusters. This competition inhibits the binding of apolar guests to the pocket.

On the other hand, apolar functionalities added to the portal such as methyl and ethyl groups induce a drying transition in the pocket. This can be via either a physical desolvation process by which water molecules evacuate a space

between two apolar moieties at a certain distance (in the case of methyl groups in TEMOA **37**), or via a steric effect where the apolar groups occupy space to remove water (ethyl groups in TEEtOA **53**), or both. The presence of the methyl groups that desolvate the pocket of **37** increase the strength of binding to the pocket due to the absence of competing water molecules in the pocket. A similar situation is true with **53**, however the conformational mobility of the ethyl groups contributes to the slightly weaker binding to **53** relative to **37** by ca. 5 $k_B T$ (~12.9 kJ mol^{-1} at 298 K). Thus, contrary to common belief, alkyl groups may be considered as functional groups, as they change the nature of the hydration of an already weakly-hydrated pocket.

Compound **53** has been shown to bind alkanes in the same fashion as **30** and **37**. Compound **53**, with its eight extra carbons which comprise the ethyl groups at the portal, sterically constrict the pocket and engenders the ability to bind small hydrocarbons which otherwise do not bind to **30**. Indeed, methane, the smallest and simplest hydrocarbon, can be held by a monomer of **53** and is not released until forced out using N_2 or by a vacuum. In comparison, at the other end of the spectrum *n*-tetradecane ($C_{14}H_{30}$) is held by a capsular dimer of **53**. *n*-Tetradecane adopts a spinning-top motif– the shortest *n*-alkane that adopts the said motif in a dimer. The presence of the constrictive ethyl groups reduces the size of the portal which allows *n*-tetradecane to adopt the spinning-top motif while completely skipping the hairpin motif as can be seen in a dimer of **30**. Compound **53** also displays a monotonic switch from monomer to dimer in the presence of

increasingly large alkane guests. This switch may be indicative of a more stable state where there is an energetic penalty to the solvation of the ethyl groups as they are turned outwards as a function of guest size, and thus induces a dimerization to reduce the solvent-exposed surface area of the host.

Part III: Positively Charged Analogues of Negatively Charged Hosts

The asymmetry in binding of charged host–guest pairs

There is no unified understanding of the mechanism of protein aggregation brought about by the presence of co-solutes salts. Ion binding to the protein is obviously key, but to date the complexity of binding has precluded the development of a clear picture. Smaller, less complicated model system may shed light into these intricacies and nuances.[240]

Anion binding and recognition in water is a relatively new facet of supramolecular chemistry.[241] Instead, there has been a fascination with anion binding in organic solvents such as chloroform, and for example, attaining very high affinities.[242] And yet, the fundamental understanding of how to apply this knowledge to more biologically relevant systems, i.e., aqueous systems, is unclear. Indeed, most anion sequestration systems involve charge neutral hosts and are driven by host–guest interactions that would be very weak in water due to its highly polar nature.

Towards this, positively charged water-soluble hosts were synthesised with the aim of studying the effect of positive electrostatic potentials on the binding of anions to weakly hydrated concavities.

Host	Guest	$\log_{10} K_a$	ΔG (kJ mol^{-1})	ΔH (kJ mol^{-1})	$-T\Delta S$ (kJ mol^{-1})
30	AdCOOH	6.5 ± 0.1	−37.2 ± 0.6	−38.3 ± 0.5	1.1 ± 0.2
30	AdNMe₃Cl	6.0 ± 0.1	−35.2 ± 0.3	−33.1 ± 3.2	−1.1 ± 2.9
36	AdCOOH	6.9 ± 0.0	−32.4 ± 0.2	−32.4 ± 1.3	−7.0 ± 1.1
36	AdNMe₃Cl	4.0 ± 0.1	−22.9 ± 0.3	−32.5 ± 2.8	9.6 ± 2.5

Table 14: Thermodynamic data[a] from ITC for the binding of guests AdCOOH and AdNMe$_3$Cl with hosts **30** and **36**. All titrations were performed by CG for a future publication. Titrations were performed at 25 ° C in 10 mM phosphate buffer at pH 11.5 for **30** and pH 7.4 for **36**.

[a] The ΔH and K_a values were obtained by carrying out at least three separate experiments, averaging each set of data, and calculating the respective standard deviations. ΔG was obtained from K_a via the standard thermodynamic equation. The average ΔH and ΔG values were then used to calculate an average $-T\Delta S$, and the corresponding standard deviations calculated using the standard equation for the propagation of uncertainties for subtraction. The deviations in ΔG were obtained by using the standard equation for the propagation of uncertainties for logarithms. The errors in $\log_{10} K_a$ are smaller than what is significant.

In unpublished work performed by Corinne Gibb, a series of experiments was conducted to probe the Coulombic effects present when a charged guest binds to the weakly hydrated pocket of a charged host. Briefly, the binding affinities of pairs of positively or negatively charged guests (adamantyl derivatives) to positively or negatively charged hosts (**30** and **36**) was determined using both ITC and ^{1}H NMR spectroscopy. The experiments reveal an asymmetry (Table 13) in binding pairs, which can be ranked as follows (**H**: host; **G**: guest; blue: positive; red: negative): **H**:**G** > **H**:**G** > **H**:**G** > **H**:**G**.

It is satisfying to observe that intuition holds true for the extreme cases: the strongest binding pair is that of dissimilar charges, specifically **H**:**G**, and the weakest is one with similar charges, **H**:**G**. However, what is not so intuitive are the

intermediate cases where H:G > H:G. It may be, just like in the case of OA **30** versus *exo*-OA **39**, that the hydration profile of the pockets may be different. In addition, there is literature precedent for the large differences in the hydration shell of carboxylates and quaternary ammoniums in so much as quaternary ammoniums suppress the formation of dangling hydrogen bonds in solution.[243] More work needs to done here to determine the causes of the observed phenomena, but what is clear is that there is no simple Coulombic relationship between the binding of charged guests to cavitands. Readers should be mindful of this in the following discussions.

The syntheses of Positand 2 and Positand 3

The syntheses of Positand 2 and Positand 3 (**67** and **68**, Fig. 61) starts with the formation of known compound tetra-*endo*-methyl octol cavitand (TEMOctol, **68**)[192] or tetra-*endo*-ethyl octol cavitand (TEEtOctol, **69**) from octa-bromide **32** via an eightfold copper(I)-catalysed Ullmann biaryl ether condensation with a 4-alkyl-3,5-dihydroxybenzyl alcohol. The crude products can be converted to the octa-halides (**69** and **70**), after which the products are converted to the octakis-trimethylammonium salt via a Menschutkin reaction in DMF. The bromide salt that is formed is subjected to ion-exchange chromatography to replace the bromide counterions with chlorides, and an eventual size-exclusion chromatography step removes any side-products to yield **67** or **68**.
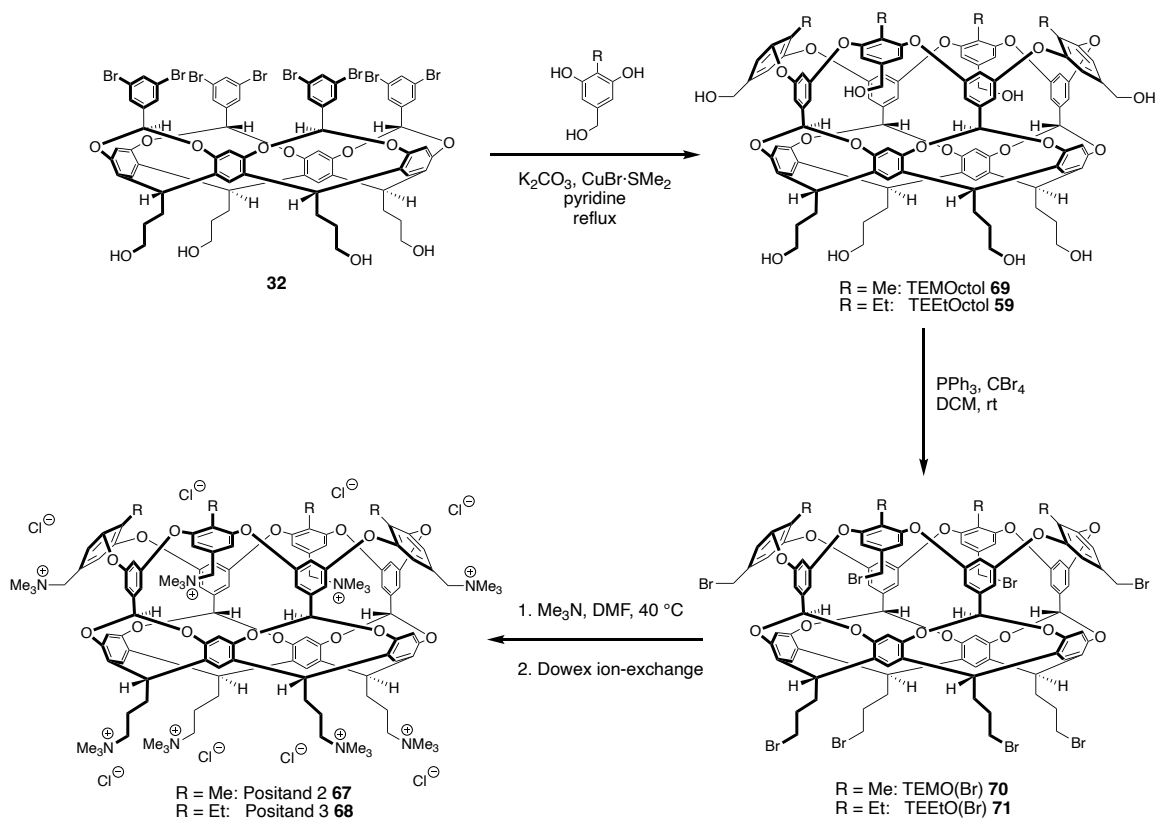
Fig. 61: Synthesis of Positand 2 (**67**) and Positand 3 (**68**) from octa-bromide **32**.
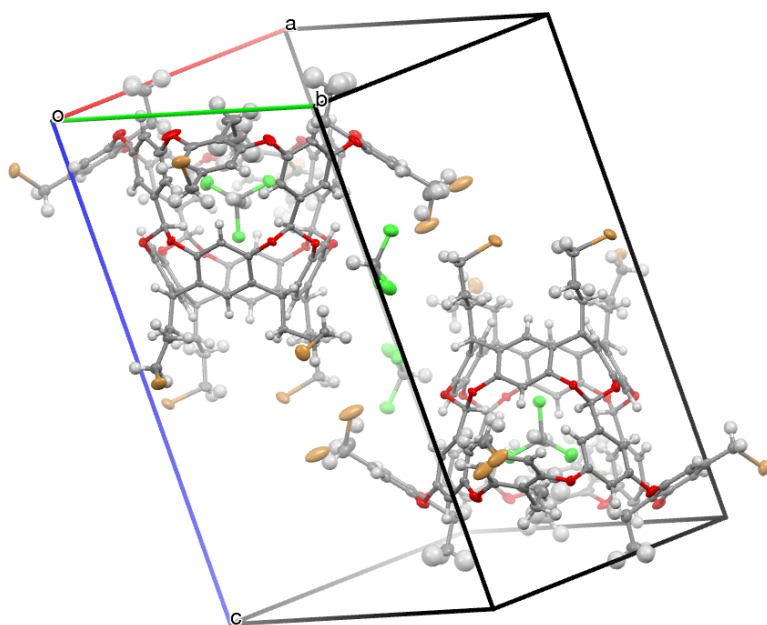
Fig. 62: Image of the unit cell of **71** showing two asymmetric units within the triclinic cell.

A crystalline sample of tetra-*endo*-ethyl octa bromide cavitand (TEEtO(X), **71**) was grown at room temperature by the layered diffusion of hexanes onto a 10 mg ml^{-1} solution of the compound in CHCl$_3$ to give colourless columns. Compound **71** crystallises in the P$\bar{1}$ space group with two cavitand molecules in the unit cell (Fig. 62). A CHCl$_3$ molecule is located outside of the cavitand; another can be found inside the cavitand and is disordered over two sites with the three chlorine atoms in common. Two of the pendent ethyl groups at the rim of the cavitand *trans* to one another are inward pointing, with the methine of the bound chloroform situated underneath them.
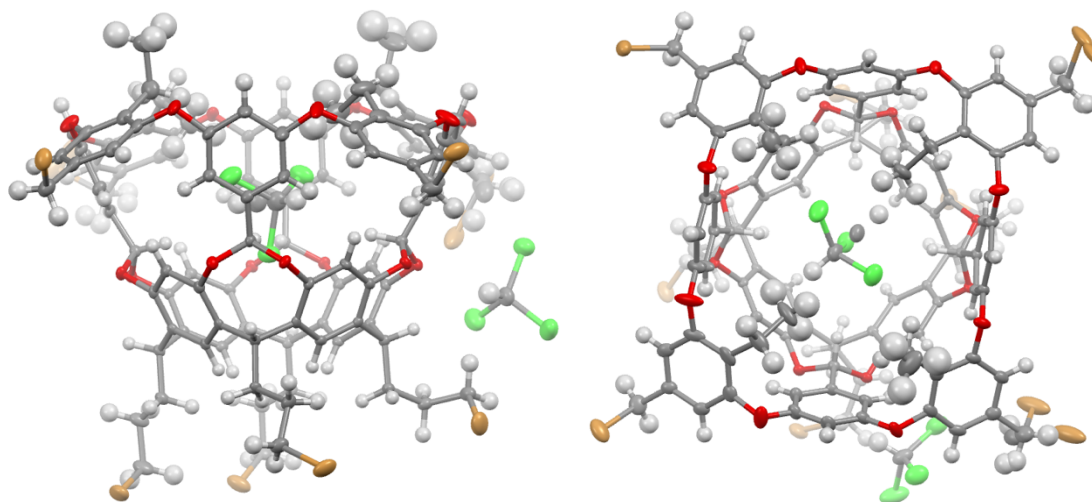
Fig. 63: Views of the asymmetric unit in the unit cell of **71**. (*left*) View from the side; (*right*) view into the cavity via the portal

It would be very easy to speculate about the favoured position of the chloroform molecule within the cavitand itself, however a cursory exploration of the space-filling model of the clathrate reveals the answer. The position of the methine in CHCl$_3$ maximises the amount of van der Waals interactions between the bound solvent and the pendent ethyl groups. The two outward pointing ethyl

groups are positioned out of the pocket in part because of the size of the $CHCl_3$

molecule in the pocket leaving no space for the remaining ethyls to turn inwards.

The mean distance between the downward pointing chlorine atom and the bottom

of the pocket is 2.854 Å; there is no C-H⋯X hydrogen bonding between the H_b

proton of the cavity to the chlorine atom via the belt of electronegativity at the

equator of the chlorine atom. The deep binding of $CHCl_3$ seems to be a crystal

packing effect where the inwards pointing ethyls push down on the $CHCl_3$.

In the course of the workup for both **70** and **71**, it was discovered that the

slight change in the alkylation state of the basket (methyl for **70** and ethyl for **71**)

changes its properties relative to the octahalide precursor of **36** which does not

have alkyl groups. For example, in order to separate the excess/unreacted

triphenylphosphane from the precursor of **36**, the mixture is taken up in anhydrous

diethyl ether to solubilise the phosphane which leaves the octahalide as a solid.[202]

However, in the case of **70** and **71** the alkylation state increases solubility in diethyl

ether, and a large loss of yield is observed during the workup. Consequently,

hexanes was used as an alternative to solubilize the excess phosphane and leave

70 and **71** as a solid. In the Menschutkin quaternisation reaction converting the

octahalides **70** and **71** to the water soluble Positand 2 (**67**) and Positand 3 (**68**) by

reaction with trimethylamine in DMF, an insoluble intermediate precipitates out of

solution which re-solubilises upon the addition of a small aliquot of absolute

ethanol. This phenomenon does not happen in the quaternisation reaction to form

36.
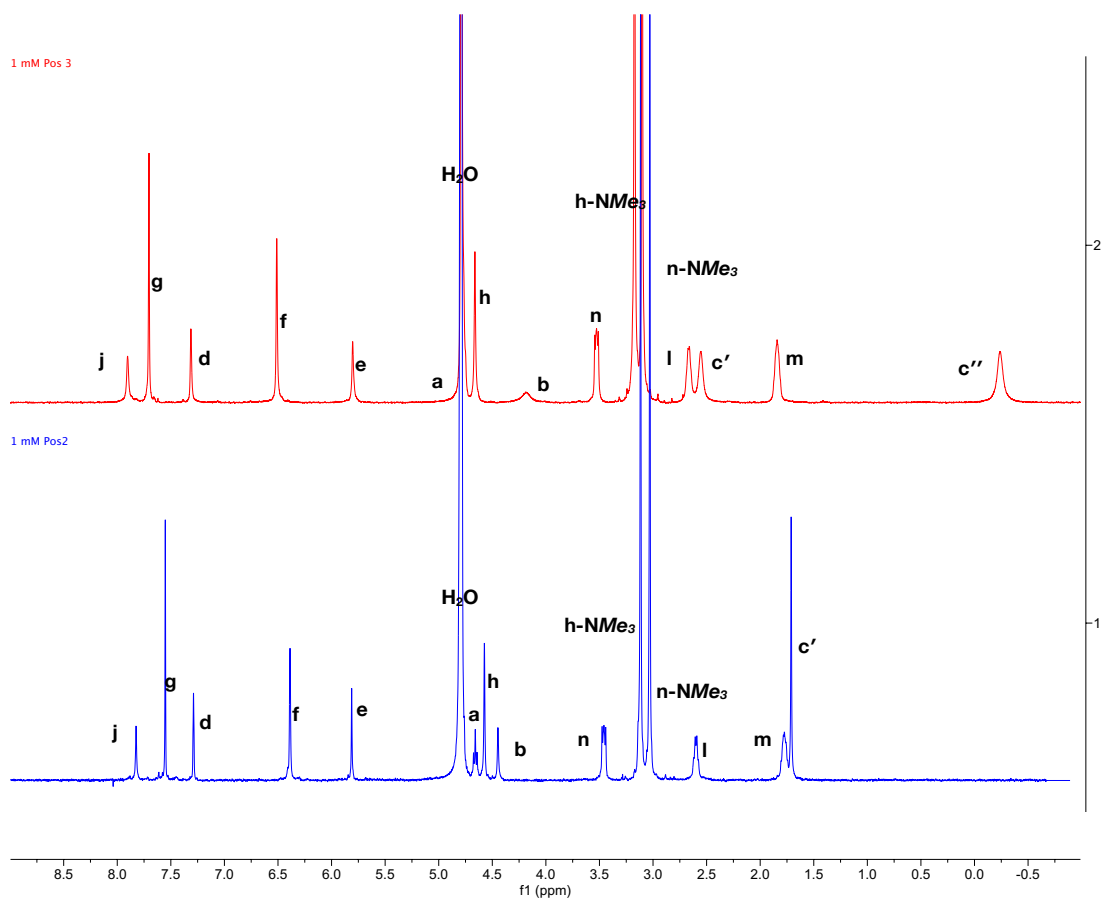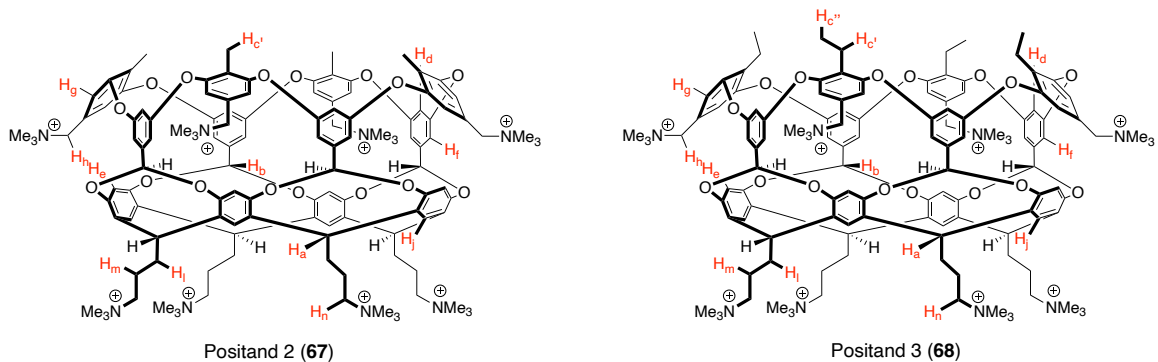
Fig. 64: (*top*) Line structures of Positand 1 (**67**) and Positand 2 (**68**) with protons labelled with assignments for their corresponding ^{1}H NMR spectra. (*bottom*) ^{1}H NMR spectra of 1 mM solutions of **67** (blue) and **68** (red) in 10 mM pD 7.4 phosphate-buffered D$_2$O, with peak assignments.

The binding properties of Positand 2 and Positand 3

The structural differences in Positand 2 (**67**) and Positand 3 (**68**) are similar to the differences between TEMOA (**37**) and TEEtOA (**53**) in so much as **53** has additional degrees of freedom at the portal. Compound **68** is expected to also have a vacuous cavity and to be drier than **67**, which is in turn expected to be drier than **36**. An inspection of the ^{1}H NMR spectra of **67** and **68** (Fig 64) shows differences that could point to the degree of vacuity within the pockets. The $H_{c'}$ position (methyl in **67** and methylene in **68**) have starkly different nuclear shielding: $H_{c'}$ in **67** is more shielded than in **68** presumably because of the flexibility of the outer flaps of the cavitand. The flaps can flex, moving the methyl groups in **67** slightly deeper into the pocket. The $H_{c'}$ resonance in **68** (methylene) is more deshielded, possibly because the pendent terminal methyl ($H_{c''}$) stops additional flexing, and thus exposing the methylene to the outer environment to a greater degree. The linewidths also point to the fact that the methylene in **68** is undergoing chemical exchange ('in' *versus* 'out', see analogous system for **53**, Fig. 46), while the methyls in **67** are rotating fast, lengthening the T_2 relaxation time, narrowing the linewidth $\Delta_{\frac{1}{2}}$ from 22.9 Hz in **68** to 4.8 Hz in **67**.[107]

An exploratory experiment to probe the hydration of the pockets of **67** and **68** involves the binding of 4-bromobenzoic acid (**72**) to **30**, **36**, **67**, and **68**. The thermodynamic parameters are summarised in Table 15 and in representative thermograms shown in Fig. 65. Going from OA (**30**) to Positand 1 (**36**), there is a two-fold increase in the affinity constant, however there is a drop in the binding

enthalpy. The enthalpic favourability is a hallmark of the non-classical hydrophobic effect; however, the drop in enthalpy is possibly because water is a better guest for **36**. It may be hypothesised that the dipoles of the water cluster within **36** are pointed towards the walls of the host and the positive charges beyond, making it a better guest in **36** than in **30**. Regardless, there is an entropic compensation in the binding of the guest to **30**, presumably because of the formation of a complex between a host and guest of like charge— this compensation is significantly less in **36**.

	4-bromobenzoic acid (72)			
	$\log_{10} K_a$	ΔG (kJ mol^{-1})	ΔH (kJ mol^{-1})	$-T\Delta S$ (kJ mol^{-1})
OA (30)[b]	5.7 ± 0.0	−32.5 ± 0.0	−45.7 ± 2.4	13.1 ± 2.4
TEMOA (37)	6.4 ± 0.0	−36.3 ± 0.1	−57.1 ± 0.3	20.8 ± 0.2
TEEtOA (53)	4.5 ± 0.0	−25.5 ± 0.2	−50.8 ± 1.4	25.3 ± 1.3
Positand 1 (36)[b]	6.1 ± 0.1	−35.0 ± 0.1	−36.9 ± 1.7	4.8 ± 0.2
Positand 2 (67)	6.3 ± 0.0	−36.2 ± 0.1	−53.0 ± 0.5	16.8 ± 0.4
Positand 3 (68)	5.8 ± 0.1	−33.1 ± 0.3	−59.6 ± 0.8	26.5 ± 0.6

Table 15: Thermodynamic data[a] from ITC for the binding of 4-bromobenzoic acid (**72**) with hosts **30**, **36**, **37**, **67**, **53**, and **68**. All titrations were performed at 25 °C in 10 mM phosphate buffer at pH 11.5 for **30**, **37**, and **53**, and pH 7.4 for **36**, **67**, and **68**.

[a] The ΔH and K_a values were obtained by carrying out at least three separate experiments, averaging each set of data, and calculating the respective standard deviations. ΔG was obtained from K_a via the standard thermodynamic equation. The average ΔH and ΔG values were then used to calculate an average $-T\Delta S$, and the corresponding standard deviations calculated using the standard equation for the propagation of uncertainties for subtraction. The deviations in ΔG were obtained by using the standard equation for the propagation of uncertainties for logarithms. The errors in $\log_{10} K_a$ are smaller than what is significant.

[b] Titrations performed by CG for future publication.

There is another two-fold increase in the binding affinity of 4-bromobenzoic acid going from **36** to **67**. This time the increase in the binding affinity is due to the lack of competition of any bound waters in the cavity of **67**. As has been

established (*vide supra*), a dry pocket will increase the binding affinity of guests that have apolar surfaces, such as that which can be found in 4-bromobenzoic acid, resulting in an increase in entropy as can be clearly seen. The resulting stark increase in enthalpic favourability, then, comes from the formation of the C–H···X hydrogen bond between the bromine atom of the guest and the H_b protons at the base of the pocket.
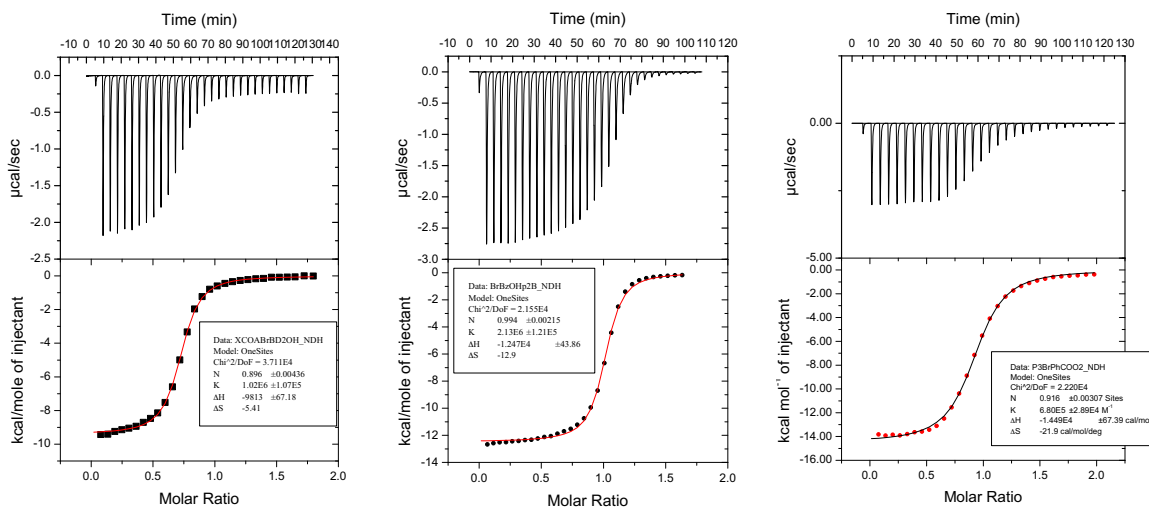
Fig. 65: Representative ITC thermograms of the binding of 4-bromobenzoic acid **72** to (*left*) Positand 1 (**36**), (*middle*) Positand 2 (**68**), and (*right*) Positand 3 (**68**). Data for **72**∈**36** was performed by CG. All data were collected on solutions in 10 mM pH 7.4 phosphate-buffered water and equilibrated at 25 °.

Again, decreasing the hydration of the pocket by switching from **67** to **68** increases the enthalpy of binding of the guest to the pocket. However, coupling both the desolvation of an apolar surface with the loss of conformational mobility in the ethyl groups introduces an entropic penalty to the binding free energy which compensates for the significant release of heat during the binding event. This

unfortunately cannot be seen in the TEMOA (**37**) *versus* TEEtOA (**53**) system for reasons which are as of yet unknown.

More work needs to be done to explore the binding profiles of Positands 1, 2, and 3 (**36**, **67**, and **68**, respectively). These experiments include ITC binding profiles of organics and inorganics, and MD simulations to visualise the hydration states of the pockets. It is believed that the combination of these experiments will elucidate the mechanism behind the enthalpy–entropy compensation phenomena that are observed in these systems.

Conclusions

The syntheses of the positively charged analogues of TEMOA (**37**) and TEEtOA (**53**), Positand 2 (**67**) and Positand 3 (**68**), respectively, have been outlined. In addition, the crystal structure of the octa-halide precursor of **68** has been obtained, and the solid-state packing has been described.

Preliminary data show that the binding of a negatively charged guest (4-bromobenzoic acid **72**) to Positand 1 (**36**), **67**, and **68** are indeed stronger than their negatively charged counterparts octa-acid **30**, **37**, and **53** as intuition would suggest. All binding events are enthalpically driven, releasing heat as the electronegative bromine atom on the guest hydrogen bonds to the reporter proton H_b. The increase in alkylation state of the portal of the hosts increases the entropic penalty of the binding event due to the loss of conformational mobility at the rim during the binding event.

Part IV: Experimental — Methods and Spectra

"A common mistake that people make when trying to design something completely foolproof is to underestimate the ingenuity of complete fools." (Douglas Adams, *Mostly Harmless*,1992)[244]

Syntheses of hosts, guests, and other small molecules

General Considerations

Room temperature (rt) is used to describe ambient laboratory temperatures ranging from 24–27 °C. All reagents were purchased from either MilliporeSigma, Fisher Scientific, TCI America, or AK Scientific and were used without further purification unless otherwise specified. Resorcinol was recrystallised from boiling toluene and dried under high vacuum at rt overnight prior to use.[245] *s*-Butyllithium was titrated against a 1.0 mM solution of *N*-benzylbenzamide in anhydrous THF prior to use.[246] Triphenylphosphane was recrystallised from boiling 95% EtOH and dried under high vacuum at 77 °C for 4 hours prior to use.[245] All reactions involving anhydrous solvents were performed under a blanket of dry N_2 gas. Anhydrous solvents were purchased from MilliporeSigma and, unless supplied with a Sure-Seal septum, stored with 3 Å molecular sieves activated at 250 °C overnight. Chromatography solvents were purchased from Fisher Scientific. Chloroform from Fisher Scientific contained up to 0.75% EtOH as preservative. Thin-layer

chromatography was performed using 60G F$_{254}$ glass-backed silica gel plates from MilliporeSigma. All flash column chromatography separations were performed using a dry load on a Teledyne Isco CombiFlash NextGen300+ instrument using SiliCycle SiliaSep silica cartridges, or Teledyne Isco RediSep Rf Gold cartridges for compounds **42** and **61**. Degassing of solvents was performed by applying a vacuum on the solvent and replacing the atmosphere with dry N$_2$. The preparation of HCl-saturated EtOH was performed by bubbling HCl gas through 250 mL absolute EtOH for 5 mins immediately prior to use. All drying steps were performed under vacuum at or below 13 Pa and, in the case of high temperature drying, in an Abderhalden apparatus charged with the appropriate refluxing solvent (EtOAc at 77 °C, PhMe at 110 °C, and xylenes at 140 °C) as necessary.

All ^{1}H NMR spectra were recorded on either a Bruker Avance 500 (500.13 MHz) instrument or a Varian UNITY INOVA 400 (399.74 MHz) instrument, or a Bruker Avance NEO 700 (700.26 MHz) instrument operating at 25 °C, using residual CHCl$_3$ (δ 7.26), DMSO-d_5 (δ 2.50), acetone-d_5 (δ 2.05), CHDCl$_2$ (δ 5.32) or H$_2$O (δ 4.79) as an internal standard. All ^{13}C NMR are broadband decoupled; spectra were recorded on either a Bruker Avance III 300 instrument (75.47 MHz ^{13}C), or a Varian UNITY INOVA 400 (100.51 MHz ^{13}C), or a Bruker Avance 500 (125.16 ^{13}C), or a Bruker Avance NEO 700 (176.10 ^{13}C) operating at 25 °C using CDCl$_3$ (δ 77.16), acetone-d_6 (δ 29.84 , 206.26), CD$_2$Cl$_2$ (δ 53.84), or DMSO-d_6 (δ 39.52) as an internal standard. For ^{13}C spectra in D$_2$O sodium 3-(trimethylsilyl)propane-1-sulfonate in a sealed capillary (DSS in D$_2$O, δ 0.00) was

used as an external standard. 2D NMR spectra were recorded on a Bruker Avance 500 operating at 25 °C. NMR spectrum data were processed using MNova 14 (Mestrelab Research, S.L.). Multiplicity abbreviations are as follows: s – singlet; d – doublet; t – triplet; q – quartet; dd – doublet of doublets; dt – doublet of triplets; td – triplet of doublets; tt – triplet of triplets; br – broad signal; m – unresolved multiplet. Coupling constants *J* are reported in hertz as positive values regardless of their real individual signs. Solvents for NMR spectroscopy were purchased from Cambridge Isotope Laboratories.

All elemental analyses were performed offsite by Midwest Microlab. All melting point (mp) data were collected using a Stanford Research Systems Digimelt MPA160 Schmelzpunktbestimmungsapparat and are uncorrected. MALDI-MS spectra were collected using a Bruker Autoflex III MALDI/TOF mass spectrometer. ESI-MS spectra were collected using a Bruker micrOTOF ESI mass spectrometer.

Purification of copper(I) bromide and the formation of its dimethyl sulfide complex

The purification of copper(I) bromide[247] and the synthesis of its dimethyl sulfide complex[248] followed literature procedures. To a dry flask was added copper(I) bromide (50.0 g, 349 mmol) and glacial acetic acid (500 mL). The green suspension was stirred vigorously at rt under a blanket of N_2 for 24 h, filtered, the solids washed with absolute ethanol until the filtrate ran colourless, then dried

under high vacuum at 110 °C for 24 h. The solids were transferred to a flame-dried, N_2-flushed flask and the solid contents cooled to –10 °C (1:1 ice/acetone). Dimethyl sulfide (300 mL) was then added dropwise via a pressure-equalising addition funnel over 30 min. and the suspension was allowed to stir at 0 °C for 30 mins. The resulting homogeneous, red-orange solution was heated to reflux (oil bath) for 24 h, after which time the solution was allowed to cool to rt. Hexanes (700 mL) was slowly poured onto the solution and the resulting suspension refrigerated for 4 h. The suspension was then filtered, and the solids washed with additional hexanes until the filtrate ran colourless. The solids were dried at rt overnight to afford the complex as a greyish-white crystalline powder (70.5 g, 98%). The complex was stored in a Dierite-charged desiccator under static vacuum until ready for use. Crystallographic data agree with the literature.[248]

Synthesis of *N*-benzyl benzamide for the titration of alkyllithiums

The synthesis of *N*-benzyl benzamide followed literature procedures.[246] To a flame-dried, N_2-flushed flask fitted with a magnetic stirrer was added DCM (300 mL), benzylamine (12 mL, 110 mmol, 1.10 equiv.), and DIPEA (25.7 mL, 150 mmol, 1.5 equiv.). The stirring solution was cooled to 0 °C (ice/water bath) for 15 minutes, after which time benzoyl chloride (11.6 mL, 100 mmol) was added dropwise via syringe over 10 mins. The solution was then allowed to stir at rt for 2 h, after which time the solution was washed sequentially with 2×200 mL 1 M HCl (aq.), 2×200 mL sat'd $NaHCO_3$ (aq.), 2×200 mL dH_2O, and 1×200 mL sat'd. NaCl (aq.).

The organics were then dried over anhydrous Na_2SO_4, filtered, and the solvent removed from the filtrate under reduced pressure to afford a white solid. The solids were dissolved a minimum amount of DCM and the concentrated solution was triturated with 20 volumes of hexanes. The suspension was refrigerated (~3 °C) overnight, after which time the suspension was filtered, the solids washed with additional hexanes, and then dried at 77 °C overnight to afford *N*-benzyl benzamide as a white solid (20.8 g, 99%). NMR spectral data and MP data agree with the literature. ^{1}H NMR (399.74 MHz, acetone-d_6 2.05 ppm) δ 4.60 (d, J = 6.0 Hz, 2H); A/A': 7.37 (2H), B/B': 7.31 (2H), C: 7.23 (1H) (J_{AB} = 7.5 Hz; J_{AC} = 1.3 Hz; J_{BC} = 7.5 Hz; $J_{AA'}$ = 1.9 Hz; $J_{BB'}$ = 1.5), D/D': 7.94 (2H), E/E': 7.45 (2H), F: 7.52 (1H) (J_{DE} = 8.9 Hz; J_{DF} = 1.4 Hz; J_{EF} = 7.5 Hz; $J_{DD'}$ = 1.8 Hz; $J_{EE'}$ = 1.3 Hz), 8.21 (br, 1H). mp 106.0–106.3 °C (lit. 105–106 °C).

Propanol-footed *meta*-basket (40)

Octabromide **32** is a known compound and synthesised according to literature procedures.[173] To a flame-dried, N_2-flushed flask was sequentially added octabromide **32** (7.34 g, 4.31 mmol), pyridine (200 mL), resorcinol (2.85 g, 25.8 mmol, 6.0 equiv.), and potassium carbonate (7.14 g, 51.7 mmol, 12 equiv.). At each of these additions, the resulting suspension was sparged with N_2 for 10 minutes to exclude dissolved and atmospheric O_2. Copper(I) bromide–dimethyl sulfide (10.6 g, 51.7 mmol, 12 equiv.) was then added in one portion, and the suspension was heated to vigorous reflux (sand bath) for 10 d. The solvent was

removed, and the residue dried under high vacuum at rt for 2 h. The solids were taken up in 250 mL THF, sonicated for 30 mins, then filtered through a THF-wet Celite pad. The Celite was washed with additional THF until the filtrate ran colourless. The solvent was removed from the combined filtrate under reduced pressure, and the residue dried under high vacuum at rt overnight. This residue was then taken up in 3 M HCl (aq.), sonicated for 45 minutes, filtered, washed with dH$_2$O until the filtrate was neutral, and dried under high vacuum at 110 °C for 6 h. The solids were taken up in 50 mL hexanes/EtOAc (1:1), sonicated for 5 mins, filtered, and washed with additional hexanes/EtOAc until the filtrate ran colourless. The solids were dried under high vacuum at 110 °C overnight to afford crude propanol-footed meta-basket **40** (5.43 g, 84% crude) as a tan solid.

Optional purification of propanol-footed *meta*-basket 40 via the tetra-acetate 40′

To a flame-dried, N$_2$-flushed flask was added crude **40** (0.109 g, 0.07 mmol) and acetic anhydride (10 mL). The suspension was stirred at 100 °C (oil bath) for 18 h, after which the homogeneous solution was cooled to rt, and the solvent removed under reduced pressure. The dark brown residue was then dried under high vacuum at 110 °C for 4 h. After this time the residue were subjected to flash column chromatography (100% CHCl$_3$, EtOH preservative, R_f = 0.10). Combining the resulting fractions containing the product, removal of the solvent under reduced pressure, and drying under high vacuum at 110 °C yielded **40′** as an off-

white solid (0.076 g, 63%). The solids were then dissolved in DMA (5 mL), and to the resulting solution was added 1 M LiOH (aq.) (0.70 mL, 16 equiv.) dropwise. The suspension was then stirred at 60 °C for 72 h, after which the solvent was removed from the homogeneous mixture under reduced pressure and the residue dried under high vacuum at rt for 3 h. The solids were then suspended in 1 M HCl (aq.) (10 mL) and sonicated for 10 mins. The suspension was filtered, washed with dH_2O until the filtrate ran neutral, and the solids were dried under high vacuum at 110 °C for 1 h. The solids were then taken up in 1:1 hexanes/$CHCl_3$ (10 ml), sonicated for 5 mins, and the suspension filtered. The solids were then dried under high vacuum at 110 °C overnight to afford pure **40** as a white powder (0.03 g, 44%). ^1H NMR (400 MHz, $CDCl_3$ 7.26 ppm) δ 1.64 (dq, J = 13.0, 6.5 Hz, 8H), 2.04 (s, 12H), 2.28 (q, J = 8.0 Hz, 8H), 4.12 (t, J = 6.5 Hz, 8H), 4.49 (s, 4H), 4.78 (t, J = 8.0 Hz, 4H), 5.95 (s, 4H), 6.46 (d, J = 2.0 Hz, 8H), 6.60 (t, J = 2.0 Hz, 4H), 6.96 (d, J = 2.5 Hz, 4H), 7.10 (s, 4H), 7.20 (dd, J = 8.0, 2.5 Hz, 8H), 7.55 (t, J = 8.0 Hz, 4H). $^{13}C\{^1H\}$ NMR (75 MHz, $CDCl_3$) δ 21.0, 26.9, 36.0, 63.9, 105.5, 107.6, 109.6, 115.4, 115.7, 120.6, 121.8, 131.2, 136.5, 139.0, 156.5, 156.6, 161.2, 171.0. HRMS (MALDI/TOF) m/z: $[M + Ag]^+$ Calcd. for $C_{100}H_{80}O_{24}Ag$ 1771.41; Found 1771.81. Anal. Calcd. for $C_{100}H_{80}O_{24} \cdot H_2O$: C, 71.34; H, 4.91. Found: C, 71.66, H, 5.21.

TIPS-footed *meta*-basket (41)

To a flame-dried, N_2-flushed flask containing anhydrous THF (200 mL) was added crude propanol-footed meta-basket **40** (5.43 g, 3.63 mmol) and imidazole

(2.17 g, 31.9 mmol, 8.8 equiv.). To the resulting dark-coloured mixture was added DIPEA (5.6 mL, 31.9 mmol, 8.8 equiv.) and TIPS-Cl (6.8 mL, 31.9 mmol, 8.8 equiv.). This mixture was heated to reflux (oil bath) for 48 h, after which time the solvent was removed under reduced pressure and the residue dried under high vacuum at rt overnight. The crude product was then subjected to flash column chromatography using a gradient of 0–5% EtOAc in hexanes (R_f = 0.36, 5% EtOAc in hexanes). After removal of the mobile phase under reduced pressure the resulting solid was suspended in 25 mL hexanes and sonicated for 3 min, refrigerated, and filtered to give the product **41** as a white powder which was dried under high vacuum at 110 °C overnight (1.96 g, 50%). ^{1}H NMR (500 MHz, CDCl$_3$, 7.26 ppm) δ 1.06 (m, 84H), 1.55 (tt, J = 7.5, 6.5 Hz, 8H), 2.27 (td, J = 8.0, 7.5 Hz, 8H), 3.75 (t, J = 6.5 Hz, 8H), 4.5 (s, 4H), 4.75 (t, J = 8.5 Hz, 4H), 5.95 (s, 4H), 6.50 (d, J = 2.5 Hz, 8H), 6.62 (t, J = 2.5 Hz, 4H), 6.97 (t, J = 2.5 Hz, 4H), 7.15 (s, 4H), 7.21 (dd, J = 8.0, 2.5 Hz, 8H), 7.55 (t, J = 8.0 Hz, 4H). ^{13}C{^{1}H} NMR (75 MHz, CDCl$_3$ 77.16 ppm) δ 12.2, 18.2, 26.7, 31.2, 36.3, 63.0, 105.8, 107.7, 109.8, 115.2, 115.9, 120.7, 122.4, 131.4, 137.0, 139.4, 156.5, 156.7, 161.3. HRMS (MALDI/TOF) m/z: [M + Na]$^+$ Calcd. for C$_{128}$H$_{152}$O$_{20}$Si$_4$Na 2144.98; Found 2144.95. Anal. Calcd. for C$_{128}$H$_{152}$O$_{20}$Si$_4$·2H$_2$O: C, 71.21; H, 7.28. Found: C, 70.98; H, 6.90.

Tetra-*exo*-ester TIPS- *meta*-basket (42)

To a flame-dried, N$_2$-flushed flask was added TIPS-*meta*-basket **41** (1.20 g, 0.57 mmol) and anhydrous THF (100 mL). The resulting solution was cooled to –

78 °C (acetone/CO$_2$) for 30 mins, before *sec*-BuLi (1.05 M in cyclohexane, 5.5 mL, 5.8 mmol, 10.2 equiv.) was added dropwise via syringe over 30 mins. The yellow solution was then left to stir for an additional 30 mins at –78 °C, after which ethyl chloroformate (0.6 mL in 5 mL anhydrous THF, 6.2 mmol, 11 equiv.) was added via syringe dropwise over 30 mins. The solution was left to stir for 1 h, after which the yellow solution was allowed to warm to rt and stirred for a total of 1 h. Aqueous HCl (1 M, 2.5 mL) was added slowly to quench the solution, the solvent was removed under reduced pressure, and the resulting solid foam residue dried under high vacuum at rt for 30 mins. The residue was taken up in 50 mL CHCl$_3$ and was washed with 3 × 20 mL dH$_2$O, and 1 × 20 mL sat'd NaCl (aq.). The organic layer was dried with anhydrous Na$_2$SO$_4$, filtered, and the solvent removed under reduced pressure. The residue was then dried under high vacuum at 110 °C overnight and the crude solids were subjected to flash column chromatography using 99:1 CHCl$_3$/EtOAc with a flow rate of 25 mL/min (R_f = 0.22, 2% EtOAc in hexanes). This afforded the product as a white solid which was dried under high vacuum at 110 °C overnight (0.58 g, 44%). ^{1}H NMR (500 MHz, CDCl$_3$ 7.26 ppm) δ 1.06 (m, 84H), 1.39 (t, *J* = 7.0 Hz, 12H), 1.54 (m, 8H), 2.26 (q, *J* = 7.0 Hz, 8H), 3.74 (t, *J* = 6.0 Hz, 4H), 4.45 (q, *J* = 7.0 Hz, 8H), 4.48 (s, 4H), 4.73 (t, *J* = 8.0 Hz, 4H), 5.87 (s 4H), 6.53 (d, *J* = 1.0 Hz, 8H), 6.72 (t, *J* = 2.0 Hz, 4H), 7.15 (s, 4H), 7.24 (dd, *J* = 2.0, 8.0 Hz, 8H), 7.56 (t, *J* = 8.0 Hz, 4H). ^{13}C{^{1}H} NMR (75 MHz, CDCl$_3$ 77.16 ppm) δ 12.2, 14.4, 18.2, 26.7, 31.1, 36.3, 62.0, 62.9, 106.0, 109.4, 115.1, 115.9, 121.0 122.5, 131.3, 137.0, 140.2, 156.3, 156.4, 158.0, 164.8. HRMS

(MALDI/TOF) m/z: [M + Na]$^+$ Calcd. for C$_{140}$H$_{168}$O$_{28}$Si$_4$Na 2432.07; Found 2432.56.

Anal. Calcd. for C$_{140}$H$_{168}$O$_{28}$Si$_4$: C, 69.74; H, 7.02. Found: C, 69.45; H, 7.15.

Tetra-*exo*-ester tetrol *meta*-basket (43)

To a dry flask was added tetra-*exo*-ester TIPS-meta-basket **42** (0.28 g, 0.12 mmol) and THF (25 mL). The mixture was stirred until homogeneous, and to which was then added TBAF·3H$_2$O (0.22 g, 0.70 mmol, 6 equiv.). The resulting solution was allowed to stir at rt overnight, after which the solvent was removed under reduced pressure, and the residue dried under high vacuum at rt for 1 h. The residue was taken up in 20 mL CHCl$_3$ and was washed with 3 × 20 mL dH$_2$O and 1 × 20 mL sat'd NaCl (aq.). The organic layer was dried with anhydrous Na$_2$SO$_4$, filtered, the solvent removed under reduced pressure, and the residue dried under high vacuum at rt for 2 h. The residue was taken up in 10 mL diethyl ether, sonicated for 3 mins, refrigerated for 2 h, filtered, washed with additional cold diethyl ether, and dried under high vacuum at 110 °C overnight to afford tetra-*exo*-ester tetrol meta-basket **43** as a white powder (0.16 g, 77%). ^{1}H NMR (300 MHz, DMSO-d_6 2.5 ppm) δ 1.27 (t, *J* = 7.0 Hz, 12H), 1.40 (m, 8H), 2.39 (m, 8H), 3.47 (q, *J* = 6.0 Hz, 8H), 4.37 (q, *J* = 7.0 Hz, 8H), 4.40 (s, 4H), 4.49 (t, *J* = 5.0 Hz, 4H), 4.54 (t, *J* = 8.0 Hz, 4H), 5.74 (s, 4H), 6.46 (s, 8H), 6.65 (t, *J* = 2.0 Hz, 8H), 7.40 (dd, *J* = 2.0, 6.2 Hz), 7.74 (m, 12H). ^{13}C{^{1}H} NMR (75 MHz, DMSO-d_6 39.52 ppm) δ 14.0, 26.0, 30.5, 36.2, 105.7, 108.6, 113.7, 114.5, 114.6, 120.6, 125.2, 132.0, 136.7, 139.6, 155.1, 155.6, 156.9, 163.6. HRMS (MALDI/TOF) m/z:

[M + Na]$^+$ Calcd. for $C_{104}H_{88}O_{28}Na$ 1807.53; Found 1807.52. Anal. Calcd. for $C_{104}H_{88}O_{28} \cdot CHCl_3 \cdot Et_2O$: C, 66.14; H, 5.04. Found: C, 66.10; H, 5.01.

Tetra-*exo*-ester tetra-acid (39′)

To a flame-dried, N$_2$-flushed flask was added tetra-*exo*-ester tetrol *meta*-basket **43** (0.160 g, 0.09 mmol), DMA (10.0 mL), and anhydrous *t*-BuOH (10.0 mL). The solution was then stirred until homogeneous, at which point KMnO$_4$ (0.198 g, 1.25 mmol, 14 equiv.) was added. The solution was allowed to stir at rt for 48 h, after which time the resulting suspension was filtered, and the residue taken up in 50 mL 1:1 DMA/H$_2$O, sonicated, filtered, and washed with 20 mL dH$_2$O. The solvent from the combined filtrates was removed under reduced pressure and the resulting residue dried under high vacuum at rt for 4 h. To the resulting solid was then added 10 mL conc. HCl. The suspension was sonicated for 5 mins, diluted with 20 mL dH$_2$O, filtered, and the solids washed with additional dH$_2$O until the filtrate ran neutral. The solids were dried under high vacuum at 110 °C overnight to afford tetra-*exo*-ester tetra-acid **39′** (0.141 g, 87%) as an off-white powder. ^{1}H NMR (300 MHz, DMSO-d_6 2.5 ppm) δ 1.28 (t, J = 7.0 Hz, 12H), 2.22 (q, J = 2.0 Hz, 8H), 2.62 (q, J = 2.0 Hz, 8H), 4.38 (q, J = 7.0 Hz, 8H), 4.40 (s, 4H), 4.60 (t, J = 8.0 Hz, 4H), 5.75 (s, 4H), 6.47 (s, 8H), 6.65 (t, J = 2.0 Hz, 4H), 7.40 (dd, J = 2.0, 8.0 Hz, 8H), 7.74 (m, 8H), 12.17 (s, 4H). ^{13}C{^{1}H} NMR (75 MHz, DMSO-d_6 39.52 ppm) δ 14.5, 25.5, 32.3, 36.3, 62.0, 106.4, 109.1, 114.6, 115.1, 115.3, 121.2, 125.3, 132.6, 136.7, 140.1, 155.9, 156.2, 157.5, 164.1, 174.3. HRMS (MALDI/TOF)

m/z: [M + Na]$^+$ Calcd for $C_{104}H_{80}O_{32}Na$ 1863.45; Found 1863.46. Anal. Calcd for $C_{104}H_{80}O_{32}\cdot 4H_2O$: C, 65.27; H, 4.63. Found: C, 65.59; H, 4.67.

exo-Octa-acid (39)

To a round bottomed flask was added tetra-*exo*-ester tetra acid (**39′**) (0.176 g, 0.096 mmol), pyridine (20 mL) and 2 M LiOH (aq.) (1.43 mL, 2.9 mmol, 30 equiv.). The suspension was stirred at reflux (sand bath) for 48 h, during which time dH$_2$O was added dropwise to dissolve any precipitate formed. After this time the homogeneous solution was allowed to cool to rt, and the solvent removed under reduced pressure. The residue was dried at rt for 2 h after which conc. HCl (10 mL) was added, and the resulting suspension sonicated for 5 mins. The suspension was diluted with dH$_2$O (20 mL), filtered, and the solids washed with additional dH$_2$O until the filtrate was neutral. The residue was dried under high vacuum at rt for 4 h, after which it was dissolved in minimum acetone, triturated with 20 volumes of dH$_2$O, refrigerated for 1 h, and filtered. The residue was dried under high vacuum at 110 °C for 24 h to afford *exo*-octa acid **39** (0.130 g, 79%) as an off-white powder. ^{1}H NMR (300 MHz, DMSO-d_6 2.5 ppm) δ 2.21 (m, 8H), 2.62 (m, 8H), 4.40 (s, 4H), 4.60 (t, J = 13.5 Hz, 4H), 5.76 (s, 4H), 6.45 (s, 8H), 6.68 (t, J = 3.5 Hz, 4H), 7.36 (dd, J = 3.5, 13.5 Hz, 8H), 7.72 (m, 12H). ^{1}H NMR (500 MHz, D$_2$O 4.79 ppm) δ 2.22 (t, J = 7.5 Hz, 8H), 2.60 (q, J = 7.5 Hz, 8H), 4.52 (s, 4H), 4.63 (t, J = 8.0, 4H), 5.95 (s, 4H), 6.51 (s, 8H), 6.93 (t, J = 2.0 Hz, 4H), 7.34 (dd, J = 2.0, 8.0 Hz, 8H), 7.51 (s, 4H), 7.67 (t, J = 8.0 Hz, 8H). ^{13}C{^{1}H} NMR (75 MHz,

DMSO-d_6 39.52 ppm) δ 25.1, 31.9, 35.9, 105.9, 108.9, 114.2, 115.0, 116.5, 120.6, 124.9, 132.0, 136.2, 138.9, 155.5, 155.9, 156.6, 165.0, 173.9. HRMS (ESI) m/z: [M – 4H$^+$]$^{4-}$ Calcd for $C_{96}H_{64}O_{32}$ 431.3281; Found 431.3261.

3,4,5-trimethoxybenzaldehyde dimethyl acetal (54)

To a dry flask flushed with N_2 and fitted with a reflux condenser and an addition funnel charged with 3 Å molecular sieves (30 g)[232] was added 3,4,5-trimethoxybenzaldehyde (50.0 g, 255 mmol), anhydrous benzene (300 mL), trimethyl orthoformate (69.7 mL, 637 mmol, 2.55 equiv.), and p-TSA hydrate (1.10 g, 6.37 mmol, 0.025 equiv.). The colour of the solution slowly changed from colourless, to purple, to yellow as the temperature increased from rt to reflux. The solution was stirred at reflux temperature (sand bath) for 48 h., after which the clear yellow solution was allowed to cool to rt. The cooled solution was diluted with 200 mL EtOAc, washed with 1 × 300 mL saturated aqueous $NaHCO_3$, 3 × 300 mL dH_2O, and 1 × 300 mL 20% w/w aqueous Na_2SO_4. The organic layer was then dried with anhydrous $MgSO_4$, filtered, and the solvent removed from the filtrate. The oily residue was then cooled to –78 °C (acetone/CO_2) to induce crystallization, and the solids dried at rt for 24 h. to afford **54** as an off-white solid (60.3 g, 98%). NMR spectroscopic data agree with the literature.[233] ^{1}H NMR (500.13 MHz, acetone-d_6, 2.05 ppm) δ 3.27 (s, 6H), 3.72 (s, 3H), 3.82 (s, 6H), 5.30 (s, 1H), 6.72 (s, 2H). ^{13}C{^{1}H} NMR (100.51 MHz, acetone-d_6) δ 52.8, 56.3, 60.5, 103.8, 104.9, 135.0, 139.1, 154.2. mp 39.1–41.1 °C.

4-Ethyl-3,5-dimethoxybenzaldehyde (55)

Compound **55** was synthesised according to a modification of a literature report.[234] To a flame-dried, N_2-flushed round-bottomed flask was added 80 mL unstabilized anhydrous THF and freshly cut sodium metal (3.0 g, 130 mmol, 3.15 equiv) pressed into leaves, and was allowed to stir at 23 °C for 15 minutes. To this was added dimethyl acetal **54** (10.0 g, 41.3 mmol) in one portion, and the mixture was allowed to stir at rt for 24 h during which the suspension went from colourless, to yellow, to deep red. The resulting deep red suspension was cooled to 0 °C (ice bath), and to which bromoethane (30 mL, 495 mmol, 3.81 equiv.) was added over 30 mins via a pressure-equalising addition funnel. The resulting yellow suspension was allowed to warm to rt and stirred for 24 h, after which the reaction was cooled to 0 °C for 1 h. The cooled solution was then quenched with 50 mL 6 M HCl added dropwise over 1 h (DANGER! H_2 released. Frequent venting required.) via a pressure-equalising addition funnel and allowed to stir at rt for 2 h. The organic solvent was then removed under reduced pressure, the remaining aqueous suspension was extracted with 3 × 75 mL EtOAc, and the combined organics washed sequentially with 1 × 50 mL satd. $NaHCO_3$, 1 × 100 mL dH_2O, and 1 × 50 mL 20% w/w aq Na_2SO_4. The organic layer was dried with anhydrous Na_2SO_4 and filtered. The solvent was removed under reduced pressure and the residue dried at rt for 12 h. The crude mixture was then subjected to column chromatography [gradient from 0–5% EtOAc in hexanes v/v, R_f = 0.46 (10%

EtOAc in hexanes)] to afford **55** as a white micaceous solid (6.70 g, 84%) which was dried at rt for 24 h. NMR spectroscopic data agree with the literature.[234] ^{1}H NMR (399.74 MHz, acetone-d_6) δ 1.05 (t, J = 7.5 Hz, 3H), 2.70 (q, J = 7.5 Hz, 2H), 3.92 (s, 6H), 7.19 (s, 2H), 9.94 (s, 1H). ^{13}C{^{1}H} NMR (75.47 MHz, acetone-d_6, 29.84, 206.26 ppm) δ 13.8, 17.5, 56.5, 105.8, 128.3, 137.0, 159.5, 192.5. mp 72–73 °C.

4-Ethyl-3,5-dimethoxybenzoic acid (56)

To a round-bottomed flask with magnetic stirrer was added **55** (2.4 g, 12.5 mmol) and THF (100 mL). To the solution was added 0.5 M aqueous Oxone (100 mL, 63 mmol, 5 equiv) and stirred for 48 h at rt, during which the triphasic suspension gradually took on an orange colour. The organic solvent was removed from the triphasic suspension under reduced pressure, and the resulting suspension was extracted with 100 mL EtOAc. The organic layer was then washed with 3 × 100 mL dH$_2$O and 1 × 100 mL 20% aq. Na$_2$SO$_4$. The organic layer was then dried with anhydrous Na$_2$SO$_4$, filtered, the solvent removed under reduced pressure, and the resulting residue dried at 77 °C. The fibrous solid was then dissolved in a minimum amount of boiling absolute EtOH, and slowly crystallised out of solution by the addition of ca. 15% boiling H$_2$O, and allowed to cool slowly to rt. The resultant needles were filtered, washed with ice-cold dH$_2$O, and dried at 77 °C to afford pure **56** (2.33 g, 90%). ^{1}H NMR (500.13 MHz, acetone-d_6 2.05 ppm) δ 1.04 (t, J = 7.5 Hz, 3H), 2.68 (q, J = 7.5 Hz, 2H), 3.88 (s, 6H), 7.27

(s, 2H), 11.2 (br, 1H). $^{13}C\{^1H\}$ NMR (75.47 MHz, acetone-d_6 29.84, 206.26 ppm) δ 13.9, 17.3, 56.3, 106.0, 126.6, 130.2, 158.9, 167.7. Calcd for $C_{11}H_{14}O_4$: C, 62.85; H, 6.71; O, 30.44. Found: C, 62.80; H, 6.71; O, 30.28. mp 194.1–195.5 °C.

Crystalline samples used for X-ray crystallography were obtained by layered diffusion of hexanes onto a solution of **56** in THF.

4-Ethyl-3,5-dihydroxybenzoic acid (57)

To a flame-dried, N_2-flushed round-bottomed flask fitted with a magnetic stirrer was added **56** (2.0 g, 9.3 mmol), anhydrous DCM (75 mL), and BBr_3 (3.6 mL, 37.3 mmol, 4 equiv). **N.B.**: Compound **56** is not immediately soluble in DCM. The solution was allowed to stir at rt for 18 h, after which the flask was opened to atmosphere for 10 mins. The solution was then cooled to 0 °C (ice bath) and 50 mL dH_2O was then added dropwise over 30 mins (CAUTION! $HBr_{(g)}$ released!) during which a tan solid precipitated. The organic solvent was then removed under reduced pressure from the triphasic mixture, and the aqueous suspension was extracted with 3 × 30 mL Et_2O. To the combined organics were added anhydrous Na_2SO_4 and decolourising carbon, after which the suspension was stirred for 5 mins. The suspension was filtered through a pad of Celite 545, and the pad was flushed with an additional 50 mL Et_2O. The solvent was removed from the filtrate under reduced pressure and the solids dissolved in minimal THF. The solution was then triturated with 20 volumes of hexanes to precipitate the product. The suspension was refrigerated (3 °C) overnight, filtered, and the solids

dried for 24 h at 77 °C to afford **57** as a fine white powder (1.6 g, 93%). ^{1}H NMR (399.74 MHz, acetone-d_6, 2.05 ppm) δ 1.12 (t, J = 7.5 Hz, 3H), 2.71 (q, J = 7.5 Hz, 2H), 7.10 (s, 2H), 8.41 (s, 2H), 10.92 (br, 1H). ^{13}C{^{1}H} NMR (75.47 MHz, acetone-d_6 29.84, 206.26 ppm) δ 13.7, 17.4, 109.0, 123.6, 129.6, 156.8, 167.7 Calcd for $C_9H_{10}O_4$: C, 59.34; H, 5.53; O, 35.13. Found: C, 59.60; H, 5.63; O, 35.41. mp 133 °C (dec.).

3,5-Dihydroxy-4-ethylbenzyl alcohol (58)

To a flame-dried, N_2-flushed round-bottomed flask fitted with a magnetic stirrer and reflux condenser was added **57** (1.3 g, 7.1 mmol) unstabilized anhydrous THF (45 mL), and $(MeO)_3B$ (3.6 mL, 32.3 mmol, 4.5 equiv.). The resulting solution was cooled to 0 °C for 10 mins, after which $BH_3 \cdot Me_2S$ complex (2.8 mL, 28.6 mmol, 4 equiv.) was added dropwise over 10 mins (CAUTION! H_2 released. Frequent venting is required during addition.). The solution was stirred at 0 °C for 15 mins, after which the solution was heated to reflux (oil bath) for 24 h. The solution was then cooled to 0 °C (ice bath), opened to atmosphere, and MeOH (25 mL) was added over 5 mins to quench the reaction (CAUTION! H_2 released). The solvent was removed under reduced pressure, and 25 mL MeOH was added and removed under reduced pressure two additional times to facilitate the evaporation of the volatile borates. The resulting residue was dried for 1 h at rt and was then dissolved in a minimal amount of THF, triturated with 20 volumes of $CHCl_3$, and filtered. The resulting solids were dried overnight at 77 °C to afford

58 as a fine white powder (1.0 g, 85%). ^{1}H NMR (399.74 MHz, acetone-d_6 2.05 ppm) δ 1.08 (t, J = 7.5 Hz, 3H), 2.65 (q, J = 7.5 Hz, 2H), 3.89 (t, J = 6.0 Hz, 1H), 4.41 (d, J = 6.0 Hz, 2H), 6.38 (s, 2H), 7.91 (s, 2H). ^{13}C{^{1}H} NMR (75.47 MHz, acetone-d_6 29.84, 206.26 ppm) δ 14.3, 17.1, 64.8, 106.0, 116.5, 142.0, 156.8. Calcd for $C_9H_{12}O_3$: C, 64.27; H, 7.19. Found: C, 64.49; H, 7.29. mp 153–156 °C

Crude tetra-*endo*-ethyl octol, TEEtOctol (59)

Octabromide **32** is a known compound and was synthesis according to literature procedures.[173] To a flame-dried, N_2-flushed round bottomed flask fitted with a magnetic stirrer and reflux condenser was added sequentially pyridine (500 mL), octabromide **32** (10.0 g, 5.87 mmol), **58** (5.92 g, 35.2 mmol, 6 equiv), and anhydrous K_2CO_3 (9.73 g, 70.4 mmol, 12 equiv). The suspension was stirred and sparged with N_2 for 10 mins between additions to exclude atmospheric and dissolved O_2. To the suspension was then added CuBr·SMe$_2$ (14.5 g, 70.4 mmol, 12 equiv), and the resulting deep green suspension was heated to a vigorous reflux for 21 d (sand bath) during which time the suspension took on a brown colour. The solvent was then removed under reduced pressure and the residue dried at rt for 10 mins. To the residue was then added THF (500 mL) and sonicated for 45 mins. The suspension was then filtered through a pad of Celite 545, and the pad flushed with additional THF until the filtrate ran colourless. The solvent was removed from the filtrate under reduced pressure, and the residue dried at rt

for 1 h. The residue was then suspended in 6 M aqueous HCl (150 mL) and sonicated for 1 h. The suspension was filtered, and the residue washed with dH$_2$O until the filtrate was pH neutral. The solids were dried at 140 °C overnight, sonicated in 150 mL EtOAc, filtered, and the dark-coloured solids washed with the same solvent until the filtrate ran colourless. The filtrate was allowed to stand at rt for 2 h during which time a tan micaceous solid precipitated out of solution. The solvent volume was then reduced to 50% under reduced pressure. The solids were filtered, then dried at 140 °C overnight to afford crude TEEtOctol **59** as a tan powder (3.92 g, 32% yield of crude **59**). Compound **59** was used in the next step without further purification.

Optional purification of tetra-*endo*-ethyl octol, TEEtOctol (59) via the octa acetate, TEEtOAc (60)

To a flame-dried, N$_2$-flushed round-bottomed flask fitted with a magnetic stirrer was added **59** (0.500 g, 0.29 mmol) and acetic anhydride (20 mL, 212 mmol, 732 equiv.). The suspension was stirred at 110 °C (oil bath) for 24 h, during which time the mixture became homogenous. The solution was then allowed to cool to rt, and the solvent was removed under reduced pressure. The residue was dried under high vacuum at 110 °C for 4 h. The residue was subjected to column chromatography [gradient from 0% EtOAc in hexanes to 10 % EtOAc in hexanes (R_f = 0.15)], and the relevant fractions dried at 110 °C overnight. The glassy

residue was then taken up in hexanes and sonicated for 10 minutes, and the resulting powder was filtered and dried at 110 °C to give **60** as a fine white powder (0.341 g, 57%). ^{1}H NMR (500.13 MHz, CDCl$_3$, 7.26 ppm) δ 0.52 (t, J = 7.5 Hz, 12H), 1.66 (tt, J = 7.0, 6.5 Hz, 8H), 2.055 (s, 12H), 2.061 (s, 12H), 2.15 (q, J = 7.5 Hz, 8H), 2.29 (dt, J = 8.0, 6.5 Hz, 8H), 4.14 (t, J = 6.5 Hz, 8H), 4.44 (s, 4H), 4.80 (t, J = 8.0 Hz, 4H), 5.20 (s, 8H), 5.90 (s, 8H), 6.486 (s, J = 2.5 Hz, 8H), 7.047 (t, J = 2.5 Hz, 4H), 7.09 (s, 4H), 7.26 (s 8H). ^{13}C{^{1}H} NMR (125.77 MHz, CDCl$_3$ 77.16 ppm) δ 13.4, 17.5, 20.85, 20.97, 26.73, 26.87, 36.0, 63.8, 64.9, 104.7, 106.1, 109.4, 115.2, 121.0, 121.7, 130.6, 136.65, 136.68, 138.9, 154.0, 156.3, 161.4, 170.6, 171.0. Calcd for C$_{120}$H$_{112}$O$_{32}$·H$_2$O: C, 69.15; H, 5.51 Found: C, 69.41; H, 5.50. mp >260 °C.

Pure tetra-*endo*-ethyl octol, TEEtOctol (59)

To a dry flask flushed with N$_2$ and fitted with a magnetic stirrer was added **60** (0.150 g, 0.073 mmol) and DMA (10 mL). The solution was allowed to stir at 70 °C (oil bath) for 30 mins, after which time 2 M aq. LiOH·H$_2$O (1.52 mL, 3.05 mmol, 42 equiv.) was added in one portion. The resulting suspension was allowed to stir for 15 mins after which dH$_2$O was added in 0.5 mL portions every 2 mins until the precipitate dissolved (~3 mL) and the resulting homogenous mixture was allowed to stir overnight. The solution was allowed to cool to rt, the solvent was removed under reduced pressure, and the residue was dried at rt

under high vacuum for 3 h. The residue was then taken up in 1 M aq. HCl (25 mL) and sonicated for 30 minutes. The suspension was filtered, and the solids washed with dH$_2$O until the eluting filtrate was pH neutral. The solids were then dried at 140 °C under high vacuum to afford pure **g** as a white powder (0.115 g, 92%). ^{1}H NMR (500.13 MHz, DMSO-d_6) δ −0.04 (t, J = 7.5 Hz, 12H), 1.41 (tt, J = 7.0, 6.5 Hz, 8H), 2.29 (q, J = 7.5 Hz, 8H), 2.40 (dt, J = 8.0, 6.5 Hz, 8H), 3.48 (dt, J = 6.0, 5.5 Hz, 8H), 4.42 (s, 4H), 4.50 (t, J = 5.0 Hz, 4H), 4.56 (t, J = 8.0 Hz, 4H), 4.58 (d, J = 5.5 Hz, 8H), 5.44 (t, J = 6.0 Hz, 4H), 5.73 (s, 8H), 6.434 (d, J = 2.0 Hz, 8H), 7.146 (t, J = 2.0 Hz, 4H), 7.26, (s, 8H), 7.71 (s, 4H). ^{13}C{^{1}H} NMR (125.76 MHz, DMSO-d_6 39.52 ppm) δ 13.0, 16.9, 26.0, 30.6, 36.2, 60.2, 61.7, 104.5, 105.6, 108.8, 114.3, 119.1, 124.9, 128.1, 137.0, 138.6, 143.6, 153.2, 155.2, 161.3. Calcd for C$_{104}$H$_{96}$O$_{24}$·2HCl·H$_2$O: C, 68.60; H, 5.54. Found: C, 68.95; H, 5.50. mp >260 °C.

Crude tetra-*endo*-ethyl octa-acid, TEEtOA (53)

To a flame-dried, N$_2$-flushed round-bottomed flask fitted with a magnetic stirrer was added crude **59** (1.4 g, 0.8 mmol) and DMA (100 mL). The solution was sparged for 5 mins, and then *t*-BuOH (100 mL) was added. The solution was again sparged for 5 mins, after which time KMnO$_4$ (3.5 g, 22.3 mmol, 28 equiv) was added in one portion. The deep purple solution was allowed to stir for 4 d at 60 °C, after which time the dark brown suspension was filtered, the residue taken up in 100 mL 4:1 dH$_2$O/DMA, sonicated for 20 mins, and filtered. The solvent was removed from the filtrate under reduced pressure and the residue dried at rt for

24 h. The residue was then suspended in conc. HCl (50 mL) and sonicated for 30 mins. The suspension was diluted with dH_2O (50 mL), sonicated for an additional 20 mins, filtered, and the solids washed with dH_2O until the filtrate was pH neutral. The solids were then dried overnight at 140 °C to afford crude **53** as a tan powder (1.1 g, 73% yield of crude **53**).

Tetra-*endo*-ethyl octa ethyl ester, TEEtOEster (61)

To a flame-dried, N_2-flushed round bottomed flask fitted with a magnetic stirrer and reflux condenser was added crude **53** (1.1 g, 0.6 mmol), HCl-saturated EtOH (90 mL), and $CHCl_3$ (140 mL). The light brown solution was heated to reflux (oil bath) under a blanket of N_2 for 4 d, after which the solvent was removed under reduced pressure and dried under high vacuum at rt for 4 h. The residue was taken up in absolute EtOH (15 mL), sonicated for 15 mins, filtered, and dried at 110 °C overnight. The solids were subjected to column chromatography [gradient from 40% hexanes in $CHCl_3$ to 100% $CHCl_3$, R_f = 0.25 (5% acetone in $CHCl_3$)], the solvent removed and dried at rt. The compound was subjected to a second round of chromatographic separation using the same conditions but using Teledyne Isco RediSep Gold cartridges. The centre 50% fractions were collected, the solvent removed, and the resulting glassy, colourless solid was dissolved in minimal $CHCl_3$ and triturated with 20 volumes of hexanes to precipitate the product. The suspension was refrigerated overnight, filtered, and the solids dried

at 140 °C overnight to afford **61** as a fine white powder. (0.98 g, 78%). ^{1}H NMR (500.13 MHz, CDCl$_3$, 7.26 ppm) δ 0.58 (t, J = 7.5 Hz, 12H), 1.24 (t, J = 7.0 Hz, 12H), 1.41 (t, J = 7.0 Hz, 12 H), 2.17 (q, J = 7.5 Hz, 8H), 2.29 (t, J = 7.5 Hz, 8H), 2.54 (td, J = 7.5, 8.0 Hz, 8H), 4.13 (q, J = 7.0 Hz, 8H), 4.40 (q, J = 7.0 Hz, 8H), 4.43 (s, 4H), 4.77 (t, J = 8.0 Hz, 4H), 5.83 (s, 4H), 6.475 (d, J = 2.5 Hz, 8H), 7.08 (t, J = 2.5 Hz, 4H), 7.12 (s, 4H), 7.91 (s, 8H). ^{13}C{^{1}H} NMR (100.51 MHz, CDCl$_3$ 77.16 ppm) δ 13.3, 14.3, 14.4, 18.1, 25.5, 32.5, 36.2, 60.8, 61.8, 104.9, 106.3, 109.3, 115.4, 122.0, 123.0, 131.0, 136.4, 136.6, 139.3, 153.9, 156.5, 161.4, 164.9, 172.9 Calcd for C$_{120}$H$_{112}$O$_{32}$: C, 69.76; H, 5.46. Found: C, 69.43; H, 5.36. mp >260 °C.

Pure tetra-*endo*-ethyl octa acid, TEEtOA (53)

To a dry round-bottomed flask fitted with a magnetic stirrer was added octa-ester **61** (0.311 g, 0.150 mmol) and DMA (33 mL). The solution was stirred at 60 °C (oil bath) for 30 mins, after which 2 M aq. LiOH·H$_2$O (0.685 mL, 1.37 mmol, 9.10 equiv) was added dropwise over 5 mins. The solution gradually became turbid, and to the suspension was slowly added dH$_2$O (~10 mL) until the precipitate redissolved. The temperature of the solution was maintained at 60 °C (oil bath) for 24 h, after which the solution was allowed to cool to rt and the solvent was removed under reduced pressure. The residue was dried at rt overnight under vacuum, after which time conc. aq. HCl (20 mL) was added to the solids. The

suspension was sonicated for 30 mins, after which the suspension was diluted with dH$_2$O (20 mL), sonicated for an additional 15 mins, then filtered. The solids were washed with additional portions of dH$_2$O until the filtrate was pH neutral. The solids were then dried at 140 °C overnight, taken up in 15 mL anhydrous acetone, then sonicated for 5 mins. The suspension was refrigerated overnight (3 °C), filtered, and the solids dried at 140 °C for 48 h to afford pure tetra-*endo*-ethyl octa acid **2** as a fine white powder (0.27 g, 97%). ^{1}H NMR (500.13 MHz, 10 mM in 10 mM pD 11.45 phosphate buffer in D$_2$O (DSS), 0.00 ppm) δ −0.35 (m, 12 H), 2.22 (t, *J* = 7.5 Hz, 8H), 2.52 (m, 8 H), 2.61 (tt, *J* = 9.0, 7.5 Hz, 8H), 4.15 (br, 4H), 4.66 (t, *J* = 9.0 Hz, 4H), 5.84 (s, 4H), 6.57 (s, 8H), 7.17 (s, 4H), 7.54 (s, 4H), 7.84 (s, 8H). ^{13}C{^{1}H} NMR (75.47 MHz, 10 mM in 10 mM pD 11.45 phosphate buffer in D$_2$O (DSS), 0.00 ppm) δ 11.9, 17.3, 26.1, 35.4, 36.4, 105.3, 106.2, 110.2, 113.9, 122.4, 123.8, 133.0, 137.1, 137.6, 138.3, 153.1, 155.7, 161.9, 172.9, 182.3. Calcd for C$_{104}$H$_{80}$O$_{32}$·4H$_2$O·HCl: C, 64.05; H, 4.60 Found: C, 64.33; H, 4.21. mp >260 °C.

Tetra-*endo*-methyl octa bromide, TEMOX-Br (70)

Tetra-*endo*-methyl octol **69** is a known compound and was synthesised according to literature procedures.[192] To a flame-dried, N$_2$-flushed flask fitted with a magnetic stirrer was added crude **69** (1.00 g, 0.597 mmol) and anhydrous DCM (120 mL). The resulting suspension was sonicated for 5 mins., after which time the suspension stirred and was sparged with N$_2$ for 15 mins. To the sparging suspension was added triphenylphosphane (2.51 g, 9.56 mmol, 16 equiv.) and

was again sparged for 15 mins. To the mixture was then added CBr$_4$ (3.57 g, 10.8 mmol, 18 equiv.) in one portion, and the resulting mixture was allowed to stir at 30 °C for 48 h, during which time the suspension partially lost its turbidity. The mixture was then flushed through a DCM-saturated silica plug, and the product was eluted with additional DCM [R_f = 1.00 (100% DCM)]. The solvent was removed from the filtrate and the residue was dried at rt for 1 h. The solids were then taken up in hexanes and sonicated for 5 minutes, filtered, washed with additional hexanes, and dried at 110 °C to afford tetra-*endo*-methyl octa bromide **70** as a white powder (0.650 g, 50%). ^{1}H NMR (500.13 MHz, CD$_2$Cl$_2$ 5.32 ppm) δ 1.63 (s, 12H), 1.90 (tt, *J* = 7.5, 6.0 Hz, 8H), 2.47 (dt, *J* = 8.0, 7.5 Hz, 8H), 3.53 (t, *J* = 6.0 Hz, 8H), 4.37 (s, 4H), 4.56 (s, 8H), 4.76 (t, *J* = 8.0 Hz, 4H), 5.94 (s, 4H), 6.49 (d, *J* = 2.5 Hz, 8H), 7.07 (t, *J* = 2.5 Hz, 4H), 7.26 (s, 4H), 7.30 (s, 8H). ^{13}C{^{1}H} NMR (100.45 MHz, CD$_2$Cl$_2$ 53.84 ppm) δ 9.4, 29.3, 31.6, 32.6, 34.6, 36.6, 104.8, 106.9, 110.2, 115.4, 122.3, 123.2, 125.9, 137.1, 139.1, 139.9, 154.5, 157.0, 161.2. mp >260 °C.

Positand 2 (67)

To a flame-dried, N$_2$-flushed flask fitted with magnetic stirrer was added **70** (0.500 g, 0.230 mmol) and anhydrous DMF (40 mL). To the homogeneous solution was added Et$_3$N (4 M in EtOH, 0.672 mL 2.76 mmol, 12.0 equiv.) and stirred at 40 °C for 24 hours, during which time a white, micaceous precipitate formed. Another aliquot of Et$_3$N was added, (4 M in EtOH, 0.672 mL, 2.76 mmol,

12.0 equiv), and additional EtOH was injected into the suspension (~5 mL) to solubilise the precipitate. The homogeneous solution was allowed to stir at 40 °C for another 24 h, after which time the solution was cooled to rt, the solvent removed under reduced pressure (**NB**: bath temperature must not exceed 30 °C), and the residues dried at rt for 4 h. The solids were then taken up in 20 mL DCM, sonicated for 1 min., filtered, and washed with additional 20 mL DCM, and dried at rt for 1 h to yield Positand 2 bromide salt as an off-white powder. The bromide salt was dissolved in 5 mL ultra-pure water and loaded onto a Dowex 1x8 chloride form ion-exchange column (15 g) and eluted with ultra-pure water until all UV-active fractions have eluted. The fractions were collected and lyophilised to give crude Positand 2 chloride as a pale yellow-brown solid. The crude product was then dissolved in a minimum amount of ultrapure water and loaded onto a Biogel P2 size-exclusion chromatography column. The first, coloured fraction was discarded, and the centre fractions of the major peak was collected. The aqueous solution was lyophilised to give pure Positand 2 chloride (**67**) as a fluffy white powder. ^{1}H NMR (500.13 MHz, D$_2$O 4.79 ppm) δ 1.73 (s, 12H), 1.80 (m, 8H), 2.63 (dd, J = 8.0, 7.5 Hz, 8H), 3.05 (s, 36H), 3.14 (s, 36H), 3.48 (m, 8H), 4.47 (s, 4H), 4.60 (s, 8H), 4.67 (t, J = 8.0 Hz, 4H), 5.83 (s, 4H), 6.41 (d, J = 2.5 Hz, 8H), 7.31 (t, J = 2.5 Hz, 4H), 7.58 (s, 8H), 7.86 (s, 4H). mp >260 °C.

Tetra-*endo*-ethyl octa bromide, TEEtOX-Br (71)

To a flame-dried, N_2-flushed flask fitted with a magnetic stirrer was added **59** (1.00 g, 0.578 mmol) and anhydrous DCM (120 mL). The resulting suspension was sonicated for 5 mins., after which time the suspension stirred and was sparged with N_2 for 15 mins. To the sparging suspension was added triphenylphosphane (2.43 g, 9.25 mmol, 16 equiv.) and was again sparged for 15 mins. To the mixture was then added CBr_4 (3.45 g, 10.4 mmol, 18 equiv.) in one portion, and the resulting mixture was allowed to stir at 30 °C for 48 h, during which time the suspension partially lost its turbidity. The mixture was then flushed through a DCM-saturated silica plug, and the product was eluted with additional DCM [R_f = 1.00 (100% DCM)]. The solvent was removed from the filtrate and the residue was dried at rt for 1 h. The solids were then taken up in hexanes and sonicated for 5 minutes, filtered, washed with additional hexanes, and dried at 110 °C to afford tetra-*endo*-ethyl octa bromide **71** as a white powder (0.844 g, 65%). ^{1}H NMR (500.13 MHz, $CDCl_3$ 7.26 ppm) δ 0.51 (t, *J* = 7.5 Hz, 12H), 1.89 (tt, *J* = 7.5, 6.0 Hz, 8H), 2.15 (q, *J* = 7.5 Hz, 8H), 2.44 (dt, *J* = 8.0, 7.5 Hz, 8H), 3.52 (t, *J* = 6.0 Hz, 8H), 4.40 (s, 4H), 4.51 (s, 8H), 4.76 (t, *J* = 8.0 Hz, 4H), 5.92 (s, 4H), 6.50 (d, *J* = 2.5 Hz, 8H), 7.04 (t, *J* = 2.5 Hz, 4H), 7.18 (s, 4H), 7.28 (s, 8H). ^{13}C{^{1}H} NMR (125.76 MHz, $CDCl_3$ 77.16 ppm) δ 13.4, 17.5, 28.7, 30.9, 31.7, 33.8, 35.9, 104.7, 106.1, 109.4, 115.2, 122.1, 122.3, 131.1, 136.7, 138.4, 139.1, 154.0, 156.3, 161.3 Calcd for $C_{104}H_{88}Br_8O_{16}$·$CHBr_3$: C, 50.73; H, 3.61. Found: C, 50.95; H, 3.85. mp >260 °C.

Positand 3 (68)

To a flame-dried, N_2-flushed flask fitted with magnetic stirrer was added **71** (0.200 g, 0.090 mmol) and anhydrous DMF (27 mL). To the homogeneous solution was added Et_3N (4 M in EtOH, 0.262 mL 1.07 mmol, 12.0 equiv.) and stirred at 40 °C for 24 hours, during which time a white, micaceous precipitate formed. Another aliquot of Et_3N was added, (4 M in EtOH, 0.262 mL, 1.07 mmol, 12.0 equiv), and additional EtOH was injected into the suspension (~5 mL) to solubilise the precipitate. The homogeneous solution was allowed to stir at 40 °C for another 24 h, after which time the solution was cooled to rt, the solvent removed under reduced pressure (**NB**: bath temperature must not exceed 30 °C), and the residues dried at rt for 4 h. The solids were then taken up in 10 mL DCM, sonicated for 1 min., filtered, and washed with additional 10 mL DCM, and dried at rt for 1 h to yield Positand 3 bromide salt as an off-white powder. The bromide salt was dissolved in 5 mL ultra-pure water and loaded onto a Dowex 1x8 chloride form ion-exchange column (15 g) and eluted with ultra-pure water until all UV-active fractions have eluted. The fractions were collected and lyophilised to give crude Positand 3 chloride as a pale yellow-brown solid. The crude product was then dissolved in a minimum amount of ultrapure water and loaded onto a Biogel P2 size-exclusion chromatography column. The first, coloured fraction was discarded, and the centre fractions of the major peak was collected. The aqueous solution was lyophilised to give pure Positand 3 chloride (**68**) as a fluffy white powder. ^{1}H NMR (700.26 MHz, D_2O 4.79 ppm) δ −0.23 (br, 12H), 1.84 (m, 8H), 2.57 (br, 8H), 2.69 (dt, J = 8.0, 7.0 Hz, 8H), 3.11 (s, 36H), 3.18 (s, 36H), 3.54 (m,

8H), 4.18 (br, 4H), 4.66 (s, 8H), 4.76 (t, *J* = 8.0 Hz, 4H), 5.80 (s, 4H), 6.51 (s, 8H), 7.33 (s, 4H), 7.70 (s, 8H), 7.94 (s, 4H). $^{13}C\{^1H\}$ DEPT135Q NMR (176.10 MHz, D_2O (DSS) 0.00 ppm) δ 11.7, 17.1, 20.8, 26.6, 36.5, 52.6, 52.7, 66.0, 68.1, 105.1, 106.9, 110.7, 113.7, 125.4, 126.4, 128.1, 133.8, 137.2, 137.9, 153.9, 155.7, 161.7. mp >260 °C.
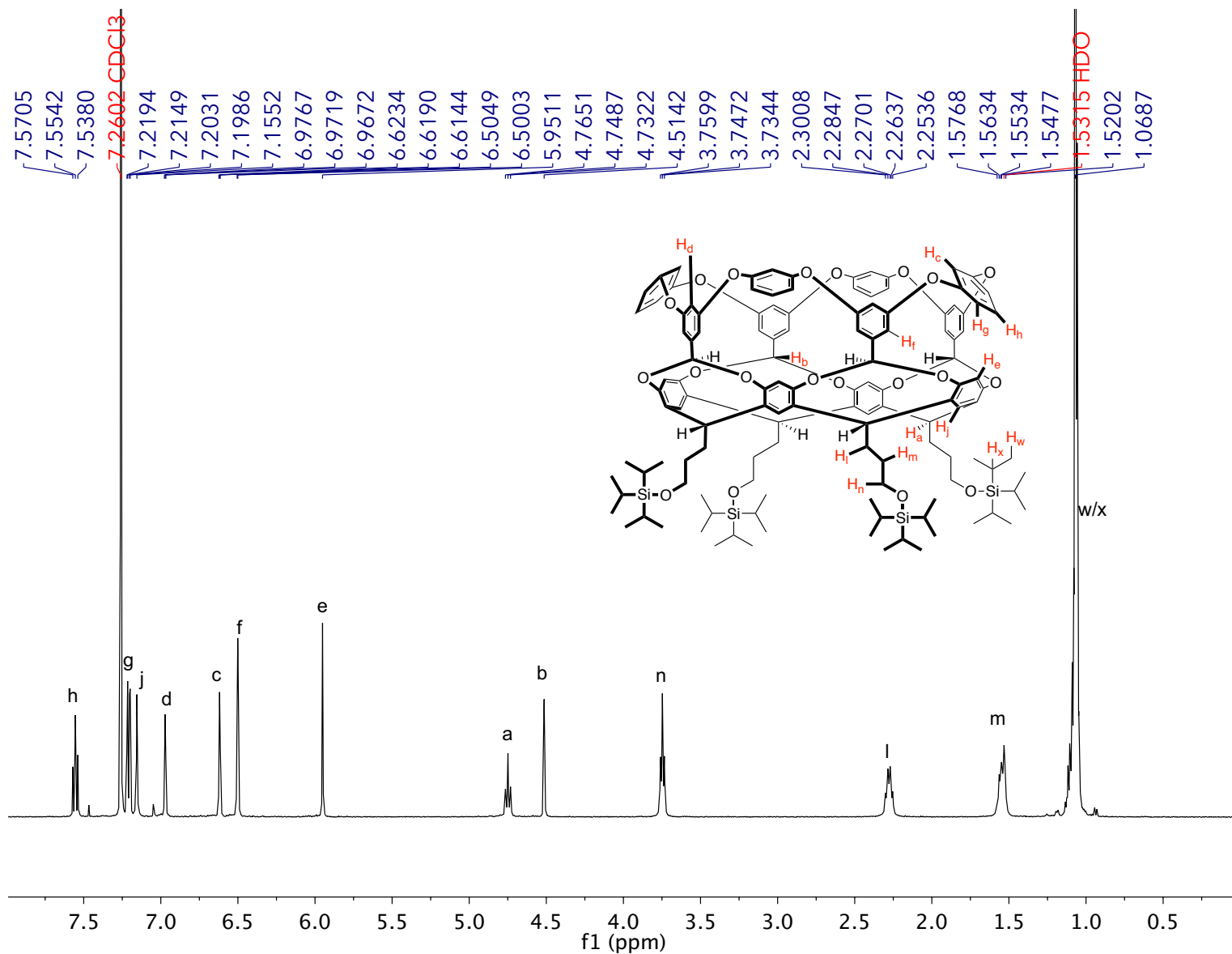
Fig. 66: ^{1}H NMR spectrum of TIPS-footed *meta*-basket **41** in CDCl$_3$.
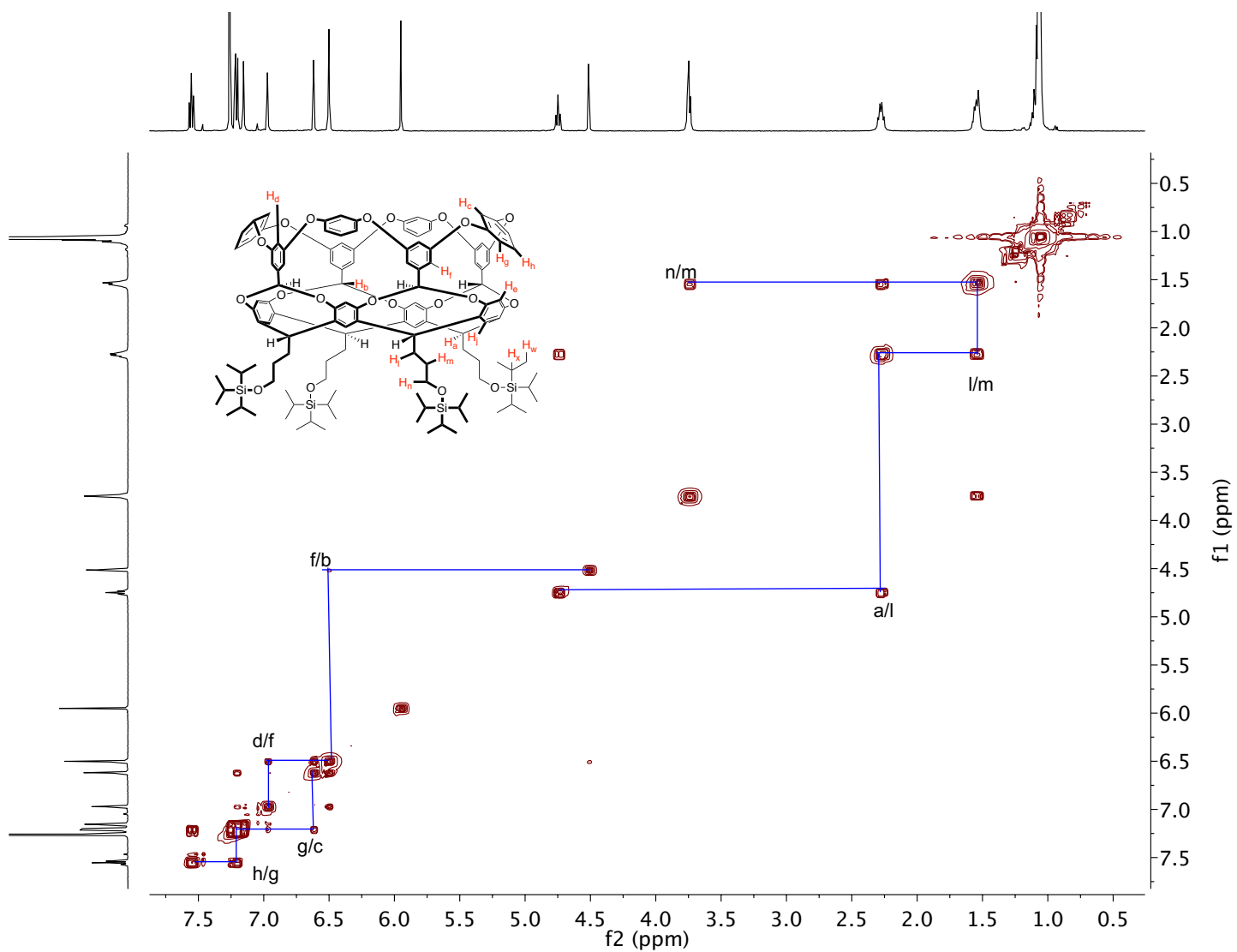
Fig. 67: ^{1}H–^{1}H COSY NMR spectrum of TIPS-footed *meta*-basket **41** in CDCl$_3$.

Fig. 68: $^{13}C\{^1H\}$ NMR spectrum of TIPS-footed *meta*-basket **41** in CDCl₃.

Calcd for $C_{128}H_{152}Si_4O_{20}$

$[M + Ag]^+$ $^{100\%}$ 2227.907;

Found $m/z^{100\%}$ 2227.904
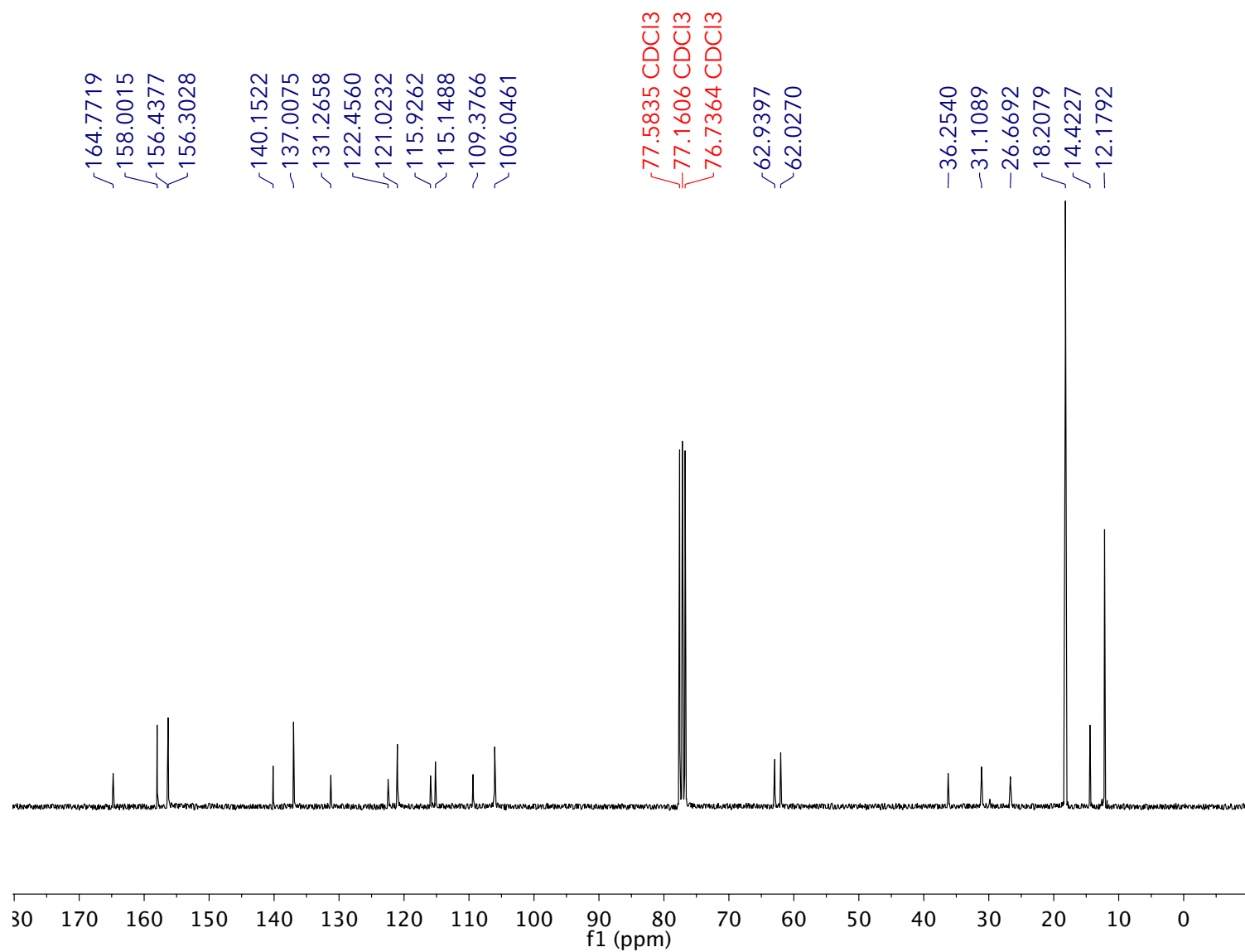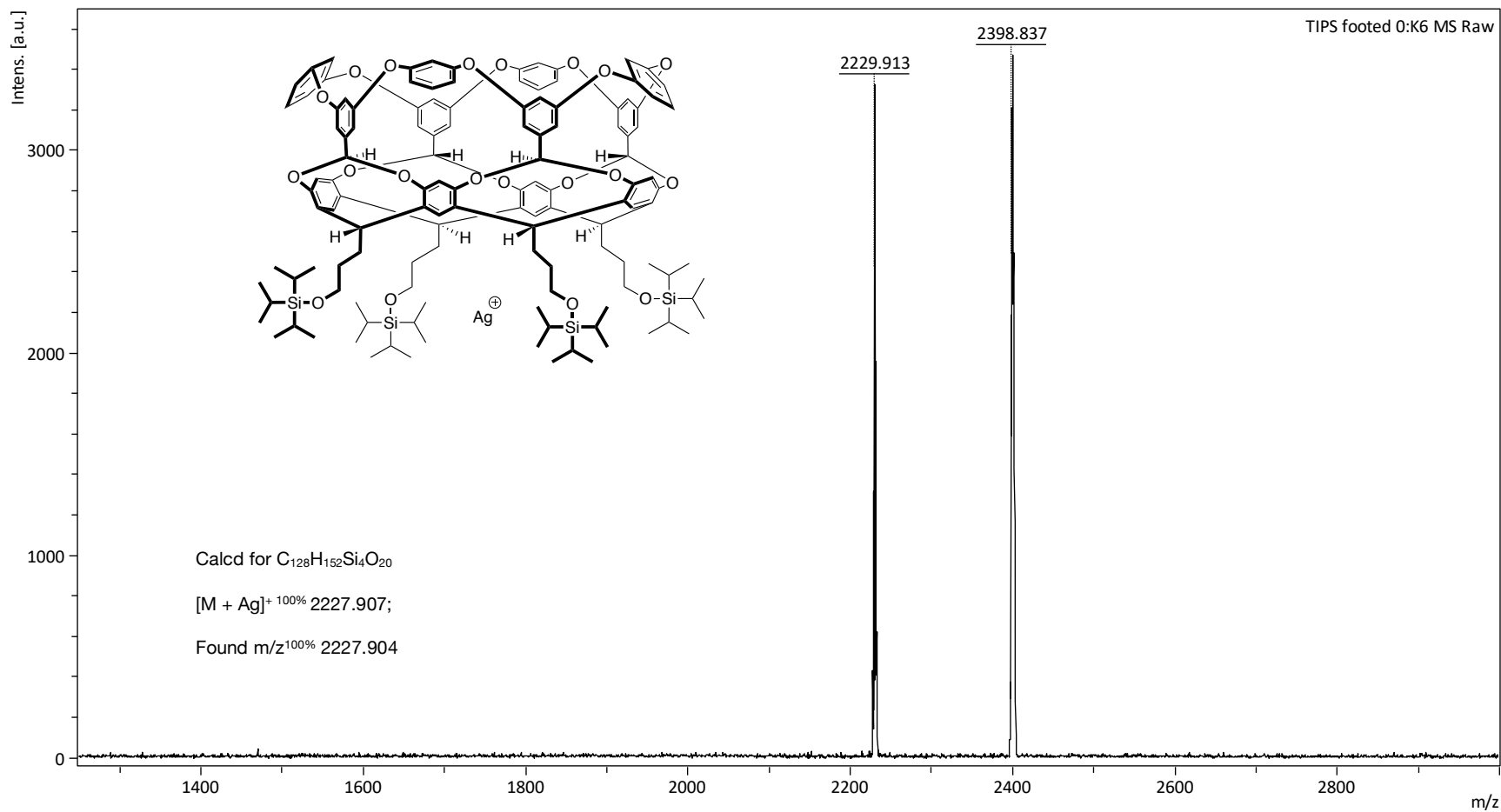
Fig. 69: MALDI-TOF MS of TIPS-footed *meta*-basket **41** (2:1:1 analyte/DCTB/AgNO$_3$), 2 mg ml^{-1} in CHCl$_3$. $[M + Ag]^+$ is indicated by signal at *m/z* 2229.913; $[M + Ag + AgNO_3]^+$ is indicated by signal at *m/z* 2398.837.
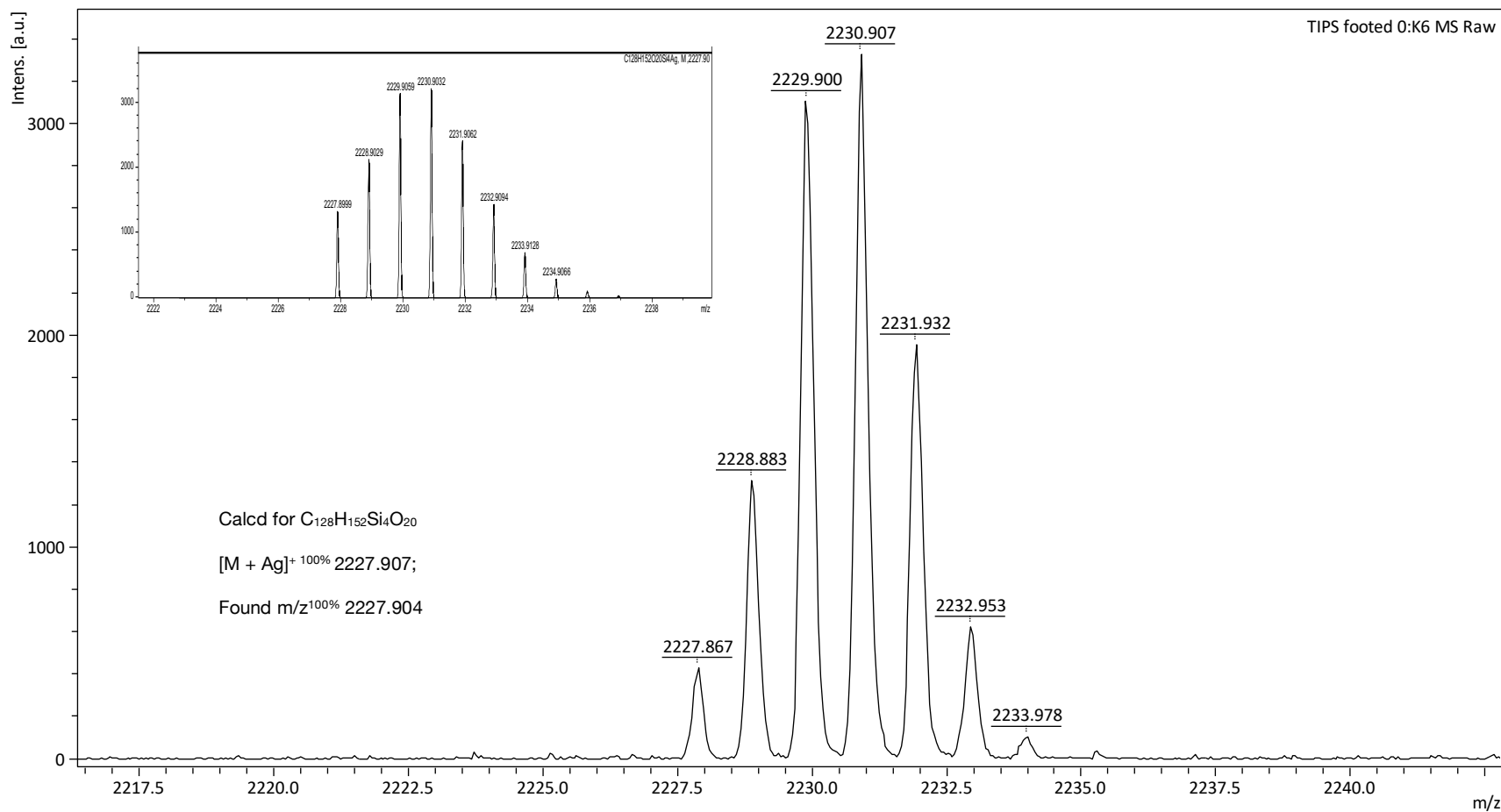
Fig. 70: Expanded view of TIPS-footed *meta*-basket **41** [M + Ag]⁺, with inset showing the theoretical spectrum for reference.
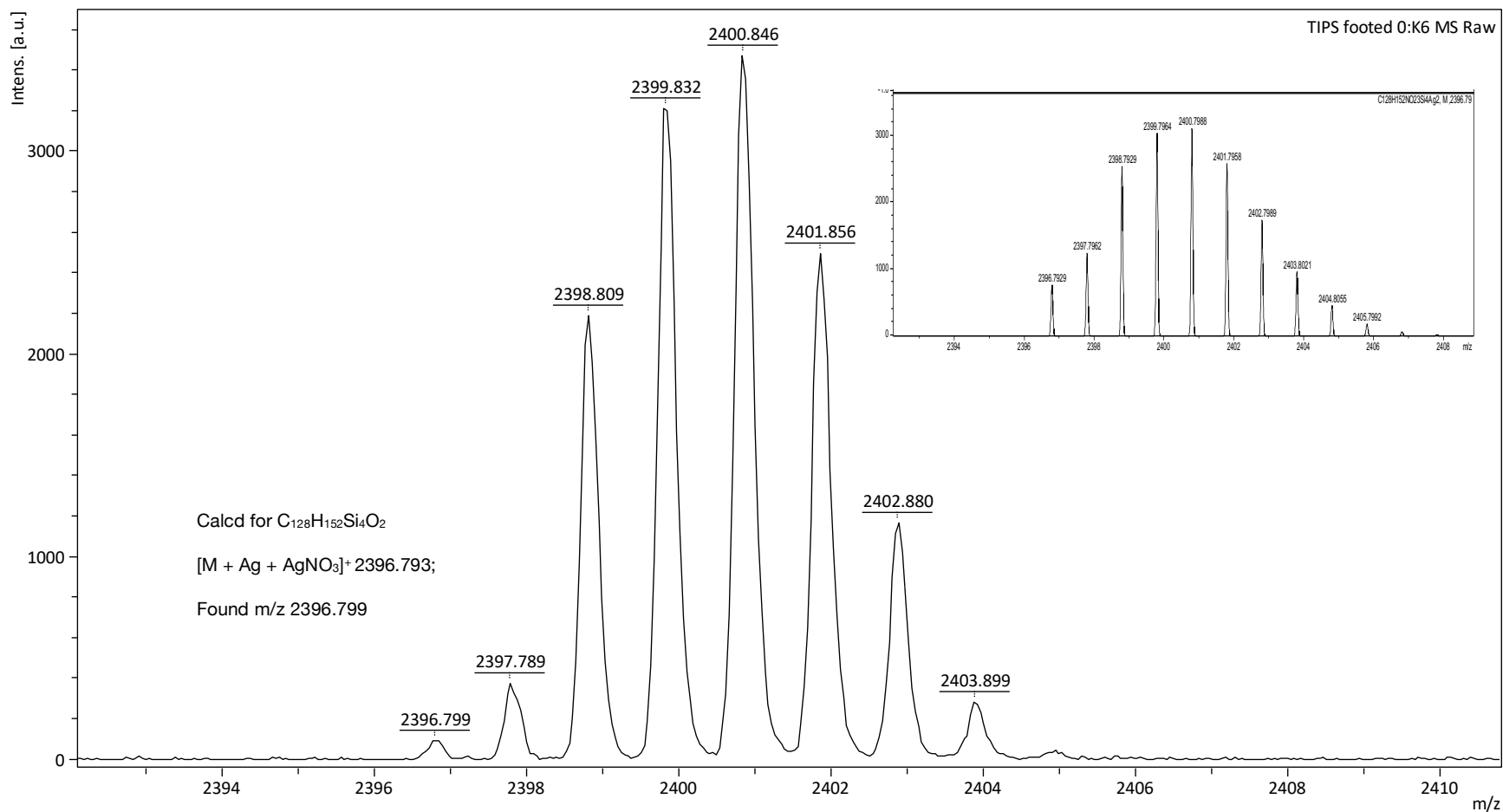
Fig. 71: Expanded view of TIPS-footed meta-basket **41** [M + Ag + AgNO₃]⁺, with inset showing the theoretical spectrum for reference.
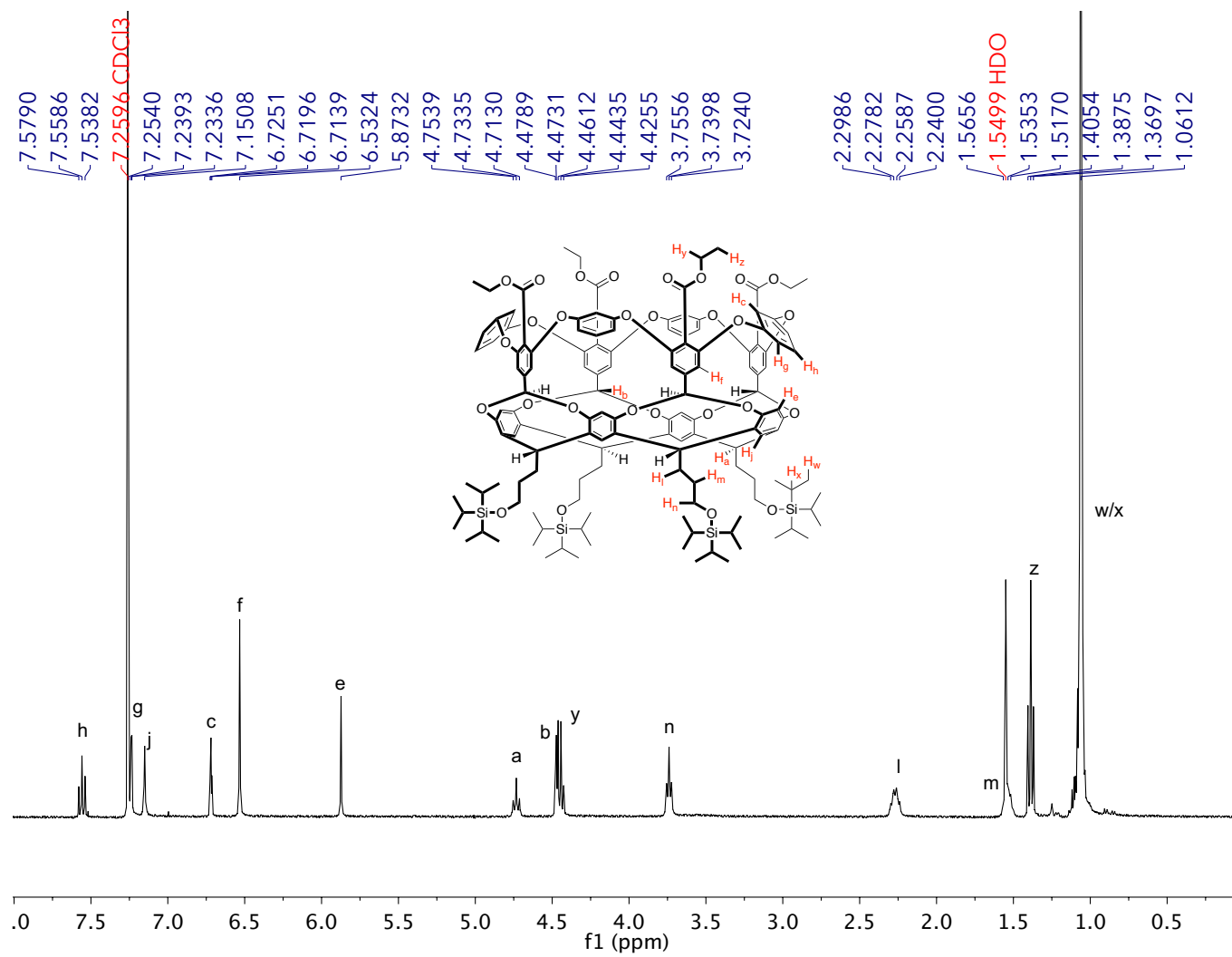
Fig. 72: ^{1}H NMR spectrum of tetra-*exo*-ester TIPS-*meta*-basket **42** in CDCl$_3$.

Fig. 73: $^{13}C\{^1H\}$ NMR spectrum of tetra-*exo*-ester TIPS-*meta*-basket **42** in CDCl$_3$.

Calcd for $C_{140}H_{168}O_{28}Si_4$ [M+Na]$^+$:

Calcd: 2432.07
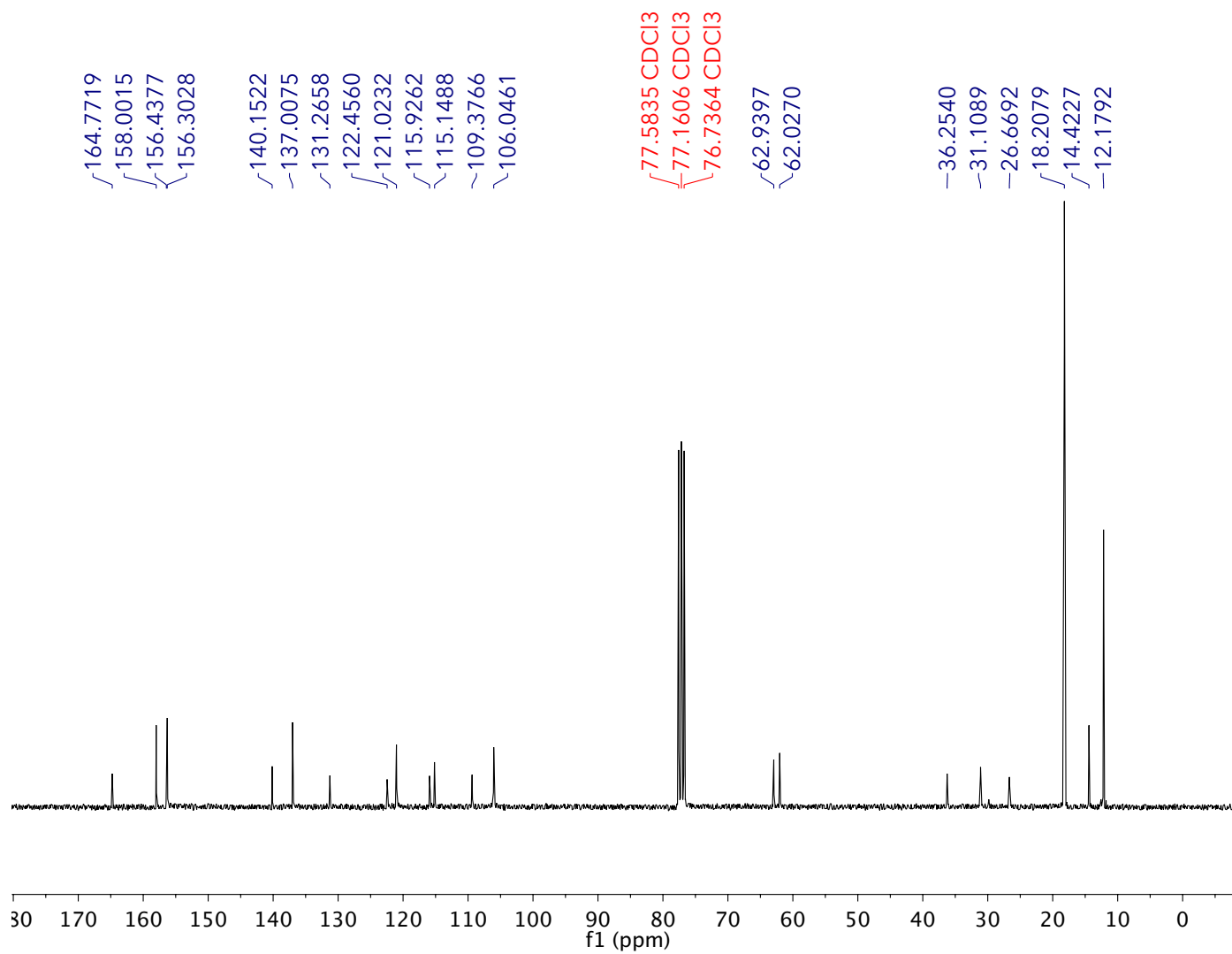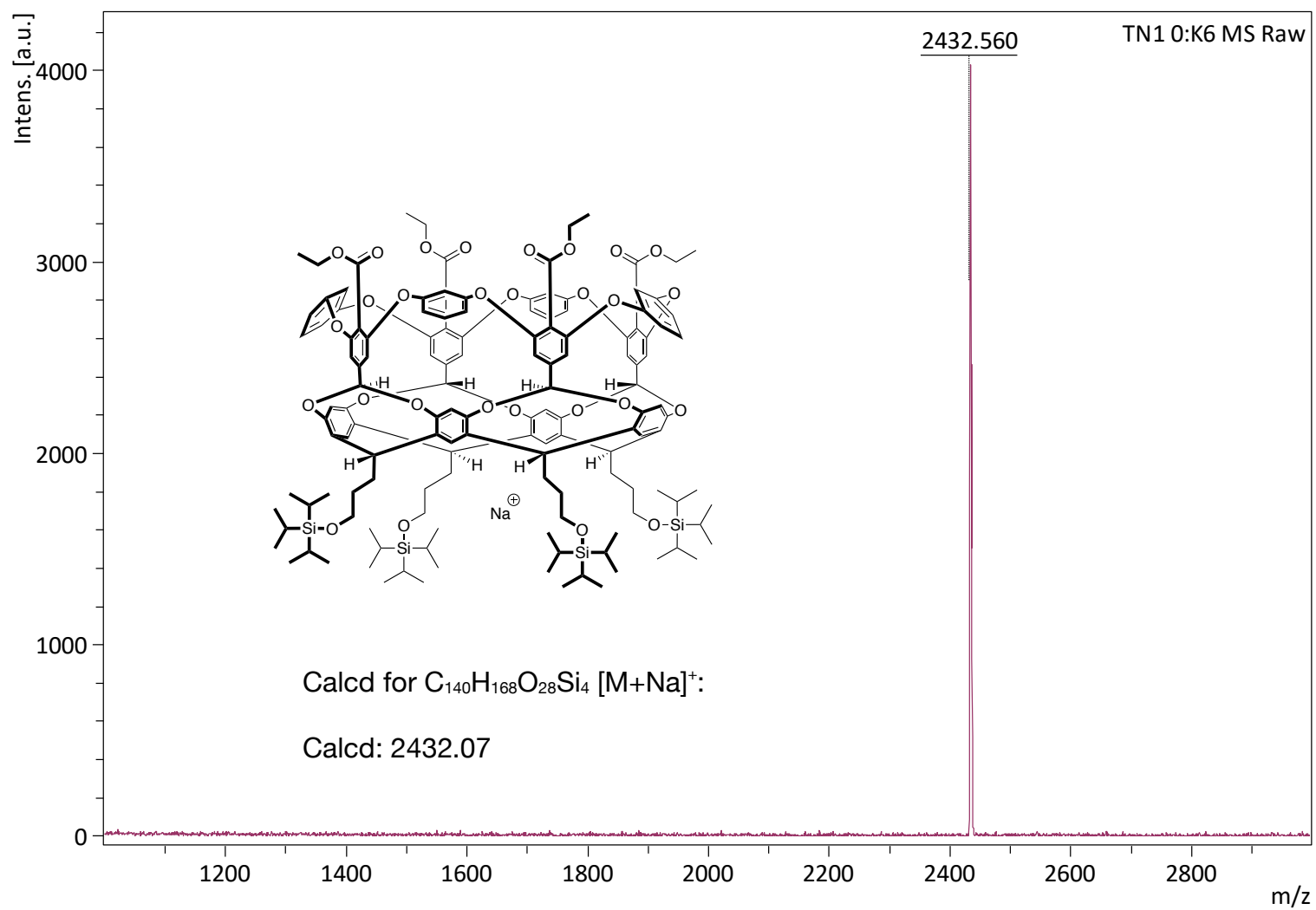
Fig. 74: MALDI-TOF MS of tetra-*exo*-TIPS *meta*-basket **42** [M + Na]$^+$ (2:1:1 analyte/DCTB/NaTFA) 2 mg ml^{-1} in CHCl$_3$.
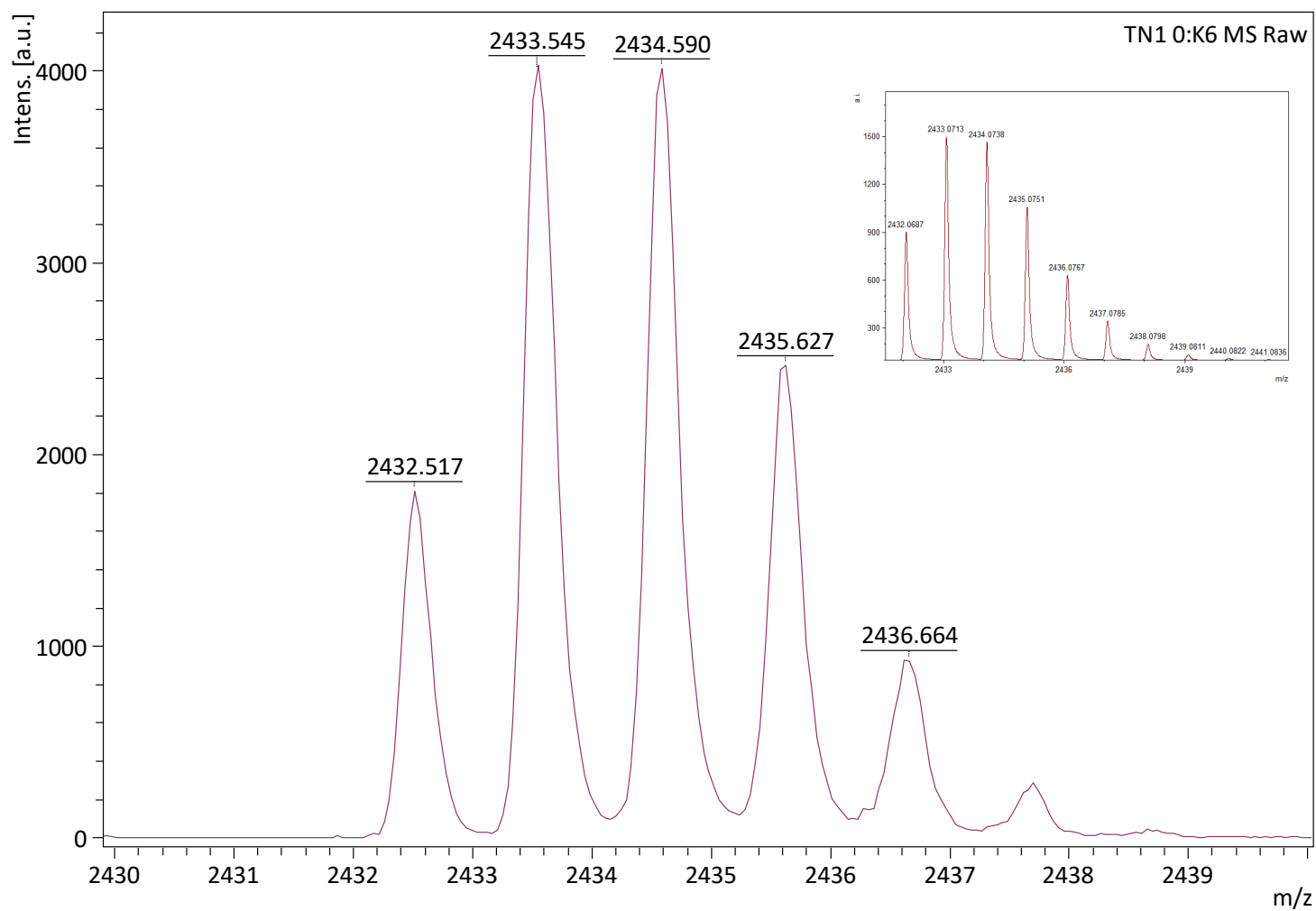
Fig. 75: Expanded view of tetra-*exo*-ester TIPS *meta*-basket **42** [M + Na]+ with theoretical calculation inset.
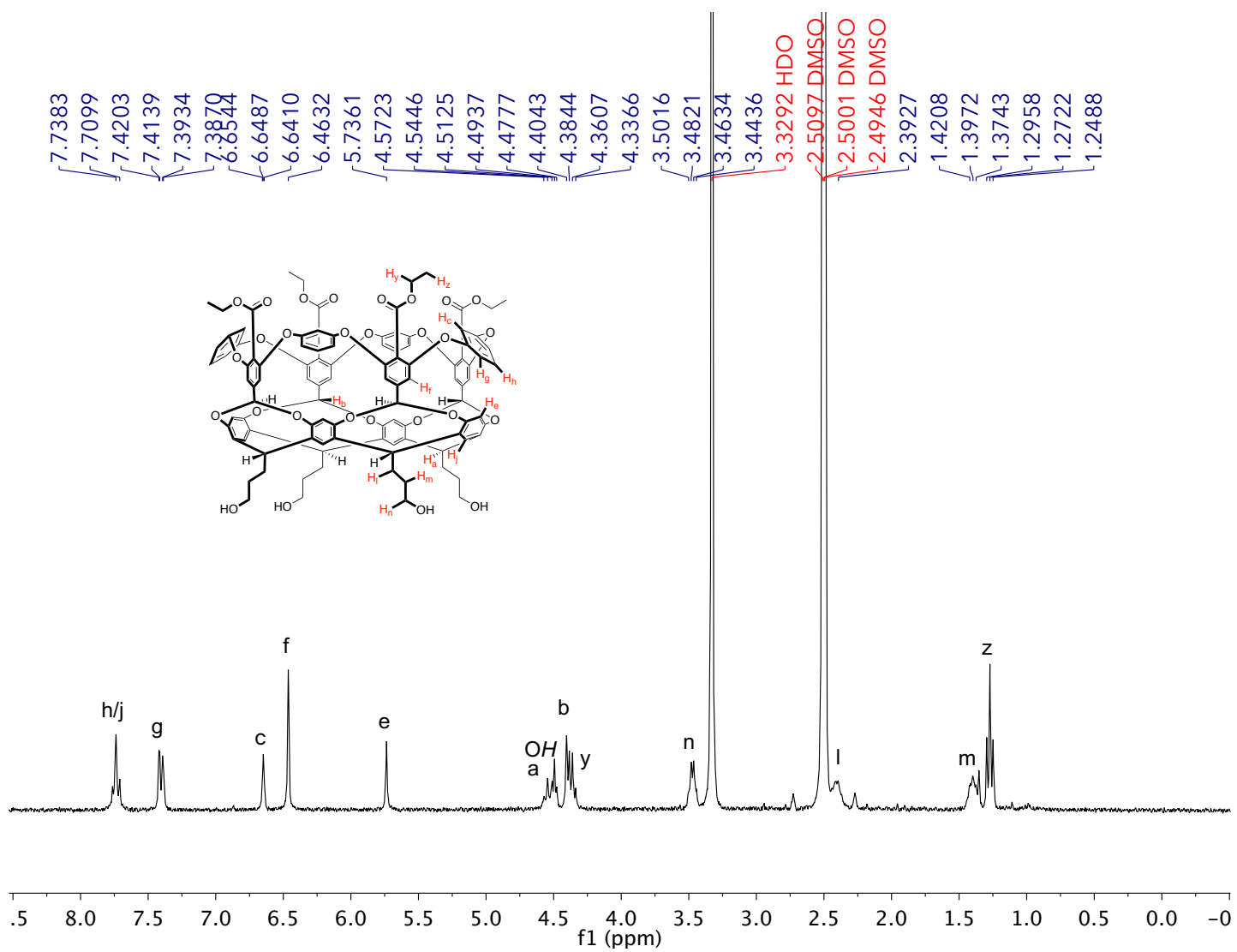
Fig. 76: ^{1}H NMR spectrum of tetra-*exo*-ester tetrol *meta*-basket **43** in DMSO-*d*$_6$.
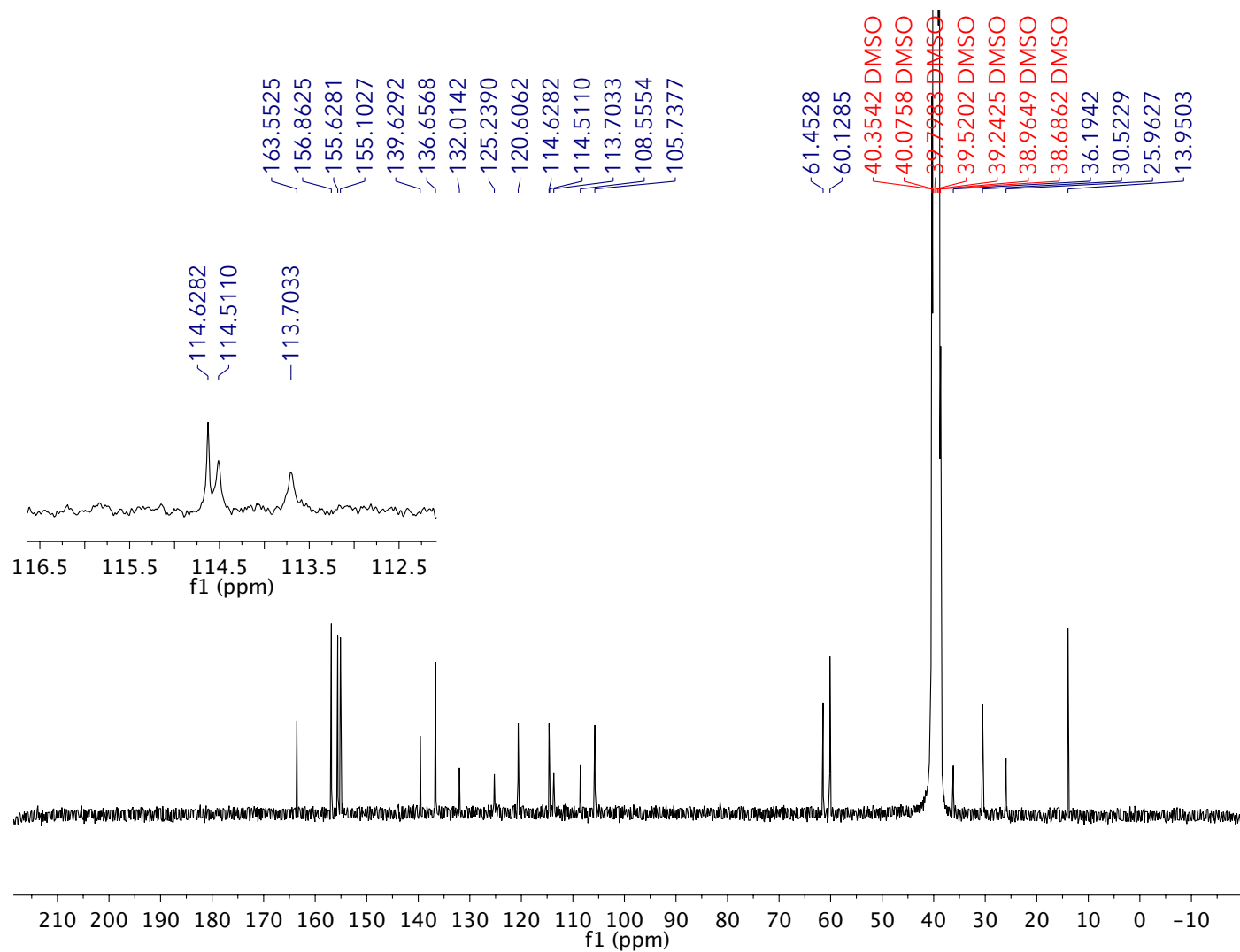
Fig. 77: $^{13}C\{^1H\}$ NMR spectrum of tetra-*exo*-ester tetrol *meta*-basket **43** in DMSO d_6. Inset shows expanded region from 112.5 ppm to 116.5 ppm.

x10⁴

1807.516

exo-ester-tetrol 0:N10 MS Raw

Calcd for $C_{104}H_{88}O_{28}$ [M+Na]⁺:

Calcd: 1807.535
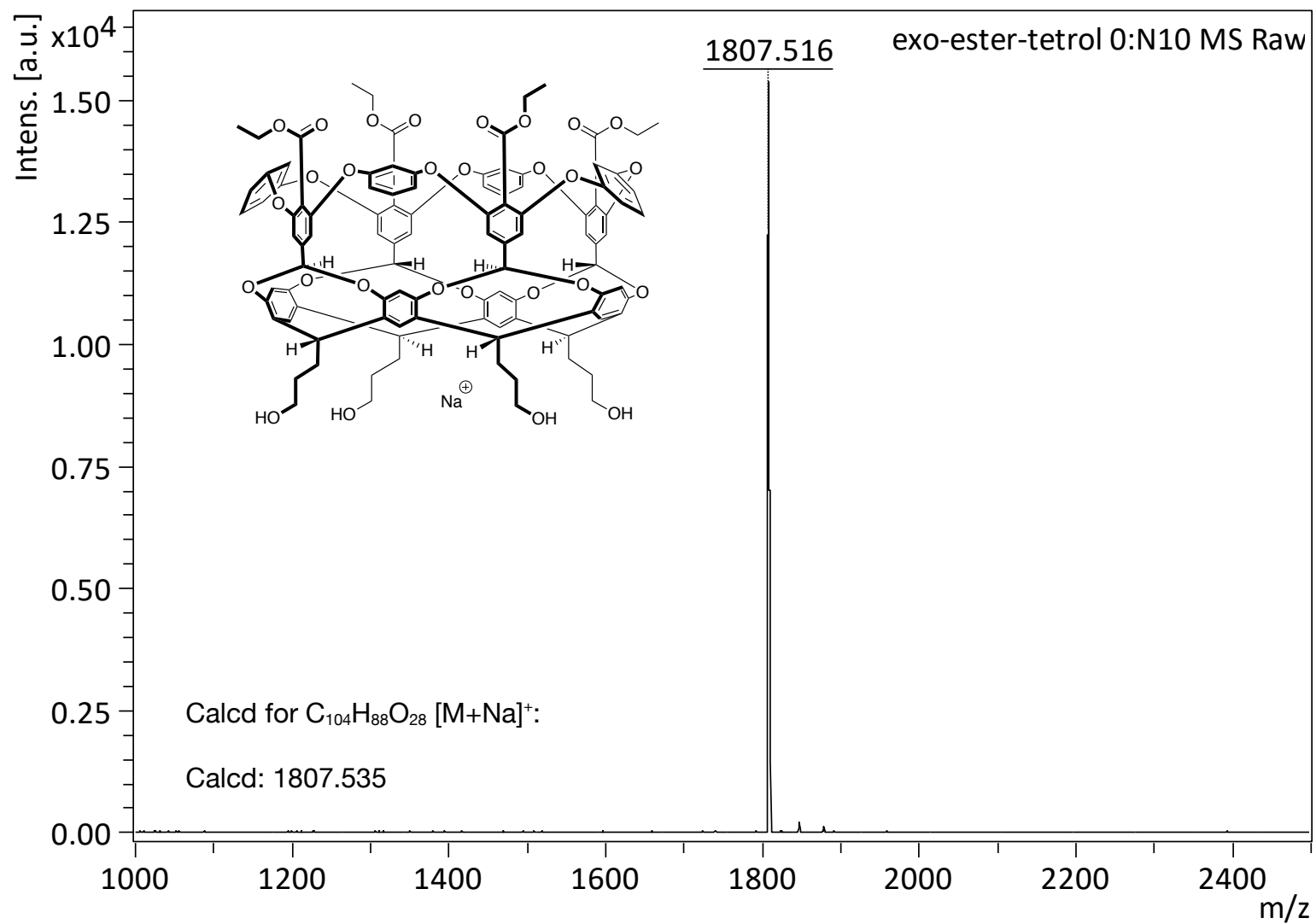
Fig. 78: MALDI-TOF MS of tetra-*exo*-ester tetrol meta-basket **43** [M + Na]⁺ (2:1:1 analyte/CHCA/NaTFA) 2 mg ml⁻¹ in THF.
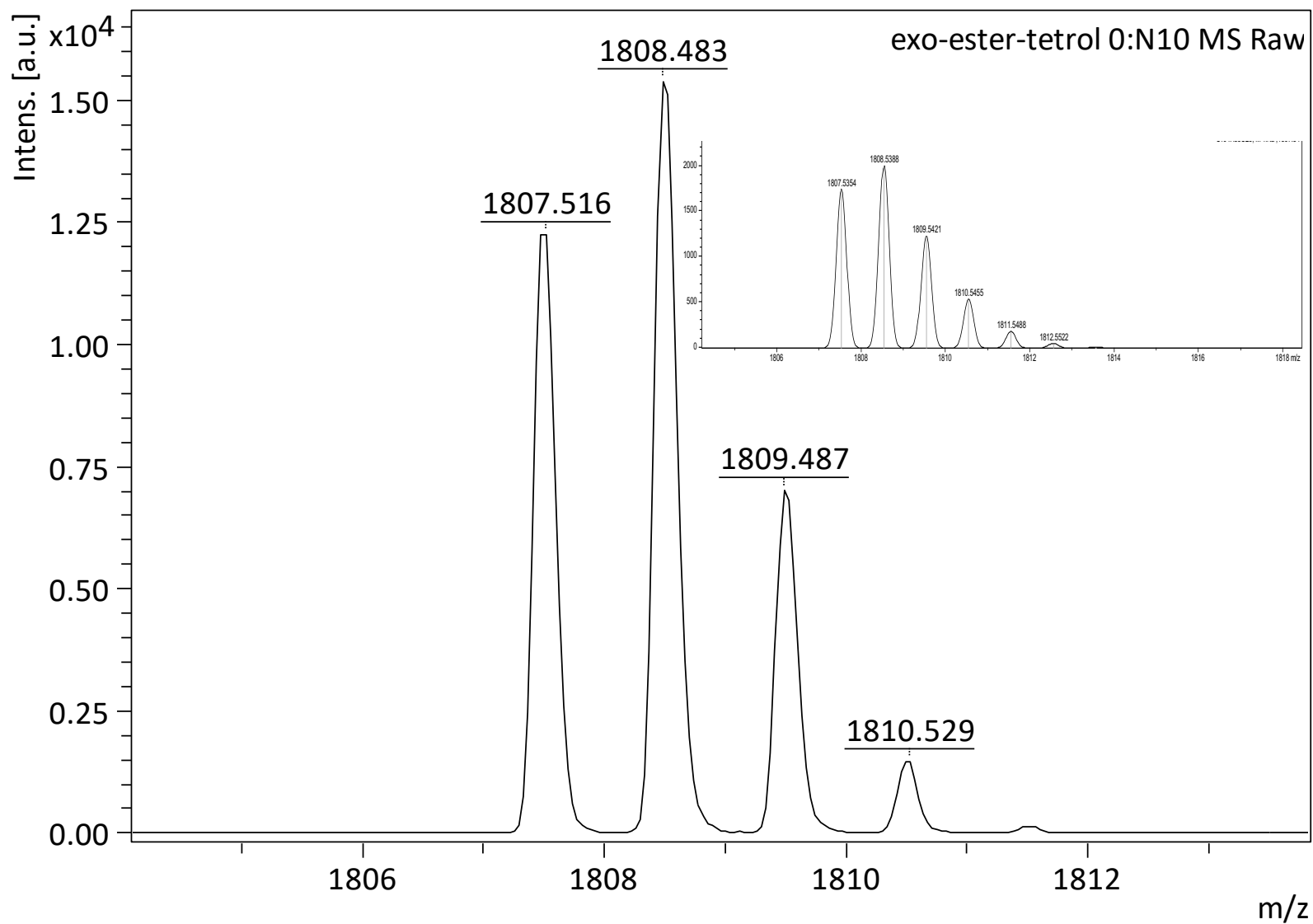
Fig. 79: Expanded view of tetra-*exo*-ester tetrol *meta*-basket **43** [M + Na]+ with theoretical calculation inset
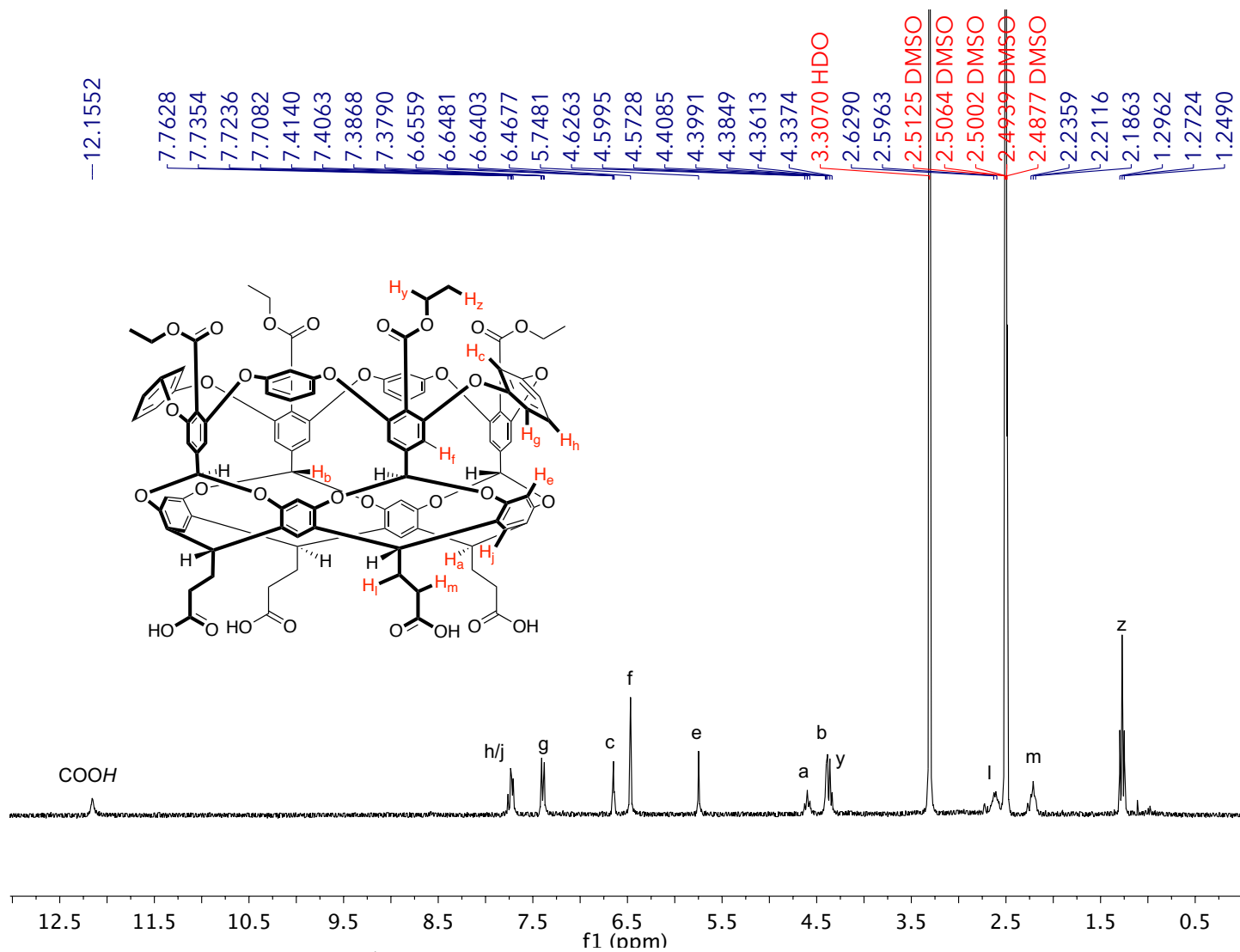
Fig. 80: ¹H NMR spectrum of tetra-*exo*-ester tetra acid **39′** in DMSO-d_6.
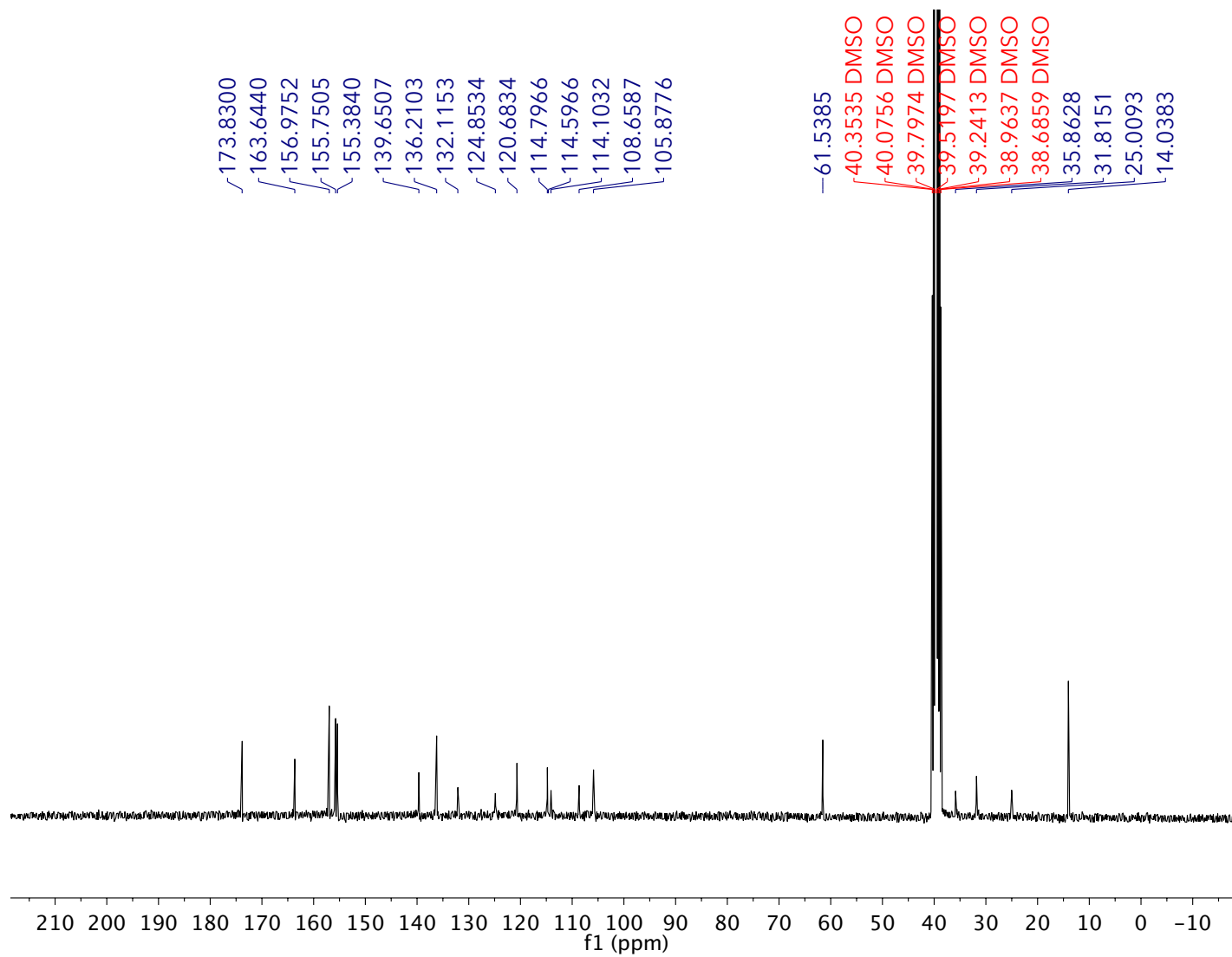
Fig. 81: ^{13}C{^{1}H} NMR spectrum of tetra-*exo*-ester tetra-acid **39'** in DMSO-d_6.
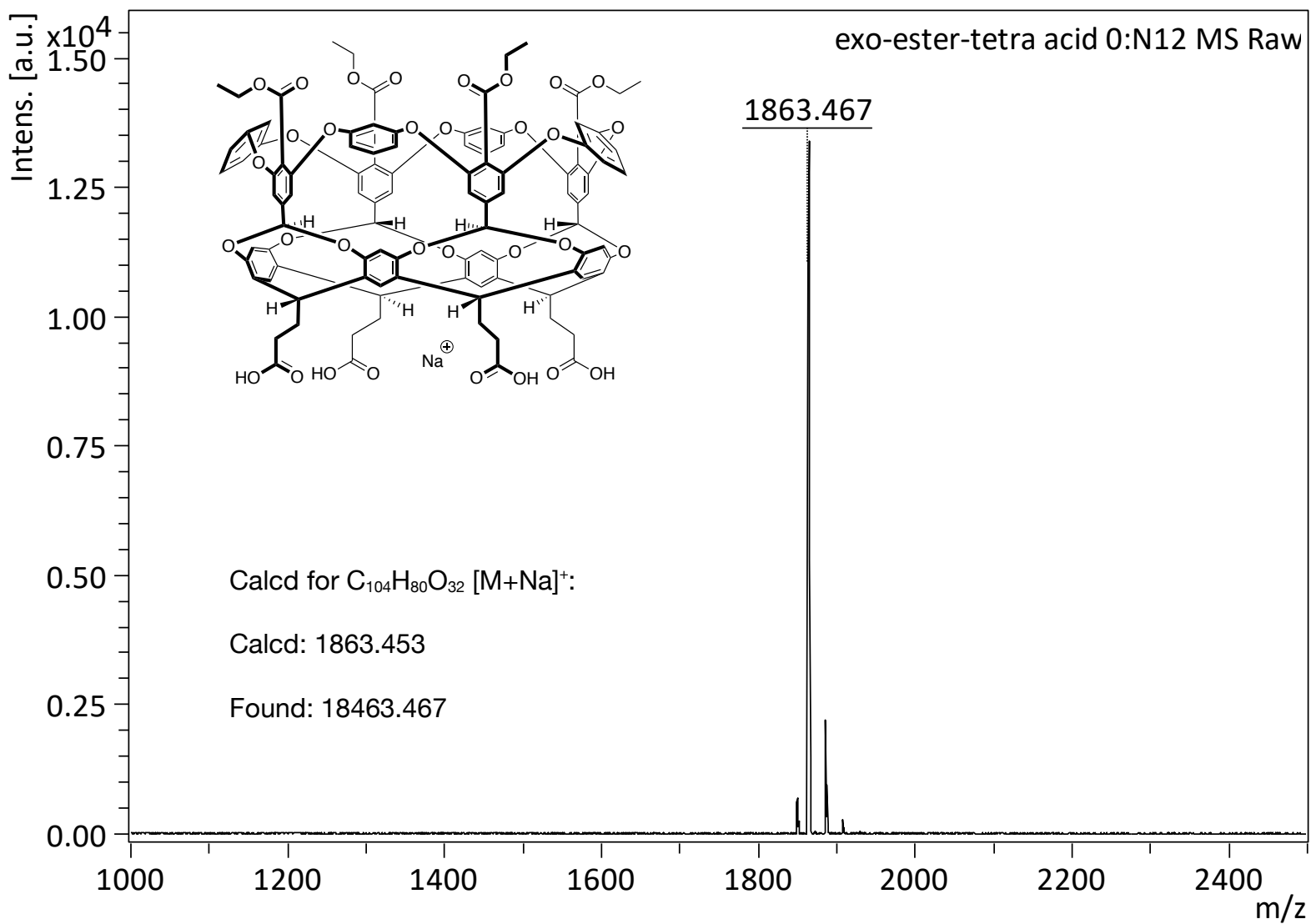
Fig. 82: MALDI-TOF MS of tetra-*exo*-ester tetra acid **39′** [M + Na]⁺ (2:1:1 analyte/CHCA/NaTFA) 2 mg ml⁻¹ in THF.
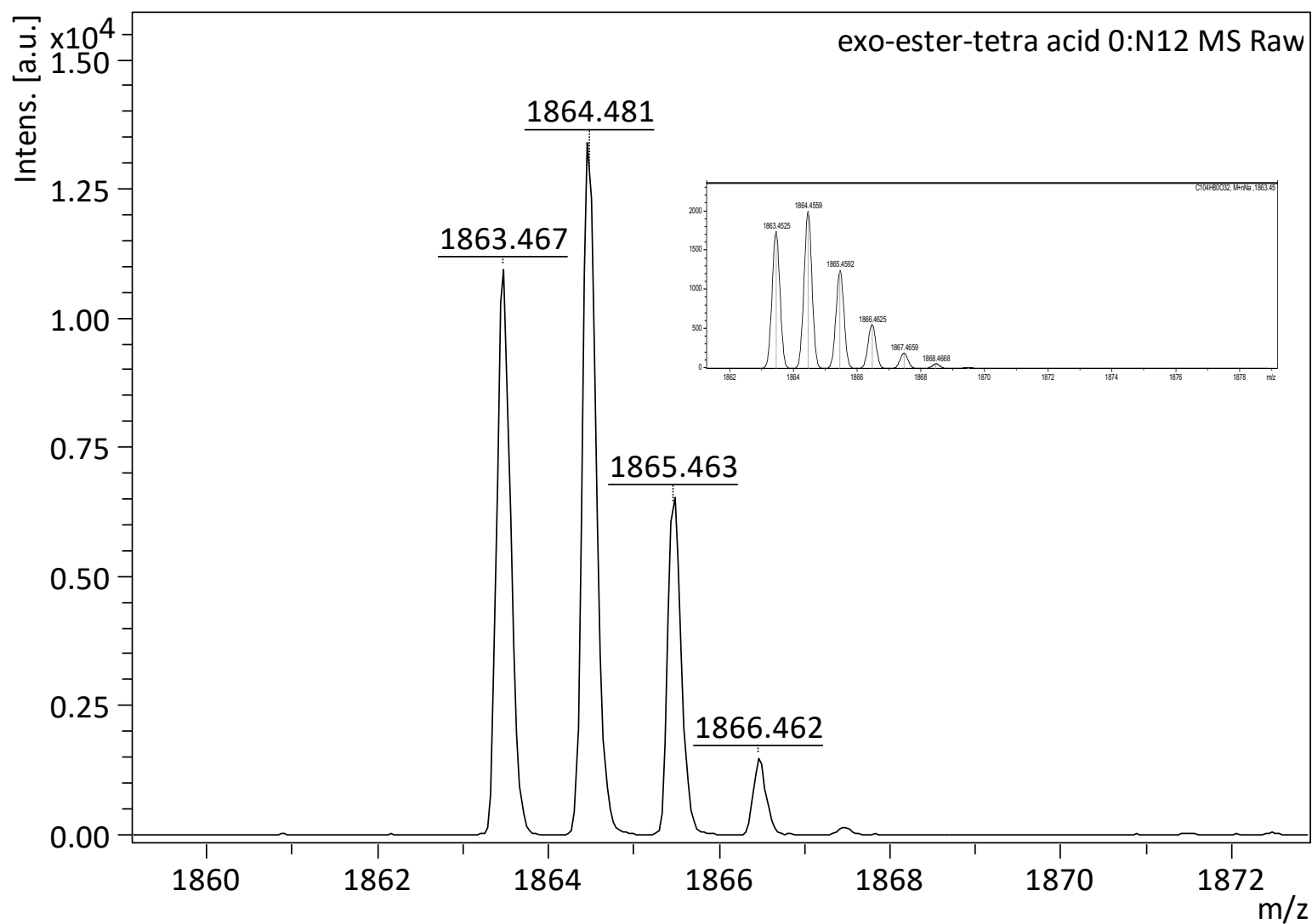
Fig. 83: Expanded view of tetra-*exo*-ester tetra acid **39′** [M + Na]⁺, with theoretical calculation inset.
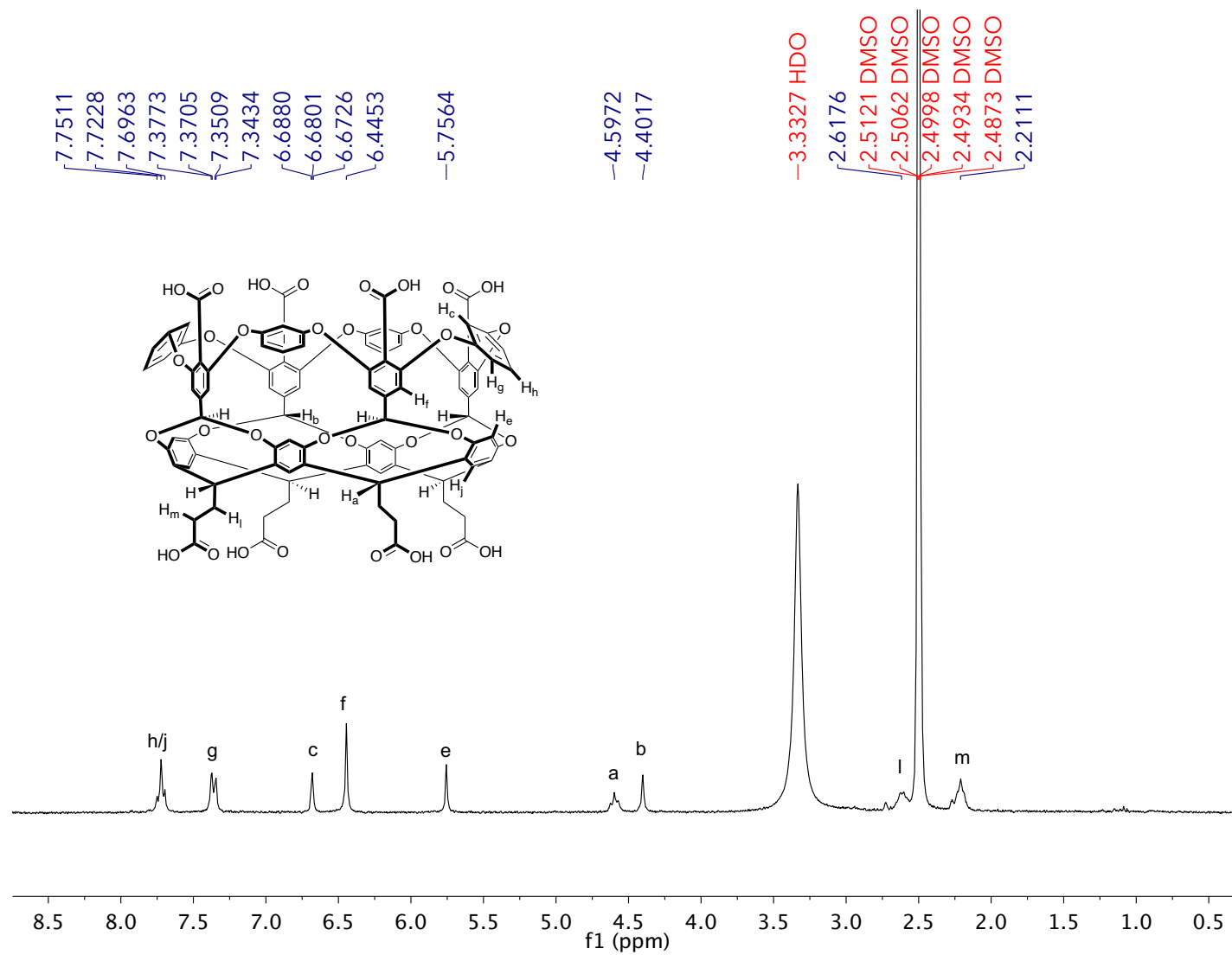
Fig. 84: ^{1}H NMR spectrum of *exo*-octa acid **39** in DMSO-d_6.
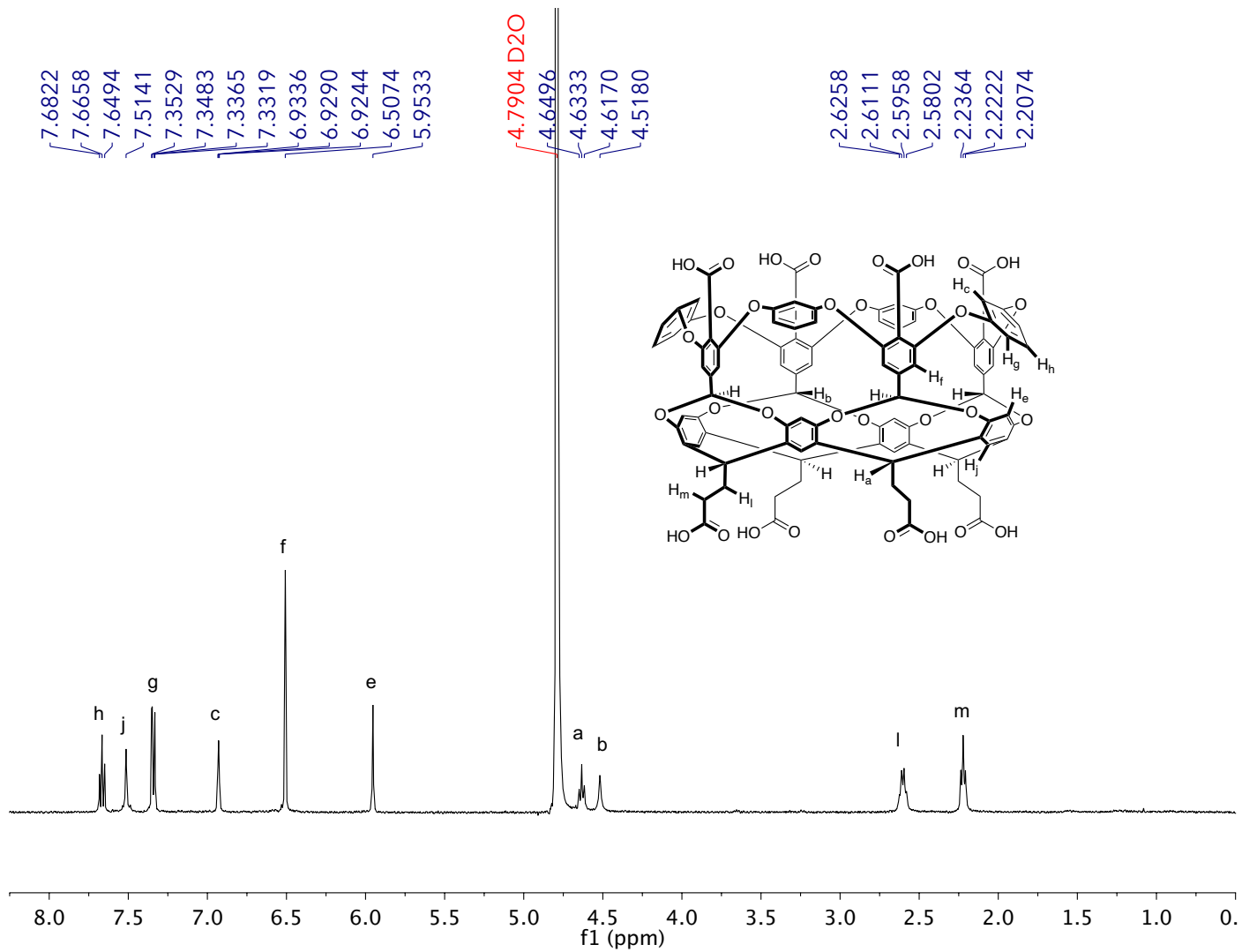
Fig. 85: ¹H NMR spectrum of 1 mM *exo*-octa acid **39** in 10 mM pD 11.5 phosphate-buffered D₂O.
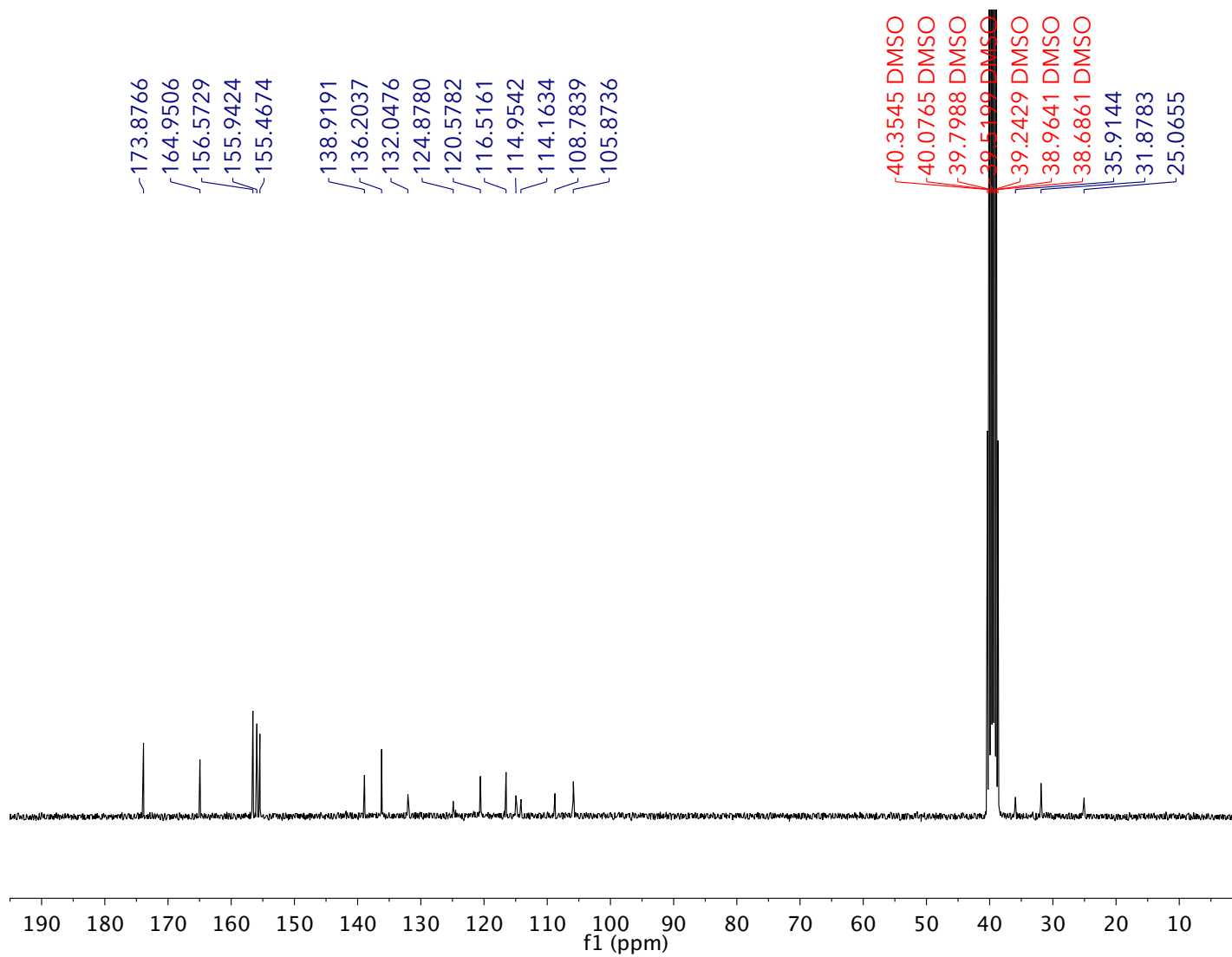
Fig. 86: $^{13}C\{^1H\}$ NMR spectrum of *exo*-octa acid **39** in DMSO-d_6.
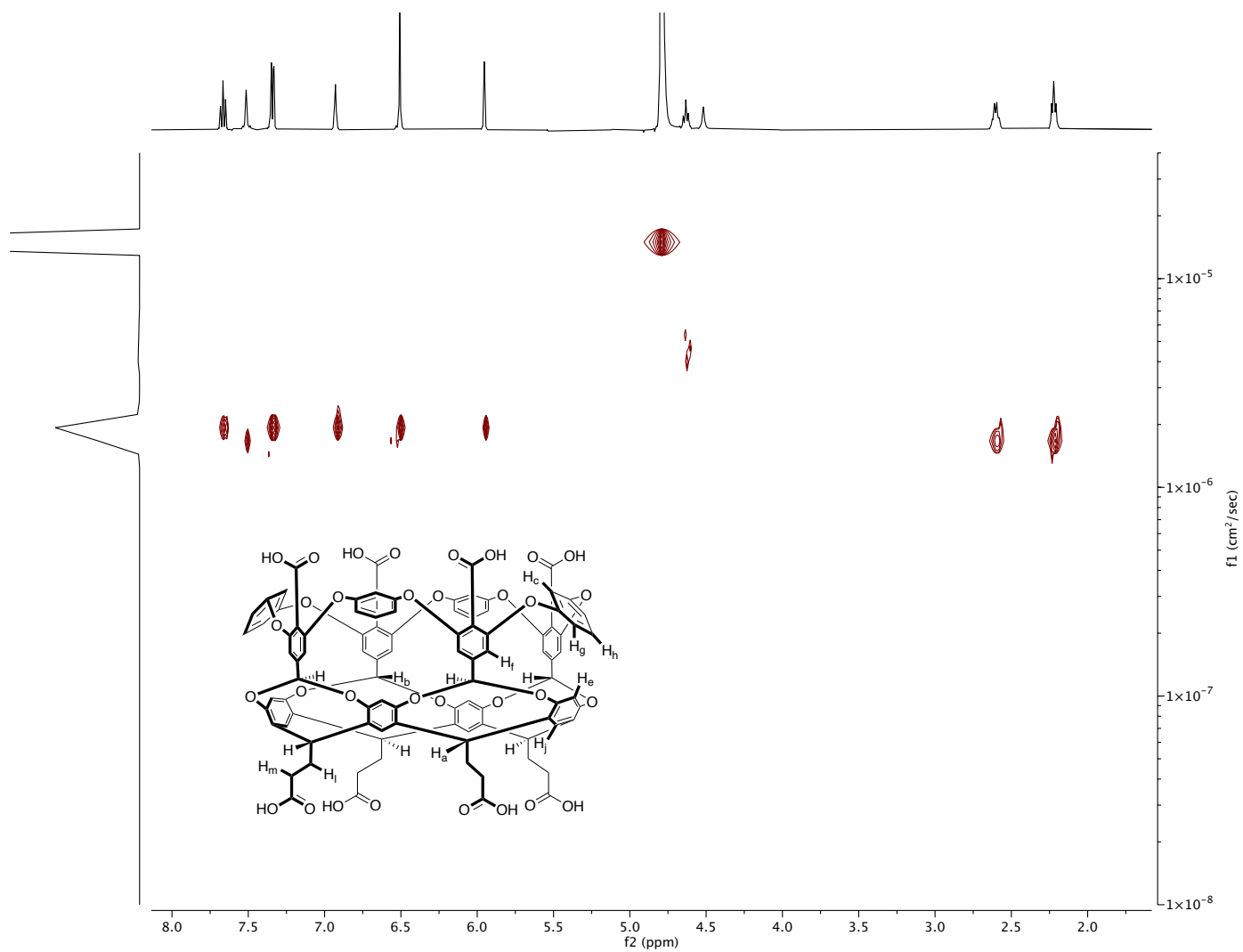
Fig. 87: DOSY NMR spectrum of 1 mM *exo*-octa acid **39** in 10 mM pD 11.5 phosphate-buffered D$_2$O.
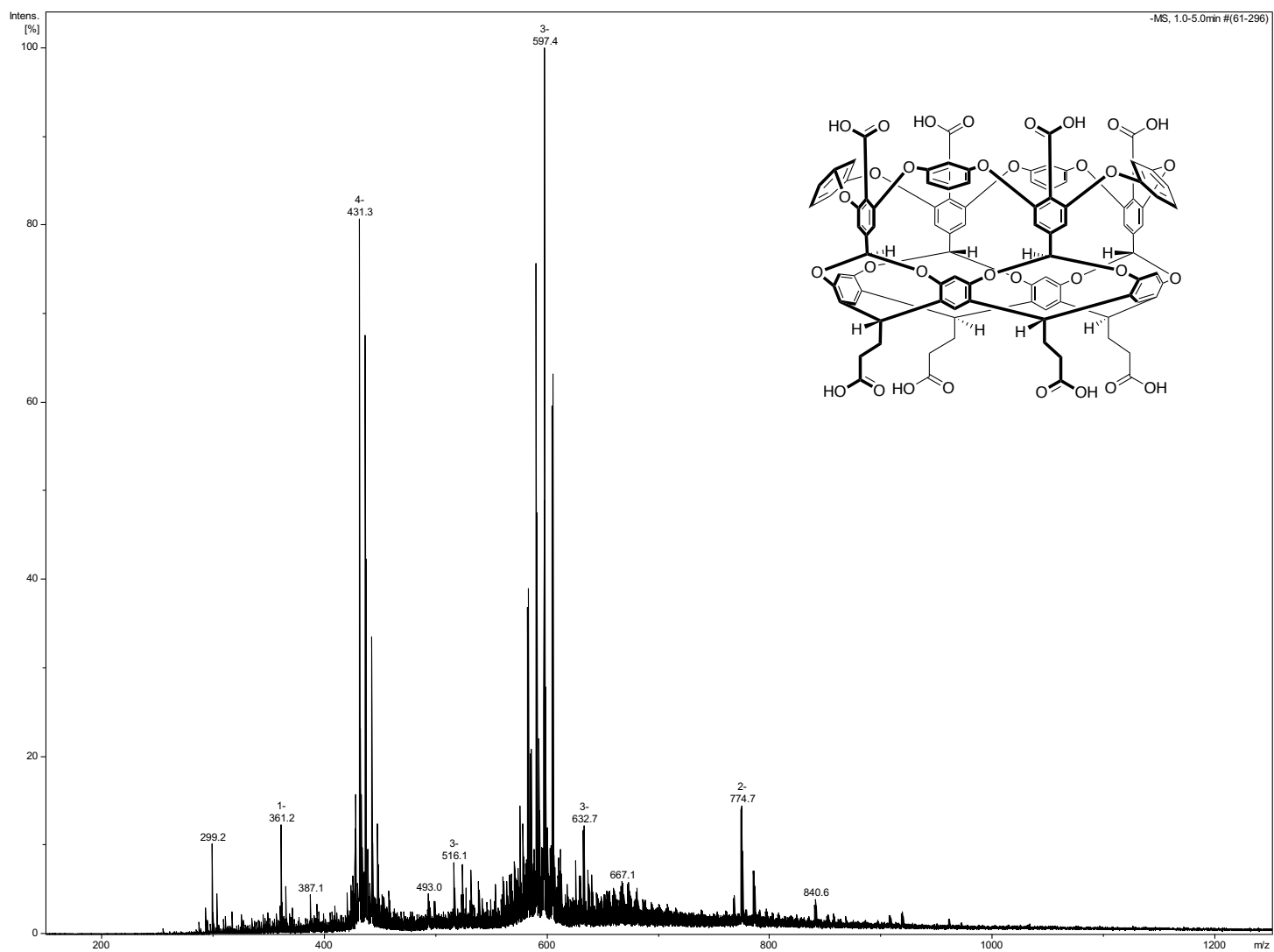
Fig. 88: ESI-MS of *exo*-octa acid **39**.

Calcd. for $C_{96}H_{60}O_{32}$ [M – 4H]$^{4-}$:
Calcd: 431.0772
Found: 431.0754
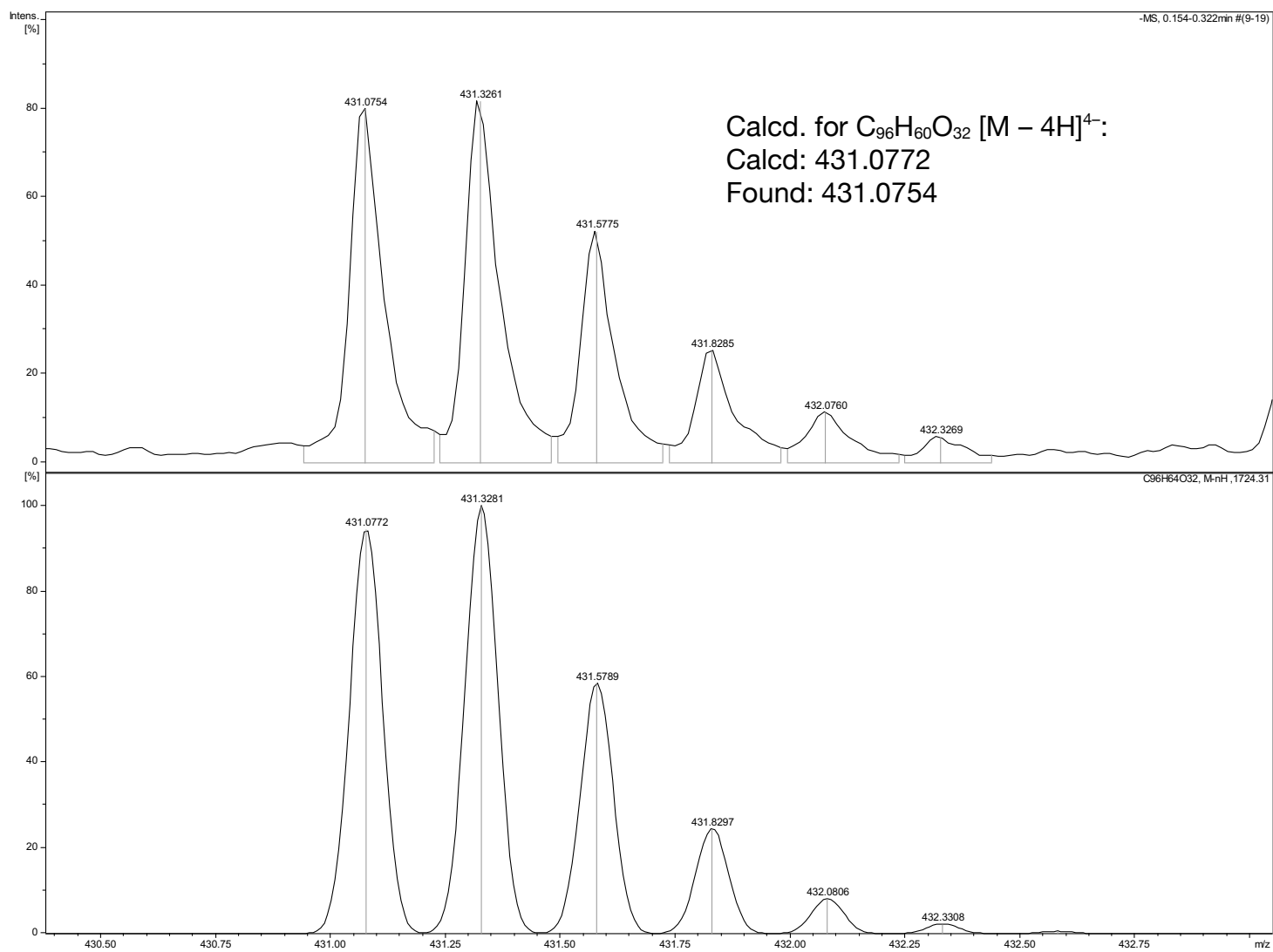
Fig. 89: Expanded view of *exo*-octa acid **39** [M – 4H]$^{4-}$ ($C_{96}H_{60}O_{32}{}^{4-}$) with theoretical calculation below.
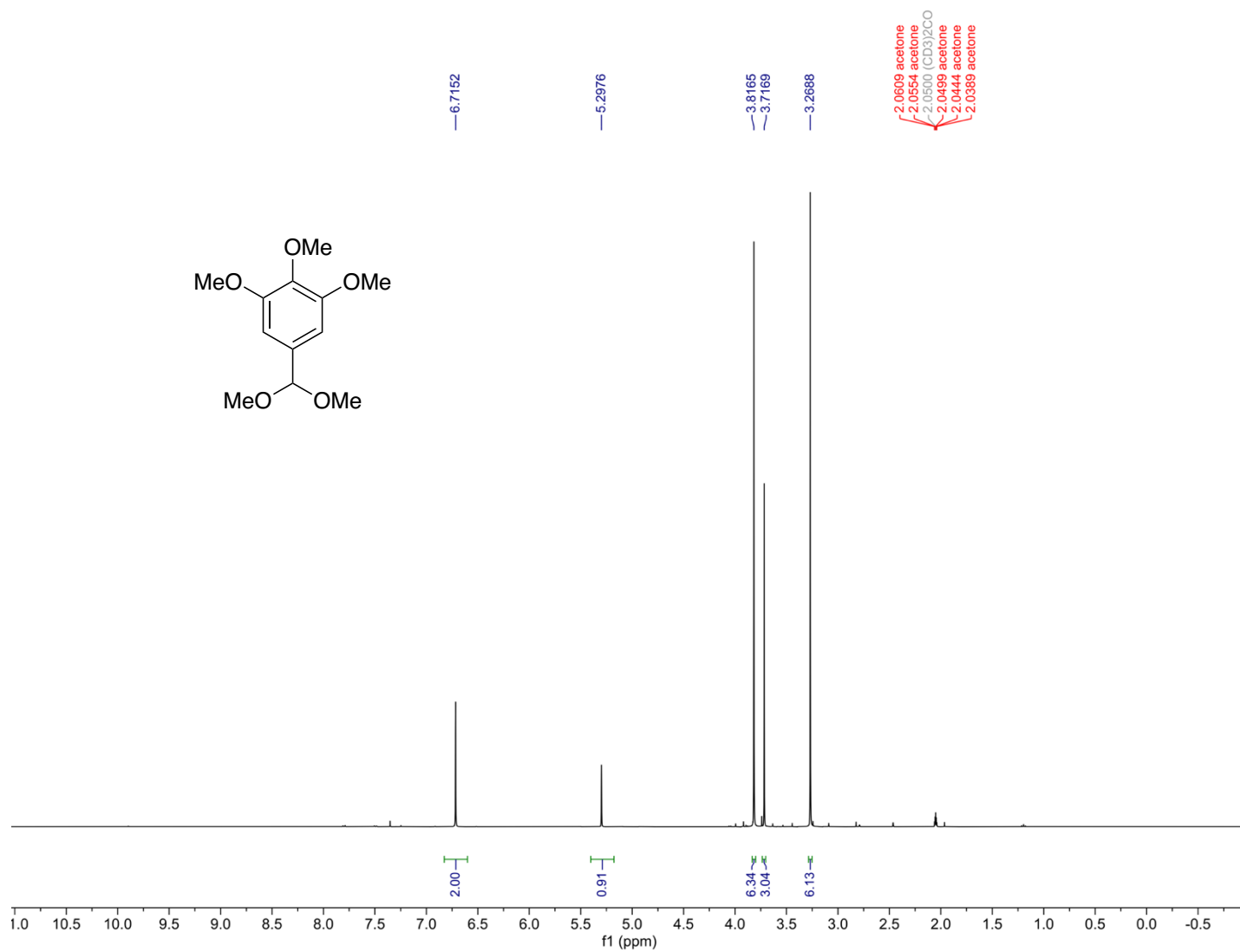
Fig. 90: ^{1}H NMR spectrum of 3,4,5-trimethoxybenzaldehyde dimethyl acetal **54** in acetone-d_6.
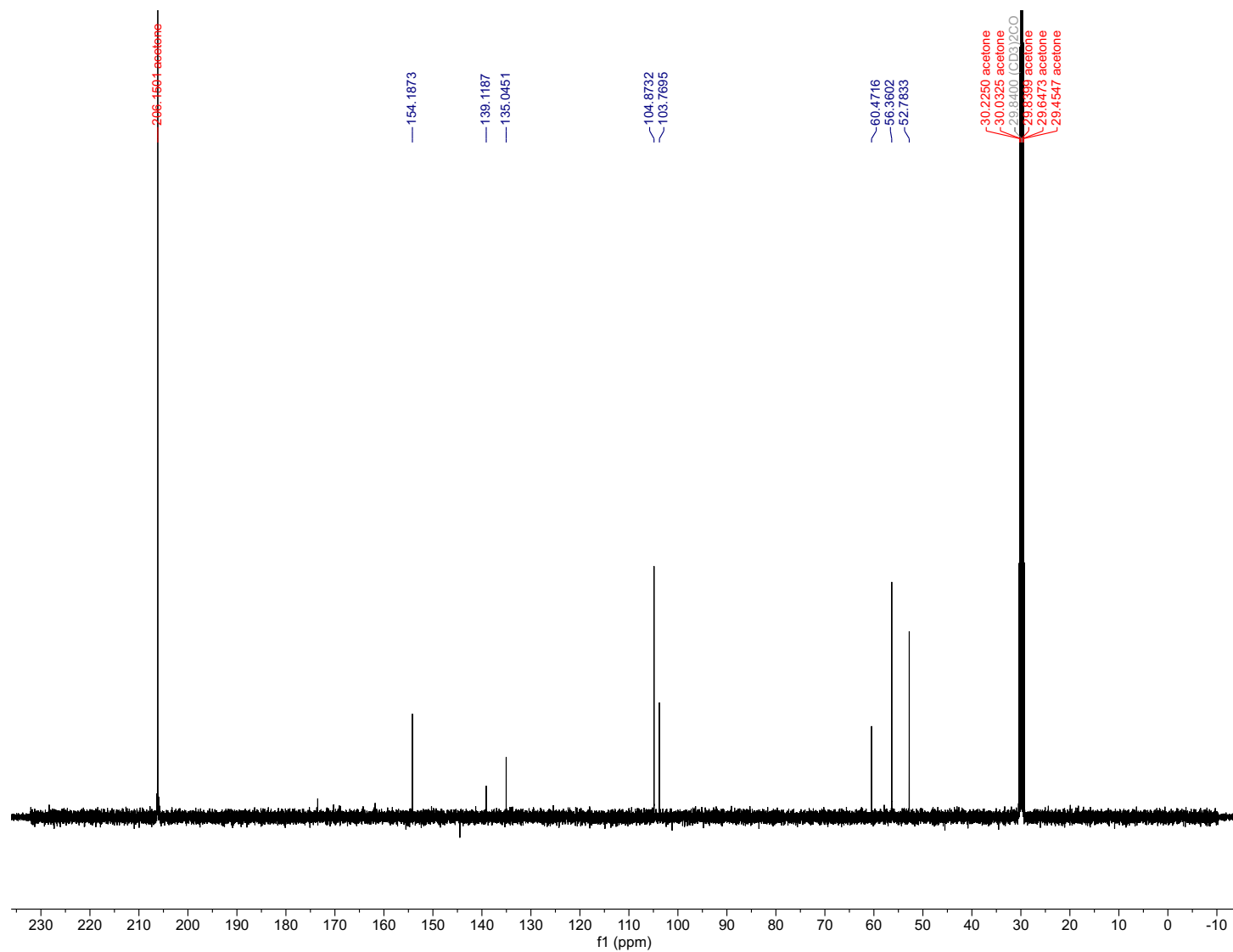
Fig. 91: ^{13}C{^{1}H} NMR spectrum of 3,4,5-trimethoxybenzaldehyde dimethyl acetal **54** in acetone-d_6.
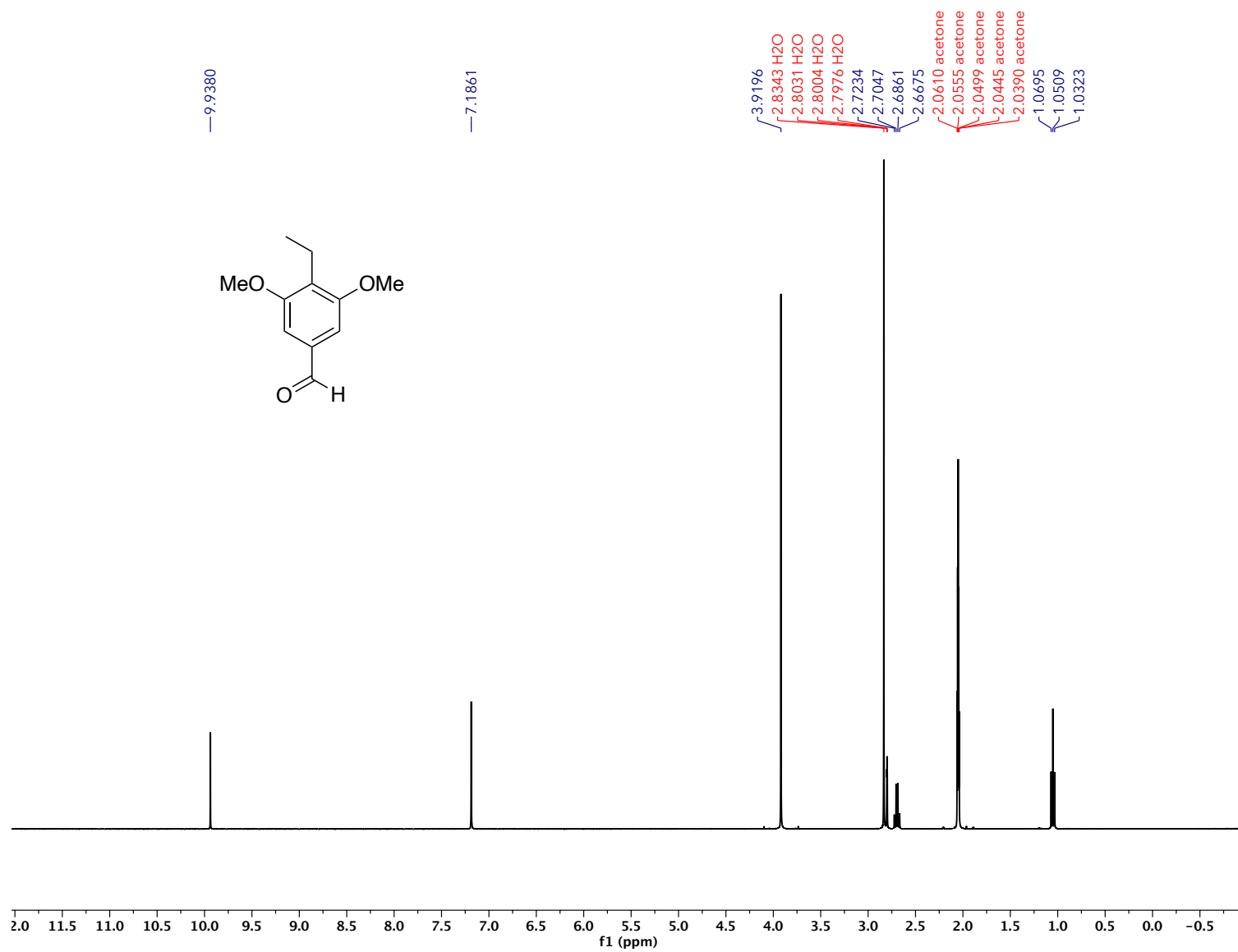
Fig. 92: ^{1}H NMR spectrum of 4-ethyl-3,5-dimethoxybenzaldehyde **55** in acetone-d_6.
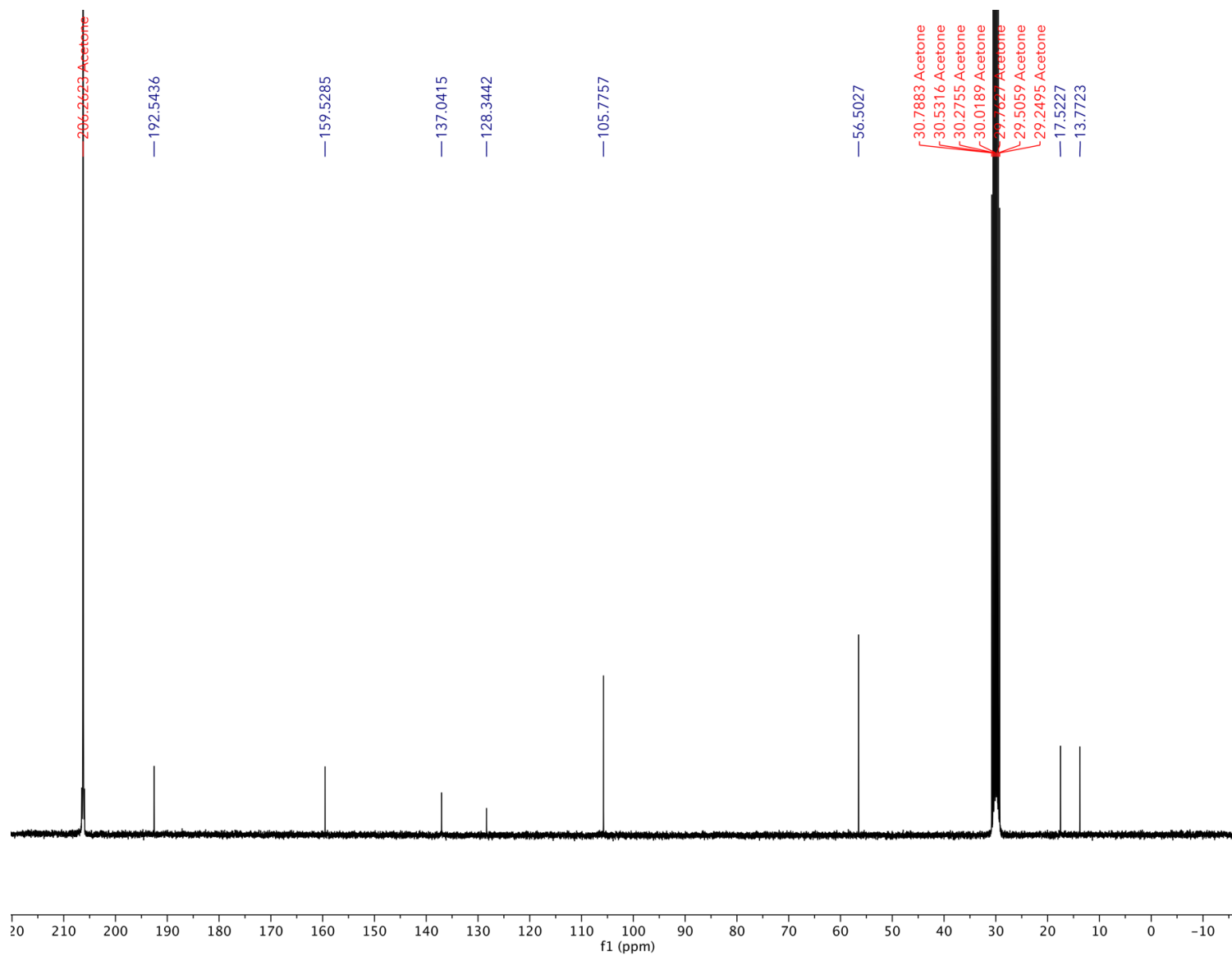
Fig. 93: $^{13}C\{^1H\}$ NMR spectrum of 4-ethyl-3,5-dimethoxybenzaldeyde **55** in acetone-d_6.
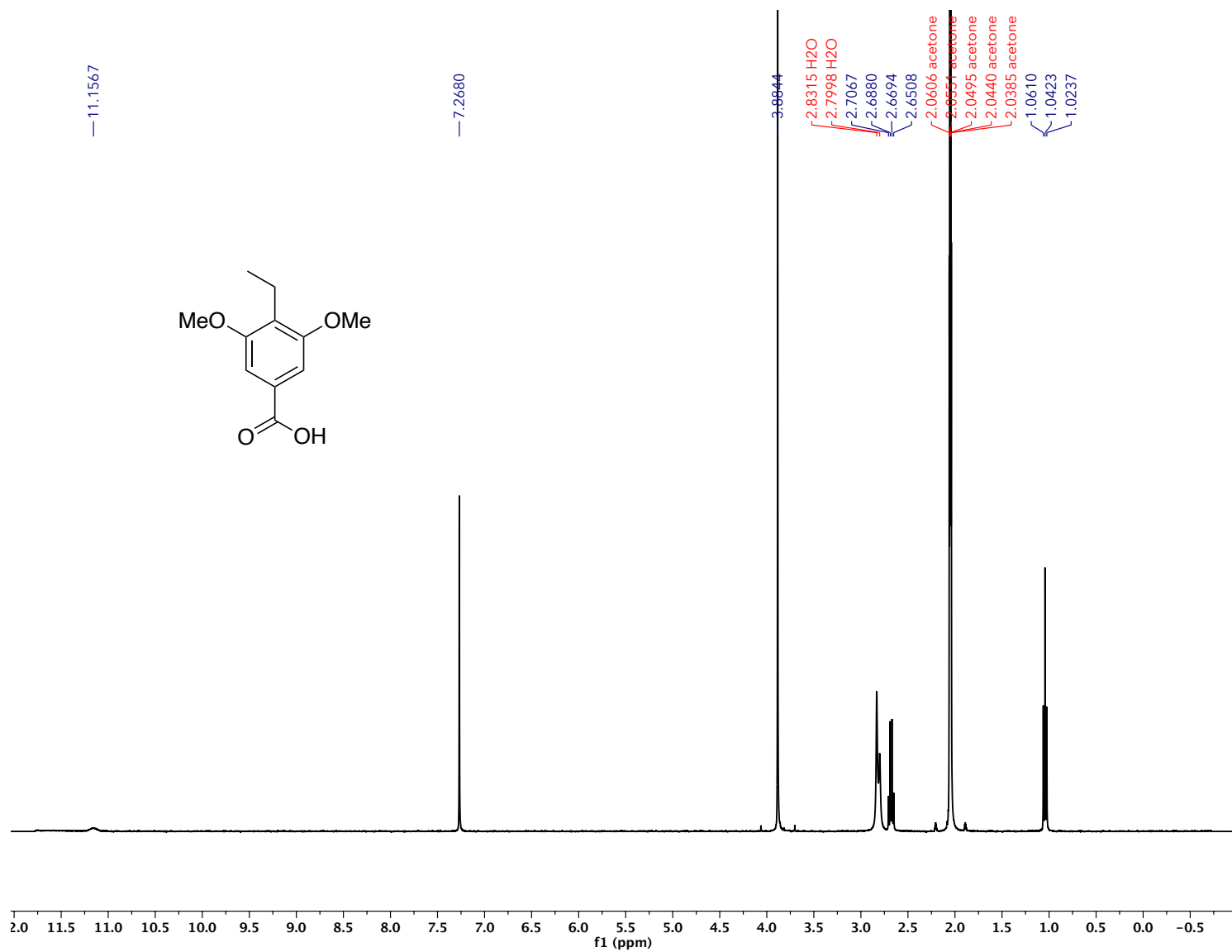
Fig. 94: ^{1}H NMR spectrum of 4-ethyl-3,5-dimethoxybenzoic acid **56** in acetone-d_6.
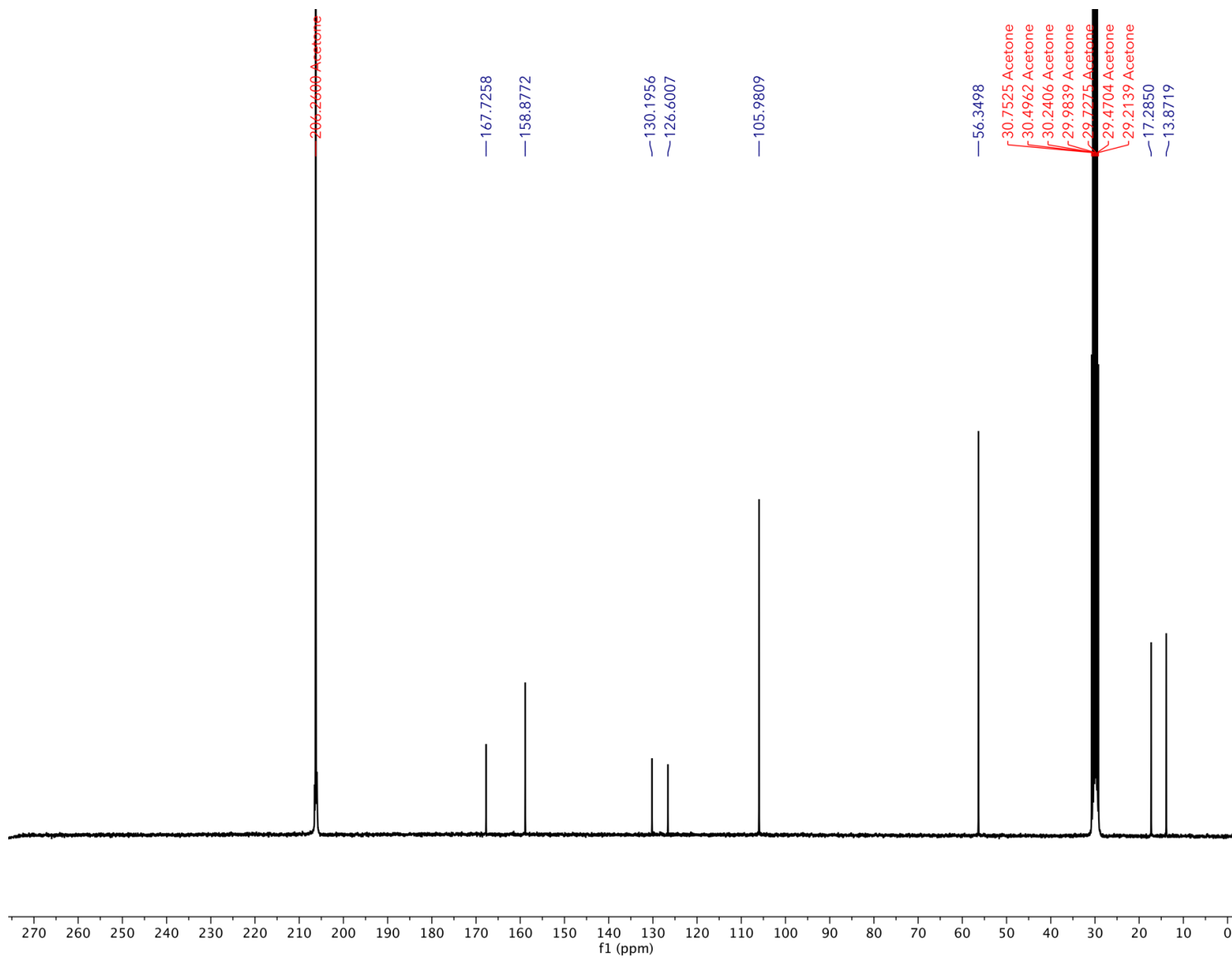
Fig. 95: $^{13}C\{^1H\}$ NMR spectrum of 4-ethyl-3,5-dimethoxybenzoic acid **56** in acetone-d_6.
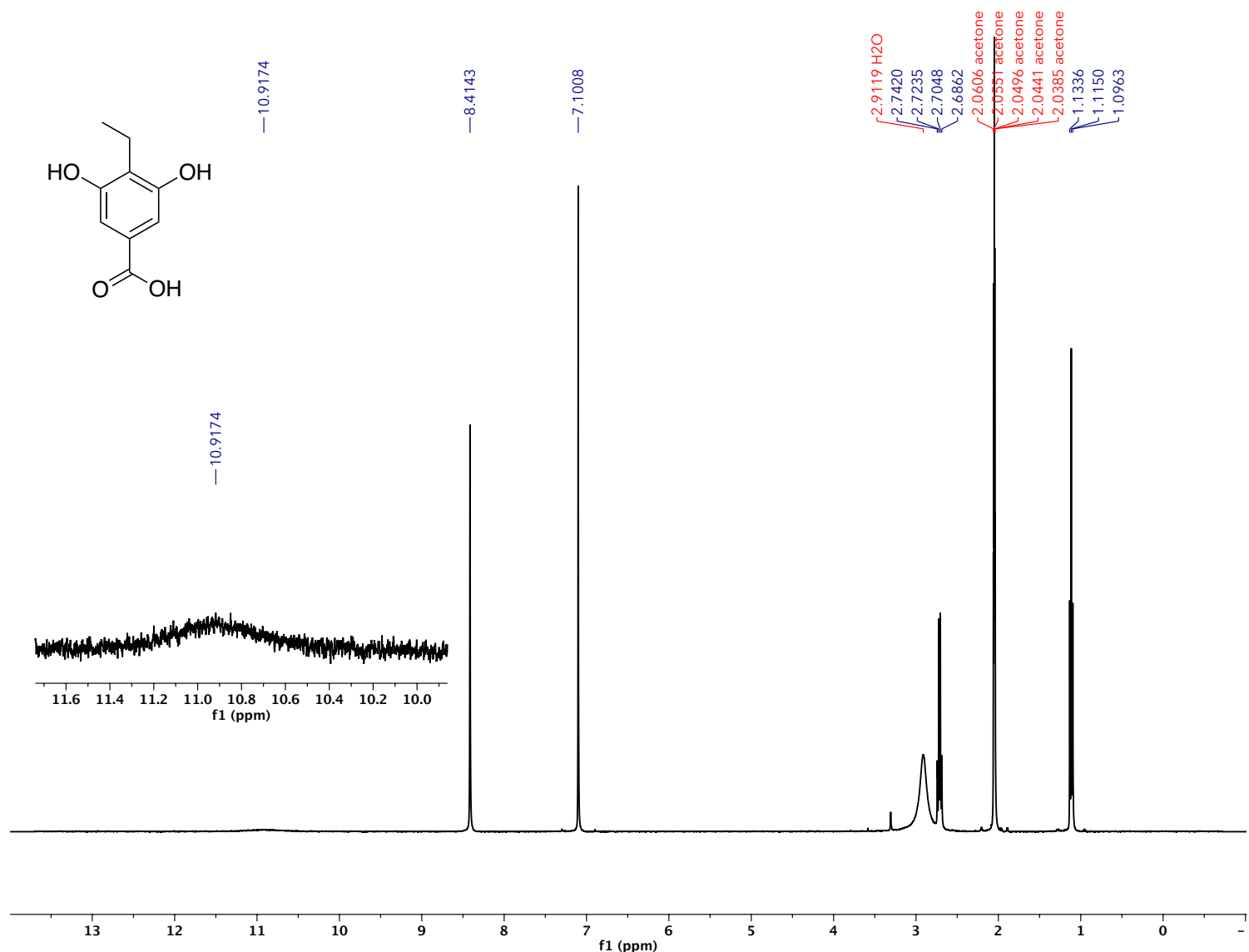
Fig. 96: ^{1}H NMR spectrum of 4-ethyl-3,5-dihydroxybenzoic acid **57** in acetone-d_6. Inset shows a broad resonance indicative of a carboxylic acid.
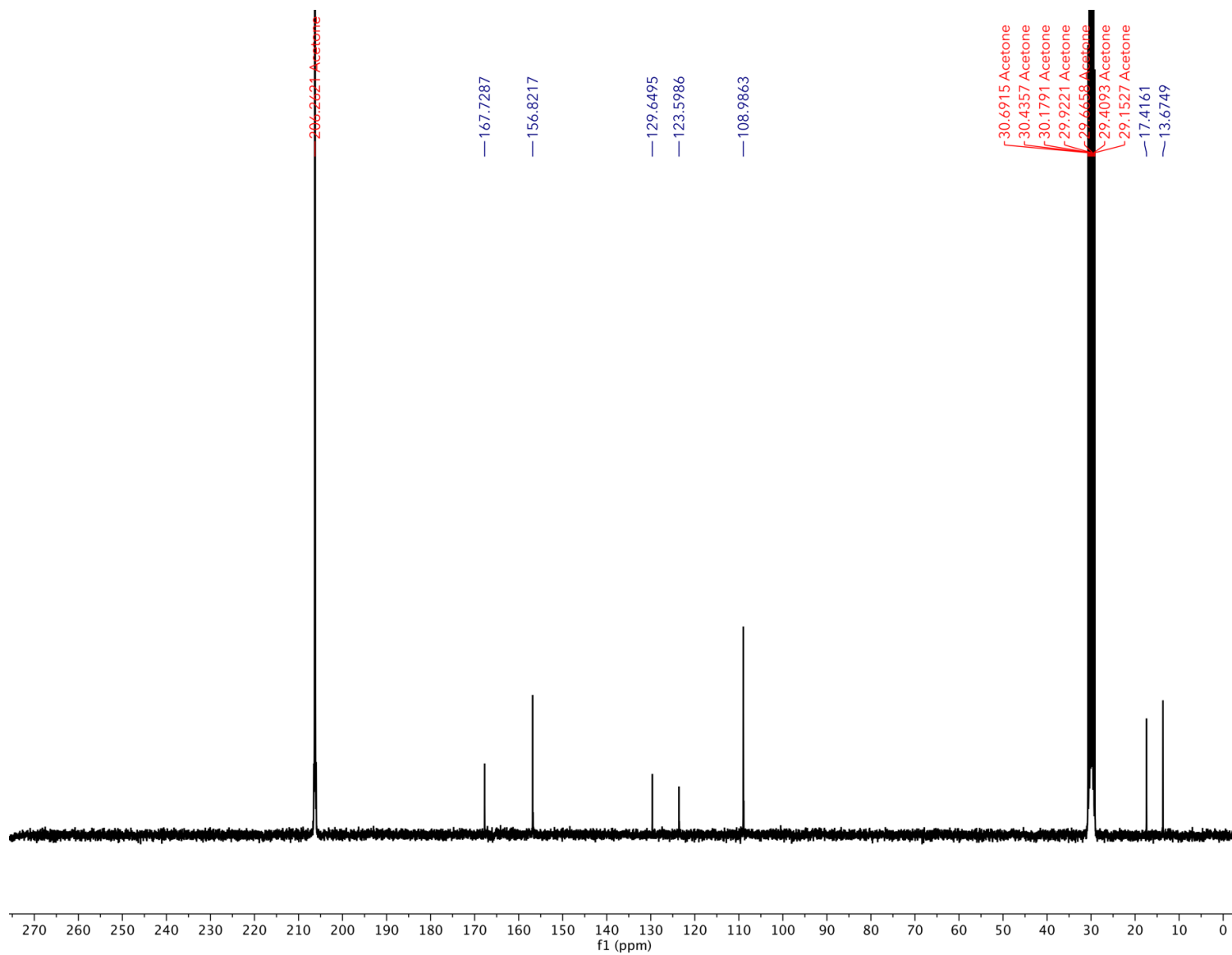
Fig. 97: $^{13}C\{^1H\}$ NMR spectrum of 4-ethyl-3,5-dihydroxybenzoic acid **57** in acetone-d_6.
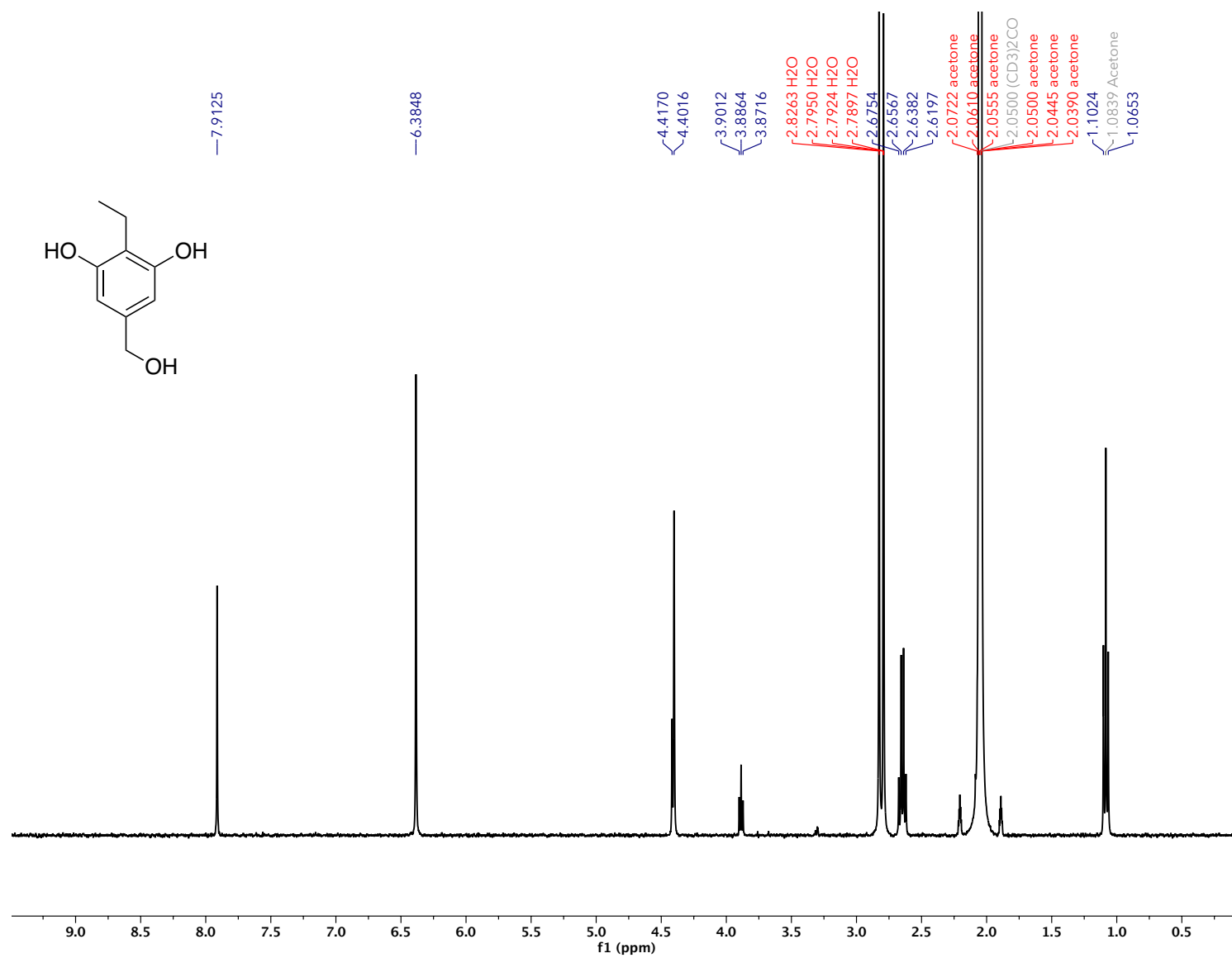
Fig. 98: ^{1}H NMR spectrum of 3,5-dihydroxy-4-ethylbenzyl alcohol **58** in acetone-d_6.
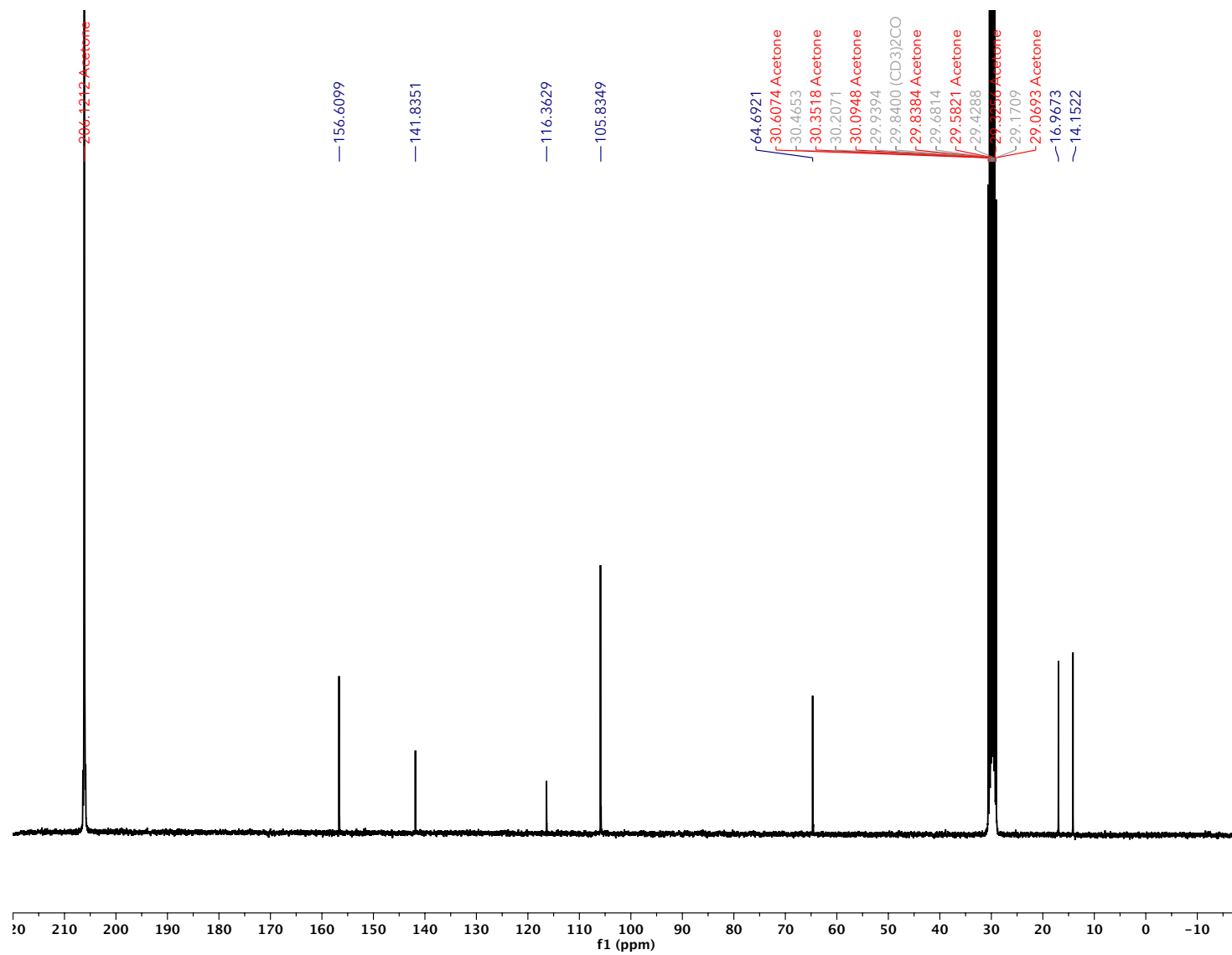
Fig. 99: $^{13}C\{^1H\}$ NMR spectrum of 3,5-dihydrozy-4-ethylbenzyl alcohol **58** in acetone-d_6.
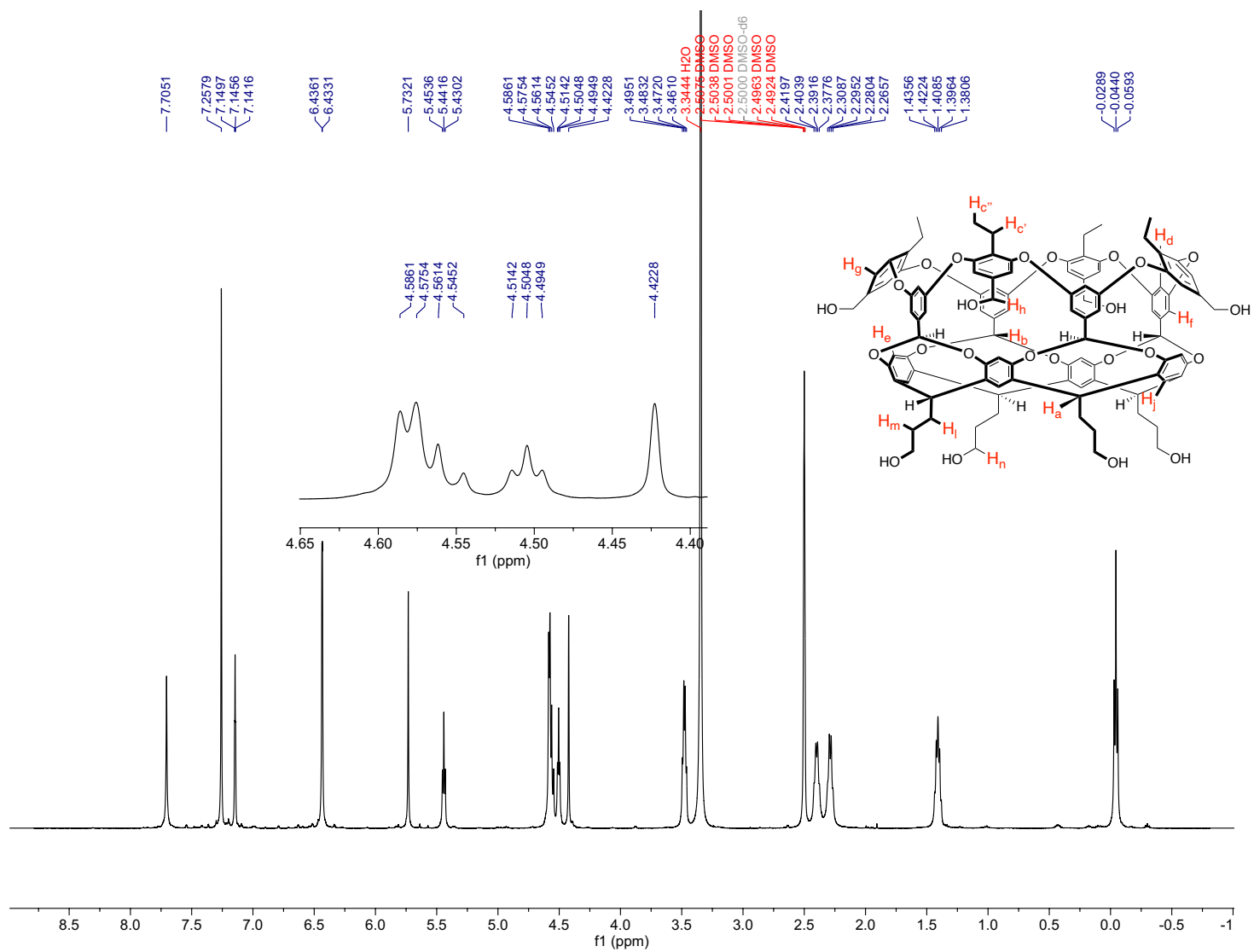
Fig. 100: ^{1}H NMR spectrum of TEEtOctol **59** in DMSO-d_6. Inset shows crowded region between 4.40–4.65 ppm.
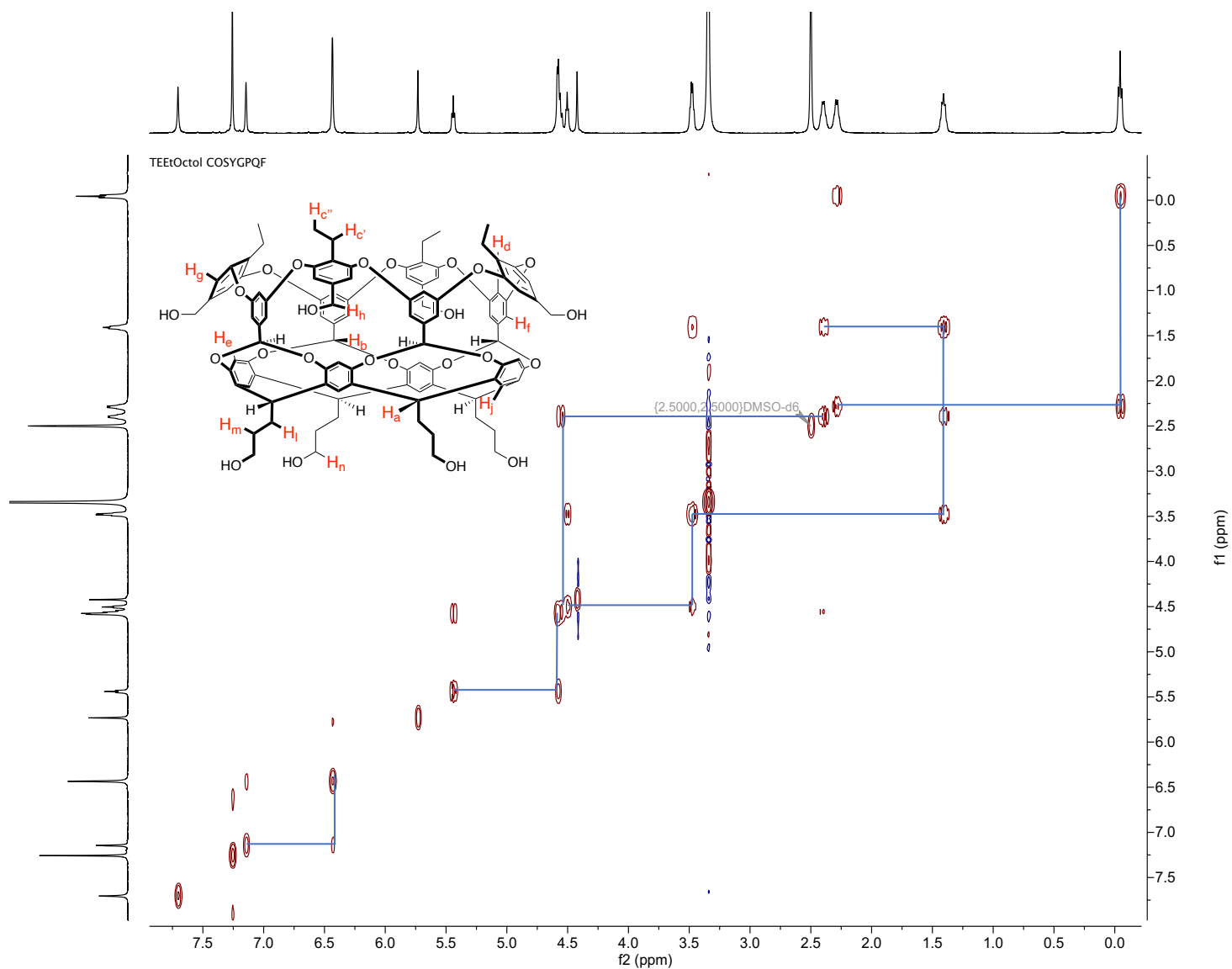
Fig. 101: ^{1}H–^{1}H COSY NMR spectrum of TEEtOctol **59** in DMSO-d_6.
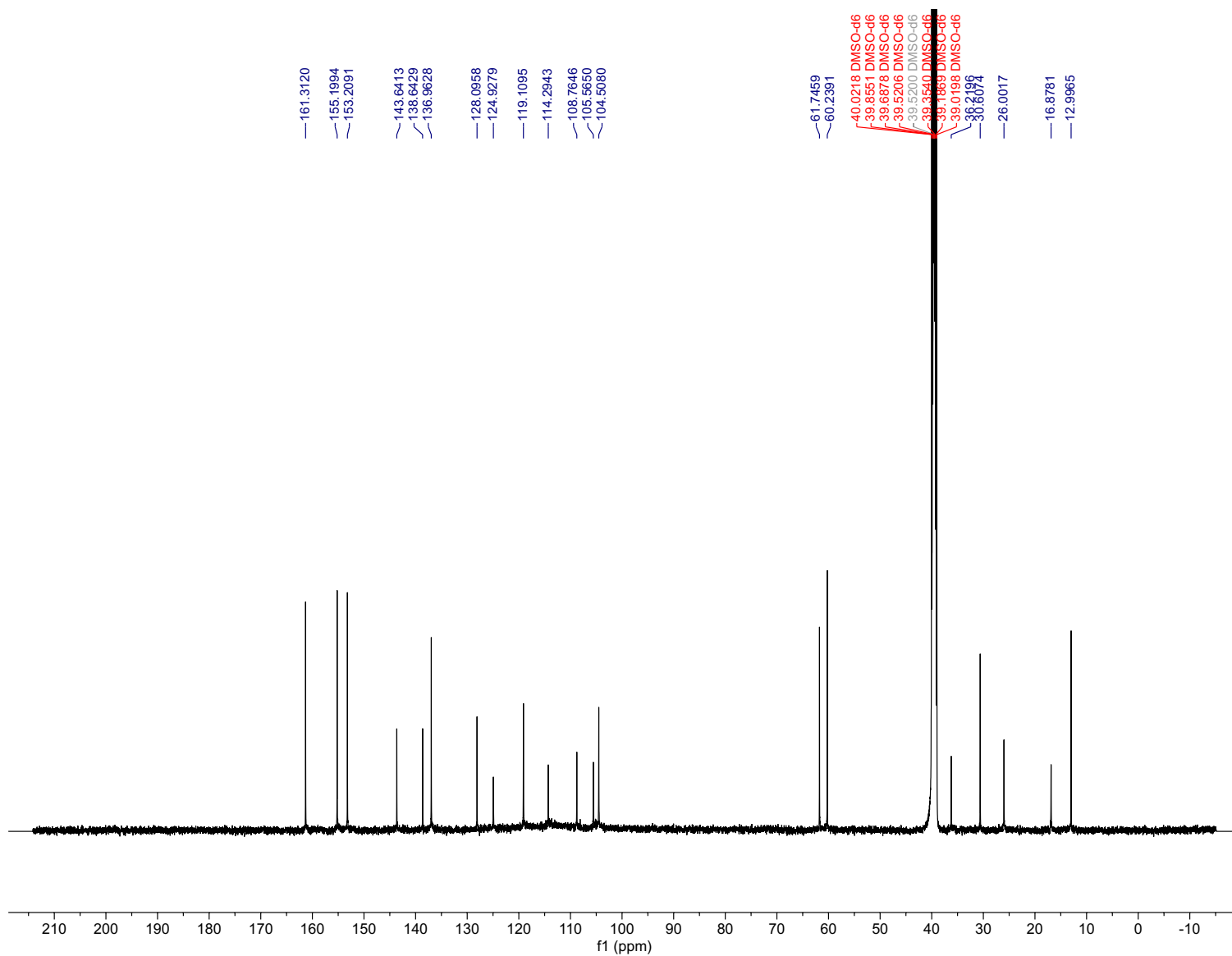
Fig. 102: $^{13}C\{^1H\}$ NMR spectrum of TEEtOctol **59** in DMSO-d_6.
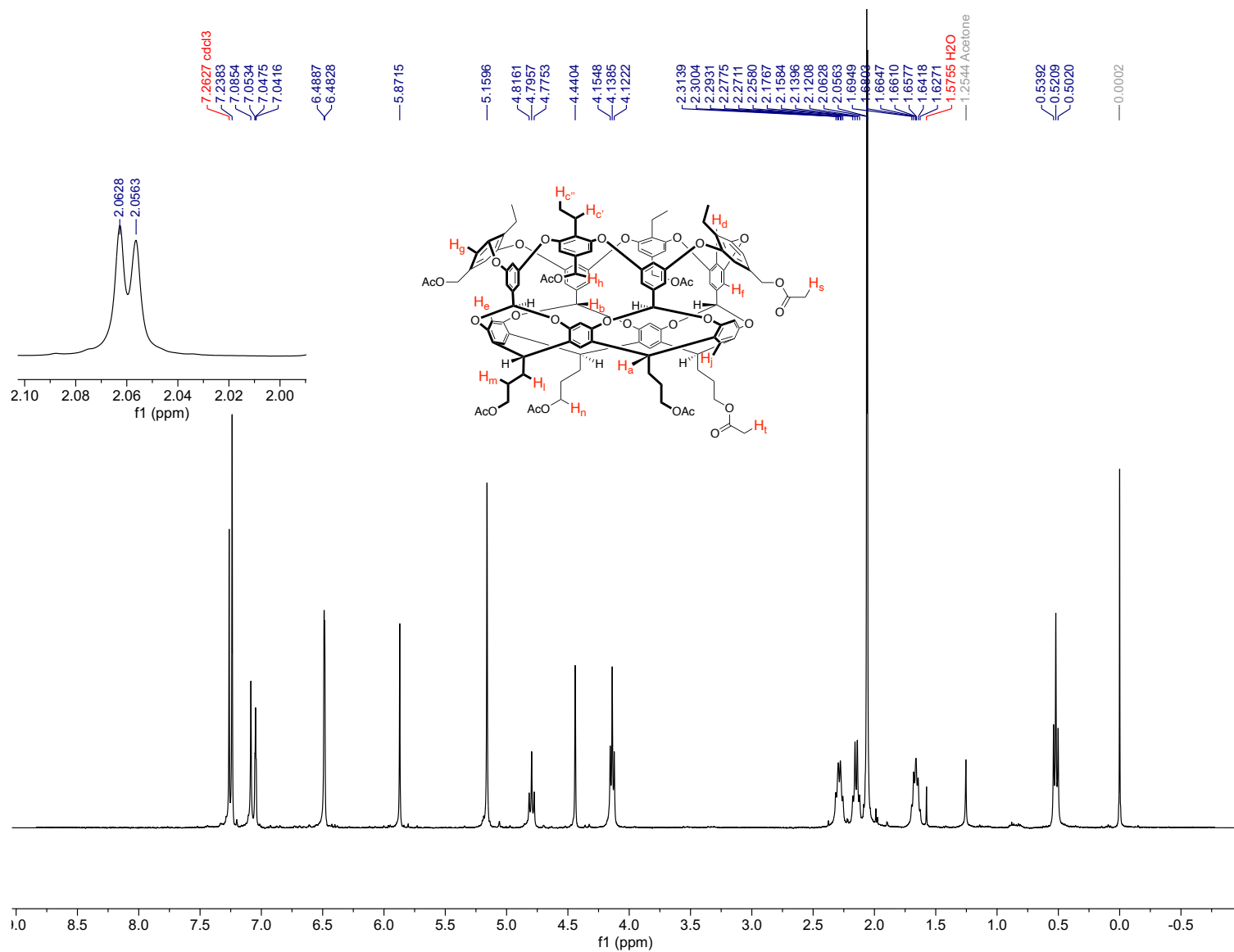
Fig. 103: ^{1}H NMR spectrum of tetra-*endo*-ethyl octa-acetate **60** in CDCl$_3$. Inset shows two close singlets corresponding to the protons of the acetyl groups.
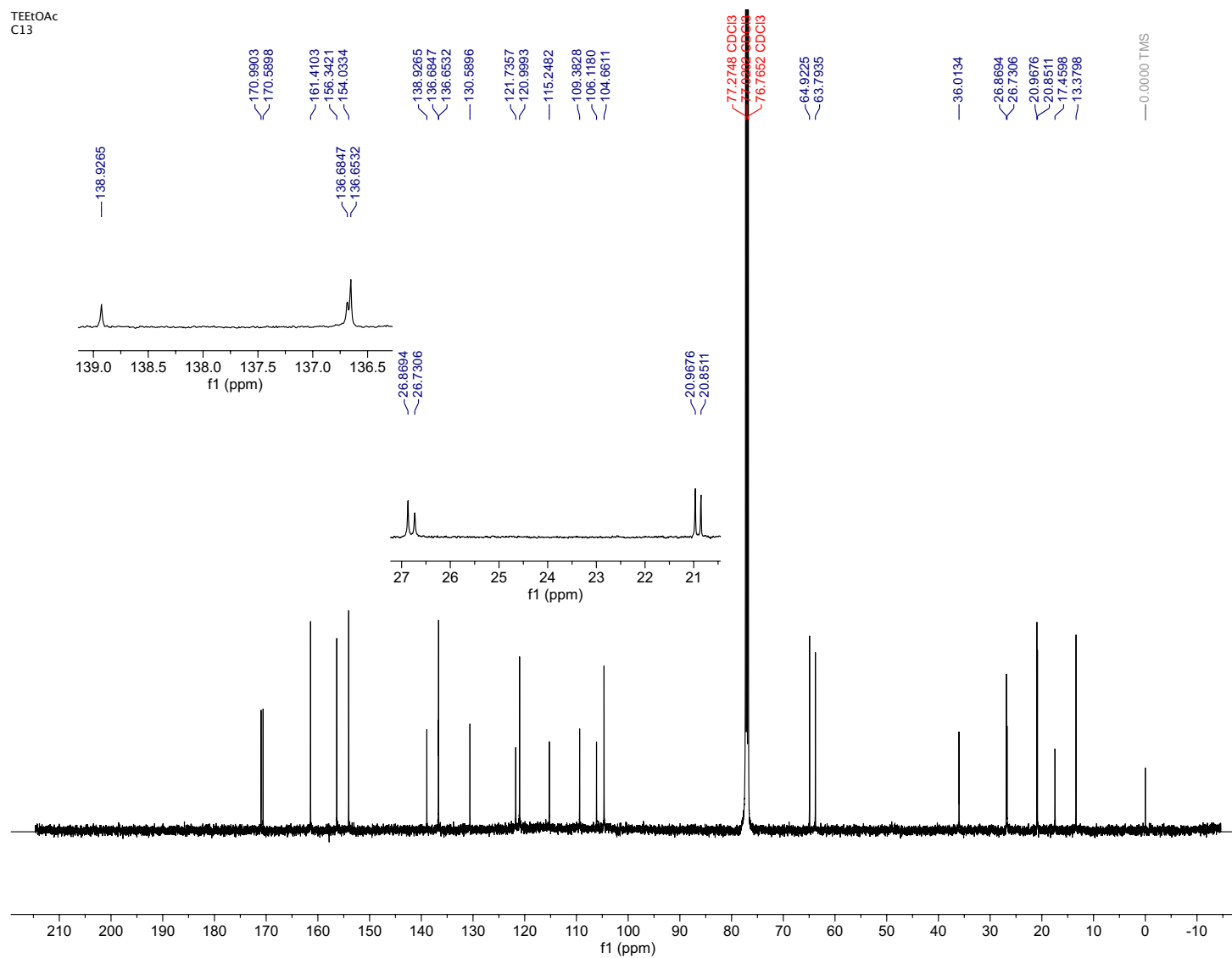
Fig. 104: $^{13}C\{^1H\}$ NMR spectrum of tetra-*endo*-ethyl octa-acetate **60** in CDCl$_3$. Insets show regions of tightly spaced signals from 136–139 ppm, and 20–27 ppm.
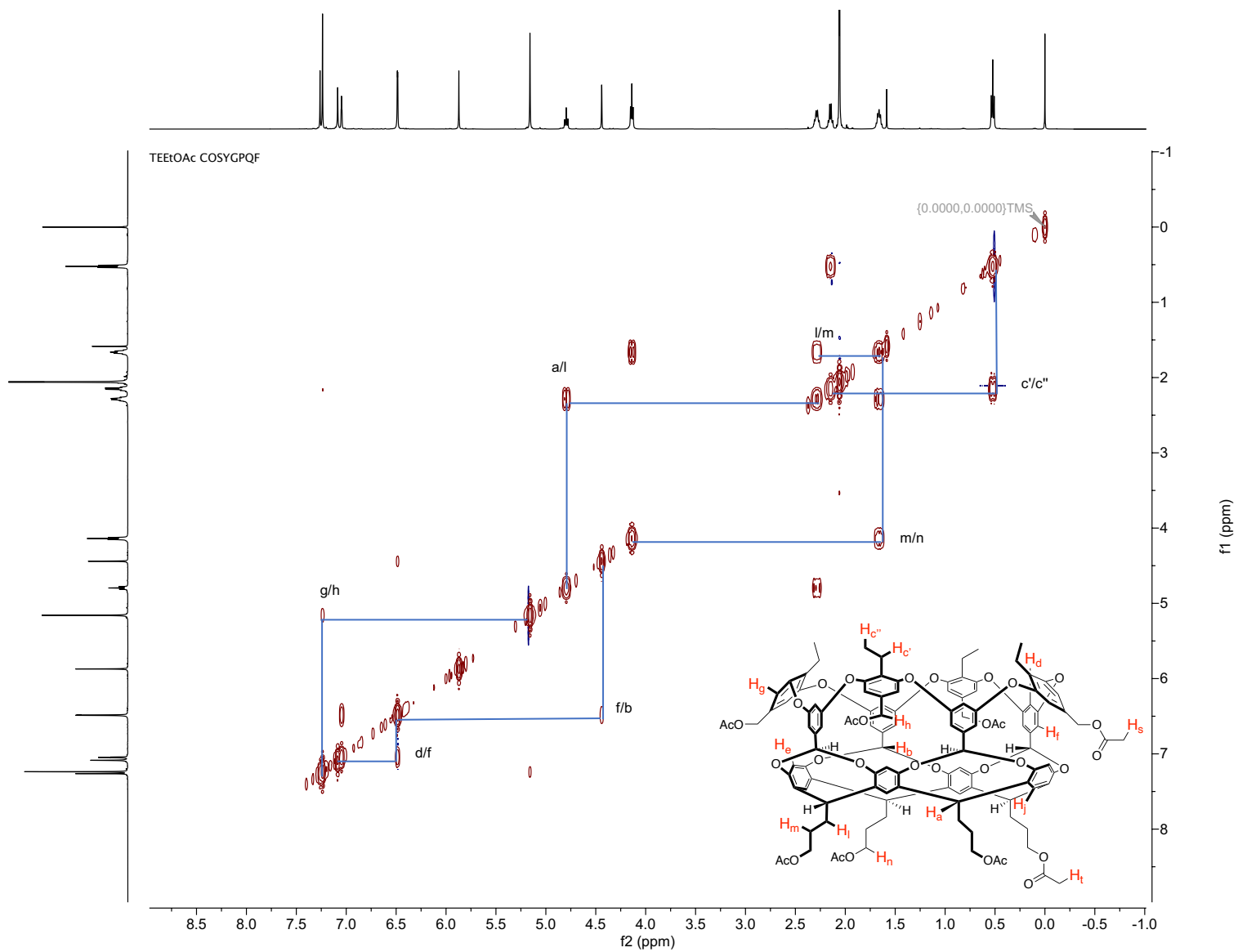
Fig. 105: ^{1}H–^{1}H COSY NMR spectrum of tetra-*endo*-ethyl octa-acetate **60** in CDCl$_3$.
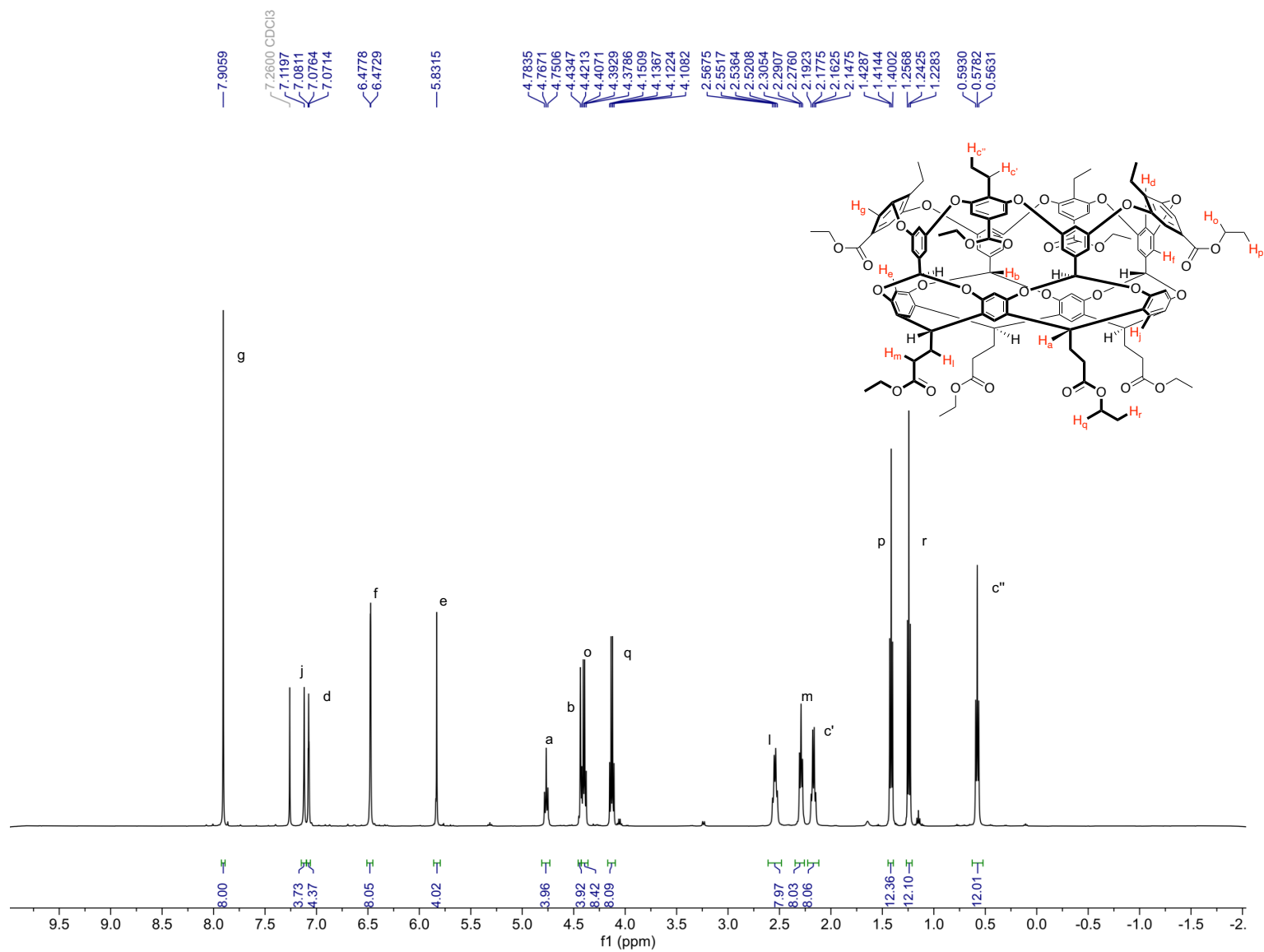
Fig. 106: ^{1}H NMR spectrum of tetra-*endo*-ethyl octaethyl ester **61** in CDCl₃.
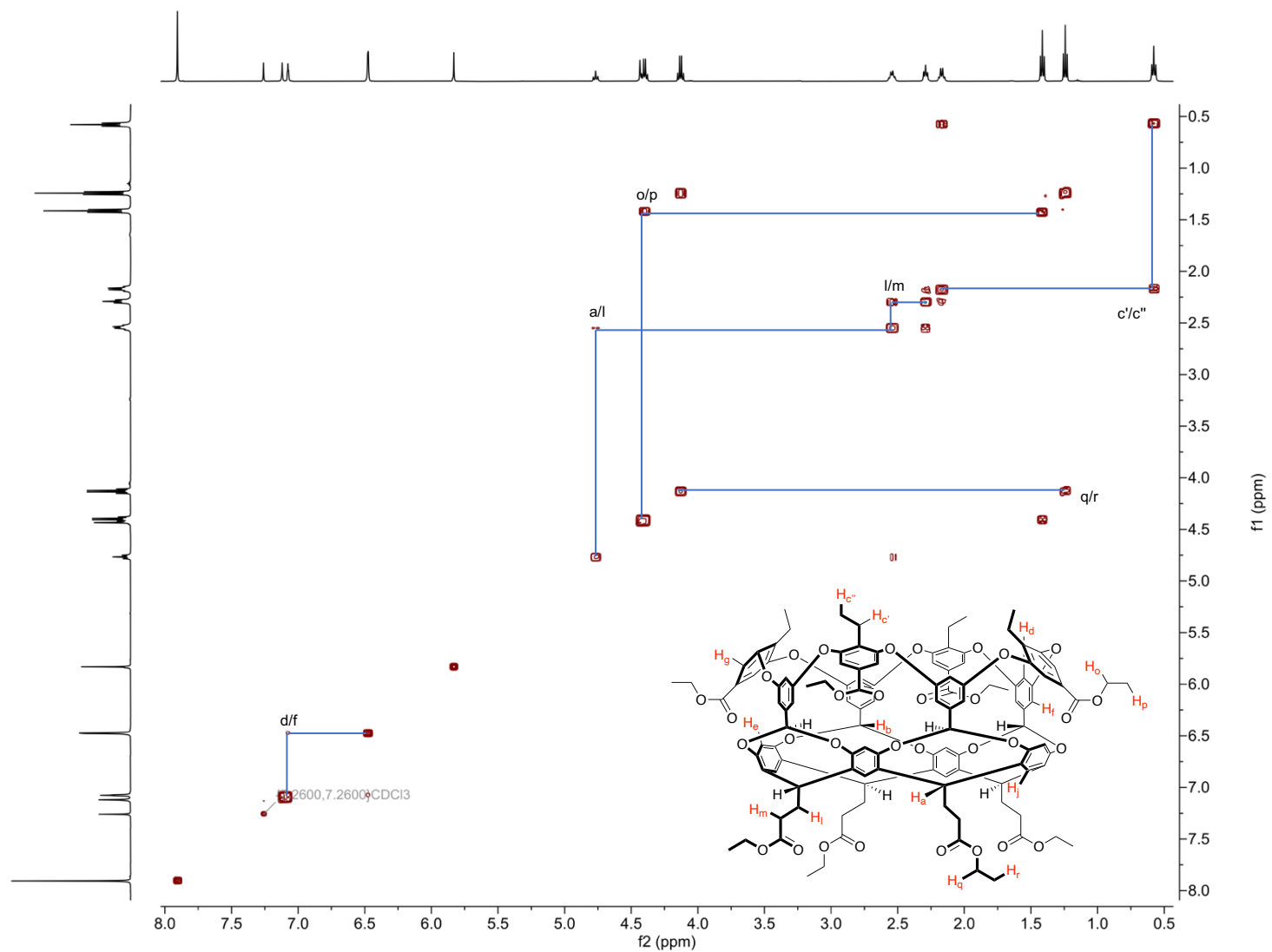
Fig. 107: ^{1}H–^{1}H COSY NMR spectrum of tetra-*endo*-ethyl octaethyl ester **61** in CDCl₃.
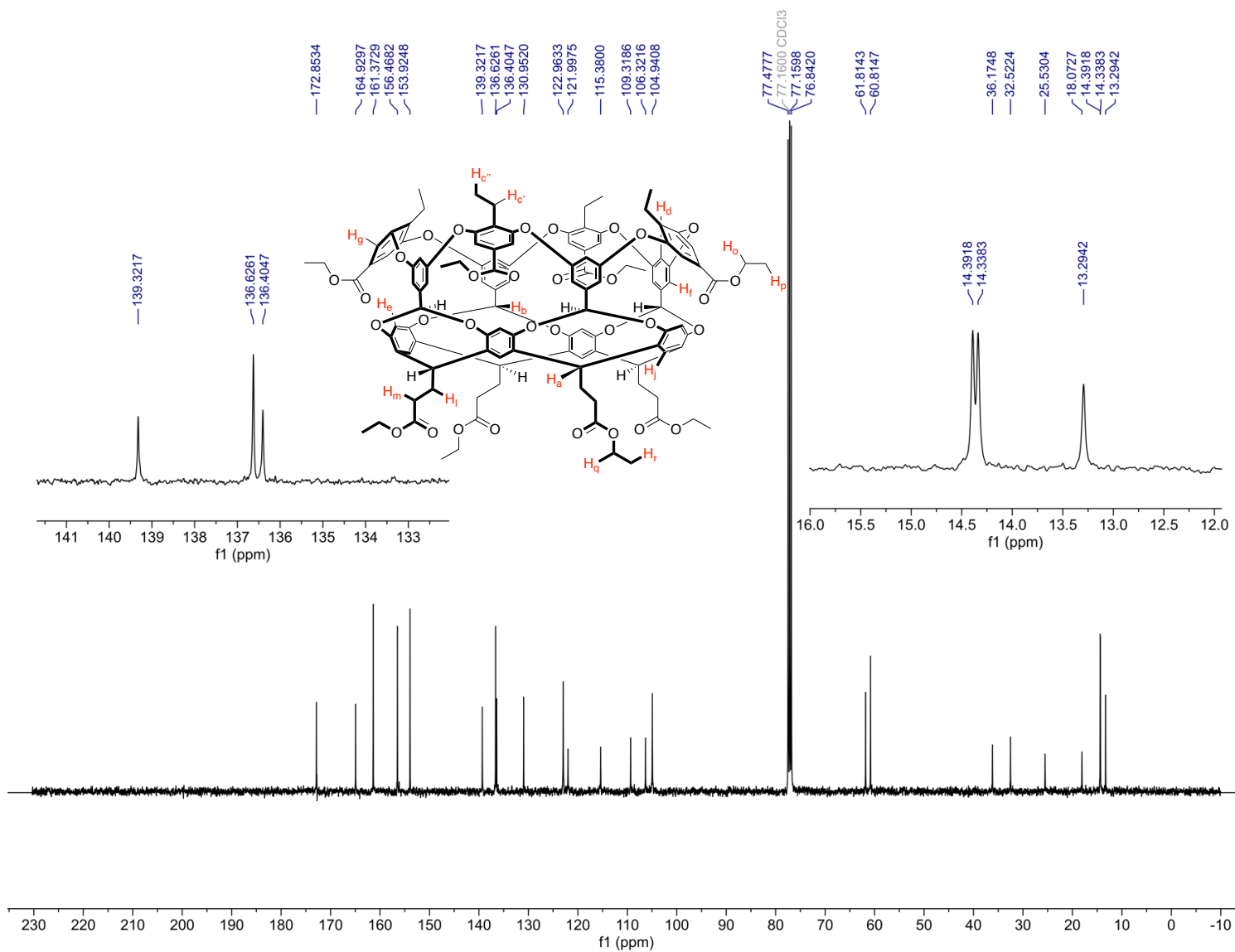
Fig. 108: $^{13}C\{^1H\}$ NMR spectrum of tetra-*endo*-ethyl octaethyl ester **61** in CDCl$_3$. Insets are expanded views of tightly spaced signals between 132–142 ppm, and 12–16 ppm.
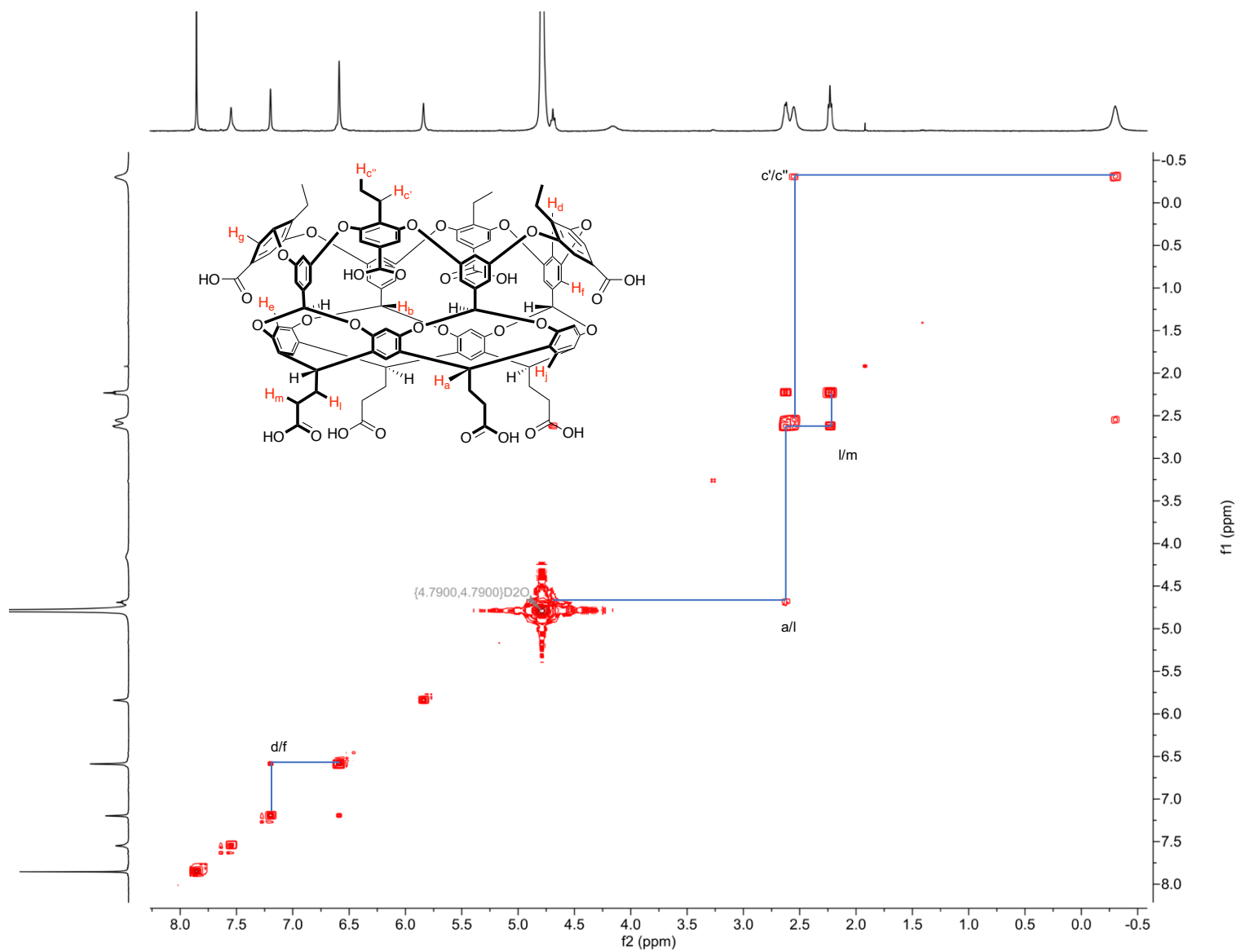
Fig. 109: ^{1}H–^{1}H COSY NMR spectrum of 1 mM tetra-*endo*-ethyl octa acid **53** in 10 mM pD 11.45 phosphate-buffered D$_2$O.
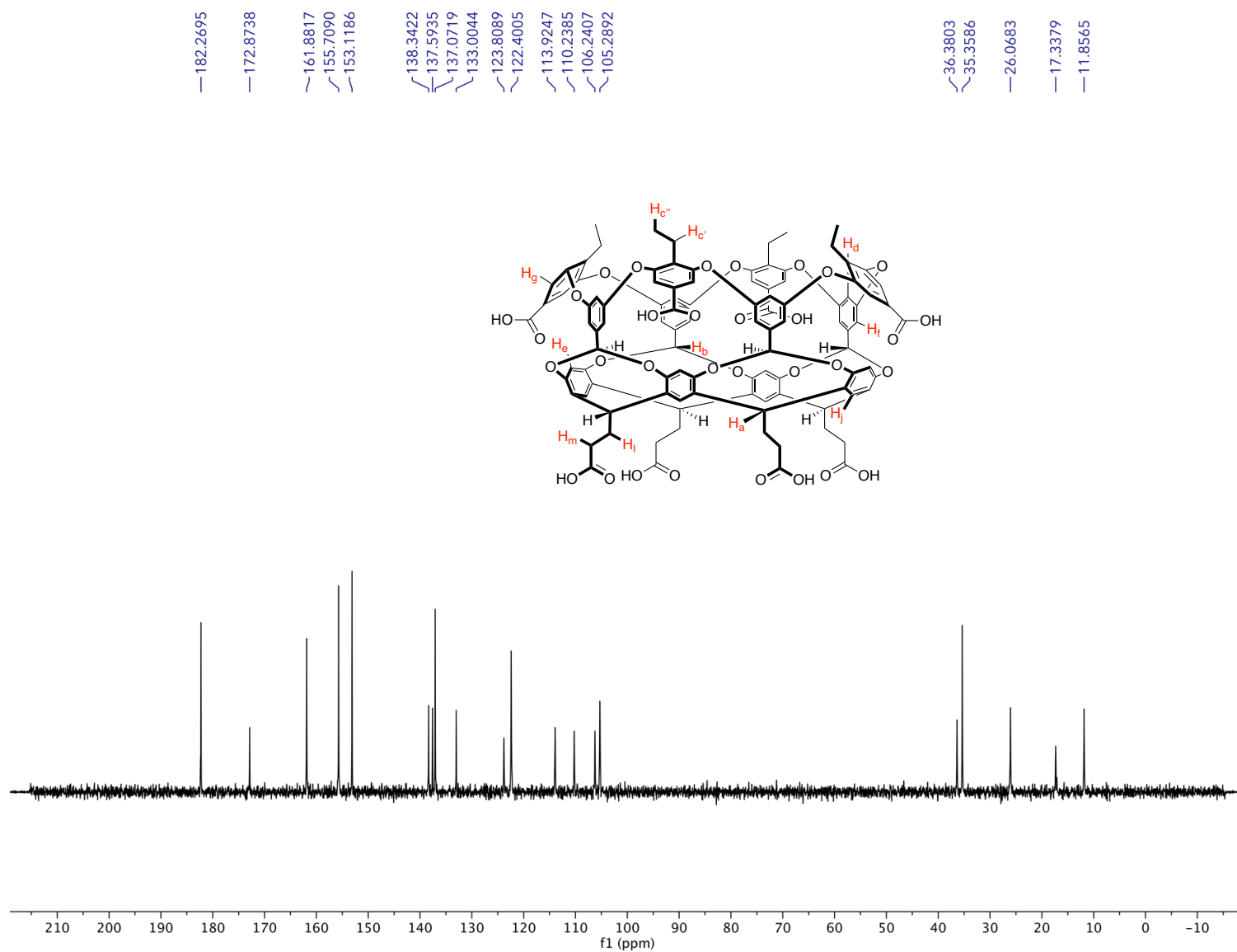
Fig. 110: $^{13}C\{^{1}H\}$ NMR spectrum of tetra-*endo*-ethyl octa acid **53** in 10 mM pD 11.45 phosphate-buffered D_2O.
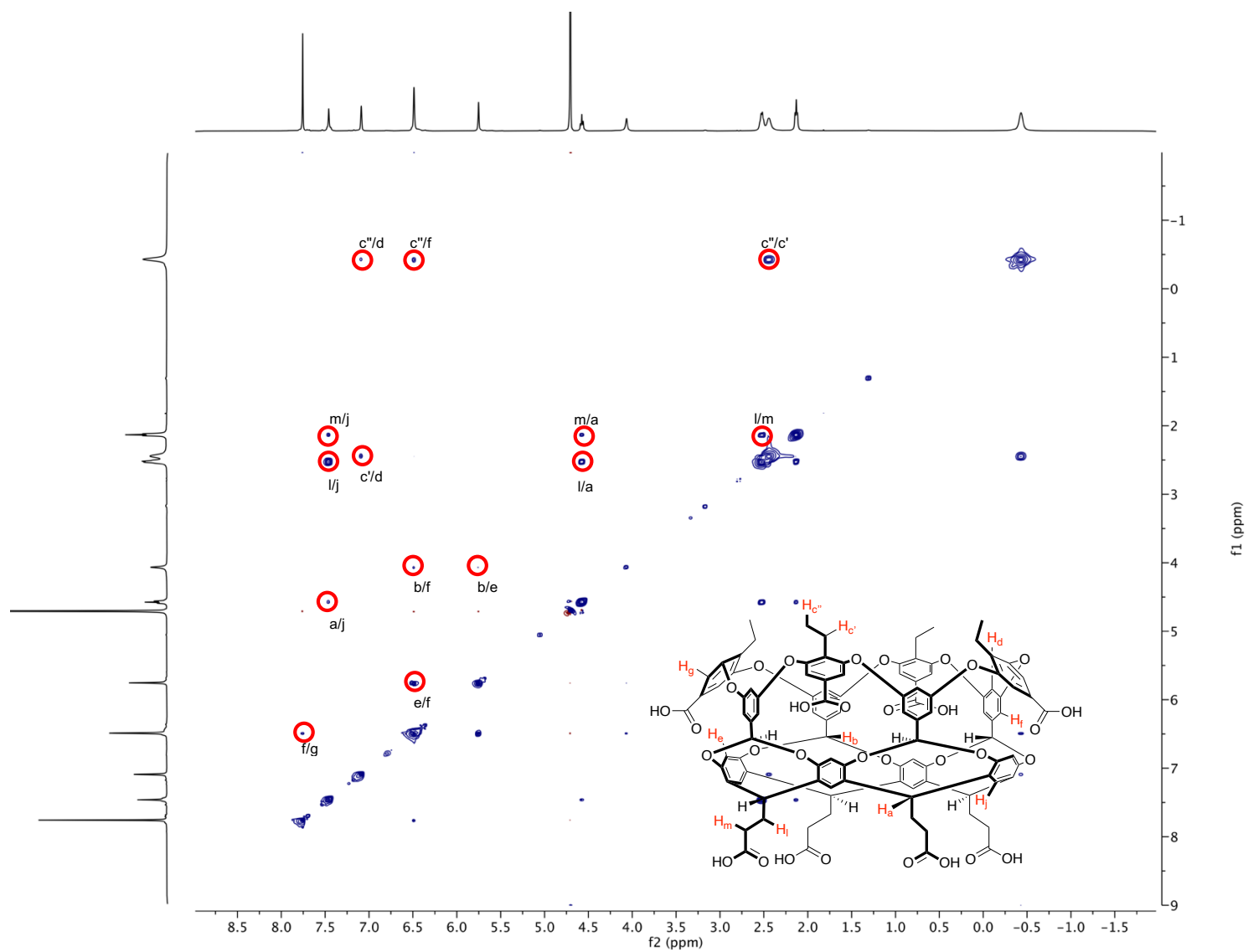
Fig. 111: 2D ^{1}H–^{1}H NOESY spectrum of 10 mM tetra-*endo*-ethyl octa acid **53** in 10 mM pD 11.45 phosphate-buffered D$_2$O
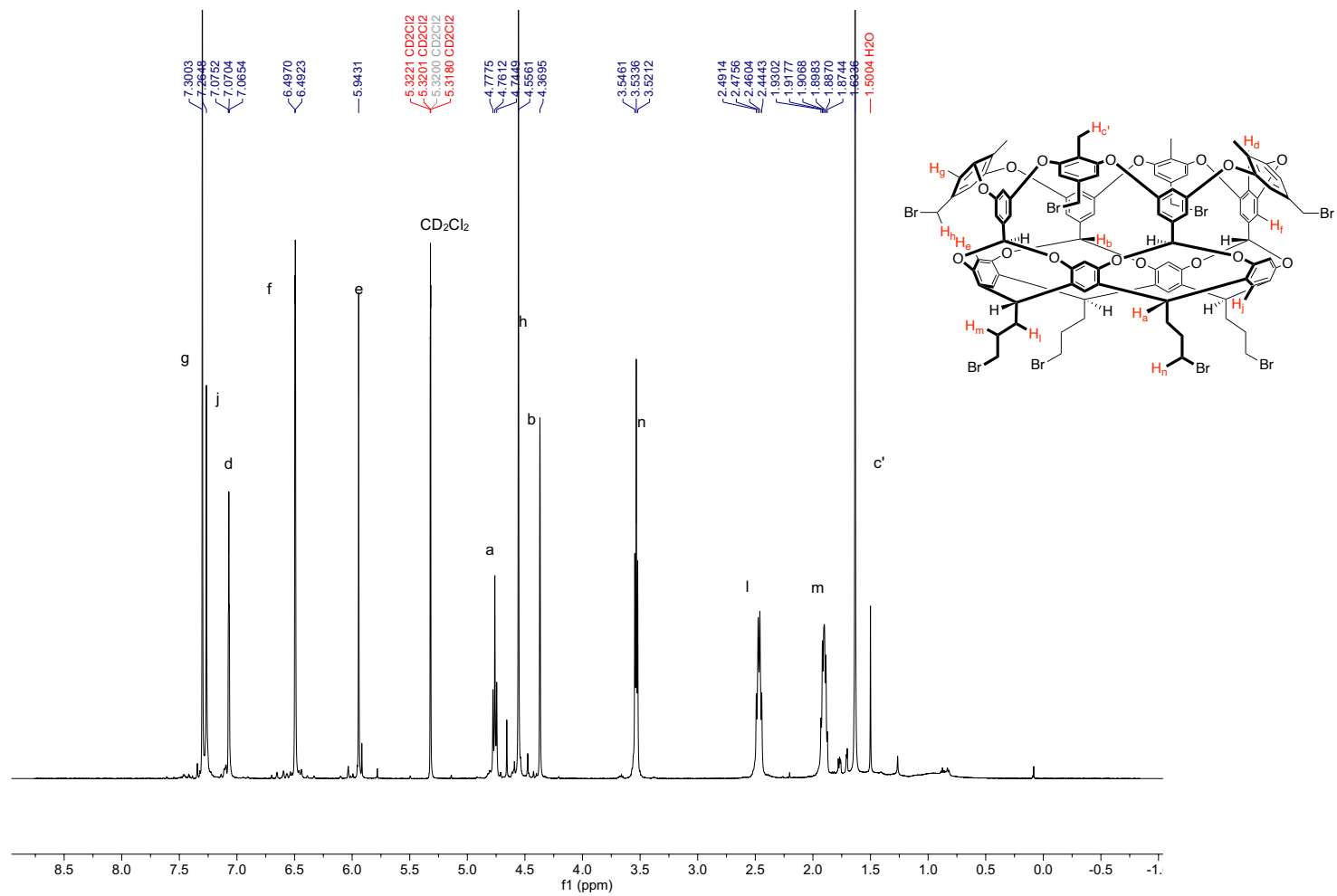
Fig. 112: ^{1}H NMR spectrum of tetra-*endo*-methyl octa-bromide **70** in CD$_2$Cl$_2$.
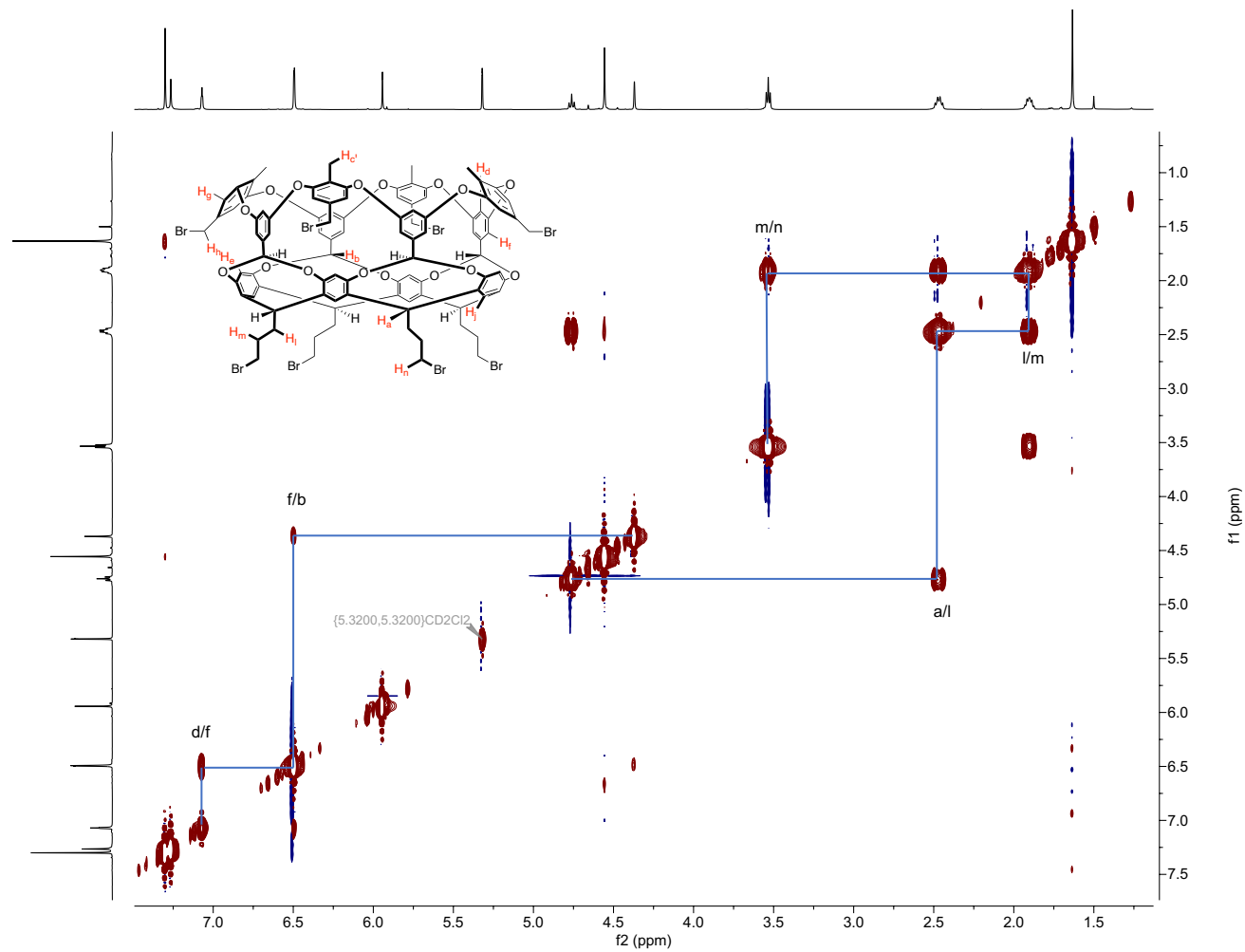
Fig. 113: ^{1}H–^{1}H COSY NMR spectrum of tetra-*endo*-methyl octa-bromide **70** in CD$_2$Cl$_2$.
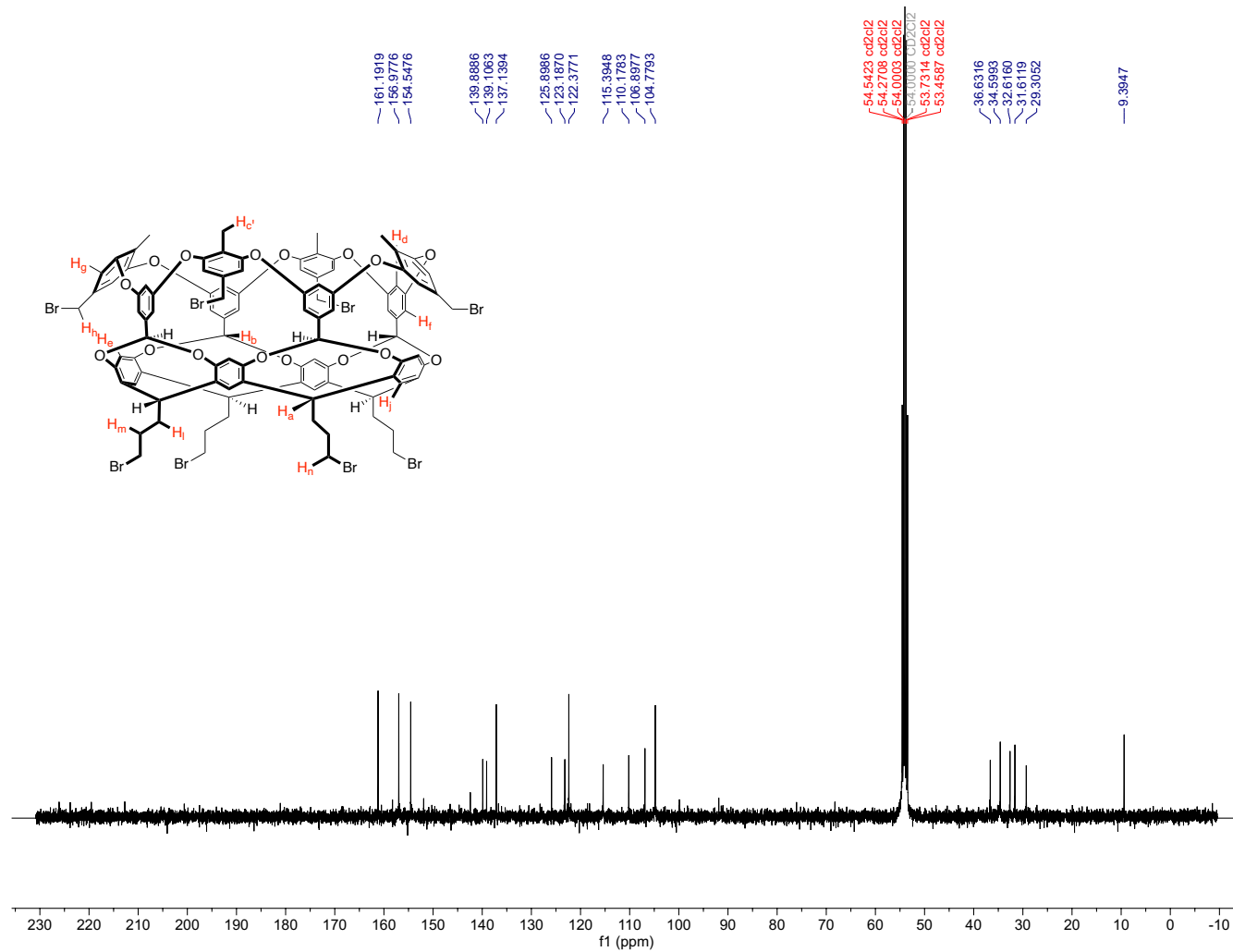
Fig. 114: $^{13}C\{^1H\}$ NMR spectrum of tetra-*endo*-methyl octa-bromide **70** in CD_2Cl_2.
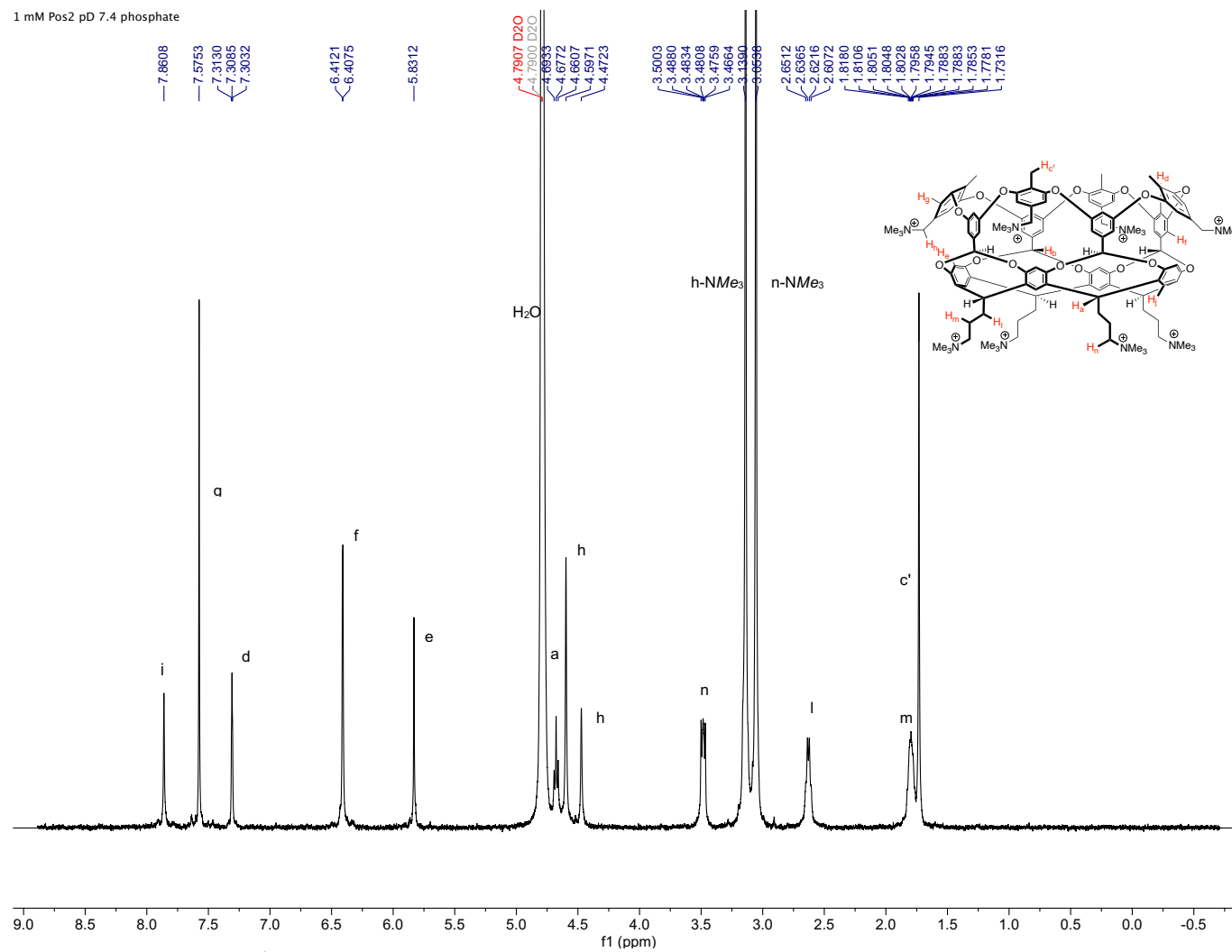
Fig. 115: ^{1}H NMR spectrum of 1 mM Positand 2 (**67**) in 10 mM pD 7.4 phosphate buffered D$_2$O.
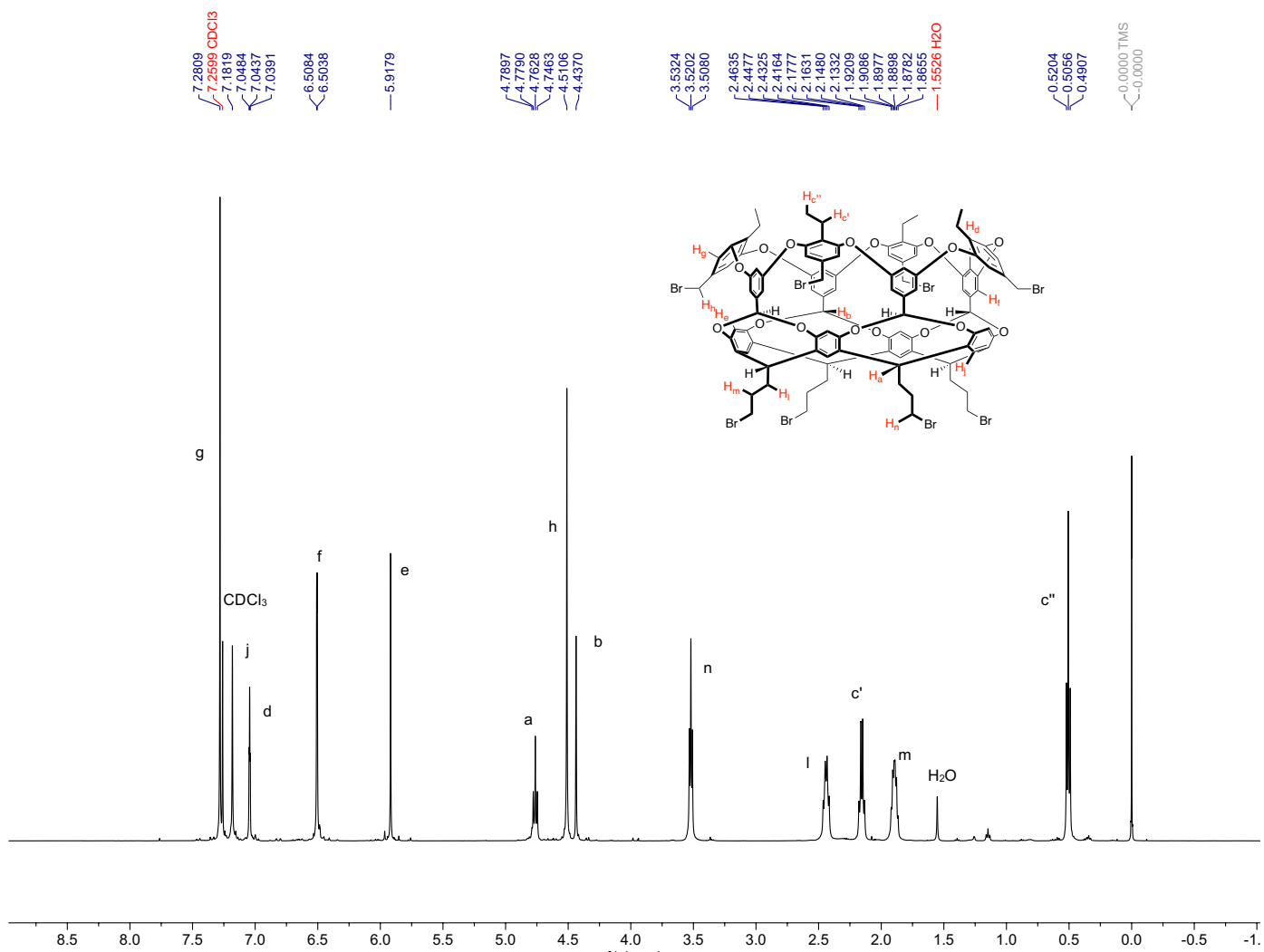
Fig. 116: ^{1}H NMR spectrum of tetra-*endo*-ethyl octa-bromide **71** in CDCl$_3$.
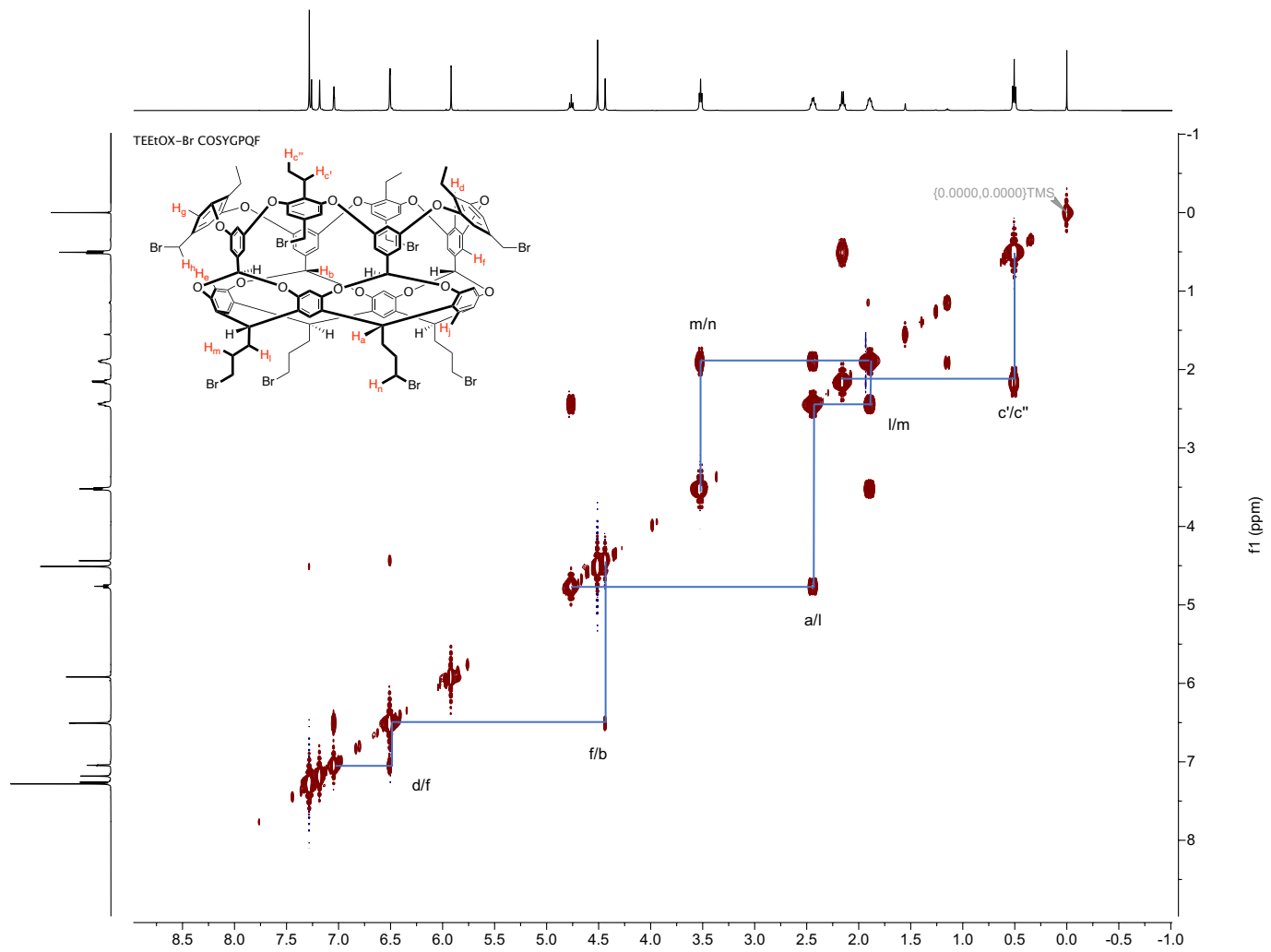
Fig. 117: ^{1}H–^{1}H COSY NMR spectrum of tetra-*endo*-ethyl octa-bromide **71** in CDCl$_3$.
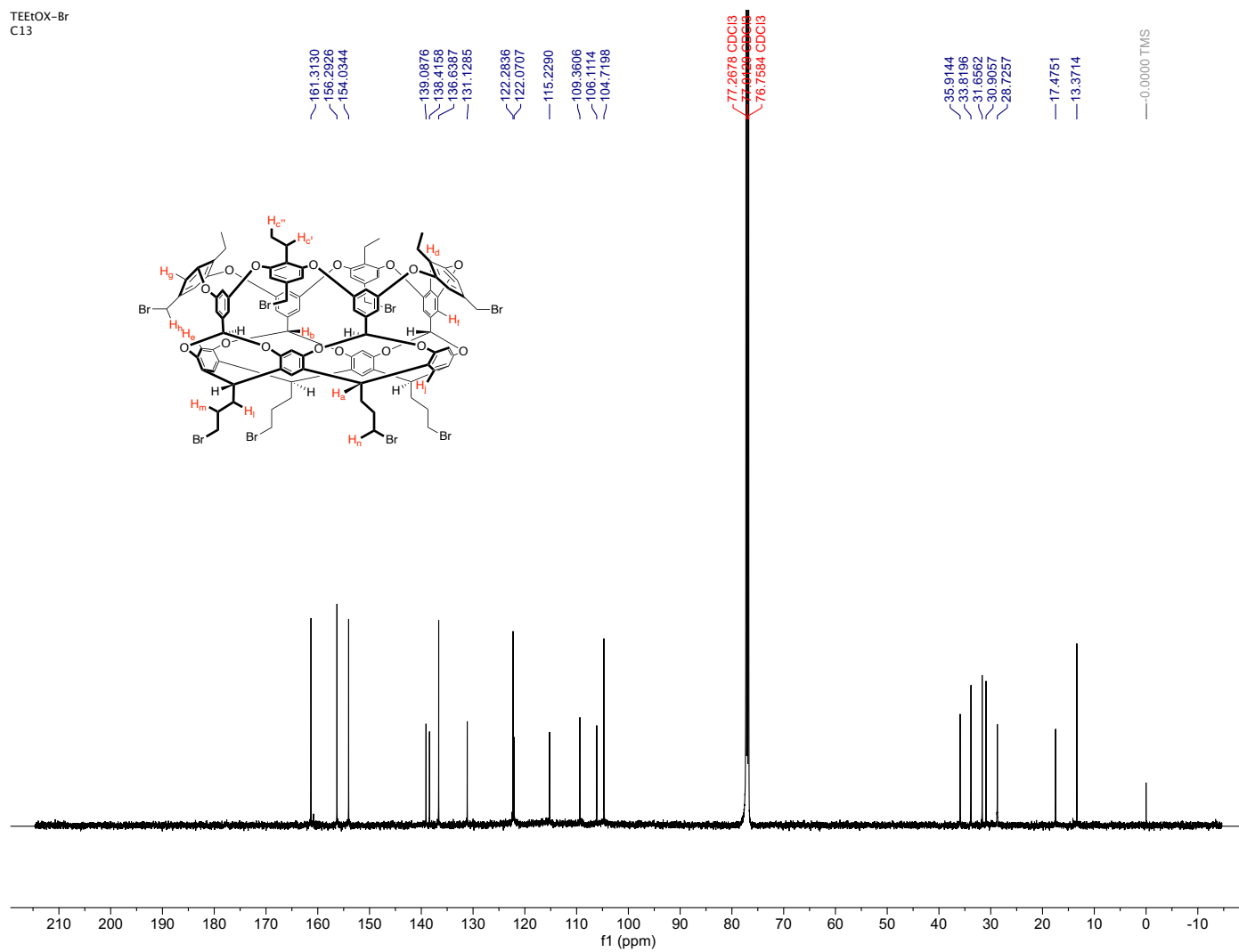
Fig. 118: ^{13}C{^{1}H} NMR spectrum of tetra-*endo*-ethyl octa-bromide **71** in CDCl$_3$.
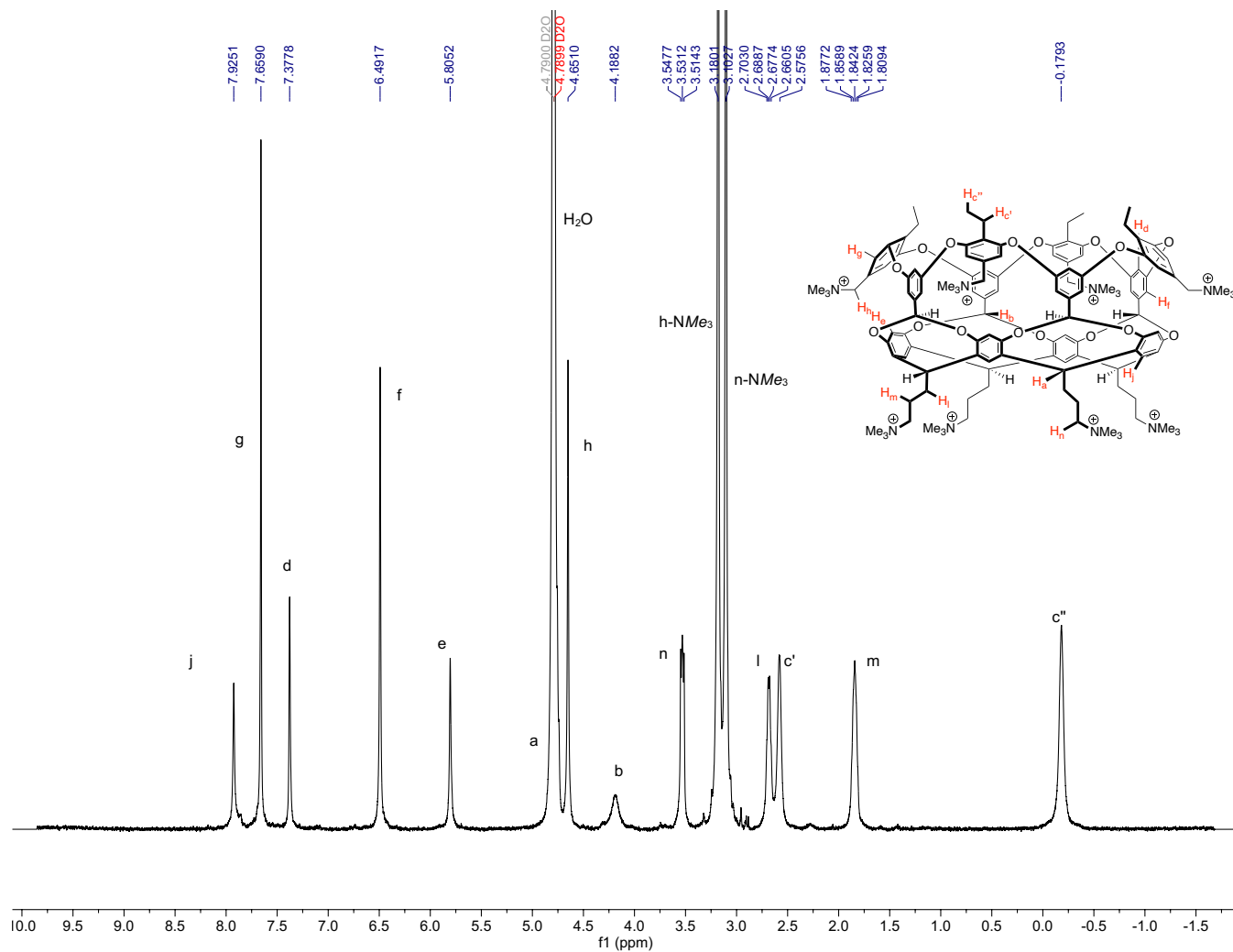
Fig. 119: ¹H NMR spectrum of 1 mM Positand 3 (**68**) in 10 mM pD 7.4 (pH 7.8) phosphate buffered D_2O.
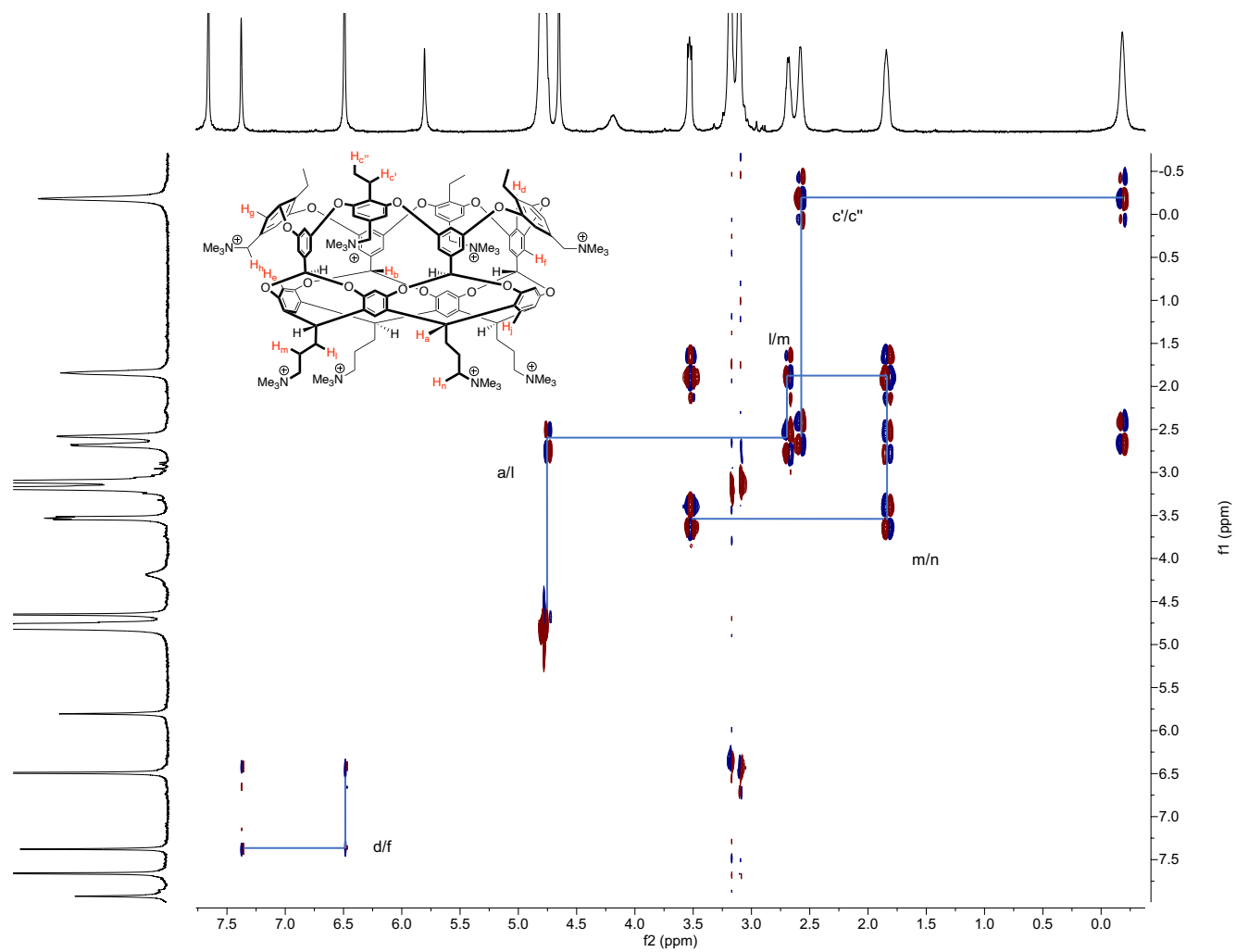
Fig. 120: ^1H–^1H DQFCOSY spectrum of 1 mM Positand 3 (**68**) in 10 mM pD 7.4 (pH 7.8) phosphate buffered D_2O.
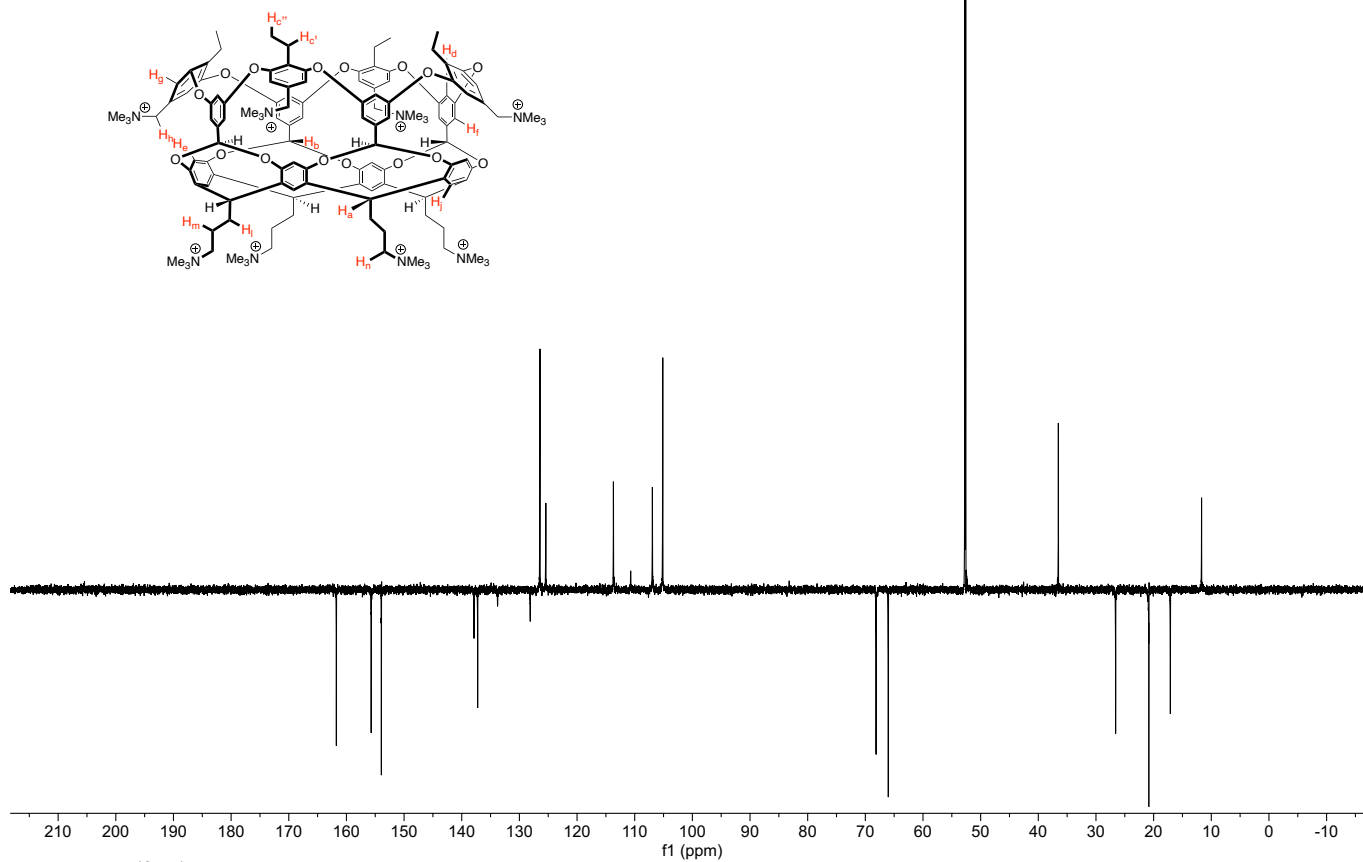
Fig. 121: ^{13}C{^{1}H} DEPT135Q NMR spectrum of 5 mM Positand 3 (**68**) in 10 mM pD 7.4 (pH 7.8) phosphate buffered D$_2$O.

Variable Temperature NMR spectroscopy data for TEEtOA (53)

The in–out dynamics of the pendent ethyl groups in **53** were probed using VT ^{1}H NMR spectroscopy. The experiment was performed on a 1 mM solution of **53** in 10 mM phosphate-buffered D_2O at pD 11.5 prepared as described in the section below, and using a Bruker Avance 500 NMR spectrometer whose probe temperature was calibrated against the Δδ difference between the residual C*H*D$_2$O*H* signals in 99.8% CD$_3$OD (–10 – 30°C) or the C*H*$_2$–O*H* signals in 80% ethylene glycol in DMSO-d_6 (30–60 °C).

Temperature (K)	⟨Δδ⟩ ± 1σ ^{a} (ppm)	Δδ H$_d$	Δδ H$_b$	Δδ H$_{c'}$	Δδ H$_{c''}$
30	0	0	0	0	0
35	0.0938 ± 0.0122	0.0924	0.0941	0.0778	0.1079
40	0.1791 ± 0.0126	0.1799	0.1863	0.1533	0.1738
45	0.2568 ± 0.0134	0.2578	0.2695	0.2236	0.3088
50	0.3022 ± 0.0140	0.3019	0.3169	0.2625	0.3608
55	0.3798 ± 0.0149	0.3777	0.3982	0.3305	0.4552
60	0.4666 ± 0.0171	0.4593	—^{b}	0.4042	0.5610

Table 16: Chemical shift changes as a function of temperature for **53** from 30–60 °C

^{a} The ⟨Δδ⟩ was calculated for protons distal to the protons of interest, i.e., H$_g$, H$_j$, H$_f$, H$_e$, H$_a$, H$_l$, and H$_m$, with the zero point at 30 °C. The errors denote one standard deviation.
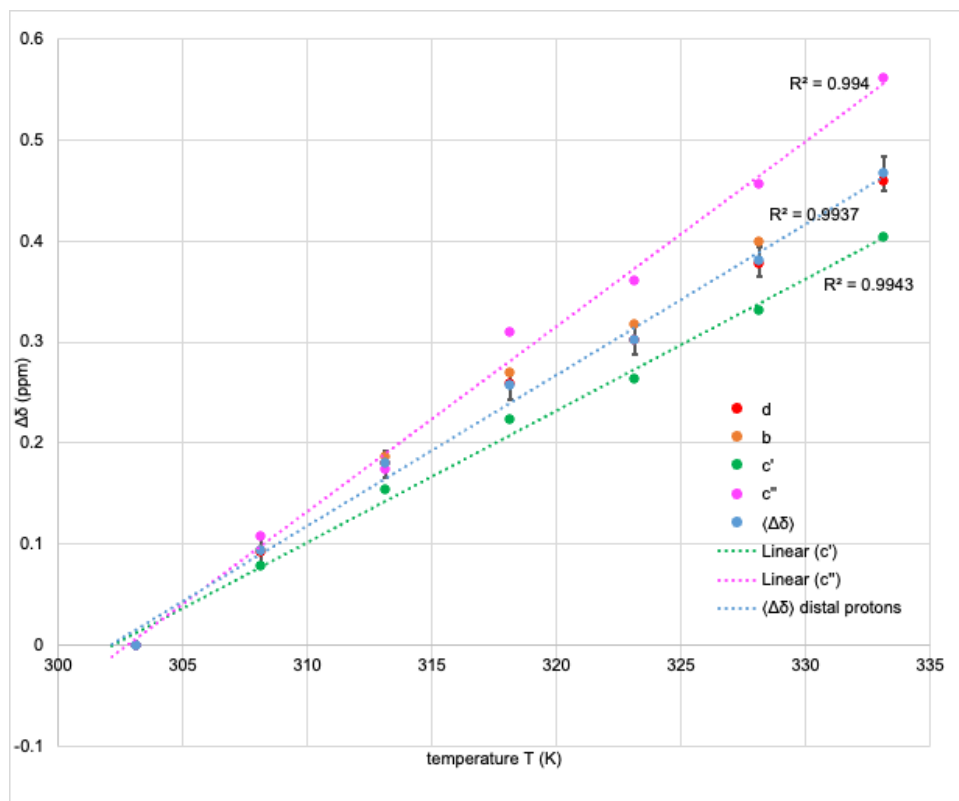
Fig. 122: Plot of Δδ as a function of temperature from 30–60 °C. The blue line indicates the average of the Δδ for distal protons (H$_j$, H$_g$, H$_f$, H$_e$, H$_a$, H$_l$, H$_m$) ; the green and pink lines show the deviation of the H$_{c'}$ and H$_{c''}$ with increasing temperature.

[b] Signal was underneath the H$_2$O peak and is thus unresolved.

Isothermal titration calorimetry (ITC): instrumentation

Isothermal Titration Calorimetric (ITC) experiments within this study were performed at 298 K using a VP-ITC MicroCalorimeter from Microcal, USA. Integrated heat data obtained for the titrations were fitted using the MicroCal-Origin 7.0 software package. All titrations were carried out in 10 mM sodium phosphate buffer of pH ~11.5 ± 0.05 at 25 °C for negatively charged hosts (octa acid **30**, TEMOA **37**, *exo*-OA **39**, and TEEtOA **53**) and pH ~7.4 ± 0.05 at 25 °C for positively charged hosts (Positand 1 **36**, Positand 2 **67**, and Positand 3 **68**). Before

each experiment, both host and guest solutions were degassed for 2–5 min to eliminate air bubbles. The injection volumes for all titrations used the computer-controlled injection procedure of guest solution into host solution. The injection volumes used for each titration are detailed in the next section.

The binding for most host-guest pairs gave adequate heats of injection such that general ITC titration procedures could be followed. However, in the case of titrations to **53** and **68**, the Wiseman "c" values (c = [host] × K_a) were less than ideal (i.e., < 5),[111] and modification procedures defined by Turnbull[112] and Tellinghuisen[113] were followed. Thus, for hosts **53** and **68**, large excesses of guest were injected into the host solution with the N parameter fixed to 1.0. We have used the same modification procedures previously.[82, 220, 249] Moreover, because the heats of complexation were relatively low, higher concentrations of the guest titrant were required which necessitated guest dilution reference titrations (guest injected into buffer solution without host) to be carried out and subtracted from the host-guest titration.

All the ITC titrations to **30**, **36**, **37**, **67** exhibited clear thermal responses and gave an excellent fit for a 1:1 complex model. Data from ITC titrations to **53** and **68** did not converge to a 1:1 model, and thus N was set to 1.00. NMR spectroscopic data are provided to corroborate 1:1 binding. All titrations were run in at least triplicate, and good reproducibility of K_a and ΔH values with the experimental error between runs less than 5%, and $-T\Delta S$ values less than 10%

ITC and NMR experimental parameters

Hosts exist as hydrates in the solid state and as such the true molar mass $\boldsymbol{M_x}$, which accounts for waters of hydration, is required for accurate determination of binding constants either by ITC or ^{1}H NMR spectroscopy. Thus, the general method for the determination of the true molar mass of all hosts is as follows. Three 2.0 mL 0.5 mM solutions of host were prepared analytically in 10 mM NaOD assuming that the host was anhydrous (e.g. M_{anh}^{37} = 1785.64 g mol^{-1}; M_{anh}^{53} = 1841.75 g mol^{-1}). Three stocks of 100 mM EtSO$_3$Na in D$_2$O were made and were used as an internal analytical standard. Nine (9) different combinations composed of 3 host stocks and 3 standard stocks were combined in 9 NMR tubes (500 µL host stock + 5 µL standard stock). An NMR spectrum of each tube was then taken using a standard 16 scan ^{1}H NMR pulse program with a spectral window spanning δ –3 – 10, and a delay time between excitation and observation pulses of 30 s. The methyl triplet of EtSO$_3^-$ was then integrated and set to a standard integral of 3.00, while the integral for the host H$_m$ resonance was allowed to float. The integrals of H$_m$ were then averaged and used in the below formula and the resulting average molar mass $\langle \boldsymbol{M_x} \rangle$ was obtained:

$$\langle M_x \rangle = \frac{W_x \cdot V_x \cdot I_{cal} \cdot N_x}{V_{Sx} \cdot (V_x + V_{cal}) \cdot \langle I_x \rangle \cdot N_{cal} \cdot C_{cal}} \cdot 10^6 \qquad \text{Eqn. 13}$$

where

$\boldsymbol{W_x}$ is the gravimetric mass of the host in the stock solution (g);

V_{Sx} is the volume of the host stock solution (mL);

$\langle I_x \rangle$ and I_{cal} are the averaged integrals of the H_m, and of the $EtSO_3^-$ methyl signals, respectively;

N_x and N_{cal} are the number of nuclei in the H_m and $EtSO_3^-$ methyl signals, respectively;

C_{cal} is the the final concentration of $EtSO_3Na$ in the NMR tube (mM);

V_x and V_{cal} are the volumes of host and $EtSO_3Na$ solutions added to the NMR tube, respectively (µL).

All solutions (including stock buffer solutions) for ITC were prepared in volumetric flasks which have been previously washed once with freshly prepared Caro's acid (1:5 30% aq. H_2O_2/98% H_2SO_4), and thrice with ultra-pure MilliQ water. Stock solutions of 10 mM pH 11.5 phosphate buffer were prepared by adding $Na_2HPO_4 \cdot 7H_2O$ (1.93 g, 7.2 mmol), Na_3PO_4 (0.44 g, 2.7 mmol), and ultra-pure MilliQ water to a 1 L volumetric flask. Stock solutions of 10 mM pH 7.4 phosphate buffer were prepared by adding NaH_2PO_4 (0.34 g, 2.8 mmol), $Na_2HPO_4 \cdot 7H_2O$ (1.92 g, 7.2 mmol), and ultra-pure MilliQ water to a 1L volumetric flask. Appropriate volumes of host and guest solutions were prepared in the normal fashion by dissolving the appropriate mass of host or guest in a volumetric flask using the above prepared stock buffer solution. The pH of the solution was measured and adjusted to pH 11.5 ± 0.05 by titrating in 5 M NaOH or 5 M HCl as appropriate. All ITC titrations utilised ultra-pure MilliQ water in the reference cell.

All solutions (including stock buffer solutions) for ^{1}H NMR spectroscopic titrations were prepared in volumetric flasks which have been previously washed once with freshly prepared Caro's acid (1:5 30% aq. H_2O_2/98% H_2SO_4), and thrice with 99.9% D_2O. Stock solutions of 10 mM pH 11.9 (pD 11.5) phosphate buffer were prepared by adding $Na_2HPO_4\cdot7H_2O$ (0.134 g, 0.5 mmol), Na_3PO_4 (0.066 g, 0.4 mmol), and 99% D_2O in a 100 mL volumetric flask. Stock solutions of pH 7.8 (pD 7.4) phosphate buffer were prepared by adding NaH_2PO_4 (0.034 g, 0.28 mmol), $Na_2HPO_4\cdot7H_2O$ (0.191 g, 0.72 mmol), and 99% D_2O in a 100 mL volumetric flask. Appropriate volumes of host and guest solutions were prepared in the normal fashion by dissolving the appropriate mass of host or guest in a volumetric flask using the above prepared stock buffer solution. The pH of the solution was measured and adjusted to pH 11.9 ± 0.05 (pD 11.5 ± 0.05) by titrating in 5 M NaOD or 5 M DCl as appropriate. All ^{1}H NMR titrations were performed on a Bruker 500.13 MHz instrument operating at 25 °C, using residual H_2O (δ 4.79) as an internal standard.

Diffusion-Ordered Spectroscopy NMR (DOSY-NMR) data were acquired using a Bruker Avance 500 MHz Instrument operating at 25 °C using 10 mM pD 11.4 phosphate buffered D_2O. Using Topspin 1.2, the LEDBPGPPR2S (2D sequence for diffusion measurement using stimulated echo and LED using bipolar gradient pulses for diffusion using 2 spoil gradients with solvent pre-saturation for suppression) was employed with an exponential ramp of the gradient strength from 2–95%, and using the following parameters:

p1 = 7.250 µs

p2 = 14.500 µs

p19 = 600.000 µs

δ = 0.004 s

Δ = 0.200 s

d1 = 2.00 s

d16 = 0.1 ms

ns = 32

TD1 = 128

DOSY NMR processing was performed using MNova 14 using a k factor of 0.996, and utilising the Peak Fit method with a single decay component and 64 points in the diffusion dimension.

Each host-guest system required specific conditions to fit within the instrumental limitations inherent of ITC. Specifically, the concentrations for host and guest, injection procedure, and DP (Differential Power) value used for each host-guest pair is listed below.

Hexanoic acid (44)

OA **30**: DP = 25 µcal s^{-1}. The ITC titration experiment used a 30-injection procedure of 15 mM guest solution titrated into 1 mM host solution. V_1 = 2.0 µL; $V_2 - V_{30}$ = 9.0 µL. $[H]_{final}$ = 0.655 mM, $[G]_{final}$ = 5.17 mM.

4-Chlorobenzoic acid (45)

OA **30**: DP = 25 μcal s^{-1}. The ITC titration experiment used a 29-injection procedure of a 1.5 mM guest solution titrated into a 0.15 mM host solution. V_1 = 2.0 μL; $V_2 - V_{29}$ = 9.0 μL. [H]$_{final}$ = 0.0995 mM, [G]$_{final}$ = 0.505 mM.

(S)-Perillic acid (46)

OA **30**: DP = 25 μcal s^{-1}. The ITC titration experiment used a 33-injection procedure of a 5 mM guest solution titrated into a 0.5 mM host solution. V_1 = 2.0 μL; $V_2 - V_7$ = 5.0 μL; $V_8 - V_{12}$ = 7.0 μL; $V_{13} - V_{33}$ = 9.0 μL. [H]$_{final}$ = 0.331 mM, [G]$_{final}$ = 1.69 mM.

exo-OA **39**: DP = 30 μcal s^{-1}. The ITC titration experiment used a 33-injection procedure of a 80 mM guest solution titrated into a 1.0 mM host solution: V_1 = 2.0 μL; $V_2 - V_5$ = 5.0 μL; $V_6 - V_9$ = 7.0 μL; $V_{10} - V_{33}$ = 9.0 μL. [H]$_{final}$ = 0.653 mM, [G]$_{final}$ = 27.8 mM.

(S)-(–)-Citronellic acid (47)

OA **30**: DP = 25 μL s^{-1}. The ITC titration experiment used a 33-injection procedure of a 5.0 mM guest solution titrated into a 0.50 mM host solution. V_1 = 2.0 μL; $V_2 - V_7$ = 5.0 μL; $V_8 - V_{12}$ = 7.0 μL; $V_{13} - V_{33}$ = 9.0 μL. [H]$_{final}$ = 0.331 mM, [G]$_{final}$ = 1.69 mM.

exo-OA **39**: DP = 35 μcal s^{-1}. The ITC titration experiment used a 33-injection procedure of a 100 mM guest solution titrated into a 1 mM host solution. V_1 = 2.0 μL; $V_2 - V_7$ = 5.0 μL; $V_8 - V_{12}$ = 7.0 μL; $V_{13} - V_{33}$ = 9.0 μL. [H]$_{final}$ = 0.661 mM, [G]$_{final}$ = 33.9 mM.

β-Phenylethyl(trimethyl)ammonium chloride (48)

OA **30**: DP = 15 µcal s^{-1}. The ITC titration experiment used a 28-injection procedure of a 7.5 mM guest solution titrated into a 0.15 mM host solution: V_1 = 1.0 µL; V_2 = 2.0 µL; V_3 = 2.5 µL; V_4 = 3.0 µL; V_5 = 3.5 µL; V_6 = 4.0 µL; V_7 = 4.5 µL; V_8 = 5.0 µL; V_9 = 5.5 µL; V_{10} = 6.0 µL; V_{11} = 6.5 µL; V_{12} = 7.0 µL; V_{13} = 7.5 µL; V_{14} = 8.0 µL; V_{15} = 8.5 µL; V_{16} = 9.0 µL; V_{17} = 9.5 µL; V_{18} = 10.0 µL; V_{19} = 10.5 µL; V_{20} = 11.0 µL; V_{21} = 11.5 µL; V_{22} = 12.0 µL; V_{23} = 12.5 µL; V_{24} = 13.0 µL; V_{25} = 13.5 µL; V_{26} = 14.0 µL; V_{27} = 14.5 µL; V_{28} = 15.0 µL. $[H]_{final}$ = 0.103 mM, $[G]_{final}$ = 2.36 mM.

exo-OA **39**: DP = 20 µcal s^{-1}. The ITC titration experiment used a 28-injection procedure of a 10 mM guest solution titrated into a 1 mM host solution: V_1 = 3.0 µL; $V_2 - V_4$ = 6.0 µL; $V_5 - V_{28}$ = 9.0 µL. $[H]_{final}$ = 0.678 mM, $[G]_{final}$ = 3.22 mM.

n-Hexyl(trimethyl)ammonium chloride (49)

OA **30**: DP = 15 µcal s^{-1}. The ITC titration experiment used a 28-injection procedure of a 7.5 mM guest solution titrated into a 0.15 mM host solution: V_1 = 1.0 µL; V_2 = 2.0 µL; V_3 = 2.5 µL; V_4 = 3.0 µL; V_5 = 3.5 µL; V_6 = 4.0 µL; V_7 = 4.5 µL; V_8 = 5.0 µL; V_9 = 5.5 µL; V_{10} = 6.0 µL; V_{11} = 6.5 µL; V_{12} = 7.0 µL; V_{13} = 7.5 µL; V_{14} = 8.0 µL; V_{15} = 8.5 µL; V_{16} = 9.0 µL; V_{17} = 9.5 µL; V_{18} = 10.0 µL; V_{19} = 10.5 µL; V_{20} = 11.0 µL; V_{21} = 11.5 µL; V_{22} = 12.0 µL; V_{23} = 12.5 µL; V_{24} = 13.0 µL; V_{25} = 13.5 µL; V_{26} = 14.0 µL; V_{27} = 14.5 µL; V_{28} = 15.0. $[H]_{final}$ = 0.103 mM, $[G]_{final}$ = 2.36 mM.

exo-OA **39**: DP = 15 µcal s^{-1}. The ITC titration experiment used a 28-injection procedure of a 7.5 mM guest solution titrated into a 0.15 mM host solution: V_1 = 1.0 µL; V_2 = 2.0 µL; V_3 = 2.5 µL; V_4 = 3.0 µL; V_5 = 3.5 µL; V_6 = 4.0 µL; V_7 = 4.5 µL; V_8 = 5.0 µL; V_9 = 5.5 µL; V_{10} = 6.0 µL; V_{11} = 6.5 µL; V_{12} = 7.0 µL; V_{13} = 7.5 µL; V_{14} = 8.0 µL; V_{15} = 8.5 µL; V_{16} = 9.0 µL; V_{17} = 9.5 µL; V_{18} = 10.0 µL; V_{19} = 10.5 µL; V_{20} = 11.0 µL; V_{21} = 11.5 µL; V_{22} = 12.0 µL; V_{23} = 12.5 µL; V_{24} = 13.0 µL; V_{25} = 13.5 µL; V_{26} = 14.0 µL; V_{27} = 14.5 µL; V_{28} = 15.0. $[H]_{final}$ = 0.678 mM, $[G]_{final}$ = 3.22 mM.

trans-4-methylcyclohexyl(trimethyl)ammonium chloride (50)

OA **30**: DP = 10 µcal s^{-1}. The ITC titration experiment used a 28-injection procedure of 1.5 mM guest solution into 0.15 mM host solution. The following variable injection volumes were used: V_1 = 3.0; $V_2 - V_{28}$ = 9.0 µL. $[H]_{final}$ = 0.101 mM, $[G]_{final}$ = 30.495 mM.

exo-OA **39**: DP = 10 µcal s^{-1}. The ITC titration experiment used a 28-injection procedure of 1.5 mM guest solution into 0.15 mM host solution. The following variable injection volumes were used: V_1 = 3.0 µL; $V_2 - V_{28}$ = 9.0 µL. $[H]_{final}$ = 0.101 mM, $[G]_{final}$ = 30.495 mM.

1-Adamantyl(trimethyl)ammonium chloride (51)

OA **30**: DP = 10 µcal s^{-1}. The ITC titration experiment used a 28-injection procedure of 1.5 mM guest solution into 0.15 mM host solution. The following

variable injection volumes were used: V_1 = 3.0 µL; V_2 – V_{28} = 9.0 µL.

$[H]_{final}$ = 0.101 mM, $[G]_{final}$ = 30.495 mM.

exo-OA **2**: DP = 10 µcal s^{-1}. The ITC titration experiment used a 28-injection procedure of 1.5 mM guest solution into 0.15 mM host solution. The following variable injection volumes were used: V_1 = 3.0 µL; V_2 – V_{28} = 9.0 µL.

$[H]_{final}$ = 0.101 mM, $[G]_{final}$ = 30.495 mM.

3-Hydroxy-2-naphthoic acid (62)

TEMOA **37**: DP = 25 µcal s^{-1}. The ITC titration experiment used a 35-injection procedure of 1.5 mM guest solution titrated into 0.15 mM host solution. V_1 = 3.0 µL; $V_2 – V_7$ = 5.0 µL; $V_8 – V_{12}$ = 7 µL; $V_{13} – V_{35}$ = 9 µL. $[H]_{final}$ = 0.0968 mM, $[G]_{final}$ = 0.532 mM.

TEEtOA **53**: DP = 15 µcal s^{-1}. The ITC titration experiment used a 28-injection procedure of 20 mM guest solution titrated into 0.10 mM host solution. V_1 = 2.0 µL; $V_2 – V_{28}$ = 9.0 µL. $[H]_{final}$ = 0.0101 mM, $[G]_{final}$ = 0.0395 mM.

p-Bromophenol (63)

TEMOA **37**: DP = 25 µcal s^{-1}. The ITC titration experiment used a 35-injection procedure of 1.5 mM guest solution titrated into 0.15 mM host solution. V_1 = 3.0 µL; $V_2 – V_7$ = 5.0 µL; $V_8 – V_{12}$ = 7 µL; $V_{13} – V_{35}$ = 9 µL. $[H]_{final}$ = 0.0968 mM, $[G]_{final}$ = 0.532 mM.

TEEtOA **53**: DP = 15 µcal s^{-1}. The ITC titration experiment used a 28-injection procedure of 7.5 mM guest solution titrated into 0.10 mM host solution. V_1 = 2.0 µL; $V_2 - V_{28}$ = 9.0 µL. [H]$_{final}$ = 0.0671 mM, [G]$_{final}$ = 2.47 mM.

Cyclopentylacetic acid (64)

TEMOA **37**: DP = 25 µcal s^{-1}. The ITC titration experiment used a 35-injection procedure of 15 mM guest solution titrated into 0.15 mM host solution. V_1 = 3.0 µL; $V_2 - V_7$ = 5.0 µL; $V_8 - V_{12}$ = 7 µL; $V_{13} - V_{35}$ = 9 µL. [H]$_{final}$ = 0.0968 mM, [G]$_{final}$ = 5.32 mM.

Piperonylic acid (65)

TEMOA **37**: DP = 25 µcal s^{-1}. The ITC titration experiment used a 35-injection procedure of 1.5 mM guest solution titrated into 0.15 mM host solution. V_1 = 3.0 µL; $V_2 - V_7$ = 5.0 µL; $V_8 - V_{12}$ = 7 µL; $V_{13} - V_{35}$ = 9 µL. [H]$_{final}$ = 0.0968 mM, [G]$_{final}$ = 0.532 mM.

TEEtOA **53**: DP = 15 µcal s^{-1}. The ITC titration experiment used a 28-injection procedure of 20 mM guest solution titrated into 0.10 mM host solution. V_1 = 2.0 µL; $V_2 - V_{28}$ = 9.0 µL. [H]$_{final}$ = 0.0671 mM, [G]$_{final}$ = 6.58 mM.

p-Toluic acid (66)

TEMOA **37**: DP = 25 µcal s^{-1}. The ITC titration experiment used a 35-injection procedure of 1.2 mM guest solution titrated into 0.15 mM host solution.

$V_1 = 3.0\ \mu L$; $V_2 - V_7 = 5.0\ \mu L$; $V_8 - V_{12} = 7\ \mu L$; $V_{13} - V_{35} = 9\ \mu L$. $[H]_{final} = 0.0968$ mM, $[G]_{final} = 0.426$ mM.

4-Bromobenzoic acid (72)

TEMOA **37**: DP = 20 $\mu cal\ s^{-1}$. The ITC titration experiment used a 31-injection procedure of 1.0 mM guest solution titrated into 0.1 mM host solution. $V_1 = 2\ \mu L$. $V_2 - V_{31} = 9\ \mu L$. $[H]_{final} = 0.0648$ mM, $[G]_{final} = 0.352$ mM.

TEEtOA **53**: DP = 20 $\mu cal\ s^{-1}$. The ITC titration experiment used a 31-injection procedure of 7.5 mM guest solution titrated into 0.115 mM host solution. $V_1 = 2$ μL. $V_2 - V_{31} = 9\ \mu L$. $[H]_{final} = 0.0728$ mM, $[G]_{final} = 2.75$ mM.

Positand 2 **67**: DP = 20 $\mu cal\ s^{-1}$. The ITC titration experiment used a 31-injection procedure of 1.0 mM guest solution titrated into 0.1 mM host solution. $V_1 = 2\ \mu L$. $V_2 - V_{31} = 9\ \mu L$. $[H]_{final} = 0.0648$ mM, $[G]_{final} = 0.352$ mM.

Positand 3 **68**: DP = 20 $\mu cal\ s^{-1}$. The ITC titration experiment used a 31-injection procedure of 1.5 mM guest solution titrated into 0.15 mM host solution. $V_1 = 2\ \mu L$. $V_2 - V_{31} = 9\ \mu L$. $[H]_{final} = 0.0972$ mM, $[G]_{final} = 0.528$ mM.

ITC and NMR spectroscopy results

The figures below show representative thermograms and binding curves for one titration experiment for each host–guest pair.

Hexanoic acid (44)
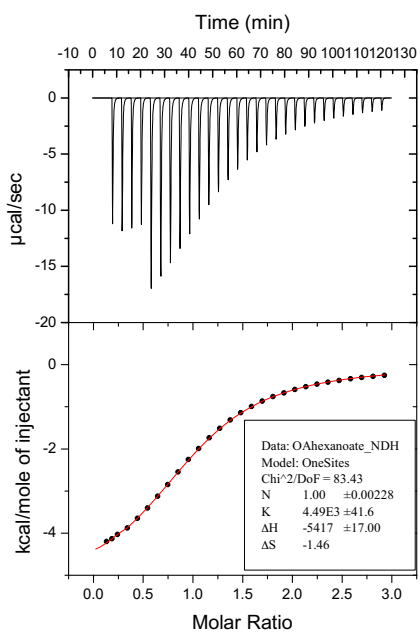
Fig. 123: ITC thermogram and 1:1 binding fit for **44**⊆**30** complexation. A 15 mM solution of **44** was titrated into a 1.0 mM solution of OA **30** equilibrated at 25 °C. Both host and guest were in 10 mM phosphate buffer, pH 11.5.

4-Chlorobenzoic acid (45)
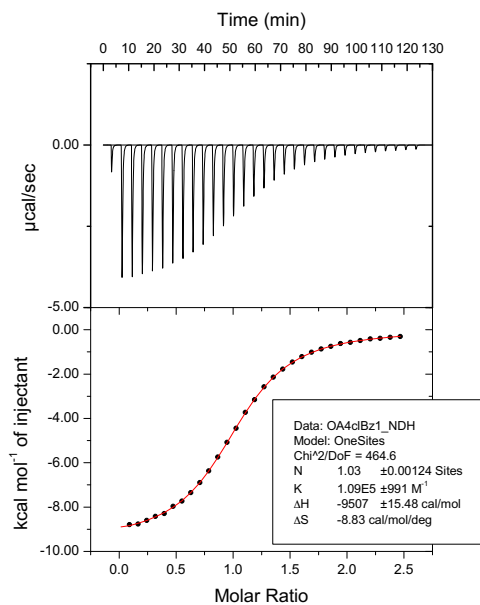
Fig. 124: ITC thermogram and 1:1 binding fit for **45**⊆**30** complexation. A 1.5 mM solution of **45** was titrated into a 0.15 mM solution of OA **30** equilibrated at 25 °C. Both host and guest were in 10 mM phosphate buffer, pH 11.5.
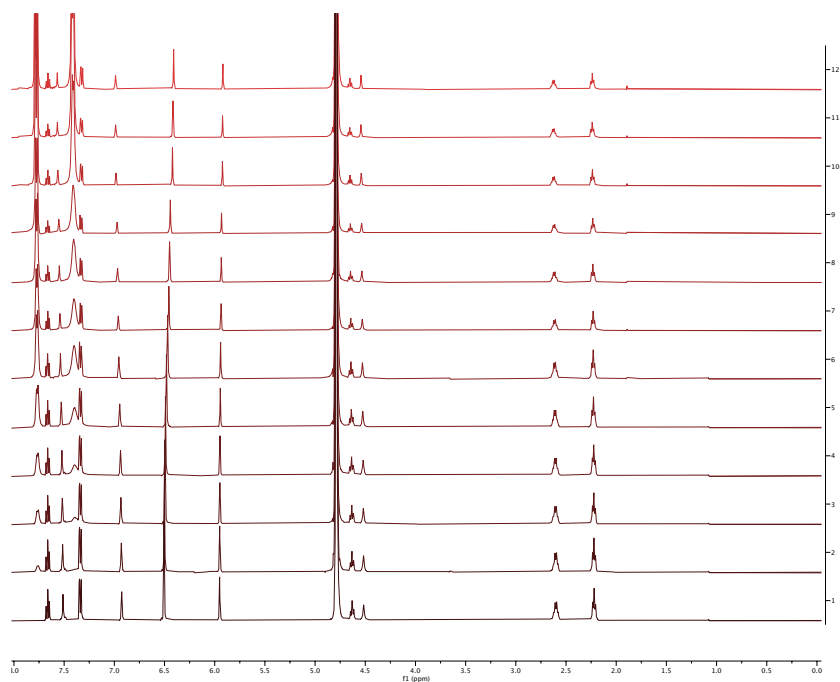
Fig. 125: ^{1}H NMR titration stack showing the addition of 250 mM **45** into a 0.5 mM solution of *exo*-OA **39**. Spectrum 1 is of the free host, while spectrum 12 is at the end of the titration at 60 equiv. **45**.
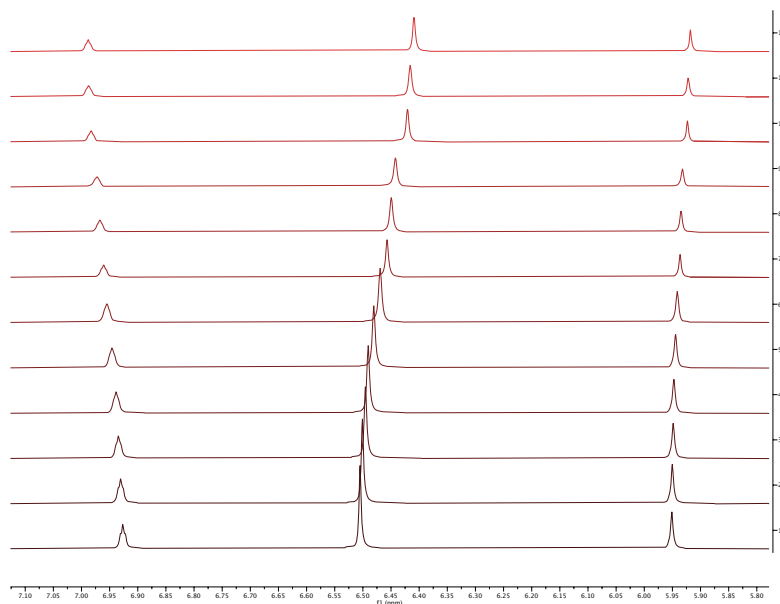
Fig. 126: Host region between 5.80 – 7.10 ppm showing the shifting of *exo*-OA **39** host peaks (H$_c$, H$_f$, and H$_e$) as a function of **45**. Spectrum 1 is of free **39**, and spectrum 12 is at the end of the titration at 60 equiv. **45**.
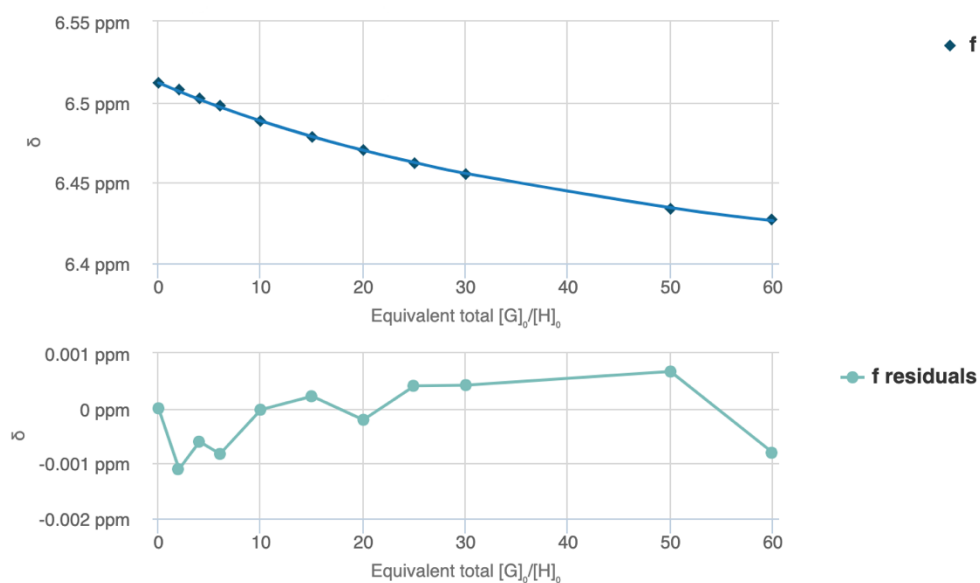
Fig. 127: Representative fitting curve (top) of the titration of 250 mM **45** to 0.5 mM *exo*-OA **39** and the corresponding residuals (bottom). Curve and residuals were calculated using the online BindFit software.[2, 3]

Perillic acid (46)
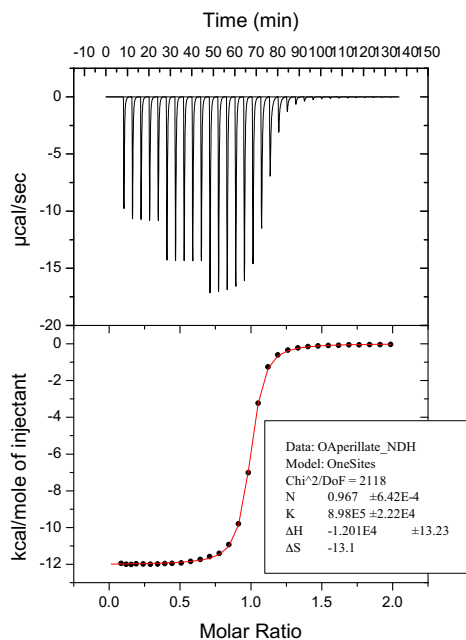
Fig. 128: ITC thermogram and 1:1 binding fit for **46**⊆**39** complexation. A 5.0 mM solution of **46** was titrated into a 0.5 mM solution of OA **39** equilibrated at 25 °C. Both host and guest were in 10 mM phosphate buffer, pH 11.5.
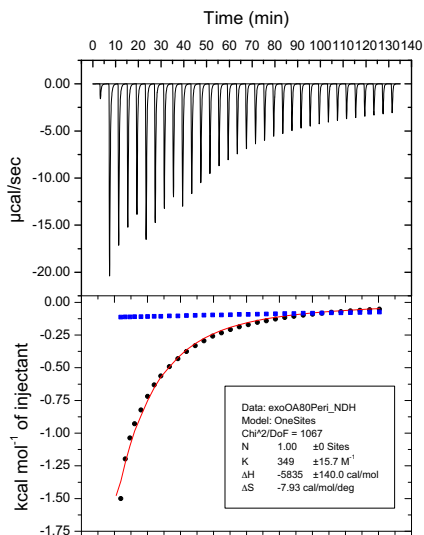
Fig. 129: ITC thermogram and 1:1 binding fit post-subtraction for **46**⊆**39** complexation. An 80 mM solution of **46** was titrated into a 1.0 mM solution of exo-OA **39** equilibrated at 25 °C. Both host and guest were in 10 mM phosphate buffer, pH 11.5.

Citronellic acid (47)
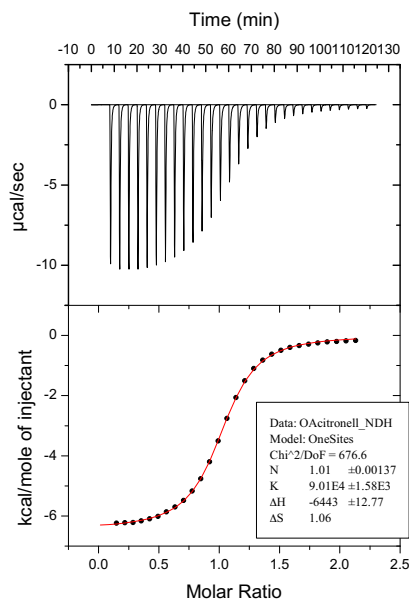
Fig. 130: ITC thermogram and 1:1 binding fit for **47**∈**30** complexation. A 5 mM solution of **47** was titrated into a 0.5 mM solution of OA **30** equilibrated at 25 °C. Both host and guest were in 10 mM phosphate buffer, pH 11.5.
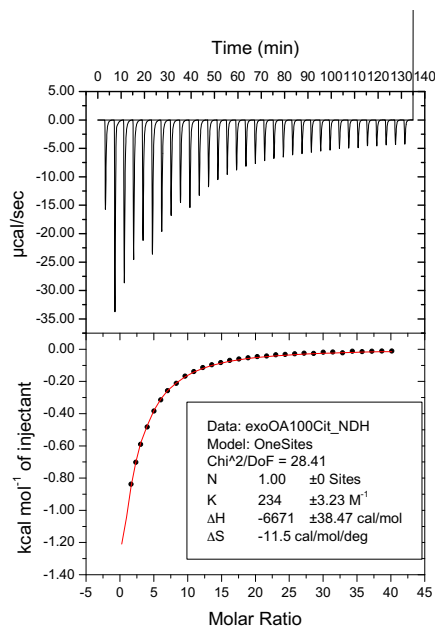
Fig. 131: ITC thermogram and 1:1 binding fit post-subtraction for **47**∈**39** complexation. A 100 mM solution of **47** was titrated into a 1.0 mM solution of *exo*-OA **39** equilibrated at 25 °C. Both host and guest were in 10 mM phosphate buffer, pH 11.5.

β-Phenylethyl(trimethyl)ammonium chloride (48)
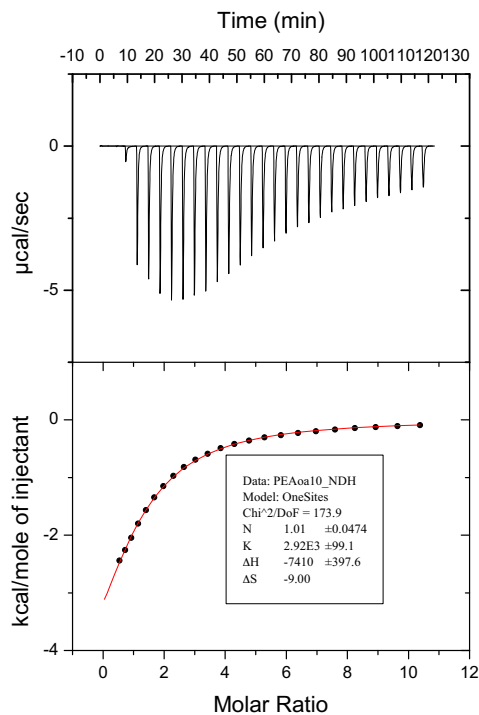
Fig. 132: ITC thermogram and 1:1 binding fit for **48**⊆**30** complexation. A 7.5 mM solution of **48** was titrated into a 0.5 mM solution of OA **30** equilibrated at 25 °C. Both host and guest were in 10 mM phosphate buffer, pH 11.5.
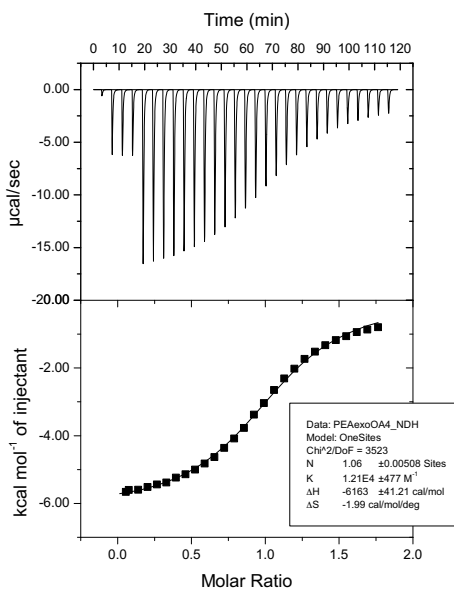
Fig. 133: ITC thermogram and 1:1 binding fit for **48**∈**39** complexation. A 10 mM solution of **48** was titrated into a 1.0 mM solution of *exo*-OA **39** equilibrated at 25 °C. Both host and guest were in 10 mM phosphate buffer, pH 11.5.

n-Hexyl(trimethyl)ammonium chloride (49)
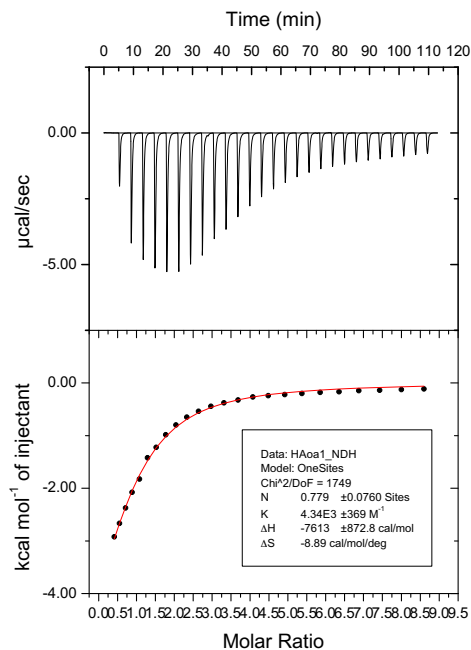
Fig. 134: ITC thermogram and 1:1 binding fit post-subtraction for **49**⊆**30** complexation. A 7.5 mM solution of **49** was titrated into a 0.15 mM solution of OA **30** equilibrated at 25 °C. Both host and guest were in 10 mM phosphate buffer, pH 11.5.
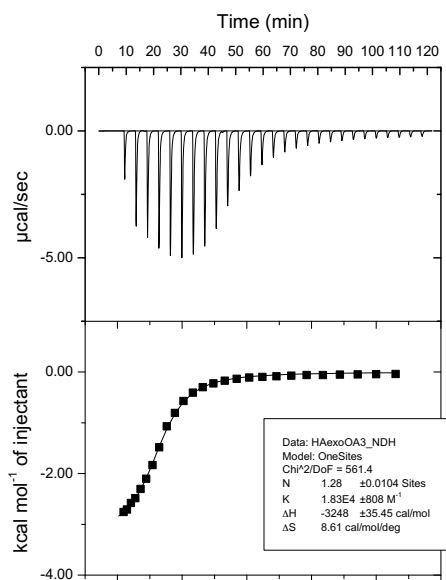
Fig. 135: ITC thermogram and 1:1 binding fit for **49**⊆**39** complexation. A 7.5 mM solution of **49** was titrated into a 0.15 mM solution of *exo*-OA **39** equilibrated at 25 °C. Both host and guest were in 10 mM phosphate buffer, pH 11.5.

trans-4-Methylcyclohexyl(trimethyl)ammonium chloride (50)
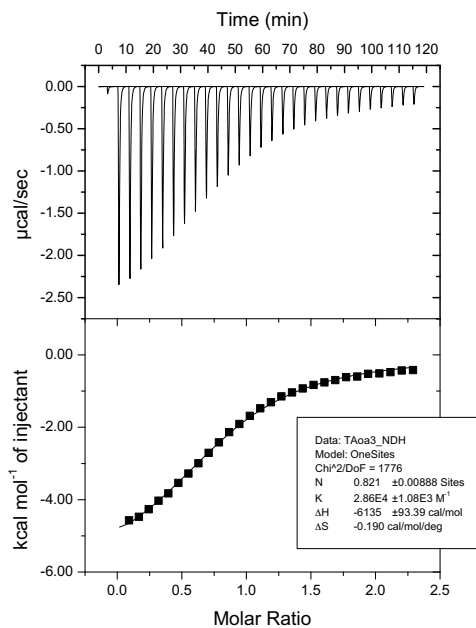
Fig. 137: ITC thermogram and 1:1 binding fit for **50**⊆**30** complexation. A 1.5 mM solution of **50** was titrated into a 0.5 mM solution of OA **30** equilibrated at 25 °C. Both host and guest were in 10 mM phosphate buffer, pH 11.5.
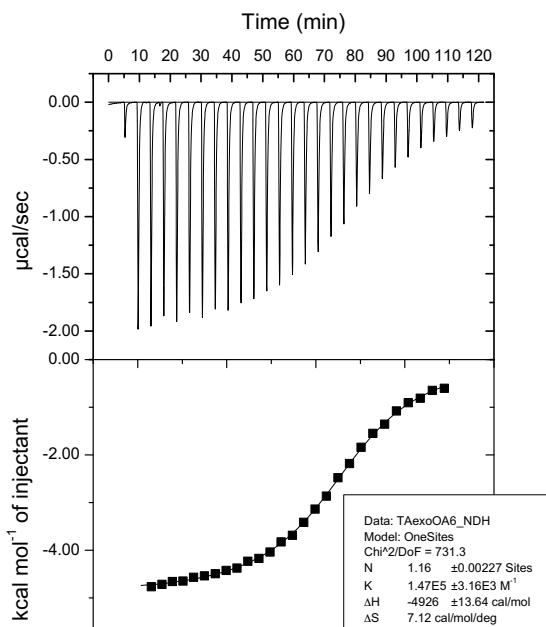
Fig. 136: ITC thermogram and 1:1 binding fit for **50**⊆**39** complexation. A 0.15 mM solution of **50** was titrated into a 0.15 mM solution of *exo*-OA **39** equilibrated at 25 °C. Both host and guest were in 10 mM phosphate buffer, pH 11.5.

1-Adamantyl(trimethyl)ammonium chloride (51)
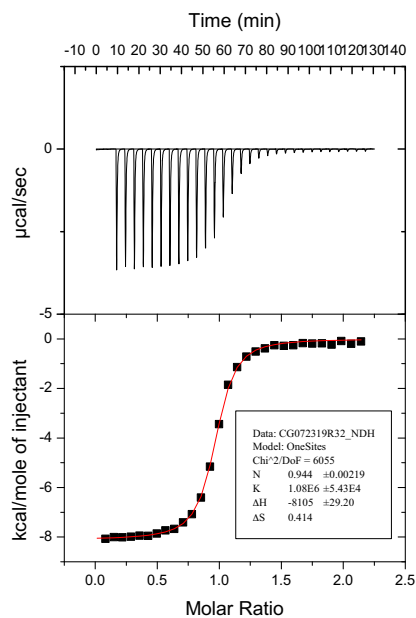
Fig. 138: ITC thermogram and 1:1 binding fit for **51**⊆**30** complexation. A 1.5 mM solution of **51** was titrated into a 0.15 mM solution of OA **30** equilibrated at 25 °C. Both host and guest were in 10 mM phosphate buffer, pH 11.5.
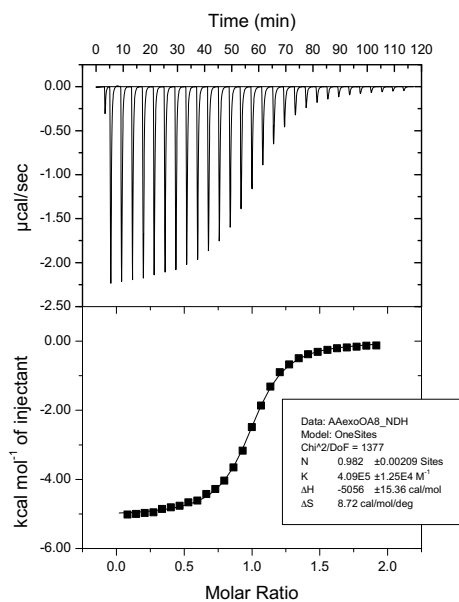
One-to-one binding of guests to *exo*-OA 39 via NMR spectroscopy

Evidence for binding of **48–50** could not be obtained by NMR as the exchange rate between the free and bound states are on the timescale of the NMR experiment. Even for the strongest binding guest to *exo*-OA (**39**) the binding is slightly faster than the NMR experiment timescale. Upon addition of one equivalent of **51** to **39**, the signals that correspond to H_b of the host and $-NMe_3$ of the guest integrate to a 4:9 ratio, indicating the formation of a 1:1 host–guest complex (Fig.).

Fig. 139: ITC thermogram and 1:1 binding fit for **51**⊆**39** complexation. A 1.5 mM solution of **51** was titrated into a 0.15 mM solution of *exo*-OA **39** equilibrated at 25 °C. Both host and guest were in 10 mM phosphate buffer, pH 11.5.
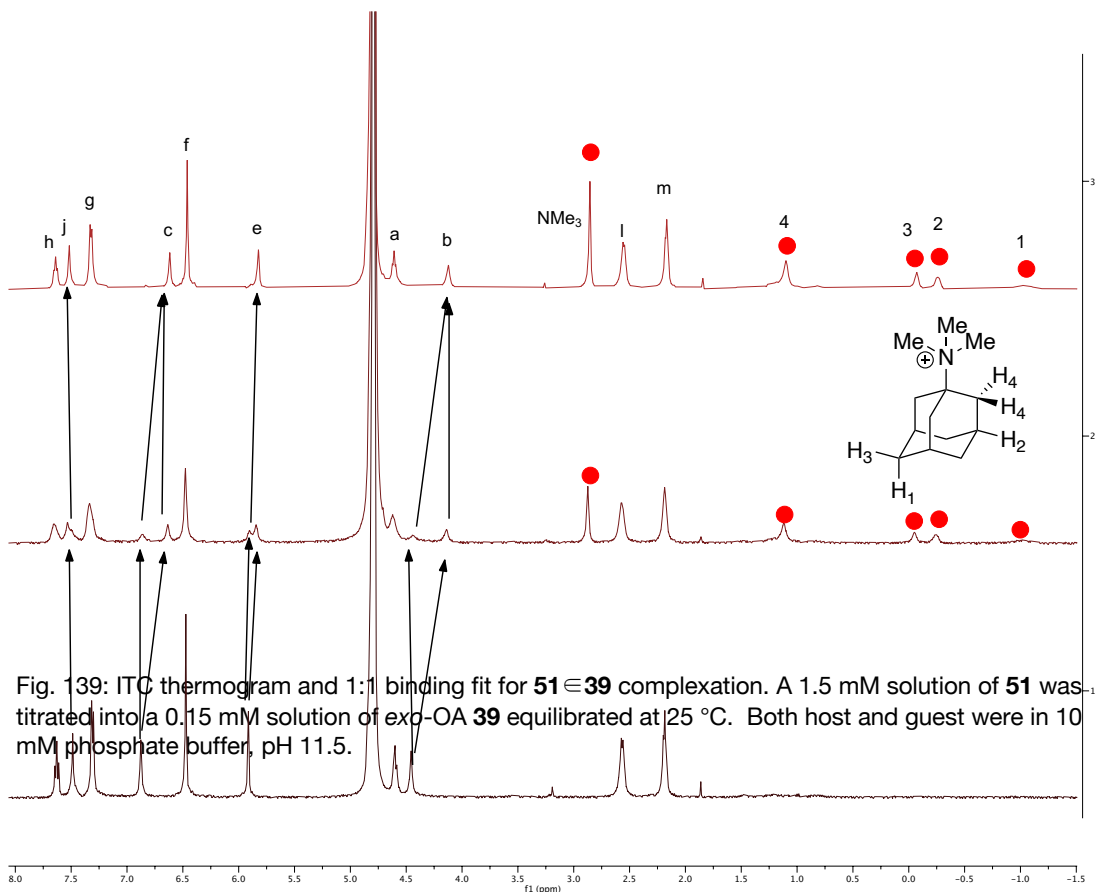
Fig. 140: ^{1}H NMR stack of the addition of **51** to *exo*-OA **39**. Spectrum 1 is of free **39**; 2 is of 0.5 equiv. **51** into **39**; 3 is of 1 equiv. **51** into **39**. Arrows indicate shifts in host peaks, red circles indicate bound guest peaks.
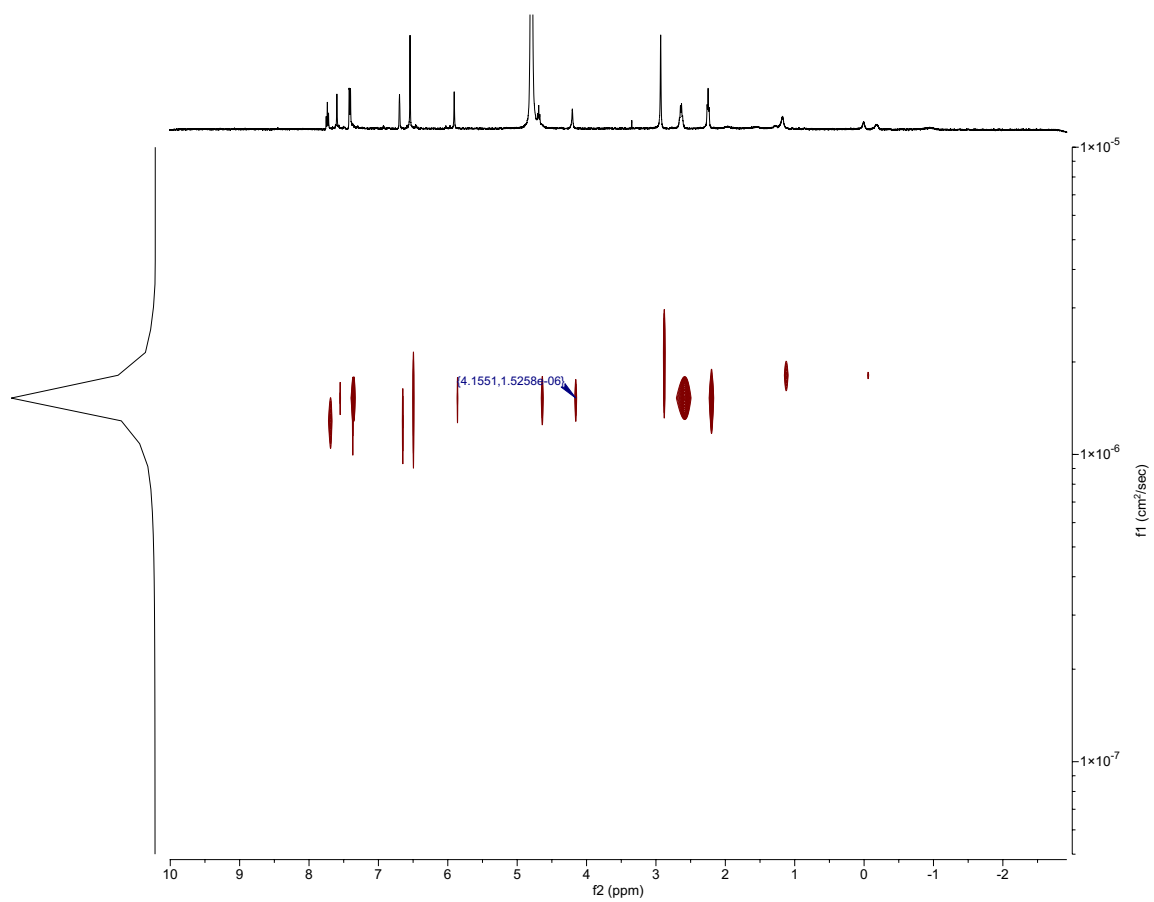
Fig. 141: DOSY NMR spectrum of the 1:1 complex of *exo*-OA **39** and **51**. $D \approx 1.53 \times 10^{-6}$ cm^2 s^{-1} corresponding to a monomeric (non-capsular) complex

3-Hydroxy-2-naphthoic acid (62)
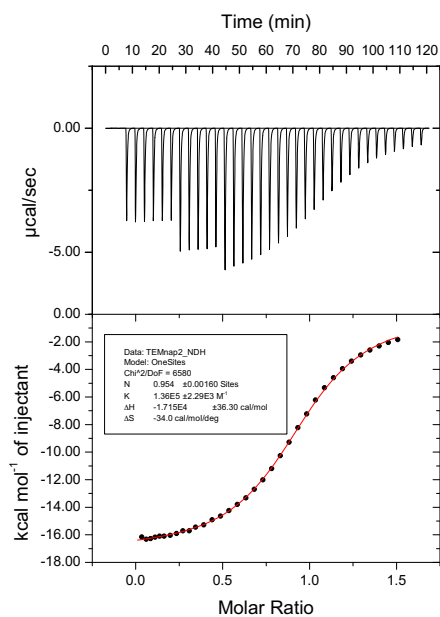
Fig. 142: ITC thermogram and 1:1 binding fit for **62**⊆**37** complexation. A 1.5 mM solution of **62** was titrated into a 0.15 mM solution of TEMOA **37** equilibrated at 25 °C. Both host and guest were in 10 mM phosphate buffer, pH 11.5.
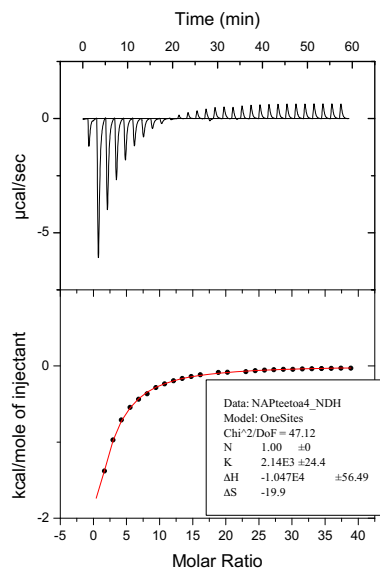
Fig. 143: ITC thermogram and 1:1 binding fit post-subtraction for **62**⊆**53** complexation. A 20.0 mM solution of **62** was titrated into a 0.10 mM solution of TEEtOA **53** equilibrated at 25 °C. Both host and guest were in 10 mM phosphate buffer, pH 11.5

p-Bromophenol (63)
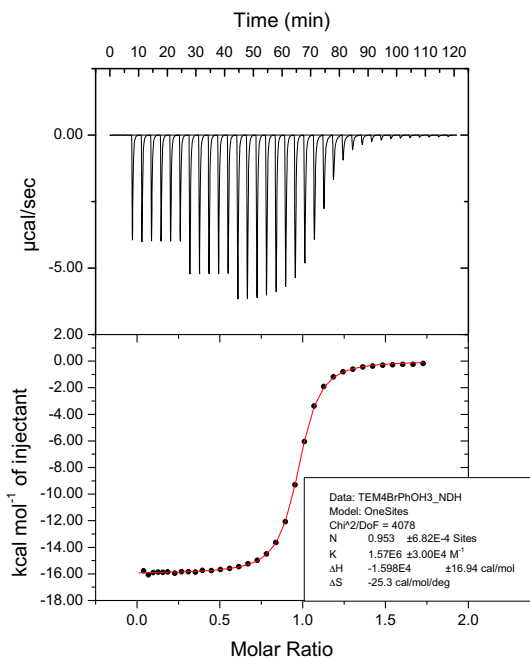
Fig. 145: ITC thermogram and 1:1 binding fit for **63**∈**37** complexation. A 1.5 mM solution of **63** was titrated into a 0.15 mM solution of TEMOA **37** equilibrated at 25 °C. Both host and guest were in 10 mM phosphate buffer, pH 11.5.
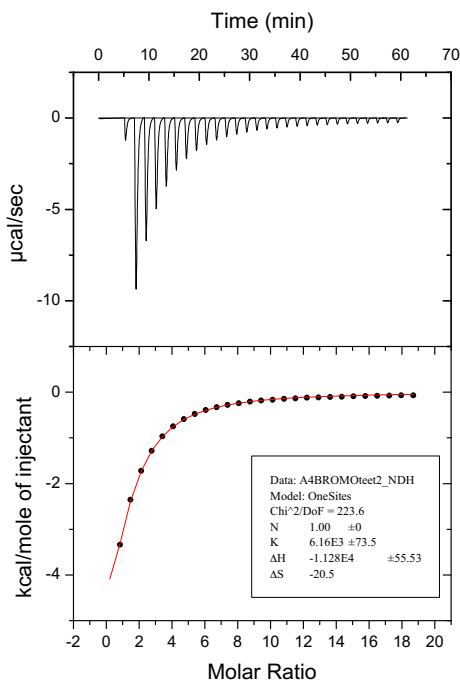
Fig. 144: ITC thermogram and 1:1 binding fit post-subtraction for **63**∈**53** complexation. A 7.5 mM solution of **63** was titrated into a 0.10 mM solution of TEEtOA **53** equilibrated at 25 °C. Both host and guest were in 10 mM phosphate buffer, pH 11.5.

Cyclopentylacetic acid (64)
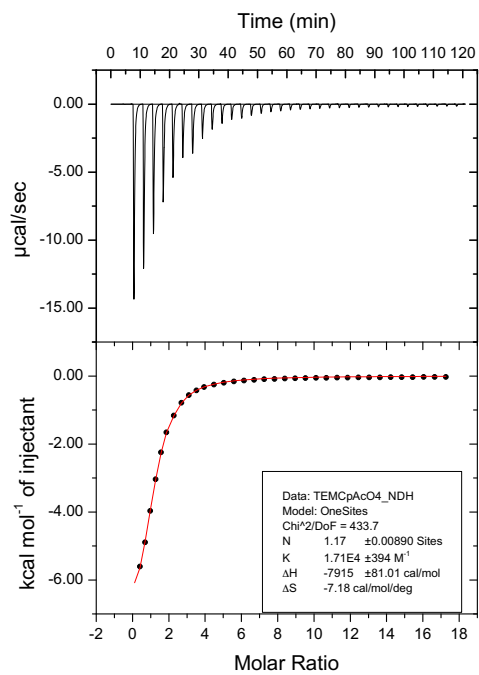
Fig. 146: ITC thermogram and 1:1 binding fit for **64**⊆**37** complexation. A 15 mM solution of **64** was titrated into a 0.15 mM solution of TEMOA **37** equilibrated at 25 °C. Both host and guest were in 10 mM phosphate buffer, pH 11.5.

Piperonylic acid (65)
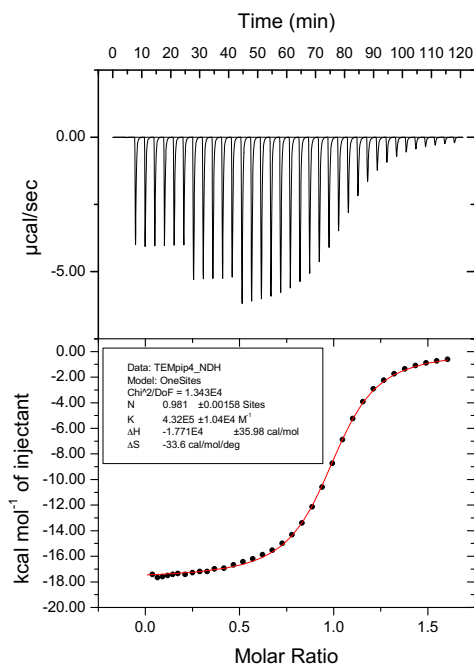
Fig. 148: ITC thermogram and 1:1 binding fit for **65**⊆**37** complexation. A 1.5 mM solution of **65** was titrated into a 0.15 mM solution of TEMOA **37** equilibrated at 25 °C. Both host and guest were in 10 mM phosphate buffer, pH 11.5.
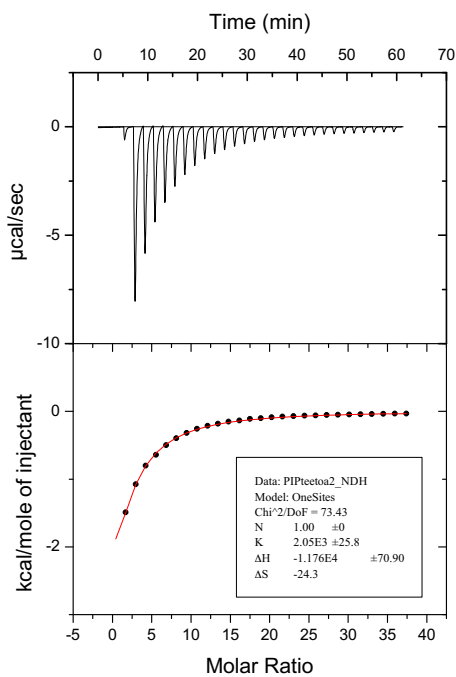
Fig. 147: ITC thermogram and 1:1 binding fit post-subtraction for **65**⊆**53** complexation. A 20.0 mM solution of **65** was titrated into a 0.10 mM solution of TEEtOA **53** equilibrated at 25 °C. Both host and guest were in 10 mM phosphate buffer, pH 11.5.

p-Toluic acid (66)
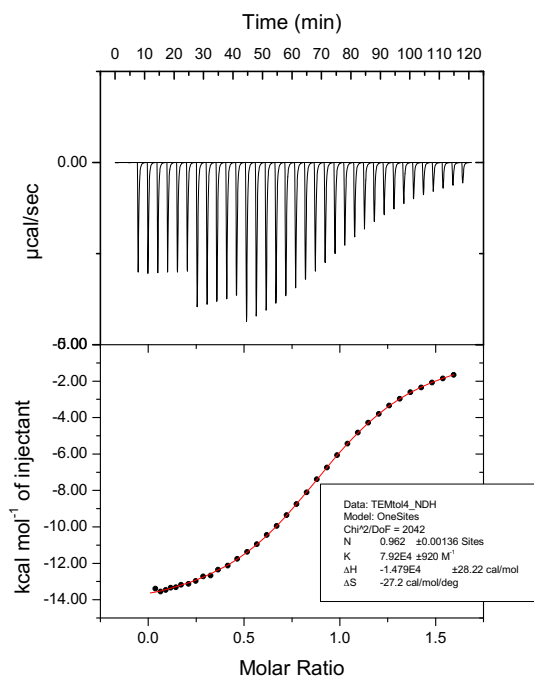
Fig. 149: ITC thermogram and 1:1 binding fit for **66**⊆**37** complexation. A 1.2 mM solution of **66** was titrated into a 0.15 mM solution of TEMOA **37** equilibrated at 25 °C. Both host and guest were in 10 mM phosphate buffer, pH 11.5.
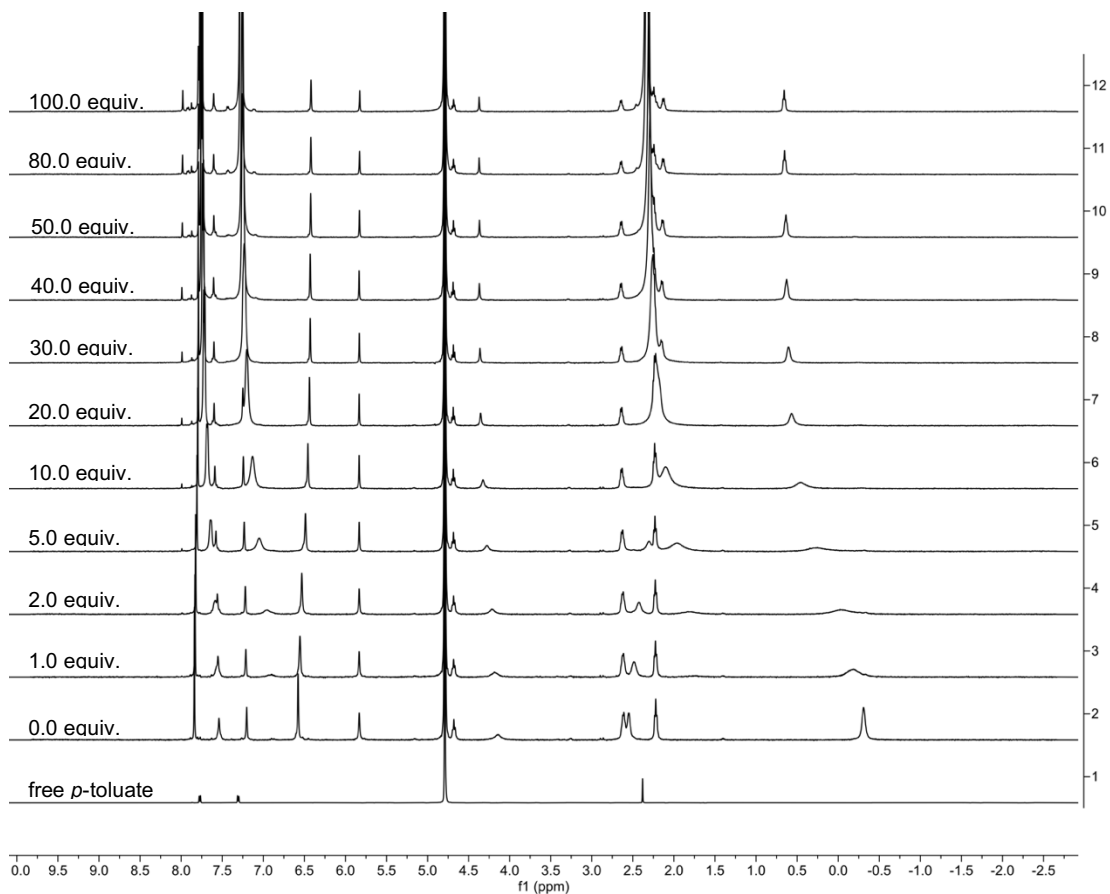
Fig. 150: ^{1}H NMR stack showing the addition of aliquots of 500 mM **66** into a 1.0 mM solution of TEEtOA **53**. Both solutions were in 10 mM pD 11.4 phosphate-buffered D2O.
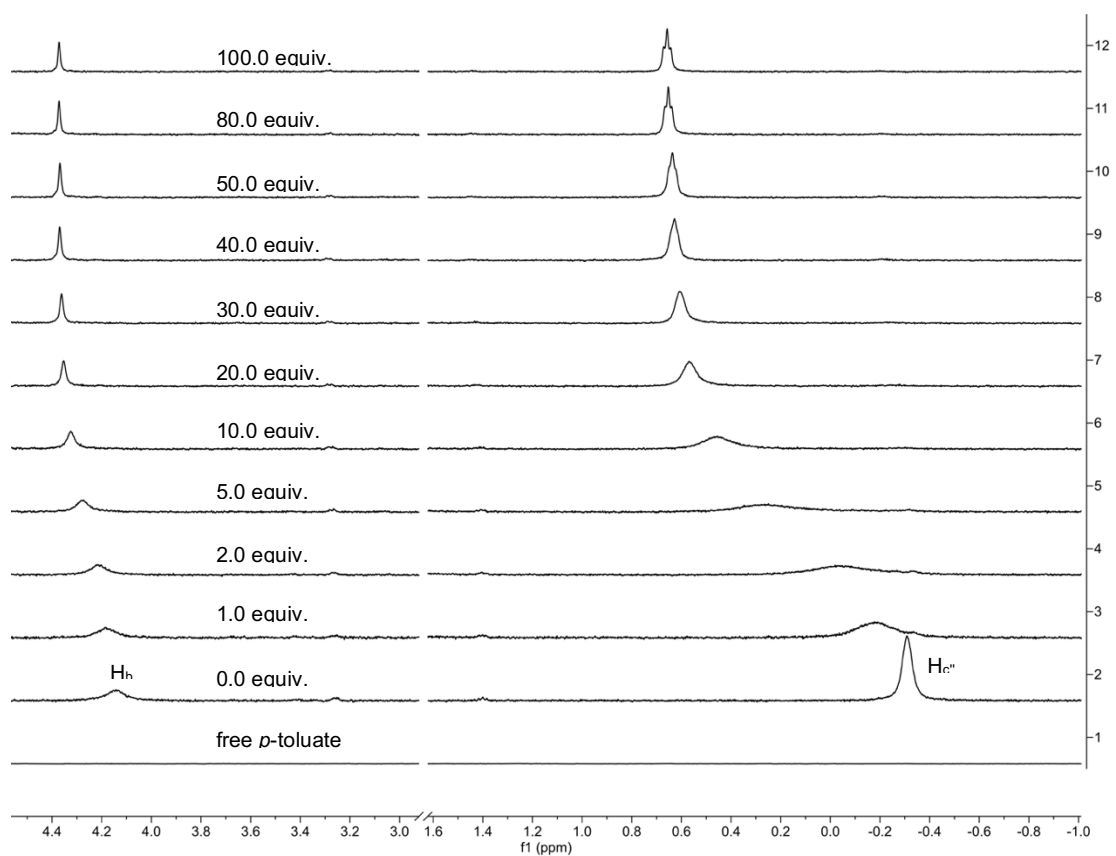
Fig. 151: Host region between –1.0 – 1.6 ppm, and 3.0 – 4.6 ppm showing the shifting of TEEtOA **53** host peaks H_b and $H_{c''}$ (see Figure S13) as a function of **66**.
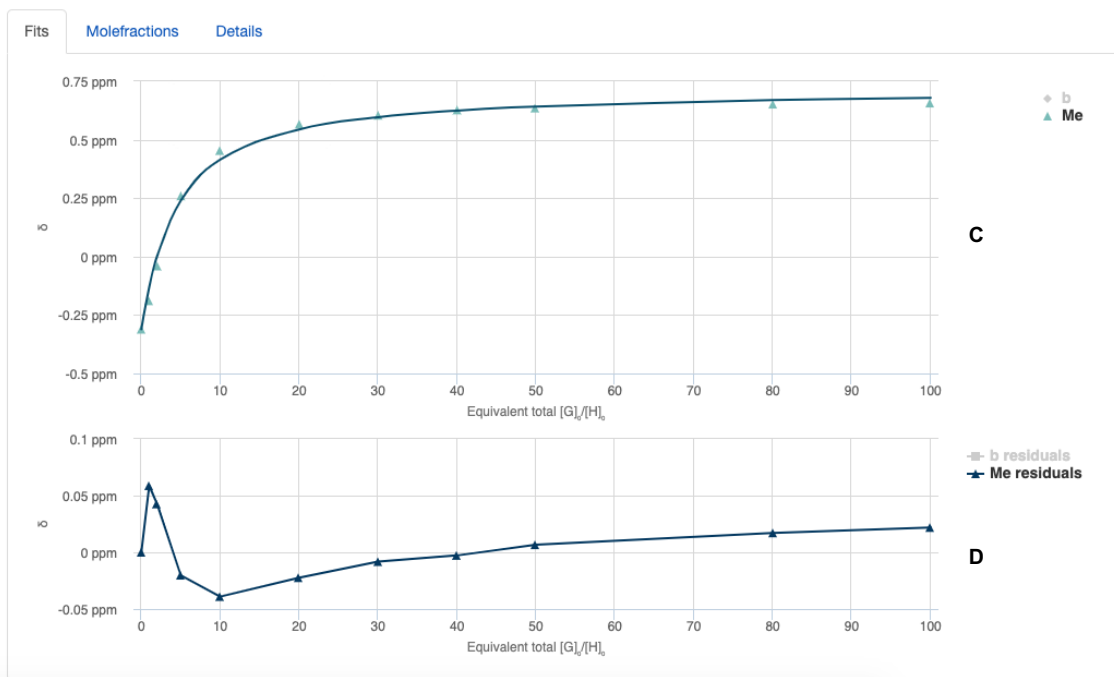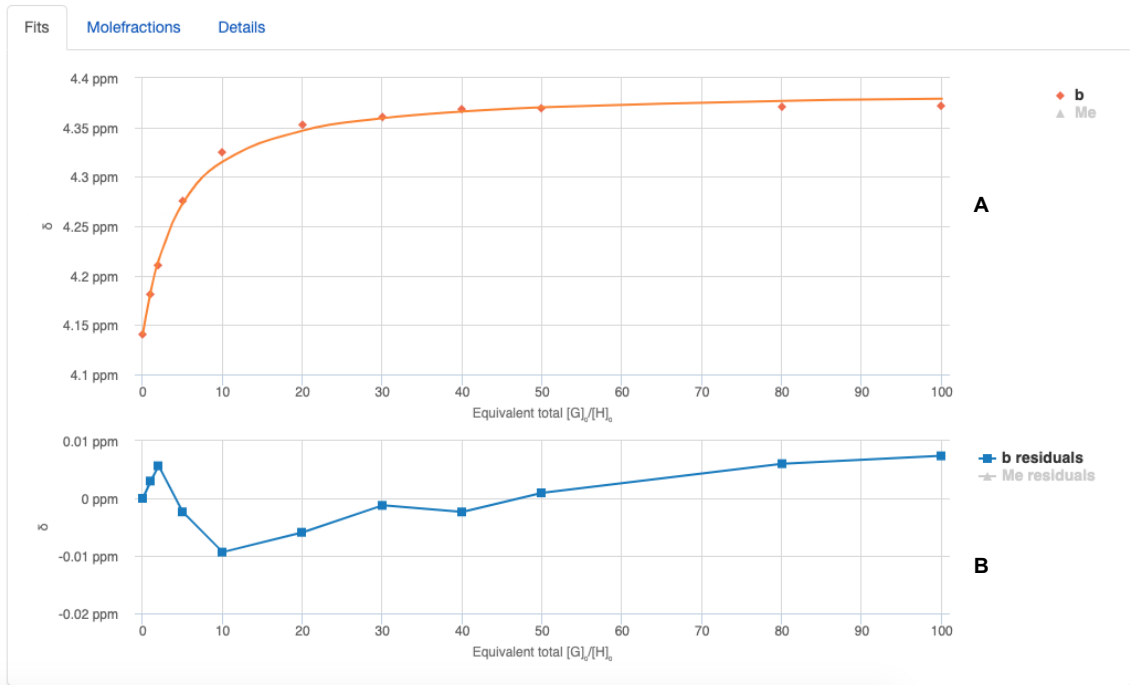
Fig. 152: (**A**, **B**) Representative fitting curve and residuals of the titration of **66** to TEEtOA **53** tracking H_b. (**C**, **D**) Representative fitting curve and residuals of the titration of **66** to TEEtOA **53** tracking $H_{c''}$. Curve and residuals were calculated using the online BindFit software.[2, 3]

4-Bromobenzoic acid (72)
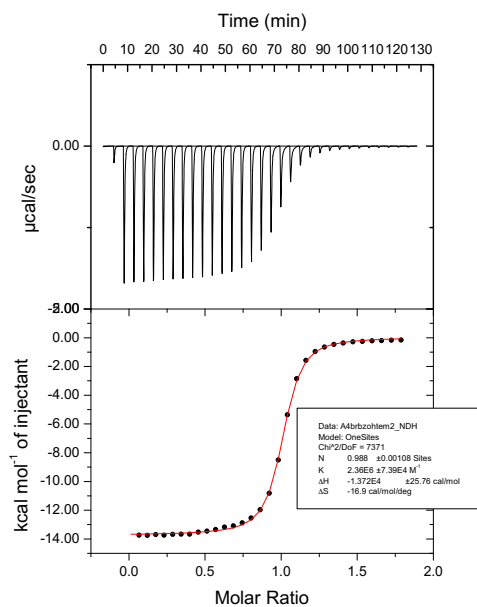
Fig. 154: ITC thermogram and 1:1 binding fit for **72**⊆**37** complexation. A 1.0 mM solution of **72** was titrated into a 0.10 mM solution of TEMOA **37** equilibrated at 25 °C. Both host and guest were in 10 mM phosphate buffer, pH 11.5.
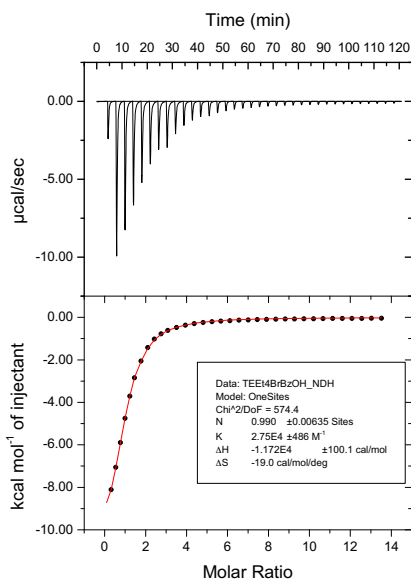
Fig. 153: ITC thermogram and 1:1 binding fit for **72**⊆**53** complexation. A 7.5 mM solution of **72** was titrated into a 0.115 mM solution of TEEtOA **37** equilibrated at 25 °C. Both host and guest were in 10 mM phosphate buffer, pH 11.5.
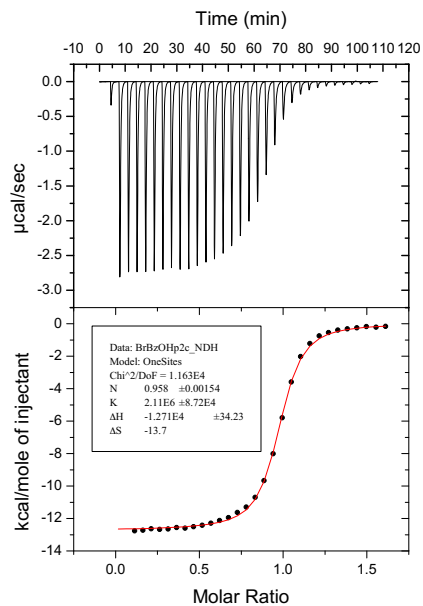
Fig. 156: ITC thermogram and 1:1 binding fit for **72**∈**67** complexation. A 1.0 mM solution of **72** was titrated into a 0.10 mM solution of Positand 2 **67** equilibrated at 25 °C. Both host and guest were in 10 mM phosphate buffer, pH 7.4.
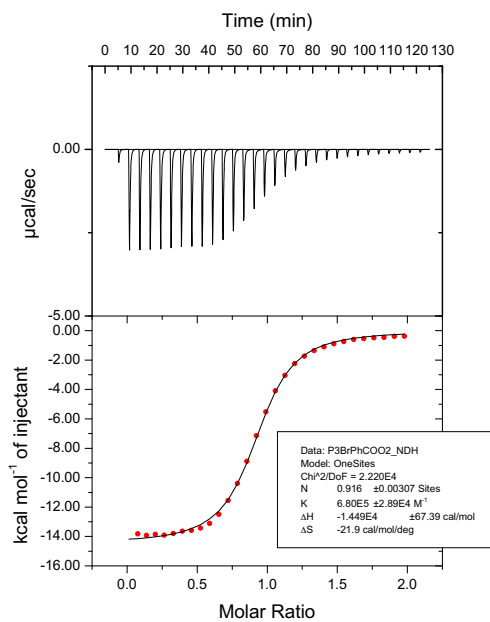
Fig. 155: ITC thermogram and 1:1 binding fit for **72**∈**68** complexation. A 1.5 mM solution of **72** was titrated into a 0.15 mM solution of Positand 3 **68** equilibrated at 25 °C. Both host and guest were in 10 mM phosphate buffer, pH 7.4.

General procedure for alkane binding

All experiments were performed at rt on solutions of 2 mM TEEtOA **53** dissolved in 10 mM pD 11.4 (pH 11.9) phosphate buffered D_2O. Standardisations of solutions were performed as described above. Sterile Millex® GV syringe filters equipped with hydrophilic Durapore® PVDF membranes with a pore size of 0.22 μm was used to filter solutions containing neat non-gaseous alkanes. The syringe filters were prepared by pushing 3 × 5 mL ultrapure water through the syringe filter and then drying under high vacuum at rt for 6 h.

Hydrocarbon gasses (CH$_4$ – *n*-C$_4$H$_{10}$)

To a standard 7-inch 5 mM OD NMR tube was added 500 μL of TEEtOA (**53**) solution, and the tube was then sealed using a rubber septum. Three freeze-pump-thaw cycles were performed on the solutions using dry N_2 to replace the atmosphere. A balloon was then filled with the appropriate hydrocarbon gas, and was then fitted with a LuerLok stopcock, a hydrophobic PTFE syringe filter, and 9-inch syringe needle. Another needle was used as a vent. The gas was then bubbled through the solution via the septum for 5 minutes, after which time the balloon was removed and the solution was allowed to equilibrate via the attached vent. NMR spectra of the gas–cavitand complexes were then taken.

Liquid hydrocarbons (C$_5$H$_{12}$ – C$_{14}$H$_{30}$)

To a 2 mL Eppendorf tube was added 1.5 mL of TEEtOA (**53**) solution and 2 µL of neat liquid hydrocarbon. The tube was then sealed and was allowed to vortex on a standard vortexer with a tube clamp attachment for 12 h. The solution was then taken up in a syringe and was then pushed through the prepared Millex® GV syringe filters and into a standard NMR tube. NMR spectra of the hydrocarbon–cavitand complexes were then taken.

Crystallographic data

Crystal structure of 4-ethyl-3,5-dimethoxybenzoic acid (56)

Identification code	BCG032_0m_a
Chemical formula	$C_{11}H_{14}O_4$
Formula weight	210.22 g/mol
Temperature	150(2) K
Wavelength	1.54178 Å
Crystal size	0.031 × 0.144 × 0.236 mm
Crystal habit	colourless plate
Crystal system	triclinic
Space group	P$\bar{1}$
Unit cell dimensions	a = 4.5802(4) Å α = 79.400(6)°
	b = 7.9822(7) Å β = 86.352(6)°
	c = 15.3535(14) Å γ = 76.197(6)°
Volume	535.70(8) Å^3
Z	2
Density (calculated)	1.303 g/cm^3
Absorption coefficient	0.827 mm^{-1}
F(000)	224

Table 17: Sample and crystal data for 4-ethyl-3,5-dimethoxydenzoic acid (**56**). CCDC 2127617.

Diffractometer	Bruker D8 VENTURE PHOTON 100 CMOS
Radiation source	INCOATEC IµS micro-focus source (Cu-Kα, λ = 1.54178 Å)
2θ range for data collection	5.80 – 71.98°
Index ranges	–5≤h≤5, –9≤k≤9, –18≤l≤17
Reflections collected	3833
Independent reflections	1949 [R_{int} = 0.0423]
Coverage of independent reflections	92.2%
Absorption correction	multi-scan
Max. and min. transmission	0.9750 and 0.8290
Refinement method	Full-matrix least-squares on F^2
Refinement program	*SHELXL-2018/1*[250]
Function minimized	Σ w(F_o^2 - F_c^2)^2
Data / restraints / parameters	1949 / 1 / 142
Goodness-of-fit on F^2	1.052
Final R indices	1471 data; I>2σ(I) R_1 = 0.0611, wR_1 = 0.1339
	all data R_2 = 0.0931, wR_2 = 0.1465
Weighting scheme	w = 1/[σ^2(F_o^2)+(0.0717P)^2+0.5831P] where P = (F_o^2+2F_c^2)/3
Largest diff. peak and hole	0.386 and –0.258 eÅ^{-3}
RMS deviation from mean	0.057 eÅ^{-3}

Table 18: Data collection and structure refinement for 4-ethyl-3,5-dimethoxybenzoic acid (**56**). CCDC 2127617.
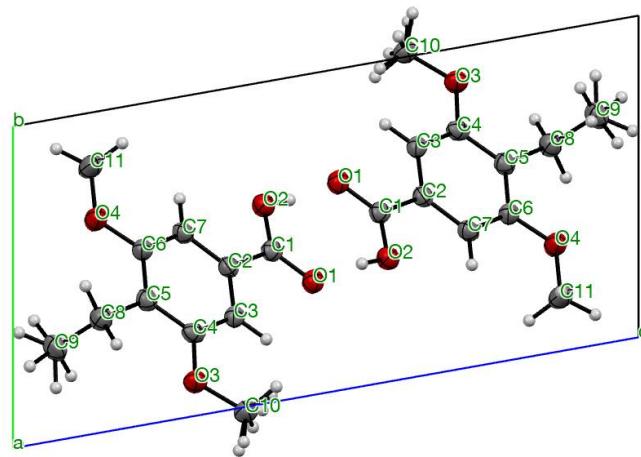
Fig. 157: ORTEP thermal ellipsoid plot of the unit cell of 4-ethyl-3,5-dimethoxybenzoic acid **56** along the crystallographic *a* axis at a 50% probability level.

Crystal structure of tetra-*endo*-ethyl octa-bromide (TEEtO(Br), 71)

Identification code	BCG034_0m_a_sq
Chemical formula	$C_{105}H_{89}Br_8Cl_3O_{16}$, $CHCl_3$
Formula weight	2471.75 g/mol
Temperature	150(2) K
Wavelength	1.54178 Å
Crystal size	0.059 × 0.133 × 0.315 mm
Crystal habit	colourless column
Crystal system	triclinic
Space group	P$\bar{1}$
Unit cell dimensions	a = 13.3248(3) Å α = 86.704(1)°
	b = 16.2858(4) Å β = 85.477(1)°
	c = 25.0430(6) Å γ = 75.034(1)°
Volume	5229.9(2) Å^3
Z	2
Density (calculated)	1.570 g/cm^3
Absorption coefficient	5.594 mm^{-1}
F(000)	2472

Table 19: Sample and crystal data for tetra-endo-ethyl octa-bromide (**71**).Figure 62 shows the image of **72** in ORTEP format.

Diffractometer	Bruker D8 VENTURE PHOTON 100 CMOS
Radiation source	INCOATEC IμS micro-focus source (Cu-Kα, λ = 1.54178 Å)
2θ range for data collection	3.26 – 72.15°
Index ranges	–16≤h≤16, –18≤k≤20, –30≤l≤30
Reflections collected	40447
Independent reflections	19470 [R_{int} = 0.0357]
Coverage of independent reflections	94.4%
Absorption correction	numerical
Max. and min. transmission	0.7340 and 0.2720
Refinement method	Full-matrix least-squares on F^2
Refinement program	*SHELXL-2018/3*[250]
Function minimized	$\Sigma\ w(F_o^2 - F_c^2)^2$
Data / restraints / parameters	19470 / 23 / 1247
Goodness-of-fit on F^2	1.045
Final R indices	15638 data; I>2σ(I) R$_1$ = 0.0600, wR$_1$ = 0.1517
	all data R$_2$ = 0.0743, wR$_2$ = 0.1633
Weighting scheme	w = 1/[σ^2(F$_o^2$)+(0.0760P)^2+18.2283P] where P = (F$_o^2$+2F$_c^2$)/3
Largest diff. peak and hole	2.703 and –1.694 eÅ^{-3}
RMS deviation from mean	0.111 eÅ^{-3}

Table 20: Data collection and structure refinement for tetra-endo-ethyl octa-bromide (**71**).

Table 21: Atomic coordinates and equivalent isotropic displacement parameters in Å² for **71**. U(eq) is defined as one-third of the trace of the orthogonalized U_{ij} tensor.

Atom	x/a	y/b	z/c	U(eq)
Br1	0.32357(5)	0.17461(4)	0.61404(2)	0.0166(6)
Br2	0.09034(5)	-0.03166(4)	0.57798(2)	0.0261(7)
Br3	-0.39375(4)	0.44035(4)	0.46354(2)	0.0320(8)
Br4	-0.08199(5)	0.70898(4)	0.46689(3)	0.0236(7)
Br5	-0.08227(5)	-0.12584(4)	0.07953(2)	0.0308(8)
Br6	1.03757(14)	-0.25362(11)	0.29848(6)	0.0320(8)
Br6A	1.0758(3)	-0.2214(2)	0.28184(12)	0.0545(13)
Br7	0.69247(11)	0.57436(5)	0.35144(3)	0.0424(10)
Br7A	0.8285(7)	0.6208(4)	0.2948(2)	0.0165(6)
Br8	-0.29418(5)	0.71719(5)	0.04958(3)	0.0182(6)
C05A	0.6781(11)	0.641(4)	0.2863(18)	0.0179(6)
C1	0.4464(3)	0.2692(3)	0.44316(15)	0.0171(6)
C10	-0.0126(3)	0.3479(2)	0.33032(16)	0.0179(6)
C100	0.1967(5)	0.4752(5)	0.0486(2)	0.0172(6)
C101	0.2534(5)	0.4132(5)	0.0917(3)	0.0169(6)
C102	-0.2278(4)	0.6568(4)	0.1126(2)	0.0310(8)
C103	0.5559(4)	0.4678(3)	0.1160(2)	0.0166(6)
C104	0.6059(7)	0.4843(6)	0.0605(3)	0.0261(7)
C105	0.7117(6)	0.6315(6)	0.2812(3)	0.0320(8)
C106	0.3064(5)	0.2793(4)	0.22077(11)	0.0236(7)
C107	0.2914(5)	0.7244(4)	0.3611(2)	0.0308(8)
C10A	0.3681(5)	0.2322(4)	0.23278(12)	0.0320(8)
C11	0.0328(3)	0.3887(3)	0.36540(15)	0.0545(13)
C12	0.0741(3)	0.4580(3)	0.34909(16)	0.0424(10)
C13	0.1271(3)	0.5020(3)	0.38597(15)	0.0165(6)
C14	0.2438(3)	0.4591(3)	0.38260(15)	0.0182(6)
C15	0.2901(3)	0.3891(3)	0.41559(15)	0.0179(6)
C16	0.3958(3)	0.3461(2)	0.40847(15)	0.0171(6)
C17	0.4087(3)	0.2746(3)	0.50268(16)	0.0179(6)
C18	0.4806(4)	0.2063(3)	0.53610(17)	0.0172(6)
C19	0.4512(4)	0.2094(3)	0.59556(18)	0.0169(6)
C2	0.4412(3)	0.1874(3)	0.41806(15)	0.0310(8)
C20	0.2030(3)	0.0473(3)	0.46948(17)	0.0166(6)
C21	0.2697(4)	-0.0086(4)	0.51089(19)	0.0261(7)
C22	0.2210(4)	0.0016(4)	0.5680(2)	0.0320(8)
C23	-0.1116(3)	0.2745(3)	0.40143(16)	0.0236(7)
C24	-0.2078(3)	0.3511(3)	0.40488(18)	0.0308(8)
C25	-0.2813(4)	0.3383(3)	0.4507(2)	0.0320(8)
C26	0.0770(3)	0.5114(3)	0.44312(15)	0.0545(13)
C27	0.1112(4)	0.5783(3)	0.47274(17)	0.0424(10)
C28	0.0688(4)	0.6689(3)	0.45283(19)	0.0165(6)
C29	0.5743(3)	0.2564(3)	0.32826(16)	0.0182(6)
C3	0.3573(3)	0.1501(3)	0.42924(15)	0.0179(6)
C30	0.5190(3)	0.1490(3)	0.38036(16)	0.0171(6)
C31	0.5160(3)	0.0757(3)	0.35578(15)	0.0179(6)
C32	0.4319(3)	0.0410(3)	0.36780(15)	0.0172(6)
C33	0.3705(3)	-0.0132(3)	0.29497(15)	0.0169(6)
C34	0.1921(3)	0.0424(3)	0.31971(16)	0.0310(8)
C35	0.1273(3)	0.0778(3)	0.27900(16)	0.0166(6)
C36	0.0497(3)	0.1518(3)	0.28862(16)	0.0261(7)
C37	0.0189(3)	0.2608(3)	0.22126(16)	0.0320(8)
C38	-0.0139(3)	0.3772(3)	0.27697(16)	0.0236(7)
C39	0.0244(3)	0.4464(3)	0.25930(16)	0.0308(8)
C4	0.3504(3)	0.0768(3)	0.40440(15)	0.0320(8)
C40	0.0683(3)	0.4855(3)	0.29539(16)	0.0545(13)
C41	0.2171(3)	0.5332(3)	0.26506(15)	0.0424(10)

C42	0.3080(3)	0.4858(3)	0.34263(16)	0.0165(6)
C43	0.4122(3)	0.4457(3)	0.33468(16)	0.0182(6)
C44	0.4549(3)	0.3748(3)	0.36675(16)	0.0179(6)
C45	0.6559(3)	0.2512(3)	0.28227(16)	0.0171(6)
C46	0.7102(3)	0.1718(3)	0.26418(17)	0.0179(6)
C47	0.8778(4)	-0.0208(3)	0.25821(19)	0.0172(6)
C48	0.8789(4)	-0.1024(3)	0.27815(18)	0.0169(6)
C49	0.8140(3)	-0.1447(3)	0.25716(18)	0.0310(8)
C5	0.2560(3)	0.0394(3)	0.41313(15)	0.0166(6)
C50	0.5363(3)	-0.0937(3)	0.24682(17)	0.0261(7)
C51	0.3725(3)	-0.0785(3)	0.20655(17)	0.0320(8)
C52	0.1992(4)	-0.1291(3)	0.12818(18)	0.0236(7)
C53	0.0947(4)	-0.0899(3)	0.12056(19)	0.0308(8)
C54	0.0708(4)	-0.0082(3)	0.09713(18)	0.0320(8)
C55	0.0629(3)	0.1813(3)	0.13636(17)	0.0545(13)
C56	0.0090(4)	0.3348(3)	0.13151(18)	0.0424(10)
C57	-0.0986(4)	0.5258(3)	0.08146(18)	0.0165(6)
C58	-0.1194(4)	0.6085(3)	0.09818(18)	0.0182(6)
C59	-0.0382(4)	0.6465(3)	0.09964(18)	0.0179(6)
C6	0.1805(3)	0.0778(3)	0.36976(16)	0.0171(6)
C60	0.1734(4)	0.5977(3)	0.17428(18)	0.0179(6)
C61	0.2432(3)	0.5799(3)	0.21430(16)	0.0172(6)
C62	0.3417(4)	0.5946(3)	0.20567(18)	0.0169(6)
C63	0.6627(3)	0.3255(3)	0.25336(17)	0.0310(8)
C64	0.4282(3)	-0.0670(3)	0.24910(16)	0.0166(6)
C65	0.0249(3)	0.2587(3)	0.16097(17)	0.0261(7)
C66	0.7694(3)	0.1675(3)	0.21556(18)	0.0320(8)
C67	0.6879(4)	0.0118(3)	0.14700(19)	0.0236(7)
C68	0.8137(4)	0.0155(3)	0.21708(18)	0.0308(8)
C69	0.7492(3)	-0.0261(3)	0.19451(18)	0.0320(8)
C7	0.0989(3)	0.1516(2)	0.37747(16)	0.0545(13)
C70	0.7503(3)	-0.1078(3)	0.21654(17)	0.0424(10)
C71	0.5876(3)	-0.1313(3)	0.20065(17)	0.0165(6)
C72	0.5346(3)	-0.1448(3)	0.15750(18)	0.0182(6)
C73	0.4268(3)	-0.1177(3)	0.16148(17)	0.0179(6)
C74	0.2756(4)	-0.0879(3)	0.11175(18)	0.0171(6)
C75	0.2538(4)	-0.0066(3)	0.08727(18)	0.0179(6)
C76	0.1484(4)	0.0311(3)	0.08063(17)	0.0172(6)
C77	0.0832(4)	0.1817(3)	0.08126(17)	0.0169(6)
C78	0.0673(4)	0.2567(3)	0.05057(17)	0.0310(8)
C79	0.0306(4)	0.3326(3)	0.07627(18)	0.0166(6)
C8	0.0323(3)	0.1896(2)	0.33801(16)	0.0261(7)
C80	0.7183(4)	0.5067(3)	0.22633(19)	0.0320(8)
C81	0.0023(5)	0.4831(3)	0.06575(17)	0.0236(7)
C82	0.0858(4)	0.5199(4)	0.06689(18)	0.0308(8)
C83	0.0621(4)	0.6027(3)	0.08399(18)	0.0320(8)
C85	0.2039(4)	0.6293(3)	0.12463(18)	0.0545(13)
C86	0.3016(4)	0.6448(3)	0.11463(18)	0.0424(10)
C87	0.3689(3)	0.6268(3)	0.15552(19)	0.0165(6)
C88	0.5476(3)	0.5944(3)	0.17319(19)	0.0182(6)
C89	0.5826(4)	0.6344(3)	0.21242(19)	0.0179(6)
C9	-0.0543(3)	0.2705(3)	0.34606(16)	0.0171(6)
C90	0.6686(4)	0.5904(3)	0.23944(19)	0.0179(6)
C91	0.5934(4)	0.5102(3)	0.15938(18)	0.0172(6)
C92	0.6801(4)	0.4688(3)	0.18752(18)	0.0169(6)
C93	0.7233(3)	0.3184(3)	0.20531(17)	0.0310(8)
C94	0.7764(3)	0.2402(3)	0.18582(17)	0.0166(6)
C95	0.5847(4)	0.0767(4)	0.1608(2)	0.0261(7)
C96	0.9495(14)	-0.1427(12)	0.3215(4)	0.0320(8)
C96A	0.953(2)	-0.147(2)	0.3192(5)	0.0236(7)

C97	0.3363(5)	0.0368(4)	0.0655(2)	0.0308(8)
C98	0.3568(5)	0.0288(5)	0.0046(2)	0.0320(8)
C99	0.0129(4)	-0.1345(4)	0.1370(2)	0.0545(13)
Cl1	0.41786(13)	0.31630(11)	0.20607(6)	0.0424(10)
Cl2	0.30869(12)	0.18932(11)	0.18527(6)	0.0165(6)
Cl3	0.28427(11)	0.26143(10)	0.28972(5)	0.0182(6)
Cl4	0.36786(14)	0.75464(11)	0.30728(6)	0.0179(6)
Cl5	0.36490(15)	0.65069(11)	0.40520(7)	0.0171(6)
Cl6	0.22083(17)	0.81497(11)	0.39599(8)	0.0179(6)
O1	0.6025(2)	0.18438(18)	0.36458(11)	0.0166(6)
O10	0.7336(3)	0.3873(2)	0.17224(13)	0.0261(7)
O11	0.8232(3)	0.0926(2)	0.19265(14)	0.0320(8)
O12	0.6956(2)	-0.1579(2)	0.19460(12)	0.0236(7)
O13	0.3792(3)	-0.1319(2)	0.11673(13)	0.0308(8)
O14	0.1237(3)	0.1096(2)	0.05252(13)	0.0320(8)
O15	0.0216(4)	0.4045(2)	0.04335(13)	0.0545(13)
O16	0.1401(3)	0.6465(3)	0.08288(14)	0.0424(10)
O2	0.4307(2)	-0.03136(17)	0.34066(11)	0.0165(6)
O3	0.2718(2)	-0.02978(18)	0.30688(12)	0.0182(6)
O4	-0.0089(2)	0.18772(18)	0.24502(11)	0.0179(6)
O5	-0.0530(2)	0.33689(18)	0.23870(11)	0.0171(6)
O6	0.1075(2)	0.55365(18)	0.27589(11)	0.0179(6)
O7	0.2677(2)	0.55490(18)	0.30809(11)	0.0172(6)
O8	0.5596(2)	0.33329(18)	0.35543(11)	0.0169(6)
O9	0.4657(2)	0.6425(2)	0.14382(14)	0.0310(8)

Table 22: Bond lengths (Å) for **72**.

Br1-C19	1.941(5)	C20-C21	1.520(6)	C62-C87	1.391(6)
Br2-C22	1.947(5)	C20-H20A	0.99	C62-H62	0.95
Br3-C25	1.952(5)	C20-H20B	0.99	C63-C93	1.388(6)
Br4-C28	1.955(5)	C21-C22	1.522(7)	C63-H63	0.95
Br5-C99	1.967(5)	C21-H21A	0.99	C66-C94	1.381(6)
Br6-C96	1.972(8)	C21-H21B	0.99	C67-C69	1.508(7)
Br6A-C96A	1.972(8)	C22-H22A	0.99	C67-C95	1.531(7)
Br7-C105	1.972(8)	C22-H22B	0.99	C67-H67A	0.99
Br7A-C05A	1.972(8)	C23-C24	1.542(6)	C67-H67B	0.99
Br8-C102	1.957(6)	C23-H23A	0.99	C68-C69	1.392(7)
O1-C30	1.400(5)	C23-H23B	0.99	C69-C70	1.406(6)
O1-C29	1.431(5)	C24-C25	1.490(7)	C71-C72	1.394(6)
O2-C32	1.397(5)	C24-H24A	0.99	C72-C73	1.387(6)
O2-C33	1.423(5)	C24-H24B	0.99	C72-H72	0.95
O3-C34	1.399(5)	C25-H25A	0.99	C74-C75	1.396(7)
O3-C33	1.415(5)	C25-H25B	0.99	C75-C76	1.398(7)
O4-C36	1.403(5)	C26-C27	1.532(6)	C75-C97	1.507(8)
O4-C37	1.421(5)	C26-H26A	0.99	C77-C78	1.382(7)
O5-C38	1.395(5)	C26-H26B	0.99	C78-C79	1.383(7)
O5-C37	1.424(5)	C27-C28	1.508(7)	C78-H78	0.95
O6-C40	1.393(5)	C27-H27A	0.99	C81-C82	1.396(8)
O6-C41	1.418(5)	C27-H27B	0.99	C80-C92	1.377(7)
O7-C42	1.397(5)	C28-H28A	0.99	C80-C90	1.398(7)
O7-C41	1.422(5)	C28-H28B	0.99	C80-H80	0.95
O8-C44	1.399(5)	C29-C45	1.511(5)	C82-C83	1.388(8)
O8-C29	1.421(5)	C29-H29	1	C82-C100	1.517(8)
O9-C87	1.384(5)	C30-C31	1.386(6)	C85-C86	1.389(7)
O9-C88	1.401(6)	C31-C32	1.385(6)	C86-C87	1.383(7)
O10-C93	1.385(5)	C31-H31	0.95	C86-H86	0.95
O10-C92	1.395(5)	C33-C64	1.519(5)	C88-C89	1.382(7)
O11-C66	1.377(5)	C33-H33	1	C88-C91	1.400(7)
O11-C68	1.396(5)	C34-C35	1.390(6)	C89-C90	1.388(7)
O12-C70	1.386(5)	C35-C36	1.389(6)	C89-H89	0.95
O12-C71	1.391(5)	C35-H35	0.95	C90-C105	1.499(8)
O13-C73	1.389(5)	C37-C65	1.508(5)	C90-C05A	1.499(8)
O13-C74	1.393(5)	C37-H37	1	C91-C92	1.398(7)
O14-C77	1.378(5)	C38-C39	1.390(6)	C91-C103	1.503(7)
O14-C76	1.397(6)	C39-C40	1.381(6)	C93-C94	1.384(6)
O15-C79	1.378(6)	C39-H39	0.95	C94-H94	0.95
O15-C81	1.381(6)	C41-C61	1.507(5)	C95-H95A	0.98
O16-C85	1.371(6)	C41-H41	1	C95-H95B	0.98
O16-C83	1.402(6)	C42-C43	1.378(6)	C95-H95C	0.98
C1-C16	1.520(6)	C43-C44	1.388(6)	C96-H96A	0.99
C1-C2	1.525(5)	C43-H43	0.95	C96-H96B	0.99
C1-C17	1.535(5)	C45-C46	1.391(6)	C96A-H96C	0.99
C1-H1	1	C45-C63	1.393(6)	C96A-H96D	0.99
C2-C30	1.392(5)	C46-C66	1.393(6)	C97-C98	1.533(8)
C2-C3	1.406(6)	C46-H46	0.95	C97-H97A	0.99
C3-C4	1.404(6)	C47-C48	1.390(7)	C97-H97B	0.99
C3-H3	0.95	C47-C68	1.395(7)	C98-H98A	0.98
C4-C32	1.393(5)	C47-H47	0.95	C98-H98B	0.98
C4-C5	1.529(6)	C48-C49	1.385(6)	C98-H98C	0.98
C5-C20	1.524(5)	C48-C96A	1.503(7)	C99-H99A	0.99
C5-C6	1.533(6)	C48-C96	1.503(7)	C99-H99B	0.99
C5-H5	1	C49-C70	1.386(6)	C100-C101	1.536(8)
C6-C34	1.390(6)	C49-H49	0.95	C100-H10A	0.99
C6-C7	1.409(6)	C50-C71	1.386(6)	C100-H10B	0.99
C7-C8	1.389(6)	C50-C64	1.389(6)	C101-H10C	0.98

C7-H7	0.95	C50-H50	0.95	C101-H10D	0.98
C8-C36	1.390(5)	C51-C73	1.385(6)	C101-H10E	0.98
C8-C9	1.522(5)	C51-C64	1.394(6)	C102-H10F	0.99
C9-C23	1.525(5)	C51-H51	0.95	C102-H10G	0.99
C9-C10	1.526(5)	C52-C74	1.382(7)	C103-C104	1.532(8)
C9-H9	1	C52-C53	1.397(7)	C103-H10H	0.99
C10-C11	1.391(6)	C52-H52	0.95	C103-H10I	0.99
C10-C38	1.392(6)	C53-C54	1.392(7)	C104-H10J	0.98
C11-C12	1.406(6)	C53-C99	1.481(7)	C104-H10K	0.98
C11-H11	0.95	C54-C76	1.376(7)	C104-H10L	0.98
C12-C40	1.395(6)	C54-H54	0.95	C105-H10M	0.99
C12-C13	1.519(5)	C55-C77	1.385(6)	C105-H10N	0.99
C13-C14	1.529(5)	C55-C65	1.391(6)	C05A-H05A	0.99
C13-C26	1.529(5)	C55-H55	0.95	C05A-H05B	0.99
C13-H13	1	C56-C65	1.382(6)	Cl1-C106	1.748(3)
C14-C42	1.390(6)	C56-C79	1.391(6)	Cl1-C10A	1.749(3)
C14-C15	1.404(6)	C56-H56	0.95	Cl2-C10A	1.748(3)
C15-C16	1.404(6)	C57-C81	1.382(8)	Cl2-C106	1.749(3)
C15-H15	0.95	C57-C58	1.386(7)	Cl3-C106	1.749(3)
C16-C44	1.391(6)	C57-H57	0.95	Cl3-C10A	1.749(3)
C17-C18	1.524(6)	C58-C59	1.382(7)	C106-H106	1
C17-H17A	0.99	C58-C102	1.483(7)	C10A-H10O	1
C17-H17B	0.99	C59-C83	1.381(7)	Cl4-C107	1.751(6)
C18-C19	1.510(6)	C59-H59	0.95	Cl5-C107	1.740(7)
C18-H18A	0.99	C60-C61	1.389(6)	Cl6-C107	1.768(6)
C18-H18B	0.99	C60-C85	1.390(6)	C107-H107	1
C19-H19A	0.99	C60-H60	0.95		
C19-H19B	0.99	C61-C62	1.392(6)		

Table 23: Bond angles (°) for **72**.

C29-O1-C30	112.7(3)	C27-C28-H28B	109.1	C71-C72-H72	121.1
C32-O2-C33	113.6(3)	H28A-C28-H28B	107.8	C71-C72-C73	117.7(4)
C33-O3-C34	114.0(3)	O1-C29-O8	110.6(3)	H72-C72-C73	121.1
C36-O4-C37	113.1(3)	O1-C29-H29	108.3	O13-C73-C51	123.5(4)
C37-O5-C38	112.7(3)	O1-C29-C45	110.6(3)	O13-C73-C72	114.6(4)
C40-O6-C41	114.6(3)	O8-C29-H29	108.3	C51-C73-C72	121.8(4)
C41-O7-C42	113.4(3)	O8-C29-C45	110.6(3)	O13-C74-C52	118.2(4)
C29-O8-C44	113.6(3)	H29-C29-C45	108.3	O13-C74-C75	118.7(4)
C87-O9-C88	116.9(3)	O1-C30-C2	121.2(4)	C52-C74-C75	122.9(5)
C92-O10-C93	118.7(4)	O1-C30-C31	117.1(4)	C74-C75-C76	115.3(4)
C66-O11-C68	119.2(4)	C2-C30-C31	121.7(4)	C74-C75-C97	123.7(5)
C70-O12-C71	116.7(3)	C30-C31-H31	120.4	C76-C75-C97	120.9(5)
C73-O13-C74	117.7(4)	C30-C31-C32	119.3(4)	O14-C76-C54	119.7(4)
C76-O14-C77	118.2(4)	H31-C31-C32	120.3	O14-C76-C75	117.2(4)
C79-O15-C81	119.5(4)	O2-C32-C4	120.7(4)	C54-C76-C75	123.0(5)
C83-O16-C85	116.7(4)	O2-C32-C31	117.2(4)	O14-C77-C55	124.1(4)
H1-C1-C2	105.7	C4-C32-C31	122.2(4)	O14-C77-C78	114.2(4)
H1-C1-C16	105.8	O2-C33-O3	110.7(3)	C55-C77-C78	121.7(4)
H1-C1-C17	105.8	O2-C33-H33	108.9	C77-C78-H78	120.8
C2-C1-C16	110.4(3)	O2-C33-C64	109.5(3)	C77-C78-C79	118.3(4)
C2-C1-C17	113.9(3)	O3-C33-H33	108.9	H78-C78-C79	120.9
C16-C1-C17	114.5(3)	O3-C33-C64	109.9(3)	O15-C79-C56	123.4(4)
C1-C2-C3	122.8(4)	H33-C33-C64	108.9	O15-C79-C78	114.8(4)
C1-C2-C30	119.9(4)	O3-C34-C6	121.8(4)	C56-C79-C78	121.7(5)
C3-C2-C30	117.3(4)	O3-C34-C35	116.0(4)	O15-C81-C57	119.8(5)
C2-C3-H3	118.6	C6-C34-C35	122.2(4)	O15-C81-C82	117.6(5)
C2-C3-C4	122.7(4)	C34-C35-H35	120.7	C57-C81-C82	122.3(5)
H3-C3-C4	118.7	C34-C35-C36	118.6(4)	H80-C80-C90	120.2
C3-C4-C5	123.2(4)	H35-C35-C36	120.7	H80-C80-C92	120.3
C3-C4-C32	116.8(4)	O4-C36-C8	121.6(4)	C90-C80-C92	119.5(5)
C5-C4-C32	119.8(4)	O4-C36-C35	116.1(4)	C81-C82-C83	116.4(5)
C4-C5-H5	106.8	C8-C36-C35	122.3(4)	C81-C82-C100	123.2(5)
C4-C5-C6	108.4(3)	O4-C37-O5	111.1(3)	C83-C82-C100	120.3(5)
C4-C5-C20	115.1(4)	O4-C37-H37	108.3	O16-C83-C59	117.6(4)
H5-C5-C6	106.8	O4-C37-C65	110.7(3)	O16-C83-C82	120.1(4)
H5-C5-C20	106.8	O5-C37-H37	108.3	C59-C83-C82	122.2(5)
C6-C5-C20	112.6(3)	O5-C37-C65	110.1(3)	O16-C85-C60	122.2(4)
C5-C6-C7	122.4(4)	H37-C37-C65	108.2	O16-C85-C86	116.3(4)
C5-C6-C34	121.0(4)	O5-C38-C10	120.8(4)	C60-C85-C86	121.5(5)
C7-C6-C34	116.6(4)	O5-C38-C39	117.2(4)	C85-C86-H86	120.9
C6-C7-H7	118.3	C10-C38-C39	122.0(4)	C85-C86-C87	118.0(4)
C6-C7-C8	123.4(4)	C38-C39-H39	120.5	H86-C86-C87	121
H7-C7-C8	118.3	C38-C39-C40	119.0(4)	O9-C87-C62	121.5(4)
C7-C8-C9	123.3(3)	H39-C39-C40	120.5	O9-C87-C86	116.2(4)
C7-C8-C36	116.9(4)	O6-C40-C12	121.0(4)	C62-C87-C86	122.3(4)
C9-C8-C36	119.8(4)	O6-C40-C39	117.2(4)	O9-C88-C89	117.9(4)
C8-C9-H9	106.2	C12-C40-C39	121.8(4)	O9-C88-C91	118.6(4)
C8-C9-C10	109.7(3)	O6-C41-O7	111.3(3)	C89-C88-C91	123.4(4)
C8-C9-C23	113.7(3)	O6-C41-H41	108.7	C88-C89-H89	120.4
H9-C9-C10	106.3	O6-C41-C61	109.5(3)	C88-C89-C90	119.3(5)
H9-C9-C23	106.2	O7-C41-H41	108.8	H89-C89-C90	120.4
C10-C9-C23	114.0(3)	O7-C41-C61	109.6(3)	C80-C90-C89	119.4(5)
C9-C10-C11	124.0(4)	H41-C41-C61	108.8	C80-C90-C105	119.1(5)
C9-C10-C38	118.6(3)	O7-C42-C14	120.4(4)	C89-C90-C105	121.5(5)
C11-C10-C38	117.2(4)	O7-C42-C43	117.2(4)	C88-C91-C92	115.1(4)
C10-C11-H11	118.6	C14-C42-C43	122.4(4)	C88-C91-C103	123.0(4)
C10-C11-C12	122.6(4)	C42-C43-H43	120.4	C92-C91-C103	121.8(4)
H11-C11-C12	118.8	C42-C43-C44	119.3(4)	O10-C92-C80	119.3(4)

C11-C12-C13	123.8(4)	H43-C43-C44	120.3	O10-C92-C91	117.3(4)
C11-C12-C40	117.3(4)	O8-C44-C16	121.3(4)	C80-C92-C91	123.3(5)
C13-C12-C40	118.8(4)	O8-C44-C43	117.4(4)	O10-C93-C63	123.8(4)
C12-C13-H13	106.2	C16-C44-C43	121.3(4)	O10-C93-C94	114.4(4)
C12-C13-C14	108.8(3)	C29-C45-C46	119.1(4)	C63-C93-C94	121.8(4)
C12-C13-C26	114.5(3)	C29-C45-C63	119.0(4)	C66-C94-C93	118.7(4)
H13-C13-C14	106.2	C46-C45-C63	121.0(4)	C66-C94-H94	120.6
H13-C13-C26	106.2	C45-C46-H46	120.6	C93-C94-H94	120.7
C14-C13-C26	114.3(3)	C45-C46-C66	118.7(4)	C67-C95-H95A	109.5
C13-C14-C15	123.5(4)	H46-C46-C66	120.6	C67-C95-H95B	109.5
C13-C14-C42	119.3(4)	H47-C47-C48	120.3	C67-C95-H95C	109.5
C15-C14-C42	117.0(4)	H47-C47-C68	120.2	H95A-C95-H95B	109.5
C14-C15-H15	118.8	C48-C47-C68	119.5(5)	H95A-C95-H95C	109.5
C14-C15-C16	122.4(4)	C47-C48-C49	118.6(4)	H95B-C95-H95C	109.4
H15-C15-C16	118.8	C47-C48-C96	119.9(7)	Br6-C96-C48	109.6(9)
C1-C16-C15	122.9(3)	C49-C48-C96	121.6(7)	Br6-C96-H96A	110
C1-C16-C44	119.4(3)	C48-C49-H49	119.3	Br6-C96-H96B	110
C15-C16-C44	117.6(4)	C48-C49-C70	121.3(4)	C48-C96-H96A	110
C1-C17-H17A	109.5	H49-C49-C70	119.3	C48-C96-H96B	110
C1-C17-H17B	109.5	H50-C50-C64	120.9	H96A-C96-H96B	108
C1-C17-C18	110.6(4)	H50-C50-C71	121	C75-C97-H97A	109.4
H17A-C17-H17B	108.1	C64-C50-C71	118.1(4)	C75-C97-H97B	109.3
H17A-C17-C18	109.5	H51-C51-C64	120.6	C75-C97-C98	111.6(5)
H17B-C17-C18	109.5	H51-C51-C73	120.6	H97A-C97-H97B	108
C17-C18-H18A	108.8	C64-C51-C73	118.8(4)	H97A-C97-C98	109.3
C17-C18-H18B	108.7	H52-C52-C53	119.8	H97B-C97-C98	109.2
C17-C18-C19	113.9(4)	H52-C52-C74	119.8	C97-C98-H98A	109.4
H18A-C18-H18B	107.7	C53-C52-C74	120.4(5)	C97-C98-H98B	109.4
H18A-C18-C19	108.8	C52-C53-C54	117.8(5)	C97-C98-H98C	109.4
H18B-C18-C19	108.7	C52-C53-C99	120.6(5)	H98A-C98-H98B	109.5
Br1-C19-C18	112.1(3)	C54-C53-C99	121.6(5)	H98A-C98-H98C	109.6
Br1-C19-H19A	109.2	C53-C54-H54	119.7	H98B-C98-H98C	109.5
Br1-C19-H19B	109.1	C53-C54-C76	120.7(5)	Br5-C99-C53	110.8(4)
C18-C19-H19A	109.3	H54-C54-C76	119.6	Br5-C99-H99A	109.5
C18-C19-H19B	109.2	H55-C55-C65	120.7	Br5-C99-H99B	109.5
H19A-C19-H19B	107.9	H55-C55-C77	120.7	C53-C99-H99A	109.6
C5-C20-H20A	109.1	C65-C55-C77	118.6(4)	C53-C99-H99B	109.5
C5-C20-H20B	109.1	H56-C56-C65	120.7	H99A-C99-H99B	108
C5-C20-C21	112.6(4)	H56-C56-C79	120.7	C82-C100-H10A	109
H20A-C20-H20B	107.9	C65-C56-C79	118.5(4)	C82-C100-H10B	109
H20A-C20-C21	109.1	H57-C57-C58	120.1	C82-C100-C101	113.0(5)
H20B-C20-C21	109.1	H57-C57-C81	120.1	H10A-C100-H10B	107.8
C20-C21-H21A	108.9	C58-C57-C81	119.8(5)	H10A-C100-C101	109
C20-C21-H21B	108.8	C57-C58-C59	119.2(5)	H10B-C100-C101	109
C20-C21-C22	113.6(4)	C57-C58-C102	120.5(5)	C100-C101-H10C	109.4
H21A-C21-H21B	107.7	C59-C58-C102	120.3(5)	C100-C101-H10D	109.5
H21A-C21-C22	108.8	C58-C59-H59	120	C100-C101-H10E	109.4
H21B-C21-C22	108.8	C58-C59-C83	120.2(5)	H10C-C101-H10D	109.6
Br2-C22-C21	113.1(4)	H59-C59-C83	119.8	H10C-C101-H10E	109.5
Br2-C22-H22A	108.9	H60-C60-C61	120.6	H10D-C101-H10E	109.5
Br2-C22-H22B	109	H60-C60-C85	120.5	Br8-C102-C58	111.0(4)
C21-C22-H22A	108.9	C61-C60-C85	118.9(4)	Br8-C102-H10F	109.4
C21-C22-H22B	109	C41-C61-C60	119.0(4)	Br8-C102-H10G	109.4
H22A-C22-H22B	107.8	C41-C61-C62	119.3(4)	C58-C102-H10F	109.4
C9-C23-H23A	109.2	C60-C61-C62	121.1(4)	C58-C102-H10G	109.5
C9-C23-H23B	109.3	C61-C62-H62	120.9	H10F-C102-H10G	108.1
C9-C23-C24	111.6(4)	C61-C62-C87	118.1(4)	C91-C103-H10H	109.2
H23A-C23-H23B	107.9	H62-C62-C87	120.9	C91-C103-H10I	109.2
H23A-C23-C24	109.3	C45-C63-H63	120.8	C91-C103-C104	112.3(5)
H23B-C23-C24	109.3	C45-C63-C93	118.4(4)	H10H-C103-H10I	107.9

C23-C24-H24A	109.5	H63-C63-C93	120.8	H10H-C103-C104	109
C23-C24-H24B	109.5	C33-C64-C50	119.5(4)	H10I-C103-C104	109.1
C23-C24-C25	110.6(4)	C33-C64-C51	118.7(4)	C103-C104-H10J	109.5
H24A-C24-H24B	108.1	C50-C64-C51	121.2(4)	C103-C104-H10K	109.4
H24A-C24-C25	109.5	C37-C65-C55	119.4(4)	C103-C104-H10L	109.5
H24B-C24-C25	109.6	C37-C65-C56	118.6(4)	H10J-C104-H10K	109.5
Br3-C25-C24	112.1(3)	C55-C65-C56	121.1(4)	H10J-C104-H10L	109.6
Br3-C25-H25A	109.2	O11-C66-C46	124.0(4)	H10K-C104-H10L	109.4
Br3-C25-H25B	109.2	O11-C66-C94	114.6(4)	Br7-C105-C90	108.9(5)
C24-C25-H25A	109.2	C46-C66-C94	121.4(4)	Br7-C105-H10M	109.9
C24-C25-H25B	109.2	H67A-C67-H67B	107.5	Br7-C105-H10N	109.9
H25A-C25-H25B	107.9	H67A-C67-C69	108.6	C90-C105-H10M	109.9
C13-C26-H26A	109.3	H67A-C67-C95	108.5	C90-C105-H10N	109.9
C13-C26-H26B	109.3	H67B-C67-C69	108.6	H10M-C105-H10N	108.3
C13-C26-C27	111.6(4)	H67B-C67-C95	108.6	Cl1-C106-Cl2	112.5(3)
H26A-C26-H26B	108	C69-C67-C95	114.8(4)	Cl1-C106-Cl3	111.7(3)
H26A-C26-C27	109.3	O11-C68-C47	118.9(4)	Cl1-C106-H106	107
H26B-C26-C27	109.3	O11-C68-C69	117.4(4)	Cl2-C106-Cl3	111.3(3)
C26-C27-H27A	108.6	C47-C68-C69	123.2(4)	Cl2-C106-H106	106.9
C26-C27-H27B	108.5	C67-C69-C68	121.8(4)	Cl3-C106-H106	107
C26-C27-C28	115.0(4)	C67-C69-C70	122.3(4)	Cl4-C107-Cl5	112.5(3)
H27A-C27-H27B	107.5	C68-C69-C70	115.8(4)	Cl4-C107-Cl6	110.0(3)
H27A-C27-C28	108.5	O12-C70-C49	117.2(4)	Cl4-C107-H107	108.2
H27B-C27-C28	108.5	O12-C70-C69	120.9(4)	Cl5-C107-Cl6	109.8(3)
Br4-C28-C27	112.7(3)	C49-C70-C69	121.6(4)	Cl5-C107-H107	108.1
Br4-C28-H28A	109	O12-C71-C50	121.8(4)	Cl6-C107-H107	108.1
Br4-C28-H28B	109	O12-C71-C72	115.9(4)		
C27-C28-H28A	109.1	C50-C71-C72	122.3(4)		

Table 24: Torsion angles (°) for **72**.

C30-O1-C29-O8	101.9(4)	C13-C14-C42-C43	-174.8(4)	H54-C54-C76-O14	-6.2
C30-O1-C29-H29	-16.6	C15-C14-C42-O7	179.9(4)	H54-C54-C76-C75	178.5
C30-O1-C29-C45	-135.1(4)	C15-C14-C42-C43	0.7(6)	H55-C55-C65-C37	9.8
C29-O1-C30-C2	-76.6(5)	C14-C15-C16-C1	-178.7(4)	H55-C55-C65-C56	178.9
C29-O1-C30-C31	101.7(4)	C14-C15-C16-C44	-0.4(6)	C77-C55-C65-C37	-170.1(4)
C33-O2-C32-C4	82.2(5)	H15-C15-C16-C1	1.2	C77-C55-C65-C56	-1.0(7)
C33-O2-C32-C31	-96.6(4)	H15-C15-C16-C44	179.5	H55-C55-C77-O14	-1.9
C32-O2-C33-O3	-100.8(4)	C1-C16-C44-O8	1.2(6)	H55-C55-C77-C78	-179.5
C32-O2-C33-H33	18.9	C1-C16-C44-C43	-178.9(4)	C65-C55-C77-O14	178.0(4)
C32-O2-C33-C64	137.8(3)	C15-C16-C44-O8	-177.2(4)	C65-C55-C77-C78	0.4(7)
C34-O3-C33-O2	97.6(4)	C15-C16-C44-C43	2.7(6)	H56-C56-C65-C37	-10.1
C34-O3-C33-H33	-22.1	C1-C17-C18-H18A	-60.7	H56-C56-C65-C55	-179.3
C34-O3-C33-C64	-141.3(3)	C1-C17-C18-H18B	56.3	C79-C56-C65-C37	170.0(4)
C33-O3-C34-C6	-77.5(5)	C1-C17-C18-C19	177.8(4)	C79-C56-C65-C55	0.8(7)
C33-O3-C34-C35	100.7(4)	H17A-C17-C18-H18A	178.5	H56-C56-C79-O15	2.8
C37-O4-C36-C8	74.4(5)	H17A-C17-C18-H18B	-64.5	H56-C56-C79-C78	-180
C37-O4-C36-C35	-104.0(4)	H17A-C17-C18-C19	57	C65-C56-C79-O15	-177.3(4)
C36-O4-C37-O5	-100.5(4)	H17B-C17-C18-H18A	60.1	C65-C56-C79-C78	-0.1(7)
C36-O4-C37-H37	18.4	H17B-C17-C18-H18B	177.1	H57-C57-C58-C59	179
C36-O4-C37-C65	136.9(4)	H17B-C17-C18-C19	-61.4	H57-C57-C58-C102	-3.1
C38-O5-C37-O4	103.5(4)	C17-C18-C19-Br1	70.2(5)	C81-C57-C58-C59	-1.0(7)
C38-O5-C37-H37	-15.3	C17-C18-C19-H19A	-50.9	C81-C57-C58-C102	176.9(5)
C38-O5-C37-C65	-133.5(4)	C17-C18-C19-H19B	-168.7	H57-C57-C81-O15	7.4
C37-O5-C38-C10	-78.6(5)	H18A-C18-C19-Br1	-51.3	H57-C57-C81-C82	-178.8
C37-O5-C38-C39	100.6(4)	H18A-C18-C19-H19A	-172.4	C58-C57-C81-O15	-172.6(5)
C41-O6-C40-C12	79.5(5)	H18A-C18-C19-H19B	69.7	C58-C57-C81-C82	1.1(8)
C41-O6-C40-C39	-100.1(4)	H18B-C18-C19-Br1	-168.3	C57-C58-C59-H59	-179.3
C40-O6-C41-O7	-98.1(4)	H18B-C18-C19-H19A	70.6	C57-C58-C59-C83	0.8(7)
C40-O6-C41-H41	21.7	H18B-C18-C19-H19B	-47.3	C102-C58-C59-H59	2.8
C40-O6-C41-C61	140.5(3)	C5-C20-C21-H21A	55.5	C102-C58-C59-C83	-177.2(5)
C42-O7-C41-O6	98.7(4)	C5-C20-C21-H21B	-61.7	C57-C58-C102-Br8	-88.6(5)
C42-O7-C41-H41	-21.1	C5-C20-C21-C22	176.9(4)	C57-C58-C102-H10F	150.6
C42-O7-C41-C61	-140.0(3)	H20A-C20-C21-H21A	-65.7	C57-C58-C102-H10G	32.3
C41-O7-C42-C14	-81.6(5)	H20A-C20-C21-H21B	177.1	C59-C58-C102-Br8	89.4(5)
C41-O7-C42-C43	97.6(4)	H20A-C20-C21-C22	55.7	C59-C58-C102-H10F	-31.5
C44-O8-C29-O1	-102.3(4)	H20B-C20-C21-H21A	176.7	C59-C58-C102-H10G	-149.7
C44-O8-C29-H29	16.3	H20B-C20-C21-H21B	59.5	C58-C59-C83-O16	175.8(4)
C44-O8-C29-C45	134.8(4)	H20B-C20-C21-C22	-61.9	C58-C59-C83-C82	-0.6(8)
C29-O8-C44-C16	76.4(5)	C20-C21-C22-Br2	62.7(5)	H59-C59-C83-O16	-4.2
C29-O8-C44-C43	-103.5(4)	C20-C21-C22-H22A	-58.6	H59-C59-C83-C82	179.4
C88-O9-C87-C62	26.1(6)	C20-C21-C22-H22B	-175.9	H60-C60-C61-C41	9.5
C88-O9-C87-C86	-153.8(4)	H21A-C21-C22-Br2	-175.8	H60-C60-C61-C62	-178.8
C87-O9-C88-C89	-106.0(5)	H21A-C21-C22-H22A	62.9	C85-C60-C61-C41	-170.6(4)
C87-O9-C88-C91	77.5(5)	H21A-C21-C22-H22B	-54.5	C85-C60-C61-C62	1.1(7)
C93-O10-C92-C80	77.7(6)	H21B-C21-C22-Br2	-58.7	H60-C60-C85-O16	-1.6
C93-O10-C92-C91	-106.7(5)	H21B-C21-C22-H22A	-180	H60-C60-C85-C86	178.7
C92-O10-C93-C63	-0.3(6)	H21B-C21-C22-H22B	62.6	C61-C60-C85-O16	178.5(4)
C92-O10-C93-C94	177.9(4)	C9-C23-C24-H24A	-78.5	C61-C60-C85-C86	-1.2(7)
C68-O11-C66-C46	4.3(7)	C9-C23-C24-H24B	39.8	C41-C61-C62-H62	-9
C68-O11-C66-C94	-174.4(4)	C9-C23-C24-C25	160.7(4)	C41-C61-C62-C87	171.0(4)
C66-O11-C68-C47	-85.2(6)	H23A-C23-C24-H24A	42.5	C60-C61-C62-H62	179.3
C66-O11-C68-C69	102.4(5)	H23A-C23-C24-H24B	160.8	C60-C61-C62-C87	-0.7(7)
C71-O12-C70-C49	117.2(4)	H23A-C23-C24-C25	-78.3	C61-C62-C87-O9	-179.6(4)
C71-O12-C70-C69	-69.3(5)	H23B-C23-C24-H24A	160.4	C61-C62-C87-C86	0.3(7)
C70-O12-C71-C50	-36.4(6)	H23B-C23-C24-H24B	-81.2	H62-C62-C87-O9	0.4
C70-O12-C71-C72	143.6(4)	H23B-C23-C24-C25	39.6	H62-C62-C87-C86	-179.7
C74-O13-C73-C51	15.2(6)	C23-C24-C25-Br3	171.3(3)	C45-C63-C93-O10	177.9(4)
C74-O13-C73-C72	-163.9(4)	C23-C24-C25-H25A	50.2	C45-C63-C93-C94	-0.0(7)
C73-O13-C74-C52	-97.5(5)	C23-C24-C25-H25B	-67.6	H63-C63-C93-O10	-2.1
C73-O13-C74-C75	86.6(5)	H24A-C24-C25-Br3	50.5	H63-C63-C93-C94	179.9
C77-O14-C76-C54	80.1(6)	H24A-C24-C25-H25A	-70.6	O11-C66-C94-C93	178.9(4)
C77-O14-C76-C75	-104.3(5)	H24A-C24-C25-H25B	171.7	O11-C66-C94-H94	-1
C76-O14-C77-C55	-1.6(7)	H24B-C24-C25-Br3	-67.9	C46-C66-C94-C93	0.2(7)
C76-O14-C77-C78	176.1(4)	H24B-C24-C25-H25A	171	C46-C66-C94-H94	-179.7
C81-O15-C79-C56	8.0(7)	H24B-C24-C25-H25B	53.3	H67A-C67-C69-C68	155.5

C81-O15-C79-C78	-169.4(4)	C13-C26-C27-H27A	-168.3	H67A-C67-C69-C70	-20.2
C79-O15-C81-C57	-83.3(6)	C13-C26-C27-H27B	-51.7	H67B-C67-C69-C68	38.8
C79-O15-C81-C82	102.6(6)	C13-C26-C27-C28	70.0(5)	H67B-C67-C69-C70	-136.9
C85-O16-C83-C59	102.6(5)	H26A-C26-C27-H27A	-47.3	C95-C67-C69-C68	-82.8(6)
C85-O16-C83-C82	-80.9(6)	H26A-C26-C27-H27B	69.3	C95-C67-C69-C70	101.5(5)
C83-O16-C85-C60	-23.7(7)	H26A-C26-C27-C28	-169	H67A-C67-C95-H95A	-59.5
C83-O16-C85-C86	156.0(4)	H26B-C26-C27-H27A	70.7	H67A-C67-C95-H95B	-179.5
H1-C1-C2-C3	156.4	H26B-C26-C27-H27B	-172.8	H67A-C67-C95-H95C	60.5
H1-C1-C2-C30	-27	H26B-C26-C27-C28	-51.1	H67B-C67-C95-H95A	57.1
C16-C1-C2-C3	-89.7(5)	C26-C27-C28-Br4	67.1(5)	H67B-C67-C95-H95B	-62.9
C16-C1-C2-C30	86.9(5)	C26-C27-C28-H28A	-54.1	H67B-C67-C95-H95C	177.1
C17-C1-C2-C3	40.7(6)	C26-C27-C28-H28B	-171.6	C69-C67-C95-H95A	178.8
C17-C1-C2-C30	-142.7(4)	H27A-C27-C28-Br4	-54.6	C69-C67-C95-H95B	58.8
H1-C1-C16-C15	-154.7	H27A-C27-C28-H28A	-175.8	C69-C67-C95-H95C	-61.2
H1-C1-C16-C44	27	H27A-C27-C28-H28B	66.6	O11-C68-C69-C67	-2.6(7)
C2-C1-C16-C15	91.4(5)	H27B-C27-C28-Br4	-171.2	O11-C68-C69-C70	173.3(4)
C2-C1-C16-C44	-86.9(4)	H27B-C27-C28-H28A	67.7	C47-C68-C69-C67	-174.7(5)
C17-C1-C16-C15	-38.7(5)	H27B-C27-C28-H28B	-49.9	C47-C68-C69-C70	1.3(7)
C17-C1-C16-C44	143.0(4)	O1-C29-C45-C46	32.4(5)	C67-C69-C70-O12	1.0(7)
H1-C1-C17-H17A	70.3	O1-C29-C45-C63	-158.3(4)	C67-C69-C70-C49	174.3(4)
H1-C1-C17-H17B	-171.3	O8-C29-C45-C46	155.4(4)	C68-C69-C70-O12	-174.9(4)
H1-C1-C17-C18	-50.5	O8-C29-C45-C63	-35.3(5)	C68-C69-C70-C49	-1.6(7)
C2-C1-C17-H17A	-174	H29-C29-C45-C46	-86.1	O12-C71-C72-H72	1.1
C2-C1-C17-H17B	-55.6	H29-C29-C45-C63	83.2	O12-C71-C72-C73	-178.8(4)
C2-C1-C17-C18	65.2(5)	O1-C30-C31-H31	3.6	C50-C71-C72-H72	-178.9
C16-C1-C17-H17A	-45.7	O1-C30-C31-C32	-176.4(4)	C50-C71-C72-C73	1.2(7)
C16-C1-C17-H17B	72.7	C2-C30-C31-H31	-178.1	C71-C72-C73-O13	179.0(4)
C16-C1-C17-C18	-166.5(4)	C2-C30-C31-C32	1.9(6)	C71-C72-C73-C51	-0.0(7)
C1-C2-C3-H3	-2.8	C30-C31-C32-O2	177.9(4)	H72-C72-C73-O13	-0.9
C1-C2-C3-C4	177.2(4)	C30-C31-C32-C4	-0.8(6)	H72-C72-C73-C51	-180
C30-C2-C3-H3	-179.5	H31-C31-C32-O2	-2.1	O13-C74-C75-C76	176.0(4)
C30-C2-C3-C4	0.5(6)	H31-C31-C32-C4	179.2	O13-C74-C75-C97	0.2(7)
C1-C2-C30-O1	-0.4(6)	O2-C33-C64-C50	-27.4(5)	C52-C74-C75-C76	0.3(7)
C1-C2-C30-C31	-178.6(4)	O2-C33-C64-C51	161.4(4)	C52-C74-C75-C97	-175.4(5)
C3-C2-C30-O1	176.5(4)	O3-C33-C64-C50	-149.2(4)	C74-C75-C76-O14	-175.1(4)
C3-C2-C30-C31	-1.8(6)	O3-C33-C64-C51	39.5(5)	C74-C75-C76-C54	0.4(7)
C2-C3-C4-C5	-175.4(4)	H33-C33-C64-C50	91.6	C97-C75-C76-O14	0.8(7)
C2-C3-C4-C32	0.6(6)	H33-C33-C64-C51	-79.7	C97-C75-C76-C54	176.2(5)
H3-C3-C4-C5	4.6	O3-C34-C35-H35	2.9	C74-C75-C97-H97A	-22
H3-C3-C4-C32	-179.4	O3-C34-C35-C36	-177.1(4)	C74-C75-C97-H97B	-140.1
C3-C4-C5-H5	-153.5	C6-C34-C35-H35	-178.8	C74-C75-C97-C98	99.0(6)
C3-C4-C5-C6	91.8(5)	C6-C34-C35-C36	1.1(7)	C76-C75-C97-H97A	162.4
C3-C4-C5-C20	-35.2(6)	C34-C35-C36-O4	176.0(4)	C76-C75-C97-H97B	44.4
C32-C4-C5-H5	30.6	C34-C35-C36-C8	-2.5(6)	C76-C75-C97-C98	-76.5(6)
C32-C4-C5-C6	-84.0(5)	H35-C35-C36-O4	-4.1	O14-C77-C78-H78	2.4
C32-C4-C5-C20	148.9(4)	H35-C35-C36-C8	177.5	O14-C77-C78-C79	-177.5(4)
C3-C4-C32-O2	-179.1(4)	O4-C37-C65-C55	-36.4(5)	C55-C77-C78-H78	-179.7
C3-C4-C32-C31	-0.4(6)	O4-C37-C65-C56	154.2(4)	C55-C77-C78-C79	0.3(7)
C5-C4-C32-O2	-3.0(6)	O5-C37-C65-C55	-159.7(4)	C77-C78-C79-O15	177.0(4)
C5-C4-C32-C31	175.7(4)	O5-C37-C65-C56	30.9(5)	C77-C78-C79-C56	-0.5(7)
C4-C5-C6-C7	-92.2(5)	H37-C37-C65-C55	82.1	H78-C78-C79-O15	-3
C4-C5-C6-C34	85.5(5)	H37-C37-C65-C56	-87.3	H78-C78-C79-C56	179.5
H5-C5-C6-C7	153.1	O5-C38-C39-H39	3	O15-C81-C82-C83	173.0(5)
H5-C5-C6-C34	-29.2	O5-C38-C39-C40	-176.9(4)	O15-C81-C82-C100	-4.6(8)
C20-C5-C6-C7	36.3(5)	C10-C38-C39-H39	-177.8	C57-C81-C82-C83	-0.9(8)
C20-C5-C6-C34	-146.0(4)	C10-C38-C39-C40	2.2(6)	C57-C81-C82-C100	-178.5(5)
C4-C5-C20-H20A	52.1	C38-C39-C40-O6	178.9(4)	H80-C80-C90-C89	178.8
C4-C5-C20-H20B	169.7	C38-C39-C40-C12	-0.7(7)	H80-C80-C90-C105	0.8
C4-C5-C20-C21	-69.1(5)	H39-C39-C40-O6	-1.1	C92-C80-C90-C89	-1.1(7)
H5-C5-C20-H20A	170.4	H39-C39-C40-C12	179.3	C92-C80-C90-C105	-179.1(5)
H5-C5-C20-H20B	-72	O6-C41-C61-C60	-30.9(5)	H80-C80-C92-O10	-3.9
H5-C5-C20-C21	49.2	O6-C41-C61-C62	157.2(4)	H80-C80-C92-C91	-179.1
C6-C5-C20-H20A	-72.7	O7-C41-C61-C60	-153.2(4)	C90-C80-C92-O10	176.1(4)
C6-C5-C20-H20B	44.9	O7-C41-C61-C62	34.8(5)	C90-C80-C92-C91	0.8(8)
C6-C5-C20-C21	166.1(4)	H41-C41-C61-C60	87.9	C81-C82-C83-O16	-175.6(5)
C5-C6-C7-H7	-3	H41-C41-C61-C62	-84	C81-C82-C83-C59	0.7(8)
C5-C6-C7-C8	177.2(4)	O7-C42-C43-H43	2.4	C100-C82-C83-O16	2.0(8)

C34-C6-C7-H7	179.2	O7-C42-C43-C44	-177.7(4)	C100-C82-C83-C59	178.3(5)
C34-C6-C7-C8	-0.6(6)	C14-C42-C43-H43	-178.5	C81-C82-C100-H10A	156.8
C5-C6-C34-O3	0.7(6)	C14-C42-C43-C44	1.5(7)	C81-C82-C100-H10B	39.4
C5-C6-C34-C35	-177.5(4)	C42-C43-C44-O8	176.6(4)	C81-C82-C100-C101	-81.9(7)
C7-C6-C34-O3	178.5(4)	C42-C43-C44-C16	-3.3(6)	C83-C82-C100-H10A	-20.6
C7-C6-C34-C35	0.4(6)	H43-C43-C44-O8	-3.4	C83-C82-C100-H10B	-138
C6-C7-C8-C9	-178.6(4)	H43-C43-C44-C16	176.7	C83-C82-C100-C101	100.7(7)
C6-C7-C8-C36	-0.6(6)	C29-C45-C46-H46	-12.7	O16-C85-C86-H86	0.9
H7-C7-C8-C9	1.6	C29-C45-C46-C66	167.2(4)	O16-C85-C86-C87	-178.9(4)
H7-C7-C8-C36	179.5	C63-C45-C46-H46	178.1	C60-C85-C86-H86	-179.4
C7-C8-C9-H9	-156.1	C63-C45-C46-C66	-1.9(7)	C60-C85-C86-C87	0.8(7)
C7-C8-C9-C10	89.4(4)	C29-C45-C63-H63	12.3	C85-C86-C87-O9	179.5(4)
C7-C8-C9-C23	-39.6(5)	C29-C45-C63-C93	-167.7(4)	C85-C86-C87-C62	-0.4(7)
C36-C8-C9-H9	26.1	C46-C45-C63-H63	-178.6	H86-C86-C87-O9	-0.3
C36-C8-C9-C10	-88.5(4)	C46-C45-C63-C93	1.4(6)	H86-C86-C87-C62	179.8
C36-C8-C9-C23	142.5(4)	C45-C46-C66-O11	-177.5(4)	O9-C88-C89-H89	4.8
C7-C8-C36-O4	-176.2(4)	C45-C46-C66-C94	1.2(7)	O9-C88-C89-C90	-175.2(4)
C7-C8-C36-C35	2.2(6)	H46-C46-C66-O11	2.5	C91-C88-C89-H89	-178.9
C9-C8-C36-O4	1.9(6)	H46-C46-C66-C94	-178.9	C91-C88-C89-C90	1.1(7)
C9-C8-C36-C35	-179.8(4)	H47-C47-C48-C49	178.5	O9-C88-C91-C92	174.9(4)
C8-C9-C10-C11	-88.8(5)	H47-C47-C48-C96	-1	O9-C88-C91-C103	-2.6(7)
C8-C9-C10-C38	87.2(4)	C68-C47-C48-C49	-1.4(7)	C89-C88-C91-C92	-1.4(7)
H9-C9-C10-C11	156.7	C68-C47-C48-C96	178.6(8)	C89-C88-C91-C103	-178.9(5)
H9-C9-C10-C38	-27.3	H47-C47-C68-O11	8.3	C88-C89-C90-C80	0.2(7)
C23-C9-C10-C11	40.0(5)	H47-C47-C68-C69	-179.7	C88-C89-C90-C105	178.2(5)
C23-C9-C10-C38	-143.9(4)	C48-C47-C68-O11	-171.7(4)	H89-C89-C90-C80	-179.8
C8-C9-C23-H23A	67	C48-C47-C68-C69	0.2(8)	H89-C89-C90-C105	-1.8
C8-C9-C23-H23B	-50.9	C47-C48-C49-H49	-179	C80-C90-C105-Br7	-67.7(6)
C8-C9-C23-C24	-172.0(3)	C47-C48-C49-C70	1.1(7)	C80-C90-C105-H10M	171.9
H9-C9-C23-H23A	-176.5	C96-C48-C49-H49	1	C80-C90-C105-H10N	52.8
H9-C9-C23-H23B	65.6	C96-C48-C49-C70	-178.9(8)	C89-C90-C105-Br7	114.3(5)
H9-C9-C23-C24	-55.5	C47-C48-C96-Br6	-125.5(7)	C89-C90-C105-H10M	-6
C10-C9-C23-H23A	-59.8	C47-C48-C96-H96A	114	C89-C90-C105-H10N	-125.2
C10-C9-C23-H23B	-177.7	C47-C48-C96-H96B	-5	C88-C91-C92-O10	-174.9(4)
C10-C9-C23-C24	61.2(5)	C49-C48-C96-Br6	54(1)	C88-C91-C92-C80	0.5(7)
C9-C10-C11-H11	-2.6	C49-C48-C96-H96A	-66	C103-C91-C92-O10	2.6(7)
C9-C10-C11-C12	177.5(4)	C49-C48-C96-H96B	175.2	C103-C91-C92-C80	178.0(5)
C38-C10-C11-H11	-178.6	C48-C49-C70-O12	174.0(4)	C88-C91-C103-H10H	-34.5
C38-C10-C11-C12	1.4(6)	C48-C49-C70-C69	0.5(7)	C88-C91-C103-H10I	-152.3
C9-C10-C38-O5	0.3(6)	H49-C49-C70-O12	-5.9	C88-C91-C103-C104	86.6(6)
C9-C10-C38-C39	-178.8(4)	H49-C49-C70-C69	-179.5	C92-C91-C103-H10H	148.2
C11-C10-C38-O5	176.6(4)	H50-C50-C64-C33	9.7	C92-C91-C103-H10I	30.4
C11-C10-C38-C39	-2.6(6)	H50-C50-C64-C51	-179.3	C92-C91-C103-C104	-90.8(6)
C10-C11-C12-C13	-178.0(4)	C71-C50-C64-C33	-170.3(4)	O10-C93-C94-C66	-178.9(4)
C10-C11-C12-C40	-0.0(6)	C71-C50-C64-C51	0.8(7)	O10-C93-C94-H94	1
H11-C11-C12-C13	2.1	H50-C50-C71-O12	-1.5	C63-C93-C94-C66	-0.7(7)
H11-C11-C12-C40	-180	H50-C50-C71-C72	178.5	C63-C93-C94-H94	179.1
C11-C12-C13-H13	-155.2	C64-C50-C71-O12	178.4(4)	C75-C97-C98-H98A	57.9
C11-C12-C13-C14	90.9(5)	C64-C50-C71-C72	-1.5(7)	C75-C97-C98-H98B	-62.1
C11-C12-C13-C26	-38.3(6)	H51-C51-C64-C33	-8.6	C75-C97-C98-H98C	178
C40-C12-C13-H13	26.9	H51-C51-C64-C50	-179.8	H97A-C97-C98-H98A	179
C40-C12-C13-C14	-87.0(5)	C73-C51-C64-C33	171.4(4)	H97A-C97-C98-H98B	59
C40-C12-C13-C26	143.8(4)	C73-C51-C64-C50	0.3(7)	H97A-C97-C98-H98C	-60.9
C11-C12-C40-O6	-179.9(4)	H51-C51-C73-O13	0.4	H97B-C97-C98-H98A	-63.1
C11-C12-C40-C39	-0.3(6)	H51-C51-C73-C72	179.4	H97B-C97-C98-H98B	176.9
C13-C12-C40-O6	-1.8(6)	C64-C51-C73-O13	-179.6(4)	H97B-C97-C98-H98C	57
C13-C12-C40-C39	177.7(4)	C64-C51-C73-C72	-0.7(7)	C82-C100-C101-H10C	59.4
C12-C13-C14-C15	-89.1(5)	H52-C52-C53-C54	178.7	C82-C100-C101-H10D	-60.7
C12-C13-C14-C42	86.2(5)	H52-C52-C53-C99	-1.4	C82-C100-C101-H10E	179.3
H13-C13-C14-C15	157	C74-C52-C53-C54	-1.3(7)	H10A-C100-C101-H10C	-179.3
H13-C13-C14-C42	-27.7	C74-C52-C53-C99	178.7(5)	H10A-C100-C101-H10D	60.6
C26-C13-C14-C15	40.3(6)	H52-C52-C74-O13	4.5	H10A-C100-C101-H10E	-59.4
C26-C13-C14-C42	-144.5(4)	H52-C52-C74-C75	-179.8	H10B-C100-C101-H10C	-61.9
C12-C13-C26-H26A	76.4	C53-C52-C74-O13	-175.5(4)	H10B-C100-C101-H10D	178
C12-C13-C26-H26B	-41.6	C53-C52-C74-C75	0.2(8)	H10B-C100-C101-H10E	58
C12-C13-C26-C27	-162.6(4)	C52-C53-C54-H54	-178	C91-C103-C104-H10J	170.6
H13-C13-C26-H26A	-166.8	C52-C53-C54-C76	2.0(7)	C91-C103-C104-H10K	50.6

H13-C13-C26-H26B	75.3	C99-C53-C54-H54	2	C91-C103-C104-H10L	-69.3
H13-C13-C26-C27	-45.8	C99-C53-C54-C76	-178.0(5)	H10H-C103-C104-H10J	-68.3
C14-C13-C26-H26A	-50.1	C52-C53-C99-Br5	-132.6(4)	H10H-C103-C104-H10K	171.7
C14-C13-C26-H26B	-168	C52-C53-C99-H99A	106.5	H10H-C103-C104-H10L	51.8
C14-C13-C26-C27	71.0(5)	C52-C53-C99-H99B	-11.8	H10I-C103-C104-H10J	49.4
C13-C14-C15-H15	-5.8	C54-C53-C99-Br5	47.4(6)	H10I-C103-C104-H10K	-70.6
C13-C14-C15-C16	174.1(4)	C54-C53-C99-H99A	-73.5	H10I-C103-C104-H10L	169.5
C42-C14-C15-H15	178.8	C54-C53-C99-H99B	168.2	H54-C54-C76-O14	-6.2
C42-C14-C15-C16	-1.3(6)	C53-C54-C76-O14	173.8(4)		
C13-C14-C42-O7	4.3(6)	C53-C54-C76-C75	-1.5(8)		

Table 25: Anisotropic displacement parameters for **72**. The anisotropic displacement factor takes the form:
$-2\pi^2[h^2a^{*2}U_{11} + \cdots + 2hka^*b^*U_{12}]$.

Atom	U_{11}	U_{22}	U_{33}	U_{23}	U_{13}	U_{12}
Br1	0.0419(3)	0.0628(4)	0.0344(3)	0.0150(3)	-0.0023(2)	-0.0237(3)
Br2	0.0526(4)	0.0475(3)	0.0379(3)	-0.0007(2)	0.0137(3)	-0.0278(3)
Br3	0.0280(3)	0.0553(4)	0.0399(3)	-0.0160(3)	0.0044(2)	0.0061(3)
Br4	0.0344(3)	0.0289(3)	0.0682(4)	0.0004(3)	0.0004(3)	0.0045(2)
Br5	0.0375(3)	0.0343(3)	0.0512(3)	-0.0059(2)	-0.0125(2)	-0.0092(2)
Br6	0.0667(10)	0.0525(9)	0.0567(8)	-0.0180(6)	-0.0300(7)	0.0314(6)
Br6A	0.0667(10)	0.0525(9)	0.0567(8)	-0.0180(6)	-0.0300(7)	0.0314(6)
Br7	0.1570(11)	0.0373(4)	0.0386(4)	-0.0019(3)	-0.0152(5)	0.0104(5)
Br7A	0.1570(11)	0.0373(4)	0.0386(4)	-0.0019(3)	-0.0152(5)	0.0104(5)
Br8	0.0388(3)	0.0638(4)	0.0404(3)	-0.0097(3)	0.0017(3)	0.0136(3)
O1	0.0135(13)	0.0159(14)	0.0191(13)	0.0029(11)	0.0005(11)	-0.0026(12)
O2	0.0180(14)	0.0128(13)	0.0182(13)	-0.0007(10)	-0.0040(11)	-0.0018(12)
O3	0.0140(13)	0.0142(14)	0.0247(14)	-0.0016(11)	0.0016(11)	-0.0011(12)
O4	0.0187(14)	0.0158(14)	0.0183(13)	0.0015(11)	-0.0055(11)	-0.0022(12)
O5	0.0160(13)	0.0159(14)	0.0185(13)	-0.0050(11)	-0.0033(11)	-0.0007(12)
O6	0.0162(14)	0.0166(14)	0.0201(14)	0.0026(11)	0.0017(11)	-0.0043(12)
O7	0.0194(14)	0.0147(14)	0.0169(13)	0.0026(10)	-0.0020(11)	-0.0036(12)
O8	0.0143(13)	0.0153(14)	0.0195(14)	-0.0026(11)	0.0012(11)	-0.0009(12)
O9	0.0159(15)	0.0315(19)	0.0410(19)	0.0183(15)	0.0025(14)	-0.0033(14)
O10	0.0284(16)	0.0174(15)	0.0275(16)	0.0044(12)	0.0091(13)	-0.0013(14)
O11	0.0356(19)	0.0184(16)	0.0385(19)	-0.0060(14)	0.0201(15)	-0.0062(15)
O12	0.0161(14)	0.0242(16)	0.0290(16)	-0.0102(13)	0.0018(12)	-0.0014(13)
O13	0.0235(16)	0.038(2)	0.0289(17)	-0.0159(14)	-0.0091(13)	0.0021(15)
O14	0.051(2)	0.0198(16)	0.0221(16)	-0.0069(13)	-0.0038(15)	-0.0015(16)
O15	0.121(4)	0.0194(18)	0.0148(16)	0.0016(13)	-0.009(2)	-0.002(2)
O16	0.038(2)	0.068(3)	0.0267(18)	0.0234(18)	-0.0111(16)	-0.027(2)
C1	0.0158(18)	0.015(2)	0.0158(18)	-0.0013(15)	-0.0027(15)	-0.0009(16)
C2	0.0151(18)	0.0155(19)	0.0119(17)	0.0011(14)	-0.0014(14)	-0.0012(16)
C3	0.0168(19)	0.016(2)	0.0147(18)	0.0009(15)	-0.0007(15)	0.0003(17)
C4	0.0145(18)	0.0152(19)	0.0147(18)	0.0022(14)	-0.0014(15)	-0.0017(16)
C5	0.0145(18)	0.0157(19)	0.0169(19)	0.0025(15)	0.0002(15)	-0.0026(16)
C6	0.0145(18)	0.0144(19)	0.0172(18)	0.0020(15)	0.0016(15)	-0.0047(16)
C7	0.0157(18)	0.0126(19)	0.0170(18)	0.0010(14)	0.0022(15)	-0.0045(16)
C8	0.0145(18)	0.0124(19)	0.0180(19)	0.0010(14)	0.0028(15)	-0.0048(16)
C9	0.0138(18)	0.0134(19)	0.0176(19)	-0.0005(14)	0.0020(15)	-0.0016(16)
C10	0.0126(17)	0.0100(18)	0.0186(19)	-0.0005(14)	0.0015(15)	0.0007(15)
C11	0.0150(18)	0.0156(19)	0.0137(17)	-0.0006(14)	0.0031(14)	-0.0004(16)
C12	0.0159(18)	0.0136(19)	0.0158(18)	-0.0035(14)	0.0016(15)	-0.0006(16)
C13	0.0145(18)	0.0149(19)	0.0151(18)	-0.0022(14)	0.0003(15)	-0.0025(16)
C14	0.0168(19)	0.0147(19)	0.0121(17)	-0.0022(14)	0.0005(14)	-0.0024(16)
C15	0.0183(19)	0.0161(19)	0.0132(17)	-0.0017(14)	0.0018(15)	-0.0032(17)
C16	0.0156(18)	0.0144(19)	0.0124(17)	0.0003(14)	-0.0013(14)	-0.0037(16)
C17	0.021(2)	0.022(2)	0.0140(18)	-0.0024(15)	-0.0016(16)	-0.0036(18)
C18	0.026(2)	0.025(2)	0.018(2)	0.0033(17)	-0.0037(17)	-0.0015(19)
C19	0.035(3)	0.031(3)	0.019(2)	0.0044(18)	-0.0072(19)	-0.007(2)
C20	0.020(2)	0.022(2)	0.020(2)	0.0045(16)	0.0010(16)	-0.0041(18)
C21	0.027(2)	0.040(3)	0.024(2)	0.011(2)	-0.0011(19)	-0.003(2)
C22	0.038(3)	0.050(3)	0.022(2)	0.010(2)	-0.005(2)	-0.014(3)
C23	0.0139(18)	0.017(2)	0.022(2)	0.0002(15)	0.0053(16)	-0.0012(17)
C24	0.021(2)	0.024(2)	0.027(2)	-0.0056(18)	0.0017(18)	0.0002(19)
C25	0.024(2)	0.037(3)	0.030(2)	-0.008(2)	0.0026(19)	-0.003(2)
C26	0.0192(19)	0.018(2)	0.0153(19)	-0.0010(15)	0.0032(15)	-0.0039(17)
C27	0.024(2)	0.025(2)	0.019(2)	-0.0041(17)	0.0021(17)	-0.0022(19)
C28	0.034(3)	0.032(3)	0.025(2)	-0.0056(19)	0.0044(19)	-0.015(2)
C29	0.0176(19)	0.0129(19)	0.0178(19)	-0.0023(15)	-0.0001(15)	-0.0018(16)
C30	0.0129(18)	0.017(2)	0.0168(18)	0.0017(15)	0.0012(15)	-0.0034(16)

C31	0.0168(19)	0.017(2)	0.0146(18)	0.0017(15)	0.0002(15)	-0.0010(17)
C32	0.0185(19)	0.0124(19)	0.0152(18)	0.0003(14)	-0.0006(15)	-0.0024(16)
C33	0.0155(18)	0.0158(19)	0.0155(18)	0.0010(15)	-0.0026(15)	-0.0025(16)
C34	0.0142(18)	0.0117(19)	0.0217(19)	-0.0002(15)	0.0002(15)	-0.0019(16)
C35	0.0183(19)	0.015(2)	0.0195(19)	-0.0034(15)	-0.0002(16)	-0.0045(17)
C36	0.0154(18)	0.015(2)	0.0198(19)	-0.0008(15)	0.0003(15)	-0.0049(17)
C37	0.0169(19)	0.0134(19)	0.0177(19)	-0.0023(15)	-0.0002(15)	-0.0012(16)
C38	0.0170(19)	0.0140(19)	0.0169(18)	-0.0034(15)	-0.0031(15)	-0.0035(16)
C39	0.0197(19)	0.017(2)	0.0143(18)	0.0027(15)	-0.0006(15)	-0.0045(17)
C40	0.0172(19)	0.0136(19)	0.0166(18)	0.0002(15)	0.0020(15)	-0.0029(16)
C41	0.0174(19)	0.018(2)	0.0152(18)	-0.0001(15)	0.0015(15)	-0.0032(17)
C42	0.019(2)	0.0123(19)	0.0169(18)	0.0008(14)	-0.0018(15)	-0.0018(16)
C43	0.0180(19)	0.016(2)	0.0175(18)	-0.0001(15)	0.0016(15)	-0.0035(17)
C44	0.0154(19)	0.017(2)	0.0170(18)	-0.0039(15)	0.0003(15)	-0.0027(17)
C45	0.0138(18)	0.018(2)	0.0181(19)	-0.0008(15)	0.0001(15)	-0.0038(16)
C46	0.021(2)	0.019(2)	0.023(2)	0.0005(16)	0.0065(17)	-0.0058(18)
C47	0.021(2)	0.030(3)	0.032(2)	-0.012(2)	0.0053(18)	-0.007(2)
C48	0.025(2)	0.023(2)	0.026(2)	-0.0064(18)	-0.0026(18)	0.0016(19)
C49	0.024(2)	0.017(2)	0.026(2)	-0.0027(17)	0.0004(17)	-0.0012(18)
C50	0.020(2)	0.019(2)	0.0187(19)	-0.0024(15)	-0.0022(16)	-0.0028(17)
C51	0.019(2)	0.021(2)	0.024(2)	-0.0055(17)	-0.0023(17)	-0.0006(18)
C52	0.031(2)	0.017(2)	0.025(2)	-0.0066(17)	-0.0065(18)	0.0017(19)
C53	0.030(2)	0.025(2)	0.028(2)	-0.0125(18)	-0.0026(19)	-0.003(2)
C54	0.025(2)	0.026(2)	0.027(2)	-0.0081(18)	-0.0075(18)	0.001(2)
C55	0.024(2)	0.019(2)	0.019(2)	-0.0017(16)	-0.0038(16)	-0.0027(18)
C56	0.048(3)	0.016(2)	0.018(2)	-0.0029(16)	-0.004(2)	0.000(2)
C57	0.045(3)	0.028(2)	0.019(2)	0.0056(18)	-0.002(2)	-0.015(2)
C58	0.033(2)	0.023(2)	0.021(2)	0.0015(17)	0.0027(18)	-0.008(2)
C59	0.038(3)	0.023(2)	0.020(2)	0.0048(17)	-0.0008(19)	-0.009(2)
C60	0.021(2)	0.030(2)	0.024(2)	0.0074(18)	-0.0010(17)	-0.008(2)
C61	0.019(2)	0.019(2)	0.0182(19)	0.0043(15)	0.0015(16)	-0.0052(17)
C62	0.022(2)	0.021(2)	0.023(2)	0.0070(17)	-0.0004(17)	-0.0019(18)
C63	0.0156(19)	0.016(2)	0.028(2)	-0.0014(16)	0.0039(17)	-0.0022(17)
C64	0.020(2)	0.0128(19)	0.0192(19)	-0.0016(15)	-0.0002(16)	-0.0017(17)
C65	0.020(2)	0.020(2)	0.019(2)	-0.0047(16)	-0.0026(16)	-0.0030(18)
C66	0.021(2)	0.019(2)	0.026(2)	-0.0060(17)	0.0064(17)	-0.0048(18)
C67	0.026(2)	0.031(3)	0.027(2)	0.0067(19)	-0.0009(19)	-0.001(2)
C68	0.023(2)	0.012(2)	0.031(2)	-0.0029(17)	0.0111(18)	0.0003(18)
C69	0.018(2)	0.020(2)	0.028(2)	-0.0046(17)	0.0070(17)	0.0006(18)
C70	0.0144(19)	0.018(2)	0.026(2)	-0.0036(16)	0.0047(16)	0.0020(17)
C71	0.018(2)	0.018(2)	0.023(2)	-0.0018(16)	0.0005(16)	0.0005(17)
C72	0.022(2)	0.021(2)	0.024(2)	-0.0079(17)	-0.0007(17)	0.0001(18)
C73	0.023(2)	0.019(2)	0.022(2)	-0.0060(16)	-0.0036(17)	-0.0013(18)
C74	0.025(2)	0.025(2)	0.025(2)	-0.0113(18)	-0.0074(18)	0.003(2)
C75	0.031(2)	0.028(2)	0.025(2)	-0.0094(18)	-0.0053(19)	-0.006(2)
C76	0.039(3)	0.021(2)	0.019(2)	-0.0072(17)	-0.0058(19)	-0.001(2)
C77	0.028(2)	0.020(2)	0.021(2)	-0.0083(17)	-0.0033(17)	-0.0007(19)
C78	0.044(3)	0.026(2)	0.015(2)	-0.0005(17)	-0.0024(19)	-0.005(2)
C79	0.051(3)	0.024(2)	0.019(2)	-0.0001(18)	-0.006(2)	-0.003(2)
C81	0.067(4)	0.020(2)	0.013(2)	0.0030(17)	-0.003(2)	-0.001(2)
C80	0.022(2)	0.022(2)	0.033(2)	0.0065(18)	0.0031(19)	-0.0029(19)
C82	0.036(3)	0.043(3)	0.016(2)	0.009(2)	-0.0058(19)	0.007(2)
C83	0.032(2)	0.039(3)	0.017(2)	0.0092(18)	-0.0059(18)	-0.009(2)
C85	0.025(2)	0.030(3)	0.024(2)	0.0088(18)	-0.0038(18)	-0.004(2)
C86	0.027(2)	0.031(3)	0.023(2)	0.0126(18)	0.0022(18)	-0.008(2)
C87	0.019(2)	0.021(2)	0.032(2)	0.0059(18)	0.0041(18)	-0.0021(18)
C88	0.018(2)	0.024(2)	0.033(2)	0.0105(19)	0.0051(18)	-0.0042(19)
C89	0.029(2)	0.017(2)	0.034(2)	0.0055(18)	0.010(2)	-0.004(2)
C90	0.034(3)	0.027(2)	0.027(2)	0.0021(18)	0.002(2)	-0.012(2)
C91	0.021(2)	0.029(2)	0.026(2)	0.0074(18)	0.0049(18)	-0.011(2)

C92	0.024(2)	0.017(2)	0.029(2)	0.0049(17)	0.0063(18)	-0.0039(18)
C93	0.020(2)	0.018(2)	0.024(2)	0.0038(16)	-0.0004(17)	-0.0057(18)
C94	0.020(2)	0.021(2)	0.021(2)	-0.0013(16)	0.0054(16)	-0.0049(18)
C95	0.034(3)	0.030(3)	0.048(3)	0.011(2)	-0.002(2)	0.003(2)
C96	0.039(3)	0.032(3)	0.037(3)	-0.012(2)	-0.011(2)	0.006(2)
C96A	0.039(3)	0.032(3)	0.037(3)	-0.012(2)	-0.011(2)	0.006(2)
C97	0.043(3)	0.040(3)	0.042(3)	-0.004(2)	-0.006(2)	-0.017(3)
C98	0.042(3)	0.068(4)	0.042(3)	-0.001(3)	0.003(3)	-0.011(3)
C99	0.034(3)	0.034(3)	0.037(3)	-0.009(2)	-0.002(2)	-0.005(2)
C100	0.048(3)	0.065(4)	0.026(3)	0.003(3)	0.000(2)	0.015(3)
C101	0.049(4)	0.065(5)	0.041(3)	-0.004(3)	-0.013(3)	0.024(3)
C102	0.035(3)	0.053(4)	0.033(3)	-0.007(2)	0.008(2)	-0.009(3)
C103	0.031(3)	0.030(3)	0.042(3)	0.002(2)	-0.003(2)	-0.010(2)
C104	0.105(6)	0.101(6)	0.031(3)	0.001(3)	-0.008(4)	-0.065(6)
C105	0.063(5)	0.039(4)	0.046(4)	-0.003(3)	-0.012(4)	-0.014(4)
C05A	0.063(5)	0.039(4)	0.046(4)	-0.003(3)	-0.012(4)	-0.014(4)
Cl1	0.0513(8)	0.0682(10)	0.0436(7)	0.0043(7)	-0.0014(6)	-0.0305(8)
Cl2	0.0484(8)	0.0644(10)	0.0536(8)	-0.0248(7)	0.0035(7)	-0.0191(8)
Cl3	0.0375(7)	0.0570(9)	0.0345(6)	-0.0050(6)	0.0010(5)	-0.0162(6)
C106	0.028(4)	0.044(5)	0.048(4)	-0.006(4)	-0.001(3)	-0.012(3)
C10A	0.028(4)	0.044(5)	0.048(4)	-0.006(4)	-0.001(3)	-0.012(3)
Cl4	0.0682(10)	0.0551(9)	0.0435(8)	-0.0040(6)	0.0112(7)	-0.0255(8)
Cl5	0.0780(11)	0.0530(9)	0.0487(8)	0.0016(7)	-0.0117(8)	-0.0314(9)
Cl6	0.0921(13)	0.0448(9)	0.0726(11)	-0.0192(8)	0.0329(10)	-0.0323(9)
C107	0.055(4)	0.036(3)	0.044(3)	-0.004(2)	0.004(3)	-0.024(3)

Table 26: Hydrogen atomic coordinates and isotropic displacement parameters ($Å^2$) for **72**.

Atom	x/a	y/b	z/c	U(eq)
H05A	0.642953	0.621042	0.319111	0.058
H05B	0.645908	0.701795	0.279463	0.058
H1	0.52198	0.267982	0.441751	0.019
H106	0.245904	0.325408	0.208993	0.047
H107	0.240281	0.697666	0.346365	0.051
H10A	0.235956	0.518389	0.038672	0.063
H10B	0.195778	0.443422	0.016179	0.063
H10C	0.215395	0.369823	0.101414	0.087
H10D	0.256817	0.444532	0.123435	0.087
H10E	0.324098	0.38572	0.077569	0.087
H10F	-0.227505	0.698267	0.139953	0.049
H10G	-0.268314	0.617156	0.128245	0.049
H10H	0.479346	0.489149	0.115463	0.041
H10I	0.572191	0.405783	0.12411	0.041
H10J	0.588569	0.448143	0.034599	0.107
H10K	0.68171	0.471063	0.062186	0.107
H10L	0.579582	0.544194	0.049378	0.107
H10M	0.675099	0.692672	0.282455	0.058
H10N	0.786647	0.626688	0.272236	0.058
H10O	0.428537	0.186047	0.244552	0.047
H11	0.035904	0.368903	0.401817	0.019
H13	0.119623	0.561098	0.370466	0.018
H15	0.24838	0.370111	0.443728	0.019
H17A	0.407072	0.331461	0.515274	0.023
H17B	0.337123	0.267024	0.507283	0.023
H18A	0.480132	0.149755	0.523774	0.029
H18B	0.552506	0.212718	0.529723	0.029
H19A	0.442213	0.268017	0.607255	0.034
H19B	0.50838	0.171488	0.615019	0.034
H20A	0.187278	0.107301	0.479701	0.025
H20B	0.136224	0.031263	0.469506	0.025
H21A	0.337994	0.005214	0.509275	0.038
H21B	0.282262	-0.068858	0.501566	0.038
H22A	0.208367	0.061823	0.577385	0.044
H22B	0.270728	-0.033341	0.592812	0.044
H23A	-0.063555	0.278878	0.428738	0.022
H23B	-0.133783	0.221331	0.409421	0.022
H24A	-0.185434	0.403555	0.409593	0.03
H24B	-0.243432	0.358173	0.371066	0.03
H25A	-0.242527	0.322151	0.48344	0.037
H25B	-0.311419	0.290953	0.443195	0.037
H26A	0.09665	0.45593	0.463039	0.021
H26B	0.000294	0.528008	0.441877	0.021
H27A	0.089181	0.573665	0.511247	0.028
H27B	0.188215	0.565081	0.469653	0.028
H28A	0.085982	0.673159	0.41375	0.035
H28B	0.103031	0.706296	0.470431	0.035
H29	0.507001	0.256019	0.313326	0.02
H3	0.303074	0.17561	0.454645	0.02
H31	0.570975	0.049464	0.330951	0.02
H33	0.360356	0.048206	0.283975	0.019
H35	0.135825	0.051938	0.245325	0.021
H37	0.089318	0.260553	0.232606	0.02
H39	0.020504	0.466465	0.222961	0.02
H41	0.24273	0.470617	0.259918	0.021
H43	0.454487	0.466303	0.307545	0.021
H46	0.7069	0.121431	0.284586	0.026

H47	0.920323	0.010147	0.272478	0.033
H49	0.813221	-0.20017	0.270893	0.028
H5	0.281649	-0.022793	0.406677	0.019
H50	0.573868	-0.086308	0.276101	0.023
H51	0.298684	-0.059883	0.208405	0.026
H52	0.217894	-0.184355	0.144747	0.031
H54	0.000232	0.020742	0.092469	0.032
H55	0.074795	0.129226	0.156924	0.025
H56	-0.016215	0.387444	0.148601	0.034
H57	-0.153442	0.49851	0.080809	0.036
H59	-0.051368	0.702945	0.111436	0.033
H60	0.105883	0.588499	0.180739	0.03
H62	0.389	0.582941	0.233258	0.028
H63	0.626774	0.379662	0.266231	0.025
H67A	0.673238	-0.034879	0.127804	0.035
H67B	0.731547	0.039742	0.122157	0.035
H7	0.088737	0.176653	0.411449	0.018
H72	0.571066	-0.171589	0.126419	0.028
H78	0.08129	0.256019	0.012783	0.035
H80	0.778021	0.476294	0.244048	0.032
H86	0.321576	0.666938	0.080688	0.033
H89	0.548183	0.691328	0.220812	0.034
H9	-0.106938	0.269833	0.319826	0.019
H94	0.816757	0.236475	0.152637	0.025
H95A	0.550768	0.098934	0.127779	0.06
H95B	0.598057	0.123581	0.179588	0.06
H95C	0.539195	0.049099	0.183959	0.06
H96A	0.907345	-0.150853	0.354863	0.046
H96B	0.99389	-0.105104	0.329068	0.046
H96C	0.918637	-0.180696	0.344983	0.046
H96D	0.974715	-0.104135	0.339205	0.046
H97A	0.401651	0.011167	0.083129	0.048
H97B	0.313821	0.097762	0.073906	0.048
H98A	0.291943	0.053191	-0.012895	0.077
H98B	0.382706	-0.03141	-0.003676	0.077
H98C	0.408883	0.059369	-0.00837	0.077
H99A	-0.027044	-0.109246	0.169717	0.043
H99B	0.045663	-0.195186	0.145552	0.043

Table 27: PLATON/SQUEEZE details for disordered solvent molecules. Probe radius: 1.2 Å. Solvent-accessible volume: 380 Å^3. Electrons found in solvent accessible volume: 91e. Atoms in void are labelled as Cxxx, and Qxxx for all others.

Atom	x/a	y/b	z/c	electron density (e Å^{-3})
C101	0.837	0.121	0.034	7.24
C102	0.685	0.249	0.009	5.58
C103	0.639	0.234	0.005	5.32
C104	0.792	0.292	0.047	4.88
C105	0.794	0.24	0.013	4.2
C106	0.624	0.232	0.044	3.87
C107	0.519	0.252	0.032	3.39
Q108	0.841	0.619	0.276	2.99
Q109	0.091	0.829	0.279	2.6
Q110	0.816	0.607	0.32	2.24
Q111	0.765	0.582	0.337	2.12
Q112	0.633	0.499	0.409	2.1
Q113	0.673	0.861	0.409	2.07
Q114	0.721	0.766	0.054	1.92
Q115	0.801	0.046	0.41	1.61
Q116	0.077	0.744	0.274	1.13
Q117	0.72	0.781	0.392	1
Q118	0.283	0.256	0.293	1
Q119	0.976	0.716	0.473	0.97
Q120	0.322	0.187	0.187	0.95
Q121	0.678	0.64	0.284	0.9
Q122	0.423	0.636	0.381	0.9
Q123	0.941	0.813	0.098	0.85
Q124	0.408	0.318	0.202	0.83
Q125	0.917	0.687	0.435	0.82
Q126	0.107	0.872	0.495	0.75
Q127	0.167	0.594	0.07	0.75
Q128	0.491	0.143	0.219	0.72
Q129	0.642	0.487	0.469	0.7
Q130	0.395	0.873	0.126	0.7
C131	0.714	0.171	0.064	0.68
Q132	0.565	0.177	0.37	0.67
Q133	0.408	0.936	0.277	0.64
Q134	0.966	0.392	0.048	0.62
Q135	0.112	0.517	0.066	0.62
Q136	0.797	0.244	0.081	0.61
Q137	0.28	0.97	0.322	0.6
Q138	0.08	0.216	0.069	0.6
Q139	0.539	0.889	0.26	0.6
Q140	0.284	0.733	0.416	0.6
Q141	0.908	0.064	0.445	0.59
Q142	0.157	0.857	0.432	0.58
Q143	0.009	0.339	0.336	0.58
Q144	0.52	0.077	0.366	0.58
Q145	0.566	0.859	0.179	0.57
Q146	0.995	0.466	0.069	0.57
Q147	0.999	0.377	0.342	0.56
Q148	0.039	0.194	0.319	0.56
Q149	0.394	0.435	0.335	0.56
Q150	0.907	0.984	0.25	0.56
Q151	0.151	0.064	0.293	0.56
Q152	0.248	0.895	0.117	0.55
Q153	0.766	0.27	0.192	0.55
Q154	0.079	0.892	0.127	0.55
Q155	0.217	0.749	0.021	0.55

Q156	0.823	0.057	0.211	0.55
Q157	0.45	0.658	0.154	0.54
Q158	0.436	0.284	0.015	0.54
Q159	0.114	0.658	0.082	0.54
Q160	0.334	0.284	0.212	0.54
Q161	0.06	0.285	0.055	0.54
Q162	0.195	0.074	0.374	0.54
Q163	0.221	0.474	0.38	0.54
Q164	0.934	0.901	0.365	0.54
Q165	0.863	0.263	0.405	0.54
Q166	0.776	0.153	0.217	0.53
Q167	0.247	1	0.309	0.53
Q168	0.971	0.863	0.058	0.53
C169	0.423	0.266	0.057	0.51
Q170	0.048	0.19	0.126	0.51
Q171	0.128	0.086	0.071	0.51
Q172	0.236	0.331	0.199	0.51
Q173	0.36	0.127	0.422	0.51
Q174	0.433	0.186	0.239	0.51
Q175	0.449	0.951	0.345	0.5
Q176	0.763	0.781	0.018	0.5
Q177	0.995	0.746	0.307	0.5
Q178	0.39	0.986	0.317	0.5
Q179	0.454	0.03	0.376	0.5

Gas-phase conformational analysis of tetra-*endo*-ethyl octa-acid (53)

The relative energies (energy profile) of the conformations of tetra-*endo*-tetra acid **53** were calculated using a gas-phase semi-empirical restricted Hartree-Fock PM6[235] model on Spartan '14.[1] The host molecule **53** used in the calculations was modified such that the pendent propanoic acid moieties at the base were truncated to methyl groups to simplify the calculation. Geometry optimisation calculations started at a conformation such that all pendent ethyl groups at the portal of the basket were pointing in (dihedral angle $\phi \doteq 0°$). Subsequent optimisation calculations involved a dihedral move of all four ethyl groups by 5° in the same direction relative to the C_{4v} symmetry axis. Table 28 gives the atomic coordinates of the global minimum, and Table 29 gives the relative energies as a function of torsion angle.

Table 28: Torsion angles and relative energies in kJ mol–1 from 0° to 360°.

H	4.519	-0.764	0.893	H	0.342	2.074	5.223
C	3.97	-0.673	1.828	H	0.762	4.52	0.89
C	2.598	-0.443	4.274	C	-2.111	2.956	4.25
C	3.405	-1.787	2.449	H	-2.734	3.834	3.888
C	3.803	0.565	2.452	C	-2.966	-2.106	4.245
C	3.121	0.712	3.675	H	-3.843	-2.73	3.882
C	2.713	-1.705	3.673	C	-3.134	-0.717	3.663
H	2.068	-0.355	5.224	C	-3.414	1.784	2.44
C	2.096	-2.962	4.254	C	-3.811	-0.568	2.437
H	2.72	-3.839	3.893	C	-2.613	0.437	4.265
C	2.951	2.1	4.259	C	-2.726	1.7	3.666
H	3.829	2.724	3.899	C	-3.976	0.67	1.815
C	0.708	-3.13	3.668	H	-2.087	0.347	5.217
C	-1.79	-3.411	2.439	H	-4.522	0.763	0.878
C	0.562	-3.809	2.443	C	2.979	2.121	5.786
C	-0.448	-2.609	4.267	H	2.167	1.543	6.238
C	-1.709	-2.722	3.664	C	2.115	-2.993	5.781
C	-0.675	-3.974	1.818	H	3.143	-2.916	6.158
H	-0.36	-2.081	5.219	O	-3.547	3.005	1.762
H	-0.765	-4.521	0.881	O	-1.678	4.333	1.767

C	1.696	2.717	3.674	O	-4.338	-1.676	1.758
C	-0.571	3.805	2.446	O	3.541	-3.007	1.771
C	0.433	2.603	4.272	O	1.672	-4.336	1.767
C	1.781	3.408	2.45	O	-3.009	-3.545	1.759
C	0.668	3.972	1.825	C	2.368	-3.335	0.996
C	-0.721	3.125	3.67	H	1.729	-2.435	0.837
C	-3.336	-2.371	0.987	C	-0.03	-7.504	-1.838
H	-2.436	-1.731	0.83	C	-0.916	-5.502	-2.978
O	4.331	1.674	1.776	C	-2.431	-7.088	-1.844
C	3.332	2.369	1.002	C	-1.332	-7.876	-1.477
H	2.433	1.73	0.841	C	0.15	-6.332	-2.578
O	3.003	3.543	1.775	H	-3.45	-7.378	-1.565
C	-2.372	3.333	0.993	H	0.832	-8.121	-1.556
H	-1.732	2.434	0.834	C	5.932	-2.204	-2.568
C	3.924	2.789	-0.325	C	7.509	-0.032	-1.819
C	4.699	3.339	-2.977	C	7.092	-2.433	-1.823
C	3.406	3.917	-0.966	C	5.51	-0.92	-2.964
C	4.827	1.935	-0.962	C	6.339	0.147	-2.563
C	5.196	2.228	-2.283	C	7.88	-1.334	-1.456
C	3.804	4.168	-2.288	H	7.382	-3.452	-1.543
H	2.737	4.592	-0.434	H	8.125	0.83	-1.536
H	5.25	1.087	-0.425	C	2.21	5.929	-2.569
C	-2.788	3.923	-0.336	C	0.036	7.507	-1.828
C	-3.332	4.696	-2.991	C	0.927	5.507	-2.967
C	-1.933	4.826	-0.972	C	2.437	7.09	-1.825
C	-3.915	3.405	-0.98	C	1.338	7.878	-1.462
C	-4.162	3.801	-2.303	C	-0.14	6.336	-2.57
C	-2.222	5.193	-2.294	H	3.456	7.38	-1.543
H	-1.086	5.25	-0.434	H	-0.826	8.124	-1.548
H	-4.591	2.736	-0.448	H	1.537	-2.182	6.235
C	-3.922	-2.789	-0.343	C	-3	-2.129	5.772
C	-4.689	-3.335	-2.999	C	-2.135	2.985	5.777
C	-4.824	-1.934	-0.982	H	3.925	1.71	6.163
C	-3.402	-3.916	-0.984	H	-1.559	2.174	6.232
C	-3.796	-4.165	-2.308	H	-1.725	3.932	6.154
C	-5.188	-2.225	-2.305	H	-2.922	-3.159	6.147
H	-5.249	-1.086	-0.445	H	-3.947	-1.718	6.146
H	-2.735	-4.591	-0.45	C	9.129	-1.512	-0.674
C	2.79	-3.923	-0.332	C	-1.511	-9.128	-0.699
C	3.342	-4.692	-2.986	C	-9.127	1.513	-0.705
C	3.919	-3.403	-0.971	C	1.514	9.129	-0.681
C	1.936	-4.825	-0.972	O	9.919	-0.677	-0.302
C	2.23	-5.19	-2.294	O	-0.676	-9.918	-0.328
C	4.17	-3.798	-2.293	O	-9.917	0.677	-0.337
H	4.592	-2.736	-0.435	O	0.677	9.919	-0.312
H	1.087	-5.249	-0.437	H	-4.98	-3.543	-4.027
O	6.057	1.443	-3.037	H	-3.539	4.99	-4.018
O	-1.436	6.054	-3.047	H	4.995	3.548	-4.004
O	-5.222	3.332	-3.065	H	3.553	-4.985	-4.012
O	5.233	-3.328	-3.051	C	-0.698	-4.268	-3.799
O	-6.046	-1.439	-3.061	H	0.188	-4.41	-4.458
O	-3.325	-5.225	-3.068	H	-1.565	-4.119	-4.483
O	1.447	-6.049	-3.05	C	4.278	-0.703	-3.788
O	3.335	5.229	-3.048	H	4.422	0.184	-4.447
C	-5.922	2.207	-2.586	H	4.131	-1.57	-4.471
C	-7.502	0.034	-1.846	C	0.712	4.273	-3.791
C	-5.499	0.924	-2.982	H	1.581	4.125	-4.472
C	-7.086	2.435	-1.845	H	-0.172	4.416	-4.452
C	-7.874	1.336	-1.483	C	-4.264	0.708	-3.802
C	-6.33	-0.143	-2.586	H	-4.115	1.576	-4.484

H	-7.377	3.454	-1.564	H	-4.406	-0.177	-4.463
H	-8.12	-0.828	-1.567	C	3.035	-0.509	-2.922
C	-2.201	-5.925	-2.585	H	3.135	0.362	-2.262
H	2.149	-0.349	-3.547	H	1.391	2.839	-2.29
C	0.516	3.032	-2.923	H	0.359	2.144	-3.547
H	-0.357	3.132	-2.266	H	-2.189	-1.552	6.229
C	-3.024	0.513	-2.932	H	-3.165	2.907	6.151
H	-2.136	0.354	-3.554	H	2.9	3.15	6.162
H	-3.127	-0.359	-2.274	O	-2.838	-9.34	-0.399
H	-2.832	1.389	-2.3	H	-2.976	-10.177	0.127
C	-0.506	-3.027	-2.93	O	9.341	-2.838	-0.373
H	0.365	-3.129	-2.27	H	10.176	-2.977	0.156
H	-1.383	-2.835	-2.3	O	2.839	9.341	-0.377
H	-0.346	-2.14	-3.553	H	2.976	10.177	0.15
H	1.703	-3.94	6.155	O	-9.34	2.839	-0.402
H	-10.177	2.976	0.123				

Table 29: Torsion angles and relative energies in kJ mol^{-1} from 0° to 360°.

Torsion ϕ (°)	rel. E (kJ/mol)		Torsion ϕ (°)	rel. E (kJ/mol)		Torsion ϕ (°)	rel. E (kJ/mol)
0	0		140	16.37		280	46.72
5	1.22		145	12.45		285	46.13
10	4.24		150	9.79		290	45.05
15	8.82		155	8.52		295	43.5
20	14.31		160	8.43		300	41.54
25	19.77		165	9.01		305	39.21
30	24.53		170	9.73		310	36.56
35	28.61		175	10.22		315	33.6
40	32.19		180	10.33		320	30.31
45	35.38		185	10.03		325	26.62
50	38.19		190	9.39		330	22.42
55	40.64		195	8.68		335	17.57
60	42.68		200	8.24		340	12.27
65	44.32		205	8.54		345	7.18
70	45.51		210	9.92		350	3.13
75	46.24		215	12.58		355	0.66
80	46.5		220	16.41		360	0.02
85	46.32		225	21.2			
90	45.74		230	26.48			
95	44.8		235	31.45			
100	43.54		240	35.45			
105	41.96		245	38.33			
110	40.14		250	40.64			
115	37.91		255	42.54			
120	35.06		260	44.16			
125	31.18		265	45.46			
130	26.33		270	46.34			

Appendix: Table of scientific abbreviations and symbols

This table of scientific abbreviations and symbols does not include units, symbols for elements, or chemical formulæ.

(aq)	aqueous solution
(g)	gas
[X]	molar concentration of species X
1D	one-dimensional
2D	two-dimensional
3D	three-dimensional
6-311+G**	split-valence Pople-type basis set with polarisation and diffuse functions
Anal.	analysis
$\boldsymbol{B}_0$	external magnetic field
BCM	bromochloromethane
br	broad signal
c	Wiseman parameter
C	concentration
C_4	molecular point group with four-fold symmetry axis
C_{4v}	molecular point group with four-fold symmetry axis and vertical mirror planes
Calc'd	calculated
CB	cucurbituril
CCDC	Cambridge Crystallographic Data Centre
CD	cyclodextrin
conc.	concentrated
CPK	Corey–Pauling–Koltun
CSD-ICSD	Cambridge Structural Database - Inorganic Crystal Structure Database
d	day
	doublet
D	diffusion constant
DBU	diazabicyclo[5.4.0]undec-7-ene
DCA	dichloroacetate
DCM	dichloromethane
dd	doublet of doublets
dH2O	deionised water
DIM	diiodomethane
DIPEA	diisopropyl(ethyl)amine, Hünig's base
d_k	kinetic diameter
DMA	N,N-dimethylacetamide
DMF	N,N-dimethylformamide
DMSO	dimethyl sulfoxide
DOSY	Diffusion-Ordered spectroscopy
DP	differential power
DSS	sodium 3-(trimethylsilyl)propane-1-sulfonate
dt	doublet of triplets
E	free energy
e	fundamental charge ($\sim 1.602 \times 10^{-19}$ C)
E_a	activation energy
equiv.	molar equivalent

ESI	electrospray ionisation
F	force
FT	Fourier transform
G	guest
$G(n)$	Gibbs free energy calculated from probability $p(n)$
H	host
h	Planck constant ($\sim 6.626 \times 10^{-34}$ J·s)
h	hour
HG	host–guest complex
HRMS	high resolution mass spectrometry
I	NMR signal integral
Imid	1H-imidazole
IR	infrared
ITC	isothermal titration calorimetry
J	coupling constant
Ka	acid dissociation constant or
	association constant
kB	Boltzmann constant ($\sim 1.381 \times 10^{-23}$ J K^{-1})
ℓ	length
LEDBPG2S	2D sequence for diffusion measurement using stimulated echo and long eddy delay using bipolar gradients for diffusion using 2 spoil gradients
$\mathcal{M}$	molar mass
m	unresolved multiplet
m/z	mass-to-charge ratio
MALDI	matrix-assisted lased desorption-ionisation
MCR	multivariate curve resolution
MD	molecular dynamics
MDT	methylene ditosylate
MEM	[(2-methoxy)ethoxy]methyl
min	minute
mp	melting point
MS	mass spectrometry
n	counting number
N_1	first hydration number
NMR	nuclear magnetic resonance
p-TSA	p-toluenesulfonic acid
$p(n)$	probability of event n
$p^{\ominus}$	standard pressure (100 kPa)
pD	negative decadic logarithm of deuterium ion molar concentration
pH	negative decadic logarithm of hydrogen ion molar concentration
pI	isoelectric point
pK_a	negative decadic logarithm of the acidity constant
PM6	Parametric Method 6
PTFE	poly(tetrafluoroethylene)
PVDF	poly(vinylidene difluoride)
q	charge or
	quartet
r	radius or
	distance
R	Regnault constant (~ 8.31447 J K^{-1} mol^{-1})
R_f	retardation factor
RMS	root-mean-square
rt	room temperature
s	singlet
SAMPL	Statistical Analysis of the Modeling of Proteins and Ligands
sat'd	saturated
S_NAr	nucleophilic aromatic substitution
s_w	molar solubility in water
T	temperature
t	triplet

T_2	transverse nuclear relaxation time
TBAF	tetrabutylammonium fluoride
TCA	trichloroacetate
td	triplet of doublets
THF	tetrahydrofuran
TIPS	triisopropylsilyl
TLC	thin-layer chromatography
TOF	time-of-flight
tt	triplet of triplets
U	potential energy
UV	ultraviolet
V	volume
v/v	volume ratio
VT	variable temperature
W	gravimetric mass
$w(r)$	work as a function of distance r
w/w	mass ratio
x∈y	complex of guest y in host x
Xt	mass-action sum of all species containing X
α	electronic polarizability
γ	gyromagnetic ratio
δ	chemical shift
$\Delta_{1/2}$	linewidth-at-half-height
ΔG	Gibbs free energy
ΔH	enthalpy
ΔS	entropy
Δδ	change in chemical shift
Δν	change in nuclear precession frequency
$\Delta\sigma_{iso}$	change in nuclear isotropic shielding
ε	Lennard-Jones potential energy minimum
ε_0	vacuum permittivity (~6.602×10^{-12} C^2 J^{-1} m^{-1})
ε_r	relative permittivity
ϑ	angle
λ	length
μ_D	dipole moment
μ_i	chemical potential
ν_x	nuclear precession frequency at state x
ρ	density
σ	particle distance at Lennard-Jones potential energy minimum
σ	standard deviation from the mean
τ	residence lifetime
φ	dihedral angle
χ	electronegativity
ω	Larmor frequency
ωB97X-D	*ab initio* range-separated hybrid correlation functional

References

1.   Deppmeier, B. J.; Driessen, A. J.; Hehre, T. S.; Hehre, W. J.; Johnson, J. A.; Klunzinger, P. E.; Leonard, J. M.; Pham, I. N.; Pietro, W. J.; Yu, J. *Spartan '14*, version 14.119p1.1.2; Wavefunction, Inc.: Irvine, Ca, 2014.

2.   Thordarson, P. Determining association constants from titration experiments in supramolecular chemistry. *Chem. Soc. Rev.* **2011,** *40* (3), 1305-1323 10.1039/c0cs00062k.

3.   Thordarson, P. BindFit. www.supramolecular.org.

4.   Johnson, G. T.; Autin, L.; Goodsell, D. S.; Sanner, M. F.; Olson, A. J. ePMV embeds molecular modeling into professional animation software environments. *Structure* **2011,** *19* (3), 293-303 10.1016/j.str.2010.12.023.

5.   Salisbury, J. o.; McGarry, D. D. *The Metalogicon of John of Salisbury: a Twelfth-Century Defence of the Logiac Arts of the Trivium*. University of California Press: California, 1955.

6.   Bullein, W. *Bulleins bulwarke of defence against all sicknesse, soarenesse, and woundes that doe dayly assaulte mankinde: which bulwarke is kept with Hilarius the gardener, & Health the phisicion, with the chirurgian, to helpe the wounded souldiours*. Thomas Marshe: England, 1579.

7.   Adams, D. *The salmon of doubt: hitchhiking the galaxy one last time*. Harmony Books: New York, 2002.

8.   Darwin, E. *The Botanic Garden, a Poem In Two Parts. Part I. Containing the Economy Of Vegetation, Part II. The Loves Of the Plants. With Philosophical Notes*. 3rd ed.; J. Johnson etc.: London, 1799.

9.   Lawson, R. M. *Science in the Ancient World: An Encyclopedia*. ABC-CLIO: Santa Barbara, California, 2004.

10.   Russell, B. *History of Western Philosophy; And its Connection with Political and Social Circumstances from the Earliest Times to the Present Day*. Routledge: 1996.

11.   Liu, A.; Major, J. S. *The Huainanzi : a guide to the theory and practice of government in early Han China*. Columbia University Press: New York, 2010.

12.   Saliba, G. *Islamic science and the making of the European Renaissance*. MIT Press: Cambridge, Mass, 2007.

13.   ibn Hayyān, J. *The works of Geber*. Dent: London, 1928.

14.   Jaffer, T. *Rāzī : master of Quranic interpretation and theological reasoning*. Oxford University Press: Oxford, 2015.

15.   Stroumsa, S. *Freethinkers of medieval Islam : Ibn al-Rawāndī, Abū Bakr al-Rāzī, and their impact on Islamic thought*. Brill: Laiden, 2016.

16.   Ronca, I. « Senior de Chemia »: A Reassessment of the Medieval Latin Translation of Ibn Umayl's Al-māʾ al-waraqī wa 'l-arḍ al-najmiyya. *Bulletin de Philosophie Médiévale* **1995,** *37*, 9-31 10.1484/j.Bpm.3.500.

17.   Morienus; Khālid ibn Yazīd, a.-U.; Stavenhagen, L. *A testament of alchemy; being the revelations of Morienus, ancient adept and hermit of Jerusalem, to Khalid ibn Yazid ibn Mu'awiyya, King of the Arabs, of the divine secrets of the magisterium and accomplishment of the alchemical art*. Published for the Brandeis University Press by the University Press of New England: Hanover, N.H, 1974.

18.   Aquinas, T. *Aurora Consurgens: a document attributed to Thomas Aquinas on the problem of opposites in alchemy*. 1966.

19.   Bacon, R.; Bridges, J. H. *The "Opus majus" of Roger Bacon edited, with introduction and analytical table*. Clarendon press: Oxford, 1897.

20.   Webster, C. *Paracelsus : medicine, magic and mission at the end of time*. Yale University Press: New Haven [Conn.] ;, 2008.

21.   Poirier, J.-P. *Lavoisier, chemist, biologist, economist*. University of Pennsylvania Press: Philadelphia, 1996.

22.   Jungnickel, C. *Cavendish: the experimental life*. Bucknell: Cranbury, NJ, 1999.

23.   Jacobsen, A. S. Discovering water: James Watt, Henry Cavendish and the nineteenth-century 'water controversy'. *Minerva* **2006,** *44* (4), 459-462 10.1007/s11024-006-9011-1.

24.   Priestley, J. *Heads of lectures on a course of experimental philosophy, particularly including chemistry*. Kraus Reprint Co.: New York, 1970.

25.   Golinski, J. Precision Instruments and the Demonstrative Order of Proof in Lavoisier's Chemistry. *Osiris* **1994,** *9*, 30-47 10.1086/368728.

26.   Roscoe, H. E. *John Dalton and the rise of modern chemistry*. Macmillan: New York, 1895.

27.   Avogadro, A. Essai d'une manière de déterminer les masses relatives des molecules élémentaires des corps, et les proportions selon lesquelles elles entrent dans ces combinaisons. *Journal de physique, de chimie, d'histoire naturelle et des arts* **1811,** *73*.

28.   Morselli, M. *Amedeo Avogadro, a scientific biography*. D. Reidel: Dordrecht, 1984.

29.   Ampère, A.-M. Lettre de M. Ampère à M. le comte Berthollet sur la détermination des proportions dans lesquelles les corps se combinent d'après le nombre et la disposition respective des molécules dont les parties intégrantes sont composées. *Ann. Chim. (Cachan, Fr.)* **1814,** *90*.

30.   Davy, H. *Collected Works*. Smith, Elder, and Co. Cornhill: London, 1839; Vol. V: Bakerian Lectures and Miscellaneous Papers from 1806 to 1815, p 554.

31.   Greenwood, N. N.; Earnshaw, A. *Chemistry of the Elements*. Butterworth Heinemann: Oxford, 1997.

32.   NIST Computational Chemistry Comparison and Benchmark Database. http://cccbdb.nist.gov/ (accessed 17 Dec.).

33.   Tantardini, C.; Oganov, A. R. Thermochemical electronegativities of the elements. *Nat. Commun.* **2021,** *12* (1), 10.1038/s41467-021-22429-0.

34.   Murphy, D. M.; Koop, T. Review of the vapour pressures of ice and supercooled water for atmospheric applications. *Q. J. R. Meteorol. Soc.* **2005,** *131* (608), 1539-1565 10.1256/qj.04.94.

35.   Atkins, P.; de Paula, J. *Physical Chemistry: Thermodynamics, Structure, and Change*. 10th ed.; W. H. Freeman and Company: New York, NY, 2014.

36.   Wagner, W. International Equations for the Pressure Along the Melting and Along the Sublimation Curve of Ordinary Water Substance. *J. Phys. Chem. Ref. Data* **1994,** *23* (3), 515-525 10.1063/1.555947.

37.   Haynes, W. M.; Lide, D. R.; Bruno, T. J., *CRC Handbook of Chemistry and Physics*. 97th Edition ed.; CRC Press: Boca Raton, 2017.

38.   Muller, P. Glossary of terms used in physical organic chemistry (IUPAC Recommendations 1994). *Pure Appl. Chem.* **1994,** *66* (5), 1077-1184 10.1351/pac199466051077.

39.　Ewing, M. B.; Lilley, T. H.; Olofsson, G. M.; Ratzsch, M. T.; Somsen, G. Standard Quantities in Chemical Thermodynamics - Fugacities, Activities, and Equilibrium-Constants for Pure and Mixed Phases (Iupac Recommendations 1994). *Pure Appl. Chem.* **1994,** *66* (3), 533-552 10.1351/pac199466030533.

40.　Gold, V. *The IUPAC Compendium of Chemical Terminology*. 2019; p 1-1670.

41.　Gasser, T. M.; Thoeny, A. V.; Fortes, A. D.; Loerting, T. Structural characterization of ice XIX as the second polymorph related to ice VI. *Nat. Commun.* **2021,** *12* (1), 1128 10.1038/s41467-021-21161-z.

42.　Bjerrum, N. Structure and Properties of Ice. *Science* **1952,** *115* (2989), 385-390 10.1126/science.115.2989.385.

43.　Leadbetter, A. J.; Ward, R. C.; Clark, J. W.; Tucker, P. A.; Matsuo, T.; Suga, H. The equilibrium low‐temperature structure of ice. *J. Chem. Phys.* **1985,** *82* (1), 424-428 10.1063/1.448763.

44.　Bernal, J. D.; Fowler, R. H. A Theory of Water and Ionic Solution, with Particular Reference to Hydrogen and Hydroxyl Ions. *J. Chem. Phys.* **1933,** *1* (8), 515-548 10.1063/1.1749327.

45.　Groom, C. R.; Bruno, I. J.; Lightfoot, M. P.; Ward, S. C. The Cambridge Structural Database. *Acta Crystallogr., Sect. B: Struct. Crystallogr. Cryst. Chem.* **2016,** *72* (Pt 2), 171-179 10.1107/S2052520616003954.

46.　Kubik, S. *Supramolecular Chemistry in Water*. 2019.

47.　Morawietz, T.; Urbina, A. S.; Wise, P. K.; Wu, X.; Lu, W.; Ben-Amotz, D.; Markland, T. E. Hiding in the Crowd: Spectral Signatures of Overcoordinated Hydrogen-Bond Environments. *J. Phys. Chem. Lett.* **2019,** *10* (20), 6067-6073 10.1021/acs.jpclett.9b01781.

48.　Franks, F. *Water: a matrix of life*. 2nd ed.; The Royal Society of Chemistry: Cambridge, 2000.

49.　Horn, H. W.; Swope, W. C.; Pitera, J. W.; Madura, J. D.; Dick, T. J.; Hura, G. L.; Head-Gordon, T. Development of an improved four-site water model for biomolecular simulations: TIP4P-Ew. *J. Chem. Phys.* **2004,** *120* (20), 9665-9678 10.1063/1.1683075.

50.　Dick, T. J. M., Jeffry D. A Review of the TIP4P, TIP4P-Ew, TIP5P, and TIP5P-E Water Models. *Annu. Rep. Comput. Chem.* **2005,** *1*, 59-74 10.1016/S1574-1400(05)01005-4.

51.   Hakala, M.; Nygard, K.; Manninen, S.; Huotari, S.; Buslaps, T.; Nilsson, A.; Pettersson, L. G.; Hamalainen, K. Correlation of hydrogen bond lengths and angles in liquid water based on Compton scattering. *J. Chem. Phys.* **2006,** *125* (8), 084504 10.1063/1.2273627.

52.   Zhu, T.; Van Voorhis, T. Understanding the Dipole Moment of Liquid Water from a Self-Attractive Hartree Decomposition. *J. Phys. Chem. Lett.* **2021,** *12* (1), 6-12 10.1021/acs.jpclett.0c03300.

53.   Head-Gordon, T.; Hura, G. Water structure from scattering experiments and simulation. *Chem. Rev.* **2002,** *102* (8), 2651-2670 10.1021/cr0006831.

54.   Batista, E. R.; Xantheas, S. S.; Jónsson, H. Molecular multipole moments of water molecules in ice Ih. *J. Chem. Phys.* **1998,** *109* (11), 4546-4551 10.1063/1.477058.

55.   Chen, H.; Ruckenstein, E. Hydrated Ions: From Individual Ions to Ion Pairs to Ion Clusters. *J. Phys. Chem. B* **2015,** *119* (39), 12671-12676 10.1021/acs.jpcb.5b06837.

56.   Migliorati, V.; Sessa, F.; Aquilanti, G.; D'Angelo, P. Unraveling halide hydration: A high dilution approach. *J. Chem. Phys.* **2014,** *141* (4), 044509 10.1063/1.4890870.

57.   Marcus, Y. Ionic radii in aqueous solutions. *Chem. Rev.* **2002,** *88* (8), 1475-1498 10.1021/cr00090a003.

58.   Molina, J. J.; Lectez, S.; Tazi, S.; Salanne, M.; Dufrêche, J.-F.; Roques, J.; Simoni, E.; Madden, P. A.; Turq, P. Ions in solutions: Determining their polarizabilities from first-principles. *J. Chem. Phys.* **2011,** *134* (1), 014511 10.1063/1.3518101.

59.   Marcus, Y. *Ions in Solution and Their Solvation*. Wiley: 2015.

60.   Mähler, J.; Persson, I. A Study of the Hydration of the Alkali Metal Ions in Aqueous Solution. *Inorg. Chem.* **2012,** *51* (1), 425-438 10.1021/ic2018693.

61.   Nguyen, M. T. H.; Tichacek, O.; Martinez-Seara, H.; Mason, P. E.; Jungwirth, P. Resolving the Equal Number Density Puzzle: Molecular Picture from Simulations of LiCl(aq) and NaCl(aq). *J. Phys. Chem. B* **2021,** *125* (12), 3153-3162 10.1021/acs.jpcb.0c10599.

62.   Carrillo-Tripp, M.; Saint-Martin, H.; Ortega-Blake, I. A comparative study of the hydration of Na+ and K+ with refined polarizable model potentials. *J. Chem. Phys.* **2003,** *118* (15), 7062-7073 10.1063/1.1559673.

63.   Jungwirth, P.; Tobias, D. J. Chloride Anion on Aqueous Clusters, at the Air–Water Interface, and in Liquid Water: Solvent Effects on Cl- Polarizability. *J. Phys. Chem. A* **2001,** *106* (2), 379-383 10.1021/jp012059d.

64.   Tessman, J. R.; Kahn, A. H.; Shockley, W. Electronic Polarizabilities of Ions in Crystals. *Phys. Rev.* **1953,** *92* (4), 890-895 10.1103/physrev.92.890.

65.   Matricon, P.; Suresh, R. R.; Gao, Z. G.; Panel, N.; Jacobson, K. A.; Carlsson, J. Ligand design by targeting a binding site water. *Chem. Sci.* **2020,** *12* (3), 960-968 10.1039/d0sc04938g.

66.   Di Tommaso, D.; de Leeuw, N. H. Structure and dynamics of the hydrated magnesium ion and of the solvated magnesium carbonates: insights from first principles simulations. *Phys. Chem. Chem. Phys.* **2010,** *12* (4), 894-901 10.1039/b915329b.

67.   Kiriukhin, M. Y.; Collins, K. D. Dynamic hydration numbers for biologically important ions. *Biophys. Chem.* **2002,** *99* (2), 155-168 10.1016/s0301-4622(02)00153-9.

68.   Zavitsas, A. A. Aqueous Solutions of Calcium Ions: Hydration Numbers and the Effect of Temperature. *J. Phys. Chem. B* **2005,** *109* (43), 20636-20640 10.1021/jp053909i.

69.   Śmiechowski, M. Anion‑water interactions of weakly hydrated anions: molecular dynamics simulations of aqueous NaBF4and NaPF6. *Mol. Phys.* **2016,** *114* (12), 1831-1846 10.1080/00268976.2016.1157219.

70.   Eklund, L.; Hofer, T. S.; Persson, I. Structure and water exchange dynamics of hydrated oxo halo ions in aqueous solution using QMCF MD simulation, large angle X-ray scattering and EXAFS. *Dalton Trans.* **2015,** *44* (4), 1816-1828 10.1039/c4dt02580f.

71.   Vchirawongkwin, V.; Rode, B. M.; Persson, I. Structure and dynamics of sulfate ion in aqueous solution--an ab initio QMCF MD simulation and large angle X-ray scattering study. *J. Phys. Chem. B* **2007,** *111* (16), 4150-4155 10.1021/jp0702402.

72.   Pribil, A. B.; Hofer, T. S.; Randolf, B. R.; Rode, B. M. Structure and dynamics of phosphate ion in aqueous solution: Anab initioQMCF MD study. *J. Comput. Chem.* **2008,** *29* (14), 2330-2334 10.1002/jcc.20968.

73.   Baldwin, R. L. Energetics of Protein Folding. *J. Mol. Biol.* **2007,** *371* (2), 283-301 10.1016/j.jmb.2007.05.078.

74.   Steed, J. W.; Atwood, J. L. *Supramolecular Chemistry*. 2nd ed.; John Wiley and Sons, Inc.: Chichester, 2009.

75.   Hillyer, M. B.; Gibb, B. C. Molecular Shape and the Hydrophobic Effect. *Annu. Rev. Phys. Chem.* **2016,** *67* (1), 307-329 10.1146/annurev-physchem-040215-112316.

76.   do Carmo, M. P. *Differential geometry of curves & surfaces*. 2nd ed.; 2018.

77.   Griffiths, D. J. *Introduction to electrodynamics*. Cambridge University Press: Cambridge, 2018.

78.   Reichardt, C.; Welton, T. *Solvents and Solvent Effects in Organic Chemistry*. 4th Edition ed.; Wiley-VCH: Weinheim, Germany, 2011.

79.   Cremer, P. S.; Flood, A. H.; Gibb, B. C.; Mobley, D. L. Collaborative routes to clarifying the murky waters of aqueous supramolecular chemistry. *Nat. Chem.* **2017,** *10* (1), 8-16 10.1038/nchem.2894.

80.   Choudhury, N.; Pettitt, B. M. On the mechanism of hydrophobic association of nanoscopic solutes. *J. Am. Chem. Soc.* **2005,** *127* (10), 3556-3567 10.1021/ja0441817.

81.   Sullivan, M. R.; Yao, W.; Gibb, B. C. The thermodynamics of guest complexation to octa-acid and tetra-endo-methyl octa-acid: reference data for the sixth statistical assessment of modeling of proteins and ligands (SAMPL6). *Supramol. Chem.* **2019,** *31* (3), 184-189 10.1080/10610278.2018.1549327.

82.   Sullivan, M. R.; Sokkalingam, P.; Nguyen, T.; Donahue, J. P.; Gibb, B. C. Binding of carboxylate and trimethylammonium salts to octa-acid and TEMOA deep-cavity cavitands. *J. Comput.-Aided Mol. Des.* **2017,** *31* (1), 21-28 10.1007/s10822-016-9925-0.

83.   Rizzi, A.; Murkli, S.; McNeill, J. N.; Yao, W.; Sullivan, M.; Gilson, M. K.; Chiu, M. W.; Isaacs, L.; Gibb, B. C.; Mobley, D. L.*, et al.* Overview of the SAMPL6 host-guest binding affinity prediction challenge. *J. Comput.-Aided Mol. Des.* **2018,** *32* (10), 937-963 10.1007/s10822-018-0170-6.

84.   Barnett, J. W.; Sullivan, M. R.; Long, J. A.; Tang, D.; Nguyen, T.; Ben-Amotz, D.; Gibb, B. C.; Ashbaugh, H. S. Spontaneous drying of non-polar deep-cavity cavitand pockets in aqueous solution. *Nat. Chem.* **2020,** *12* (7), 589-594 10.1038/s41557-020-0458-8.

85.   Marquez, C.; Nau, W. M. Polarizabilities Inside Molecular Containers. *Angew. Chem., Int. Ed. Engl.* **2001,** *40* (23), 4387-4390 10.1002/1521-3773(20011203)40:23<4387::aid-anie4387>3.0.co;2-h.

86.   He, S.; Biedermann, F.; Vankova, N.; Zhechkov, L.; Heine, T.; Hoffman, R. E.; De Simone, A.; Duignan, T. T.; Nau, W. M. Cavitation energies can outperform dispersion interactions. *Nat. Chem.* **2018,** *10* (12), 1252-1257 10.1038/s41557-018-0146-0.

87.   Biedermann, F.; Vendruscolo, M.; Scherman, O. A.; De Simone, A.; Nau, W. M. Cucurbit[8]uril and blue-box: high-energy water release overwhelms electrostatic interactions. *J. Am. Chem. Soc.* **2013,** *135* (39), 14879-14888 10.1021/ja407951x.

88.   Biedermann, F.; Nau, W. M.; Schneider, H. J. The hydrophobic effect revisited--studies with supramolecular complexes imply high-energy water as a noncovalent driving force. *Angew. Chem., Int. Ed.* **2014,** *53* (42), 11158-11171 10.1002/anie.201310958.

89.   Assaf, K. I.; Nau, W. M. Cucurbiturils: from synthesis to high-affinity binding and catalysis. *Chem. Soc. Rev.* **2015,** *44* (2), 394-418 10.1039/c4cs00273c.

90.   Assaf, K. I.; Holub, J.; Bernhardt, E.; Oliva-Enrich, J. M.; Fernandez Perez, M. I.; Canle, M.; Santaballa, J. A.; Fanfrlik, J.; Hnyk, D.; Nau, W. M. Face-Fusion of Icosahedral Boron Hydride Increases Affinity to gamma-Cyclodextrin: closo,closo-[B21 H18](-) as an Anion with Very Low Free Energy of Dehydration. *ChemPhysChem* **2020,** *21* (10), 971-976 10.1002/cphc.201901225.

91.   Hummer, G.; Rasaiah, J. C.; Noworyta, J. P. Water conduction through the hydrophobic channel of a carbon nanotube. *Nature* **2001,** *414* (6860), 188-190 10.1038/35102535.

92.   Vaitheeswaran, S.; Yin, H.; Rasaiah, J. C.; Hummer, G. Water clusters in nonpolar cavities. *Proc. Natl. Acad. Sci. U. S. A.* **2004,** *101* (49), 17002-17005 10.1073/pnas.0407968101.

93.   Hofmeister, F. Zur Lehre von der Wirkung der Salze. *Arch. Exp. Pathol. Pharmakol.* **1888,** *24* (4-5), 247-260 10.1007/bf01918191.

94.   Duong-Ly, K. C.; Gabelli, S. B. Salting out of proteins using ammonium sulfate precipitation. *Methods Enzymol.* **2014,** *541*, 85-94 10.1016/B978-0-12-420119-4.00007-0.

95.   Marcus, Y. Effect of Ions on the Structure of Water: Structure Making and Breaking. *Chem. Rev.* **2009,** *109* (3), 1346-1370 10.1021/cr8003828.

96.   Marcus, Y. *Ion Properties*. CRC Press: 1997.

97.   Marcus, Y. Viscosity B-coefficients, structural entropies and heat capacities, and the effects of ions on the structure of water. *J. Solution Chem.* **1994,** *23* (7), 831-848 10.1007/bf00972677.

98.   Assaf, K. I.; Nau, W. M. The Chaotropic Effect as an Assembly Motif in Chemistry. *Angew. Chem., Int. Ed.* **2018,** *57* (43), 13968-13981 10.1002/anie.201804597.

99.   Gregory, K. P.; Wanless, E. J.; Webber, G. B.; Craig, V. S. J.; Page, A. J. The electrostatic origins of specific ion effects: quantifying the Hofmeister series for anions. *Chem. Sci.* **2021,** *12* (45), 15007-15015 10.1039/d1sc03568a.

100.   Rembert, K. B.; Paterová, J.; Heyda, J.; Hilty, C.; Jungwirth, P.; Cremer, P. S. Molecular Mechanisms of Ion-Specific Effects on Proteins. *J. Am. Chem. Soc.* **2012,** *134* (24), 10039-10046 10.1021/ja301297g.

101.   Paterová, J.; Rembert, K. B.; Heyda, J.; Kurra, Y.; Okur, H. I.; Liu, W. R.; Hilty, C.; Cremer, P. S.; Jungwirth, P. Reversal of the Hofmeister Series: Specific Ion Effects on Peptides. *J. Phys. Chem. B* **2013,** *117* (27), 8150-8158 10.1021/jp405683s.

102.   Jungwirth, P.; Cremer, P. S. Beyond Hofmeister. *Nat. Chem.* **2014,** *6* (4), 261-263 10.1038/nchem.1899.

103.   Okur, H. I.; Hladilkova, J.; Rembert, K. B.; Cho, Y.; Heyda, J.; Dzubiella, J.; Cremer, P. S.; Jungwirth, P. Beyond the Hofmeister Series: Ion-Specific Effects on Proteins and Their Biological Functions. *J. Phys. Chem. B* **2017,** *121* (9), 1997-2014 10.1021/acs.jpcb.6b10797.

104.   Okur, H. I.; Hladílková, J.; Rembert, K. B.; Cho, Y.; Heyda, J.; Dzubiella, J.; Cremer, P. S.; Jungwirth, P. Beyond the Hofmeister Series: Ion-Specific Effects on Proteins and Their Biological Functions. *J. Phys. Chem. B* **2017,** *121* (9), 1997-2014 10.1021/acs.jpcb.6b10797.

105.   Hyde, A. M.; Zultanski, S. L.; Waldman, J. H.; Zhong, Y. L.; Shevlin, M.; Peng, F. General Principles and Strategies for Salting-Out Informed by the Hofmeister Series. *Org. Process Res. Dev.* **2017,** *21* (9), 1355-1370 10.1021/acs.oprd.7b00197.

106.   Zerbe, O.; Jurt, S. *Applied NMR spectroscopy for chemists and life scientists*. Weinheim : Wiley-VCH: Weinheim, 2014.

107.   Günther, H. *NMR Spectroscopy: Basic Principles, Concepts and Applications in Chemistry, 3rd Edition*. Wiley-VCH Verlag GmbH & Co. KGaA: Weinheim, Germany, 2013.

108.	Harris, R. K.; Becker, E. D.; Cabral de Menezes, S. M.; Granger, P.; Hoffman, R. E.; Zilm, K. W. Further conventions for NMR shielding and chemical shifts (IUPAC Recommendations 2008). *Pure Appl. Chem.* **2008,** *80* (1), 59-84 10.1351/pac200880010059.

109.	Bryant, R. G. The Nmr Time Scale. *J. Chem. Educ.* **1983,** *60* (11), 933-935 10.1021/ed060p933.

110.	Gibb, C. L. D.; Gibb, B. C., The Thermodynamics of Molecular Recognition. In *Supramolecular Chemistry: From Molecules to Nanomaterials*, Gale, P. A.; Steed, J. W., Eds. John Wiley & Sons, Ltd: 2012; Vol. 2.

111.	Sun, H.; Gibb, C. L. D.; Gibb, B. C. Calorimetric analysis of the 1 : 1 complexes formed between a water-soluble deep-cavity cavitand, and cyclic and acyclic carboxylic acids. *Supramol. Chem.* **2008,** *20* (1-2), 141-147 10.1080/10610270701744302.

112.	Turnbull, W. B.; Daranas, A. H. On the value of c: can low affinity systems be studied by isothermal titration calorimetry? *J. Am. Chem. Soc.* **2003,** *125* (48), 14859-14866 10.1021/ja036166s.

113.	Tellinghuisen, J. Isothermal titration calorimetry at very low c. *Anal. Biochem.* **2008,** *373* (2), 395-397 10.1016/j.ab.2007.08.039.

114.	Pedersen, C. J. The Discovery of Crown Ethers (Reprinted from Current Topics in Macrocyclic Chemistry in Japan, 1987). *J. Inclusion Phenom. Mol. Recognit. Chem.* **1992,** *12* (1-4), 7-10 10.1007/Bf01053852.

115.	Pedersen, C. J. Cyclic polyethers and their complexes with metal salts. *J. Am. Chem. Soc.* **2002,** *89* (26), 7017-7036 10.1021/ja01002a035.

116.	Steed, J. W. First- and second-sphere coordination chemistry of alkali metal crown ether complexes. *Coord. Chem. Rev.* **2001,** *215* (1), 171-221 10.1016/S0010-8545(01)00317-4.

117.	Parks, F. C.; Sheetz, E. G.; Stutsman, S. R.; Lutolli, A.; Debnath, S.; Raghavachari, K.; Flood, A. H. Revealing the Hidden Costs of Organization in Host–Guest Chemistry Using Chloride-Binding Foldamers and Their Solvent Dependence. *J. Am. Chem. Soc.* **2022**, 10.1021/jacs.1c10758.

118.	Tsuchiya, T.; Shimizu, T.; Kamigata, N. Unsaturated Thiacrown Ethers: Synthesis, Physical Properties, and Formation of a Silver Complex. *J. Am. Chem. Soc.* **2001,** *123* (47), 11534-11538 10.1021/ja0102742.

119.   Tsuchiya, T.; Shimizu, T.; Hirabayashi, K.; Kamigata, N. Formation and Structures of Mercury Complexes of 18-Membered Unsaturated and Saturated Thiacrown Ethers. *J. Org. Chem.* **2003,** *68* (9), 3480-3485 10.1021/jo020668r.

120.   Ferrier, M. G.; Valdez, C. A.; Singh, S. K.; Hok, S.; Ray, D.; Gagliardi, L.; Despotopulos, J. D. Unsaturated Sulfur Crown Ethers Can Extract Mercury(II) and Show Promise for Future Copernicium(II) Studies: A Combined Experimental and Computational Study. *Inorg. Chem.* **2021,** 10.1021/acs.inorgchem.1c01869.

121.   Pitzer, K. S. Are elements 112, 114, and 118 relatively inert gases? *J. Chem. Phys.* **1975,** *63* (2), 1032-1033 10.1063/1.431398.

122.   Mewes, J. M.; Smits, O. R.; Kresse, G.; Schwerdtfeger, P. Copernicium: A Relativistic Noble Liquid. *Angew. Chem., Int. Ed.* **2019,** *58* (50), 17964-17968 10.1002/anie.201906966.

123.   Cram, D. J. Cavitands: organic hosts with enforced cavities. *Science* **1983,** *219* (4589), 1177-1183 10.1126/science.219.4589.1177.

124.   Bender, M. L.; Komiyama, M. *Cyclodextrin Chemistry*. 1978.

125.   Wimmer, T., Cyclodextrins. In *Ullmann's Encyclopedia of Industrial Chemistry*.

126.   Gu, A.; Wheate, N. J. Macrocycles as drug-enhancing excipients in pharmaceutical formulations. *J. Inclusion Phenom. Macrocyclic Chem.* **2021,** *100* (1-2), 55-69 10.1007/s10847-021-01055-9.

127.   Pühringer, K., Friedrich; Rex, C.; Sielenkämper, W., Andreas; Claudius, C.; Larsen, B., Per; Prins, E., Martine; Eikermann, M.; Khuenl-Brady, S., Karin Reversal of Profound, High-dose Rocuronium–induced Meeting Abstracts by Sugammadex at Two Different Time Points. *Anesthesiology* **2008,** *109* (2), 188-197 10.1097/aln.0b013e31817f5bc7.

128.   Bom, A.; Bradley, M.; Cameron, K.; Clark, J. K.; van Egmond, J.; Feilden, H.; MacLean, E. J.; Muir, A. W.; Palin, R.; Rees, D. C.*, et al.* A Novel Concept of Reversing Neuromuscular Block: Chemical Encapsulation of Rocuronium Bromide by a Cyclodextrin-Based Synthetic Host. *Angew. Chem., Int. Ed.* **2002,** *41* (2), 10.1002/1521-3773(20020118)41:2<265::Aid-anie265>3.0.Co;2-q.

129.   Liu, Z.; Samanta, A.; Lei, J.; Sun, J.; Wang, Y.; Stoddart, J. F. Cation-Dependent Gold Recovery with alpha-Cyclodextrin Facilitated by Second-Sphere Coordination. *J. Am. Chem. Soc.* **2016,** *138* (36), 11643-11653 10.1021/jacs.6b04986.

130.   Forgan, R. S.; Smaldone, R. A.; Gassensmith, J. J.; Furukawa, H.; Cordes, D. B.; Li, Q.; Wilmer, C. E.; Botros, Y. Y.; Snurr, R. Q.; Slawin, A. M.*, et al.* Nanoporous carbohydrate metal-organic frameworks. *J. Am. Chem. Soc.* **2012,** *134* (1), 406-417 10.1021/ja208224f.

131.   Liu, Z.; Frasconi, M.; Lei, J.; Brown, Z. J.; Zhu, Z.; Cao, D.; Iehl, J.; Liu, G.; Fahrenbach, A. C.; Botros, Y. Y.*, et al.* Selective isolation of gold facilitated by second-sphere coordination with alpha-cyclodextrin. *Nat. Commun.* **2013,** *4* (May), 1855 10.1038/ncomms2891.

132.   Lee, J. W.; Samal, S.; Selvapalam, N.; Kim, H. J.; Kim, K. Cucurbituril homologues and derivatives: new opportunities in supramolecular chemistry. *Acc. Chem. Res.* **2003,** *36* (8), 621-630 10.1021/ar020254k.

133.   Lagona, J.; Mukhopadhyay, P.; Chakrabarti, S.; Isaacs, L. The Cucurbit[n]uril Family. *Angew. Chem., Int. Ed.* **2005,** *44* (31), 4844-4870 10.1002/anie.200460675.

134.   Scott, M. P.; Sherburn, M. S., Resorcinarenes and Pyrogallolarenes. In *Comprehensive Supramolecular Chemistry II*, Elsevier: 2017; pp 337-374.

135.   Hoegberg, A. G. S. Cyclooligomeric phenol-aldehyde condensation products. 2. Stereoselective synthesis and DNMR study of two 1,8,15,22-tetraphenyl[14]metacyclophan-3,5,10,12,17,19,24,26-octols. *J. Am. Chem. Soc.* **1980,** *102* (19), 6046-6050 10.1021/ja00539a012.

136.   Weinelt, F.; Schneider, H. J. Host-guest chemistry. 27. Mechanisms of macrocycle genesis. The condensation of resorcinol with aldehydes. *J. Org. Chem.* **1991,** *56* (19), 5527-5535 10.1021/jo00019a011.

137.   Zhang, Q.; Tiefenbacher, K. Terpene cyclization catalysed inside a self-assembled cavity. *Nat. Chem.* **2015,** *7* (3), 197-202 10.1038/nchem.2181.

138.   Catti, L.; Zhang, Q.; Tiefenbacher, K. Advantages of Catalysis in Self-Assembled Molecular Capsules. *Chem. - Eur. J.* **2016,** *22* (27), 9060-9066 10.1002/chem.201600726.

139.   Pollok, C. H.; Zhang, Q.; Tiefenbacher, K.; Merten, C. Chirality Induction from a Chiral Guest to the Hydrogen-Bonding Network of Its Hexameric Resorcinarene Host Capsule. *ChemPhysChem* **2017,** *18* (15), 1987-1991 10.1002/cphc.201700610.

140.   Zhang, Q.; Catti, L.; Pleiss, J.; Tiefenbacher, K. Terpene Cyclizations inside a Supramolecular Catalyst: Leaving-Group-Controlled Product Selectivity and Mechanistic Studies. *J. Am. Chem. Soc.* **2017,** *139* (33), 11482-11492 10.1021/jacs.7b04480.

141.   Köster, J. M.; Tiefenbacher, K. Elucidating the Importance of Hydrochloric Acid as a Cocatalyst for Resorcinarene-Capsule-Catalyzed Reactions. *ChemCatChem* **2018,** *10* (14), 2941-2944 10.1002/cctc.201800326.

142.   Zhang, Q.; Catti, L.; Tiefenbacher, K. Catalysis inside the Hexameric Resorcinarene Capsule. *Acc. Chem. Res.* **2018,** *51* (9), 2107-2114 10.1021/acs.accounts.8b00320.

143.   Nemat, S. J.; Tiefenbacher, K. Thioderivatives of Resorcin[4]arene and Pyrogallol[4]arene: Are Thiols Tolerated in the Self-Assembly Process? *Org. Lett.* **2021,** *23* (17), 6861-6865 10.1021/acs.orglett.1c02426.

144.   MacGillivray, L. R.; Atwood, J. L. A chiral spherical molecular assembly held together by 60 hydrogen bonds. *Nature* **1997,** *389* (6650), 469-472 10.1038/38985.

145.   Dalgarno, S. J.; Power, N. P.; Atwood, J. L. Metallo-supramolecular capsules. *Coord. Chem. Rev.* **2008,** *252* (8-9), 825-841 10.1016/j.ccr.2007.10.010.

146.   Jin, P.; Dalgarno, S. J.; Atwood, J. L. Mixed metal-organic nanocapsules. *Coord. Chem. Rev.* **2010,** *254* (15-16), 1760-1768 10.1016/j.ccr.2010.04.009.

147.   Hu, X.; Feng, S.; Du, J.; Shao, L.; Lang, J.; Zhang, C.; Kelley, S. P.; Lin, J.; Dalgarno, S. J.; Atwood, D. A*., et al.* Controlled hierarchical self-assembly of networked coordination nanocapsules via the use of molecular chaperones. *Chem. Sci.* **2020,** *11* (46), 12547-12552 10.1039/d0sc05002d.

148.   Cram, D. J.; Tanner, M. E.; Thomas, R. The Taming of Cyclobutadiene. *Angew. Chem., Int. Ed. Engl.* **1991,** *30* (8), 1024-1027 10.1002/anie.199110241.

149.   MacGillivray, L. R.; Atwood, J. L. Structural classification and general principles for the design of spherical molecular hosts. *Angew. Chem., Int. Ed.* **1999,** *38* (8), 1018-1033 10.1002/(SICI)1521-3773(19990419)38:8<1018::AID-ANIE1018>3.0.CO;2-G.

150.   Warmuth, R.; Yoon, J. Recent highlights in hemicarcerand chemistry. *Acc. Chem. Res.* **2001,** *34* (2), 95-105 10.1021/ar980082k.

151.   Tunstad, L. M.; Tucker, J. A.; Dalcanale, E.; Weiser, J.; Bryant, J. A.; Sherman, J. C.; Helgeson, R. C.; Knobler, C. B.; Cram, D. J. Host-guest complexation. 48. Octol building blocks for cavitands and carcerands. *J. Org. Chem.* **2002,** *54* (6), 1305-1312 10.1021/jo00267a015.

152.   Cram, D. J.; Karbach, S.; Kim, Y. H.; Baczynskyj, L.; Kallemeyn, G. W. Shell closure of two cavitands forms carcerand complexes with components of the

medium as permanent guests. *J. Am. Chem. Soc.* **2002,** *107* (8), 2575-2576 10.1021/ja00294a076.

153.   Tanner, M. E.; Knobler, C. B.; Cram, D. J. Hemicarcerands permit entrance to and egress from their inside phases with high structural recognition and activation free energies. *J. Am. Chem. Soc.* **2002,** *112* (4), 1659-1660 10.1021/ja00160a072.

154.   Cram, D. J. Molecular Container Compounds. *Nature* **1992,** *356* (6364), 29-36 10.1038/356029a0.

155.   Cram, D. J.; Cram, J. M. *Container Molecules and Their Guests*. Royal Society of Chemistry: Cambridge, 1997.

156.   Cram, D. J.; Tanner, M. E.; Knobler, C. B. Host-guest complexation. 58. Guest release and capture by hemicarcerands introduces the phenomenon of constrictive binding. *J. Am. Chem. Soc.* **1991,** *113* (20), 7717-7727 10.1021/ja00020a039.

157.   Gibb, B. C.; Chapman, R. G.; Sherman, J. C. Synthesis of hydroxyl-footed cavitands. *J. Org. Chem.* **1996,** *61* (4), 1505-1509 10.1021/jo951633c.

158.   Jordan, J. H.; Ashbaugh, H. S.; Mague, J. T.; Gibb, B. C. Buffer and Salt Effects in Aqueous Host–Guest Systems: Screening, Competitive Binding, or Both? *J. Am. Chem. Soc.* **2021,** *143* (44), 18605-18616 10.1021/jacs.1c08457.

159.   Moran, J. R.; Ericson, J. L.; Dalcanale, E.; Bryant, J. A.; Knobler, C. B.; Cram, D. J. Vases and kites as cavitands. *J. Am. Chem. Soc.* **1991,** *113* (15), 5707-5714 10.1021/ja00015a026.

160.   Heinz, T.; Rudkevich, D. M.; Rebek, J. Pairwise selection of guests in a cylindrical molecular capsule of nanometre dimensions. *Nature* **1998,** *394* (6695), 764-766 10.1038/29501.

161.   Scarso, A.; Trembleau, L.; Rebek, J., Jr. Encapsulation induces helical folding of alkanes. *Angew. Chem., Int. Ed.* **2003,** *42* (44), 5499-5502 10.1002/anie.200352235.

162.   Scarso, A.; Trembleau, L.; Rebek, J., Jr. Helical folding of alkanes in a self-assembled, cylindrical capsule. *J. Am. Chem. Soc.* **2004,** *126* (41), 13512-13518 10.1021/ja047952f.

163.   Carey, F. A.; Sundberg, R. J. *Advanced Organic Chemistry, Part A: Structure and Mechanisms*. Fifth Edit ed.; Springer: New York, NY, 2007.

164. Smith, M. *March's Advanced Organic Chemistry: Reactions, Mechanisms, and Structure*. 7th Ed. ed.; Wiley: Hoboken, New Jersey, 2013.

165. Wu, N. W.; Rebek, J., Jr. Cavitands as Chaperones for Monofunctional and Ring-Forming Reactions in Water. *J. Am. Chem. Soc.* **2016,** *138* (24), 7512-7515 10.1021/jacs.6b04278.

166. Choi, H.-J.; Nguyen, Q.-T.; Park, Y. S.; Choi, C.-H.; Paek, K.; Kim, E.-H. New deep cavitand with imidazoquinoxaline flaps: formation of static helical alkane inclusion complexes by enhanced CH/π interactions. *Chem. Commun. (Cambridge, U. K.)* **2009,** (33), 4971 10.1039/b908650a.

167. Xi, H. P.; Gibb, C. L. D.; Gibb, B. C. Functionalized deep-cavity cavitands. *J. Org. Chem.* **1999,** *64* (25), 9286-9288 10.1021/jo9909913.

168. Fleming, I. *Molecular Orbitals and Organic Chemical Reactions*. John Wiley & Sons, Ltd: Chichester, 2010.

169. Green, J. O.; Baird, J. H.; Gibb, B. C. Reduced-symmetry deep-cavity cavitands. *Org. Lett.* **2000,** *2* (24), 3845-3848 10.1021/ol006569m.

170. Gibb, C. L. D.; Stevens, E. D.; Gibb, B. C. C-H...X-R Hydrogen Bonds Drive the Complexation Properties of a Nano-scale Molecular Basket. *J. Am. Chem. Soc.* **2001,** *123*, 5849-5850 10.1021/ja005931p.

171. Li, J. J., Ullmann coupling. In *Name Reactions*, 5th ed.; Springer: 2014; pp 611-612.

172. Gibb, C. L. D.; Gibb, B. C. Well Defined, Organic Nano-Environments in Water: The Hydrophobic Effect Drives a Capsular Assembly. *J. Am. Chem. Soc.* **2004,** *126*, 11408-11409 10.1021/ja0475611.

173. Liu, S.; Whisenhunt-Ioup, S. E.; Gibb, C. L.; Gibb, B. C. An improved synthesis of 'octa-acid' deep-cavity cavitand. *Supramol. Chem.* **2011,** *23* (6), 480-485 10.1080/10610278.2010.550290.

174. Ewell, J.; Gibb, B. C.; Rick, S. W. Water inside a hydrophobic cavitand molecule. *J. Phys. Chem. B* **2008,** *112* (33), 10272-10279 10.1021/jp804429n.

175. Kaanumalle, L. S.; Gibb, C. L.; Gibb, B. C.; Ramamurthy, V. Controlling photochemistry with distinct hydrophobic nanoenvironments. *J. Am. Chem. Soc.* **2004,** *126* (44), 14366-14367 10.1021/ja0450197.

176. Kaanumalle, L. S.; Gibb, C. L.; Gibb, B. C.; Ramamurthy, V. A hydrophobic nanocapsule controls the photophysics of aromatic molecules by suppressing

their favored solution pathways. *J. Am. Chem. Soc.* **2005,** *127* (11), 3674-3675 10.1021/ja0425381.

177. Natarajan, A.; Kaanumalle, L. S.; Jockusch, S.; Gibb, C. L.; Gibb, B. C.; Turro, N. J.; Ramamurthy, V. Controlling photoreactions with restricted spaces and weak intermolecular forces: exquisite selectivity during oxidation of olefins by singlet oxygen. *J. Am. Chem. Soc.* **2007,** *129* (14), 4132-4133 10.1021/ja070086x.

178. Kaanumalle, L. S.; Gibb, C. L.; Gibb, B. C.; Ramamurthy, V. Photo-Fries reaction in water made selective with a capsule. *Org. Biomol. Chem.* **2007,** *5* (2), 236-238 10.1039/b617022f.

179. Gibb, C. L.; Sundaresan, A. K.; Ramamurthy, V.; Gibb, B. C. Templation of the excited-state chemistry of alpha-(n-alkyl) dibenzyl ketones: how guest packing within a nanoscale supramolecular capsule influences photochemistry. *J. Am. Chem. Soc.* **2008,** *130* (12), 4069-4080 10.1021/ja7107917.

180. Sundaresan, A. K.; Gibb, C. L.; Gibb, B. C.; Ramamurthy, V. Chiral Photochemistry in a Confined Space: Torquoselective Photoelectrocyclization of Pyridones within an Achiral Hydrophobic Capsule. *Tetrahedron* **2009,** *65* (35), 7277-7288 10.1016/j.tet.2009.01.110.

181. Samanta, S. R.; Kulasekharan, R.; Choudhury, R.; Jagadesan, P.; Jayaraj, N.; Ramamurthy, V. Gold nanoparticles functionalized with deep-cavity cavitands: synthesis, characterization, and photophysical studies. *Langmuir* **2012,** *28* (32), 11920-11928 10.1021/la302478e.

182. Jagadesan, P.; Mondal, B.; Parthasarathy, A.; Rao, V. J.; Ramamurthy, V. Photochemical reaction containers as energy and electron-transfer agents. *Org. Lett.* **2013,** *15* (6), 1326-1329 10.1021/ol400267k.

183. Ramamurthy, V. Photochemistry within a water-soluble organic capsule. *Acc. Chem. Res.* **2015,** *48* (11), 2904-2917 10.1021/acs.accounts.5b00360.

184. Gibb, C. L.; Gibb, B. C. Anion binding to hydrophobic concavity is central to the salting-in effects of Hofmeister chaotropes. *J. Am. Chem. Soc.* **2011,** *133* (19), 7344-7347 10.1021/ja202308n.

185. Carnegie, R. S.; Gibb, C. L.; Gibb, B. C. Anion complexation and the Hofmeister effect. *Angew. Chem., Int. Ed.* **2014,** *53* (43), 11498-11500 10.1002/anie.201405796.

186. Gibb, C. L.; Oertling, E. E.; Velaga, S.; Gibb, B. C. Thermodynamic profiles of salt effects on a host-guest system: new insight into the Hofmeister effect. *J. Phys. Chem. B* **2015,** *119* (17), 5624-5638 10.1021/acs.jpcb.5b01708.

187. Jordan, J. H.; Gibb, C. L. D.; Wishard, A.; Pham, T.; Gibb, B. C. Ion-Hydrocarbon and/or Ion-Ion Interactions: Direct and Reverse Hofmeister Effects in a Synthetic Host. *J. Am. Chem. Soc.* **2018,** *140* (11), 4092-4099 10.1021/jacs.8b00196.

188. Sullivan, M. R.; Yao, W.; Tang, D.; Ashbaugh, H. S.; Gibb, B. C. The Thermodynamics of Anion Complexation to Nonpolar Pockets. *J. Phys. Chem. B* **2018,** *122* (5), 1702-1713 10.1021/acs.jpcb.7b12259.

189. Hillyer, M. B.; Gan, H.; Gibb, B. C. Precision Switching in a Discrete Supramolecular Assembly: Alkali Metal Ion-Carboxylate Selectivities and the Cationic Hofmeister Effect. *ChemPhysChem* **2018,** *19* (18), 2285-2289 10.1002/cphc.201800554.

190. Gibb, B. C. The synthesis and structural examination of 3a, 5-cyclo-5a-androstane steroids : [a thesis] submitted in partial fulfilment of the requirements of the degree of Doctor of Philosophy. Robert Gordon University, Aberdeen, 1992.

191. Gibb, C. L.; Gibb, B. C. Straight-chain alkanes template the assembly of water-soluble nano-capsules. *Chem. Commun. (Cambridge, U. K.)* **2007,** *2* (16), 1635-1637 10.1039/b618731e.

192. Gan, H.; Benjamin, C. J.; Gibb, B. C. Nonmonotonic assembly of a deep-cavity cavitand. *J. Am. Chem. Soc.* **2011,** *133* (13), 4770-4773 10.1021/ja200633d.

193. Laughrey, Z.; Gibb, B. C. Water-soluble, self-assembling container molecules: an update. *Chem. Soc. Rev.* **2011,** *40* (1), 363-386 10.1039/c0cs00030b.

194. Liu, S.; Russell, D. H.; Zinnel, N. F.; Gibb, B. C. Guest packing motifs within a supramolecular nanocapsule and a covalent analogue. *J. Am. Chem. Soc.* **2013,** *135* (11), 4314-4324 10.1021/ja310741q.

195. Barnett, J. W.; Gibb, B. C.; Ashbaugh, H. S. Succession of Alkane Conformational Motifs Bound within Hydrophobic Supramolecular Capsular Assemblies. *J. Phys. Chem. B* **2016,** *120* (39), 10394-10402 10.1021/acs.jpcb.6b06496.

196. Barnett, J. W.; Tang, D.; Gibb, B. C.; Ashbaugh, H. S. Alkane guest packing drives switching between multimeric deep-cavity cavitand assembly states. *Chem. Commun. (Cambridge, U. K.)* **2018,** *54* (21), 2639-2642 10.1039/c8cc00036k.

197. Liu, S.; Gan, H.; Hermann, A. T.; Rick, S. W.; Gibb, B. C. Kinetic resolution of constitutional isomers controlled by selective protection inside a

supramolecular nanocapsule. *Nat. Chem.* **2010,** *2* (10), 847-852 10.1038/nchem.751.

198.   Gan, H.; Gibb, B. C. Guest-controlled self-sorting in assemblies driven by the hydrophobic effect. *Chem. Commun. (Cambridge, U. K.)* **2012,** *48* (11), 1656-1658 10.1039/c2cc16603h.

199.   Sullivan, M. R.; Gibb, B. C. Differentiation of small alkane and alkyl halide constitutional isomers via encapsulation. *Org. Biomol. Chem.* **2015,** *13* (6), 1869-1877 10.1039/c4ob02357a.

200.   Wang, K.; Gibb, B. C. Mapping the Binding Motifs of Deprotonated Monounsaturated Fatty Acids and Their Corresponding Methyl Esters within Supramolecular Capsules. *J. Org. Chem.* **2017,** *82* (8), 4279-4288 10.1021/acs.joc.7b00264.

201.   Wang, K.; Jordan, J. H.; Gibb, B. C. Molecular protection of fatty acid methyl esters within a supramolecular capsule. *Chem. Commun. (Cambridge, U. K.)* **2019,** *55* (78), 11695-11698 10.1039/c9cc06501f.

202.   Hillyer, M. B.; Gibb, C. L.; Sokkalingam, P.; Jordan, J. H.; Ioup, S. E.; Mague, J. T.; Gibb, B. C. Synthesis of Water-Soluble Deep-Cavity Cavitands. *Org. Lett.* **2016,** *18* (16), 4048-4051 10.1021/acs.orglett.6b01903.

203.   Appel, R. Tertiary Phosphane/Tetrachloromethane, a Versatile Reagent for Chlorination, Dehydration, and P–N Linkage. *Angew. Chem., Int. Ed. Engl.* **1975,** *14* (12), 801-811 10.1002/anie.197508011.

204.   Menschutkin, N. Über die Affinitätskoeffizienten der Alkylhaloide und der Amine. *Zeitschrift für Physikalische Chemie* **1890,** *6U* (1), 41-57 10.1515/zpch-1890-0607.

205.   Keserű, G. M.; Makara, G. M. Hit discovery and hit-to-lead approaches. *Drug Discovery Today* **2006,** *11* (15-16), 741-748 10.1016/j.drudis.2006.06.016.

206.   Bleicher, K. H.; Bohm, H. J.; Muller, K.; Alanine, A. I. Hit and lead generation: beyond high-throughput screening. *Nat. Rev. Drug Discovery* **2003,** *2* (5), 369-378 10.1038/nrd1086.

207.   Olano, L. R.; Rick, S. W. Hydration free energies and entropies for water in protein interiors. *J. Am. Chem. Soc.* **2004,** *126* (25), 7991-8000 10.1021/ja049701c.

208.   Young, T.; Hua, L.; Huang, X.; Abel, R.; Friesner, R.; Berne, B. J. Dewetting transitions in protein cavities. *Proteins* **2010,** *78* (8), 1856-1869 10.1002/prot.22699.

209.   Snyder, P. W.; Mecinovic, J.; Moustakas, D. T.; Thomas, S. W., 3rd; Harder, M.; Mack, E. T.; Lockett, M. R.; Heroux, A.; Sherman, W.; Whitesides, G. M. Mechanism of the hydrophobic effect in the biomolecular recognition of arylsulfonamides by carbonic anhydrase. *Proc. Natl. Acad. Sci. U. S. A.* **2011,** *108* (44), 17889-17894 10.1073/pnas.1114107108.

210.   Setny, P.; Wang, Z.; Cheng, L. T.; Li, B.; McCammon, J. A.; Dzubiella, J. Dewetting-controlled binding of ligands to hydrophobic pockets. *Philos. Trans. R. Soc., A* **2009,** *103* (18), 187801 10.1103/PhysRevLett.103.187801.

211.   Baron, R.; Setny, P.; McCammon, J. A. Water in cavity-ligand recognition. *J. Am. Chem. Soc.* **2010,** *132* (34), 12091-12097 10.1021/ja1050082.

212.   Rizzi, V.; Bonati, L.; Ansari, N.; Parrinello, M. The role of water in host-guest interaction. *Nat. Commun.* **2021,** *12* (1), 93 10.1038/s41467-020-20310-0.

213.   Klebe, G. Applying thermodynamic profiling in lead finding and optimization. *Nat. Rev. Drug Discovery* **2015,** *14* (2), 95-110 10.1038/nrd4486.

214.   Mobley, D. L.; Gilson, M. K. Predicting Binding Free Energies: Frontiers and Benchmarks. *Annu. Rev. Biophys.* **2017,** *46*, 531-558 10.1146/annurev-biophys-070816-033654.

215.   Yin, J.; Henriksen, N. M.; Slochower, D. R.; Shirts, M. R.; Chiu, M. W.; Mobley, D. L.; Gilson, M. K. Overview of the SAMPL5 host-guest challenge: Are we doing better? *J. Comput.-Aided Mol. Des.* **2017,** *31* (1), 1-19 10.1007/s10822-016-9974-4.

216.   Laury, M. L.; Wang, Z.; Gordon, A. S.; Ponder, J. W. Absolute binding free energies for the SAMPL6 cucurbit[8]uril host–guest challenge via the AMOEBA polarizable force field. *J. Comput.-Aided Mol. Des.* **2018,** *32* (10), 1087-1095 10.1007/s10822-018-0147-5.

217.   Stephanie, B. A. d. B.; Nico, P. E. V.; Chris, O. The Role of Water Molecules in Computational Drug Design. *Curr. Top. Med. Chem. (Sharjah, United Arab Emirates)* **2010,** *10* (1), 55-66 10.2174/156802610790232288.

218.   Tang, D.; Dwyer, T.; Bukannan, H.; Blackmon, O.; Delpo, C.; Barnett, J. W.; Gibb, B. C.; Ashbaugh, H. S. Pressure Induced Wetting and Dewetting of the Nonpolar Pocket of Deep-Cavity Cavitands in Water. *J. Phys. Chem. B* **2020,** *124* (23), 4781-4792 10.1021/acs.jpcb.0c02568.

219.   Ashbaugh, H. S.; Gibb, B. C.; Suating, P. Cavitand Complexes in Aqueous Solution: Collaborative Experimental and Computational Studies of the Wetting, Assembly, and Function of Nanoscopic Bowls in Water. *J. Phys. Chem. B* **2021,** *125* (13), 3253-3268 10.1021/acs.jpcb.0c11017.

220.   Suating, P.; Nguyen, T. T.; Ernst, N. E.; Wang, Y.; Jordan, J. H.; Gibb, C. L. D.; Ashbaugh, H. S.; Gibb, B. C. Proximal charge effects on guest binding to a non-polar pocket. *Chem. Sci.* **2020,** *11* (14), 3656-3663 10.1039/c9sc06268h.

221.   Yin, J.; Henriksen, N. M.; Slochower, D. R.; Gilson, M. K. The SAMPL5 host-guest challenge: computing binding free energies and enthalpies from explicit solvent simulations by the attach-pull-release (APR) method. *J. Comput.-Aided Mol. Des.* **2017,** *31* (1), 133-145 10.1007/s10822-016-9970-8.

222.   The SAMPL Challenges. https://samplchallenges.github.io.

223.   Coleridge, S. T., Rime of the Ancient Mariner. In *Sibylline Leaves. A collection of poems*, Rest Fenner: London, 1817.

224.   Qvist, J.; Davidovic, M.; Hamelberg, D.; Halle, B. A dry ligand-binding cavity in a solvated protein. *Proc. Natl. Acad. Sci. U. S. A.* **2008,** *105* (17), 6296-6301 10.1073/pnas.0709844105.

225.   Collins, M. D.; Hummer, G.; Quillin, M. L.; Matthews, B. W.; Gruner, S. M. Cooperative water filling of a nonpolar protein cavity observed by high-pressure crystallography and simulation. *Proc. Natl. Acad. Sci. U. S. A.* **2005,** *102* (46), 16668-16671 10.1073/pnas.0508224102.

226.   Rasaiah, J. C.; Garde, S.; Hummer, G. Water in nonpolar confinement: from nanotubes to proteins and beyond. *Annu. Rev. Phys. Chem.* **2008,** *59*, 713-740 10.1146/annurev.physchem.59.032607.093815.

227.   Laughrey, Z. R.; Gibb, C. L.; Senechal, T.; Gibb, B. C. Guest binding and orientation within open nanoscale hosts. *Chem. - Eur. J.* **2003,** *9* (1), 130-139 10.1002/chem.200390008.

228.   Srinivasan, K.; Laughrey, Z. R.; Gibb, B. C. Broad Functionalization of Deep‐Cavity Cavitands by Directed *ortho*-Metalation. *Eur. J. Org. Chem.* **2008,** *2008* (19), 3265-3271 10.1002/ejoc.200800206.

229.   Schwierz, N.; Horinek, D.; Netz, R. R. Anionic and cationic Hofmeister effects on hydrophobic and hydrophilic surfaces. *Langmuir* **2013,** *29* (8), 2602-2614 10.1021/la303924e.

230.   Schwierz, N.; Horinek, D.; Netz, R. R. Specific ion binding to carboxylic surface groups and the pH dependence of the Hofmeister series. *Langmuir* **2015,** *31* (1), 215-225 10.1021/la503813d.

231.   Remko, M.; Van Duijnen, P. T.; von der Lieth, C.-W. Structure and stability of Li(I) and Na(I) – Carboxylate, sulfate and phosphate complexes. *J. Mol. Struct.: THEOCHEM* **2007,** *814* (1-3), 119-125 10.1016/j.theochem.2007.03.004.

232. Wright, A. C.; Du, Y. E.; Stoltz, B. M. Small-Scale Procedure for Acid-Catalyzed Ketal Formation. *J. Org. Chem.* **2019,** *84* (17), 11258-11260 10.1021/acs.joc.9b01541.

233. Das, P.; McNulty, J. Dichotomous Reactivity in the Reaction of Triethyl- and Triphenylphosphane HBr Salts with Dimethyl Acetals: A Novel Entry to α-Alkoxy-Functionalized Ylides and General Synthesis of Vinyl Ethers and Alkoxy Dienes. *Eur. J. Org. Chem.* **2010,** *2010* (19), 3587-3591 10.1002/ejoc.201000601.

234. Azzena, U.; Idini, M. V.; Pilo, L. Synthesis of antibiotic stilbenes by reductive metalation of 3,4,5-trimethoxybenzaldehyde dimethyl acetal. *Synth. Commun.* **2003,** *33* (8), 1309-1317 10.1081/Scc-120018690.

235. Stewart, J. J. Optimization of parameters for semiempirical methods V: modification of NDDO approximations and application to 70 elements. *J. Mol. Model.* **2007,** *13* (12), 1173-1213 10.1007/s00894-007-0233-4.

236. Scott, L. T.; Hashemi, M. M.; Bratcher, M. S. Corannulene bowl-to-bowl inversion is rapid at room temperature. *J. Am. Chem. Soc.* **2002,** *114* (5), 1920-1921 10.1021/ja00031a079.

237. Yalkowsky, S. H.; He, Y.; Jain, P. *Handbook of Aqueous Solubility Data*. 2nd ed. ed.; CRC Press: Boca Raton, 2010.

238. Tang, D.; Barnett, J. W.; Gibb, B. C.; Ashbaugh, H. S. Guest Controlled Nonmonotonic Deep Cavity Cavitand Assembly State Switching. *J. Phys. Chem. B* **2017,** *121* (47), 10717-10725 10.1021/acs.jpcb.7b09021.

239. Saltzman, A.; Tang, D.; Gibb, B. C.; Ashbaugh, H. S. Emergence of non-monotonic deep cavity cavitand assembly with increasing portal methylation. *Mol. Syst. Des. Eng.* **2020,** *5* (3), 656-665 10.1039/c9me00076c.

240. Langton, M. J.; Serpell, C. J.; Beer, P. D. Anion Recognition in Water: Recent Advances from a Supramolecular and Macromolecular Perspective. *Angew. Chem., Int. Ed.* **2016,** *55* (6), 1974-1987 10.1002/anie.201506589.

241. Escobar, L.; Ballester, P. Molecular Recognition in Water Using Macrocyclic Synthetic Receptors. *Chem. Rev.* **2021,** *121* (4), 2445-2514 10.1021/acs.chemrev.0c00522.

242. Liu, Y.; Zhao, W.; Chen, C. H.; Flood, A. H. Chloride capture using a C-H hydrogen-bonding cage. *Science* **2019,** *365* (6449), 159-161 10.1126/science.aaw5145.

243.   Davis, J. G.; Zukowski, S. R.; Rankin, B. M.; Ben-Amotz, D. Influence of a Neighboring Charged Group on Hydrophobic Hydration Shell Structure. *The Journal of Physical Chemistry B* **2015,** *119* (29), 9417-9422 10.1021/jp510641a.

244.   Adams, D. *Mostly harmless*. [1st]. ed.; Harmony Books: New York, 1992.

245.   Armarego, W. L. F. *Purification of laboratory chemicals*. Eighth edition.. ed.; Amsterdam : Butterworth-Heinemann: Amsterdam, 2017.

246.   Burchat, A. F.; Chong, J. M.; Nielsen, N. Titration of alkyllithiums with a simple reagent to a blue endpoint. *J. Organomet. Chem.* **1997,** *542* (2), 281-283 10.1016/S0022-328x(97)00143-5.

247.   Kakwere, H.; Payne, R. J.; Jolliffe, K. A.; Perrier, S. Self-assembling macromolecular chimeras: controlling fibrillization of a β-sheet forming peptide by polymer conjugation. *Soft Matter* **2011,** *7* (8), 10.1039/c0sm01237h.

248.   House, H. O.; Chu, C.-Y.; Wilkins, J. M.; Umen, M. J. Chemistry of carbanions. XXVII. Convenient precursor for the generation of lithium organocuprates. *J. Org. Chem.* **2002,** *40* (10), 1460-1469 10.1021/jo00898a019.

249.   Gibb, C. L.; Gibb, B. C. Binding of cyclic carboxylates to octa-acid deep-cavity cavitand. *J. Comput.-Aided Mol. Des.* **2014,** *28* (4), 319-325 10.1007/s10822-013-9690-2.

250.   Sheldrick, G. M. Crystal structure refinement with SHELXL. *Acta Crystallogr., Sect. C: Cryst. Struct. Commun.* **2015,** *71* (Pt 1), 3-8 10.1107/S2053229614024218.

Biography

Paolo Suating was born in Manila, Philippines where he completed is elementary and high school education. He briefly attended the Chemistry Program at the University of Santo Tomas. In 2008 he then emigrated from Manila, Philippines to Chicago, United States. After a brief pause in his education during which he worked as a board-certified pharmacy technician, he continued his undergraduate studies in Chemistry at Northern Illinois University (NIU) in 2013. During his undergraduate education he joined the research group of Dr Marc Adler studying the synthesis, reactivity, and applications of organosilanes and silicon atranes. He graduated with a BS in Chemistry from NIU in 2016 and he subsequently attended the graduate program in Chemistry at Tulane University and was supervised by Dr Bruce Gibb. While at Tulane University he was active in student government, serving two terms as treasurer, and one term as president of the Graduate Studies Student Association.